RESTORING VISION USING HUMAN OPSINS

A thesis submitted to the University of Manchester for the degree of

Doctor of Philosophy

in the Faculty of Medical and Human Sciences

2015

Jasmina Cehajic-Kapetanovic

School of Medicine

Contents

Figures

Tables

Abbreviations

AAV-	adeno-associated virus
AAQ	acrylamide-azobenzane-quaternary ammonium
ABCA4	ATP-binding cassette, subfamily A, member 4
AC	amacrine cell
AIPL1	aryl hydrocarbon receptor interacting protein-like 1
AMPA	α-amino-3-hydroxy-5-methylisoxazole-4-propionic acid
BC	bipolar cell
CABP	calcium binding protein
CACNA1	calcium channel, voltage dependent N type, alpha subunit 1
CRB1	crumbs family member 1
cGMP	cyclic guanosine monophosphate
CHM	choroideraemia gene
ChR2	channelrhodopsin , type 2
CNGA	cyclic nucleotide gated channel
CNGA	cyclic nucleotide gated channel alpha
CNGB	cyclic nucleotide gated channel beta
CNS	central nervous system
CORD	cone-rod dystrophy
CRX	cone-rod homeobox
CS	chondroitin sulphate
DENAQ	red-shifted azobenzane-based photoswitch
dLGN	dorsal lateral geniculate nucleus
DS	dermatan sulphate
ERG	electroretinogram
GABA	gamma-aminobutryic acid
GAG	glycosaminoglycan
GCL	ganglion cell layer
GDP	guanosine diphosphate
GNAT2	guanine nucleotide binding protein (G protein), alpha transducing activity polypeptide 2
GPCR	G-protein coupled receptor
GPR	G-protein receptor

GTP	guanosine triphosphate
GUCY2D	guanylate cyclase 2D
HC	horizontal cell
HS	heparan sulphate
HSPG	heparan sulphate proteoglycan
iGluR	ionotropic glutamate receptor
ILM	inner limiting membrane
INL	inner nuclear layer
IPL	inner plexiform layer
IPM	interphotoreceptor matrix
ipRGC	intrinsically photosensitive retinal ganglion cell
IRD	inherited retinal degenerations
ITR	inverted terminal repeat
KS	keratin sulphate
LCA	leber congenital amaurosis
LRIT	leucine rich repeat immunoglobulin –like and transmembrane domains
LiGluR	light-gated ionotropic glutamate receptor
MAG	malemide-azobenzene-glutamate
MC	Muller cell
mGluR	metabotropic glutamate receptor
MY07A	myosin VIIA
NFL	nerve fibre layer
NMDAN	methyl-D-aspartate acid
NpHR	*Natronomas pharaonic* halorhodopsin
NR2E3	nuclear receptor subfamily 2, group E, member 3
NRL	neutral retina leucine zipper
OLM	outer limiting membrane
ONL	outer nuclear layer
OPL	outer plexiform layer
OPN4	melanopsin
OptomGluR	chimera of melanopsin light sensing portion (Opto) and metabotropic glutamate receptor

OS	outer segments
PDE	phosphodiesterase
PG	proteoglycan
PLR	pupillary light reflex
PRPH2	peripherin 2 (retinal degeneration, slow)
RdCVF	rod-derived cone viability factor
REP1	Rab escort protein –1
RGC	retinal ganglion cell
RGR	retinal G protein coupled receptor
RHO	rod opsin or rhodopsin
RLBPRal	A binding protein 1
ROM1	retinal outer segment membrane protein 1
RP	retinitis pigmentosa
RPE	retinal pigment epithelium
RPE65	retinal pigment epithelium specific protein 65kDa protein
RPGR	retinitis pigmentosa GTPase regulator interacting protein
RS1	retinoschisin 1
SAG	S-antigen (retinal S-arrestin)
TMD	transmembrane domain
TRPM1	transient receptor potential cation channel subfamily M member 1
WPRE	woodchuck hepatitis posttranscriptional regulatory element
polyA	polyadenylation signal sequence

Abstract
Restoring vision using human opsins
Jasmina Cehajic-Kapetanovic; The University of Manchester, Doctor of Philosophy, 2015

Inherited retinal degenerations (IRDs) are progressive degenerative conditions that affect around 1 in 2500 people worldwide and lead to severe visual impairment due to irreversible loss of photoreceptors. These conditions are currently untreatable. However, inner retinal neurons, including bipolar and ganglion cells, can survive representing promising targets for emerging optogenetic therapies that aim to convert them into photoreceptors and recreate the lost photosensitivity. However, efficient targeting of these surviving cells, such as ON-bipolar cells, has not been achieved. In addition, current optogenetic actuators have low sensitivity posing major limitations to vision restoration. The overall aim of this research was to develop an optimised adeno-associated virus (AAV) based gene delivery system for efficient targeting of optogenetic sensors to surviving retinal cells, and to investigate whether this optimised approach can restore visual function in an *rd*^{1} mouse model of advanced IRD.

Transduction efficiency of AAV serotype 2, AAV2 (carrying enhanced green fluorescent protein, GFP, driven by a non-selective promoter) in conjunction with glycosidic enzymes, was determined by qualitative and quantitative analysis of GFP positive cells in the treated *wild-type* retinas. In addition, using an optimised AAV2-enzyme combination, GFP expression was analysed in *rd*^{1} mice after both untargeted delivery and when GFP was selectively targeted to ON-bipolar cells. Lastly, effects of glycosidic enzymes on the retinal function were determined by flash electroretinograms (ERGs) and pupillometry. The data revealed that a combination of heparinase III and hyaluronan lyase produced the greatest enhancement of gene delivery to the healthy *wild-type* retinas and that this optimised approach led to a marked improvement in transduction in degenerate *rd*^{1} retinas. Retinal function and photosensitivity were unaffected as determined by ERGs and pupillometry at a range of irradiances tested in the acute period and up to at least 12 months post enzymatic treatment.

Using the optimised AAV2-enzyme combination, human melanopsin (driven by a non-selective promoter) and human rod opsin (driven by non-selective or ON-bipolar cell-specific promoters) were expressed in *rd*^{1} retinas. Mice treated with melanopsin showed enhanced pupil light reflex compared to controls. Analysis of *in vivo* electrophysiology recordings from the lateral geniculate nucleus (LGN) in the thalamus of melanopsin treated revealed that light-evoked excitatory neuronal responses were more numerous, larger, and of higher sensitivity and shorter latency than those derived from control eyes. Importantly, restored responses were orders of magnitude more sensitive than current microbial or chemical-based optogenetic strategies. Electrophysiological recordings from retinal explants and the LGN in rod opsin treated *rd*^{1}mice (driven by either promoter) revealed light-evoked responses (excitatory and inhibitory) at light intensities similar to melanopsin-driven responses, but with significantly shorter latencies and these could be induced by simple light pulses, luminance increases, and naturalistic movies. Mice with rod opsin expression driven by the ON-bipolar promoter displayed behavioural responses to increases in luminance, flicker, coarse spatial patterns, and elements of a natural movie at levels of contrast and illuminance typical of natural indoor environments.

Collectively, these data reveal that enhanced AAV-mediated ectopic expression of both human melanopsin and rod opsin can drive responses at moderate light intensities, but that rod opsin has superior response qualities. The inherent advantages in employing a human protein, the simplicity of this intervention, and the quality of vision restored, all suggest that rod opsin has the potential to restore vision in patients with advanced IRDs and that it should be evaluated in clinical trials.

Declaration

No portion of the work referred to in this dissertation has been submitted in support of an application for another degree or qualification of this or any other university or other institute of learning.

Copyright statement

i. The author of this thesis (including any appendices and/or schedules to this thesis) owns certain copyright or related rights in it (the "Copyright") and s/he has given The University of Manchester certain rights to use such Copyright, including for administrative purposes.

ii. Copies of this thesis, either in full or in extracts and whether in hard or electronic copy, may be made **only** in accordance with the Copyright, Designs and Patents Act 1988 (as amended) and regulations issued under it or, where appropriate, in accordance with licensing agreements which the University has from time to time. This page must form part of any such copies made.

iii. The ownership of certain Copyright, patents, designs, trade marks and other intellectual property (the "Intellectual Property") and any reproductions of copyright works in the thesis, for example graphs and tables ("Reproductions"), which may be described in this thesis, may not be owned by the author and may be owned by third parties. Such Intellectual Property and Reproductions cannot and must not be made available for use without the prior written permission of the owner(s) of the relevant Intellectual Property and/or Reproductions.

iv. Further information on the conditions under which disclosure, publication and commercialisation of this thesis, the Copyright and any Intellectual Property and/or Reproductions described in it may take place is available in the University IP Policy (see http://documents.manchester.ac.uk/DocuInfo.aspx?DocID=487), in any relevant Thesis restriction declarations deposited in the University Library, The University Library's regulations (see http://www.manchester.ac.uk/library/aboutus/regulations) and in The University's policy on presentation of Theses.

Acknowledgements

I should like to thank my supervisors Professor Paul Bishop and Professor Robert Lucas for their expert advice and support throughout this research, together with all the members of the Lucas lab for their invaluable advice and enthusiasm. I should also like to express my gratitude to Medical Research Council and the University of Manchester, as well as the Manchester Royal Eye Hospital for allowing me to balance my research and clinical activities. Finally I am extremely grateful to my family, especially my husband Kemal, and my children Riad and Emina, for their support and encouragement.

Rationale for alternative format

The research naturally lends itself to the presentation in the alternative format because this is how the body of research was conceived, developed and written up, i.e. as several separate but related pieces of original research for publication in scientific peer-reviewed journals. There is a natural progression in the body of research from the first paper (which develops an optimised system for intravitreal vector delivery for gene therapy and is presented in Chapter 3) to the second paper (which uses the optimised system to deliver human melanopsin as an optogenetic sensor to enhance sensitivity in advanced retinal degeneration and is presented in Chapter 4) to the third paper (which uses human rod opsin to reliably recover visual responses to spatial stimuli, flicker and natural scenes at the retinal, brain and behavioural levels in a model of advanced retinal degeneration). This last paper, presented in Chapter 5, has already been successfully peer-reviewed and has been published in the journal *Current Biology* (doi: 10.1016/j.cub.2015.07.029). The two other papers have been successfully reviewed by co-authors and are ready to be submitted towards publication in peer-reviewed journals.

Contributions to papers

Efficacy and safety of glycosidic enzymes for improved gene delivery to the retina following intravitreal injection

Authors: Jasmina Cehajic-Kapetanovic, Nina Milosavljevic, Robert A. Bedford, Robert J. Lucas, Paul N. Bishop

JCK, PNB and RJL designed the research; JCK performed intraocular injections, ERGs, pupillometry, and retinal histology. JCK performed all data processing and analysis. RAB assisted with pupillometry. NM performed ERG recordings at 12 months post treatment with assistance from RAB. JCK wrote and revised the manuscript with comments from all authors. PNB and RJL supervised research.

Enhancing visual responses in retinal degeneration with human melanopsin

Authors: Jasmina Cehajic-Kapetanovic, Annette E. Allen, Nina Milosavljevic, Timothy M. Brown, Paul N. Bishop, Robert J. Lucas.

JCK, AEA, TB, PNB and RJL designed the research; JCK performed intraocular injections, pupillometry, LGN recordings and retinal histology. JCK performed all data processing and analysis with assistance from AEA. NM assisted with pupillometry. JCK wrote and revised the manuscript with comments from all authors. PNB and RJL supervised research.

Restoration of vision with ectopic expression of human rod opsin

Authors: Jasmina Cehajic-Kapetanovic, Cyril Eleftheriou, Annette E. Allen, Nina Milosavljevic, Abigail Pienaar, Robert A. Bedford, Katherine E. Davis, Paul N. Bishop, and Robert J. Lucas.

JCK, AEA, CE, NM, KED, PNB, and RJL designed the research. JCK performed intraocular injections, retinal histology, LGN recordings and behavioural experiments. JCK and CE performed MEA recordings. AP performed behavioural experiments involving spatial stimuli with assistance from KED, RB and NM. JCK performed all data processing and analysis with assistance from AEA. NM assisted with histology. JCK, PNB and RJL wrote and revised the manuscript with input from all authors. PNB and RJL supervised the research.

Chapter 1: Introduction

1.1. The human eye and retina

The human eye is a complex sensory organ that has evolved to promote survival and excel in the processing of constantly changing natural visual scenes. This processing of visual information begins at the neurosensory retina, a highly specialised photoreceptive tissue that has the ability to detect light and convert it to neural signals that are then sent to the brain for visual perception. The highly sophisticated optics of the eye allow the light to pass through the cornea, crystalline lens and the vitreal cavity in order to focus an image on the neurosensory retina which lines the innermost layer at the back of the eye (Figure 1.1).

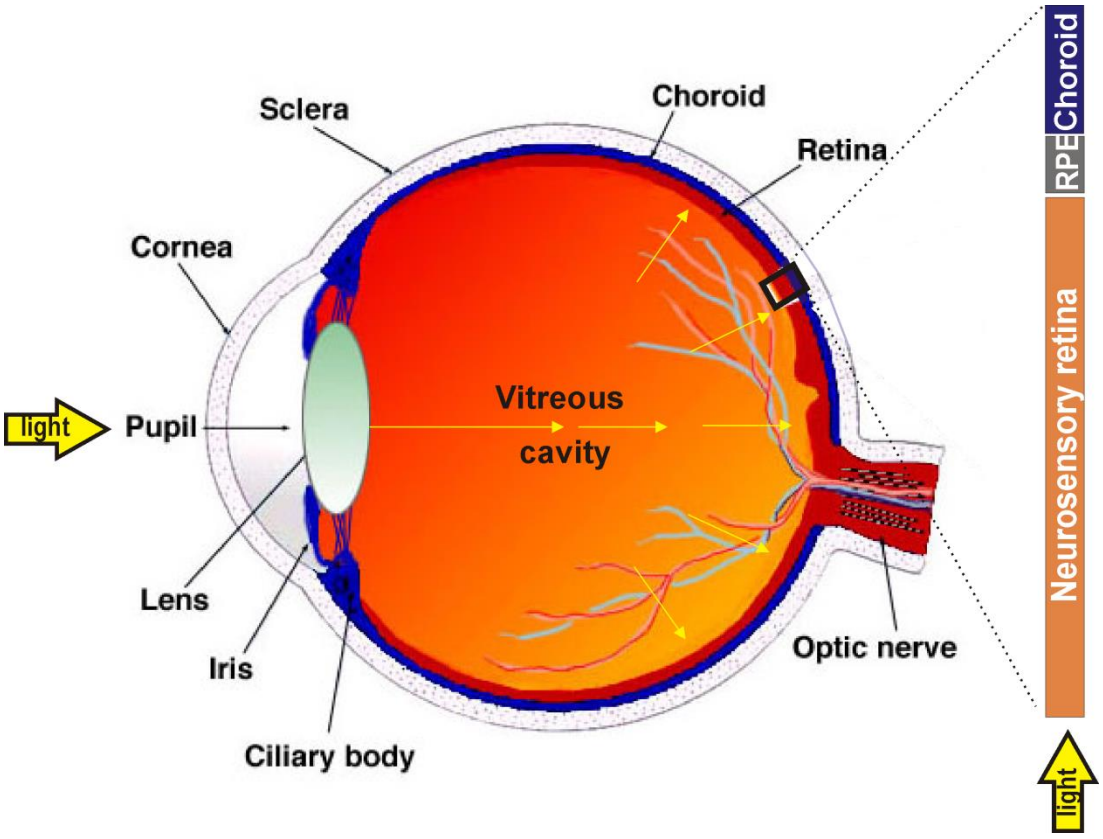

Figure 1.1. Schematic of the human eye. A transverse section through the human eye showing the different components ultimately designed to allow light passage through the front of the eye (the cornea and crystalline lens) and image detection at the back of the eye (the neurosensory retina). Adapted from webvision.med.utah.edu/simple-anatomy-of-the-retina.

The neurosensory retina has a highly ordered anatomy organised into distinct layers which contain a range of neuronal and glial cells (along with blood vessels) that are intricately connected, both vertically and laterally, and embedded in the extracellular matrix. Ultimately this allows for the detection, complex processing and propagation of the visual signal to the higher centres in the brain, which are able to extract relevant information into a coherent percept so that we can appreciate the order and beauty of our surroundings.

The image-forming vision begins at outer retinal photoreceptors, the rods and cones. These are highly specialised cells containing visual pigment that absorbs photons of light resulting in biochemical signalling and ultimately electrical impulses that are propagated to the downstream neurons of the retina. This signal propagation occurs through the so called primary vertical pathway, from photoreceptors to bipolar cells to retinal ganglion cells (RGCs), and is outputted via RGC axons and the optic nerve to the brain. The signal can however be modulated at various stages by the laterally positioned cells (amacrine and horizontal cells) to enable processing of more complex components of the visual scene and achieve both high sensitivity and high spatial acuity. Beneath the neurosensory retina lies the retinal pigment epithelium (RPE), a monolayer of non-dividing hexagonal cells predominantly involved in the transport of nutrients to and metabolic waste from the photoreceptors as well as the phagocytosis of photoreceptor outer segments. Figure 1.2 depicts the basic arrangement of these key retinal components and their connections.

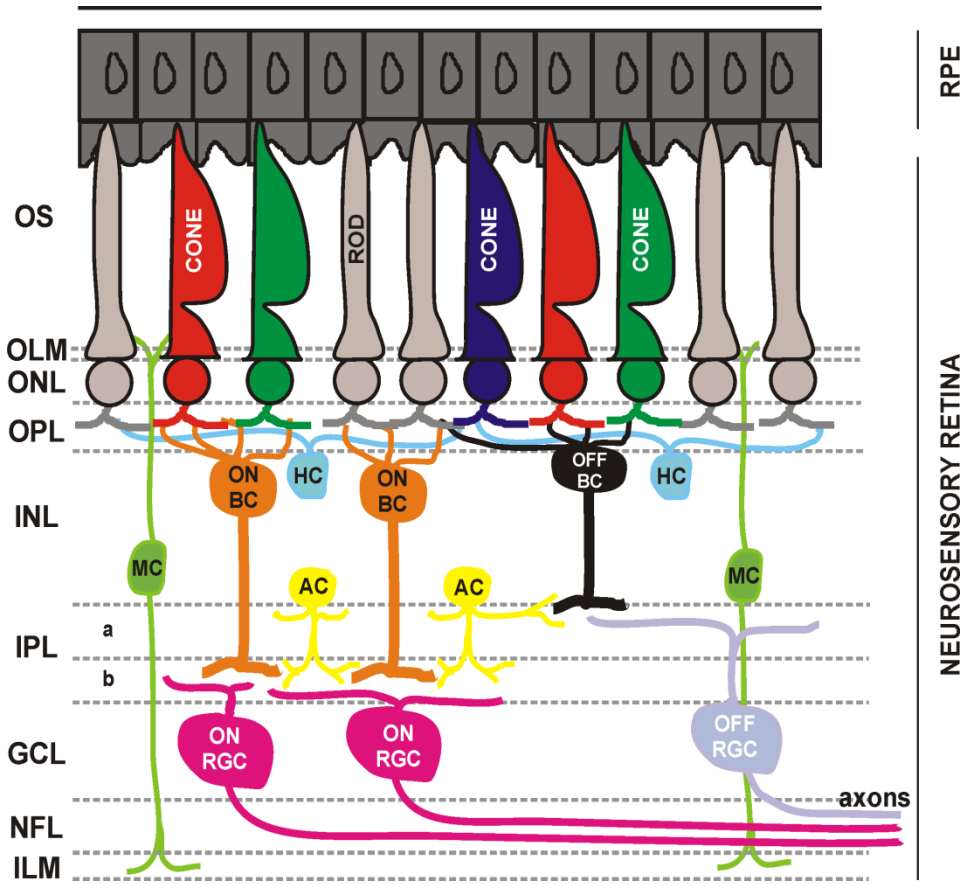

Figure 1.2. Schematic of the retina showing basic organisation of cells in the neurosensory retina and the retinal pigment epithelium (RPE). The neurosensory retina is divided into several distinct layers: outer photoreceptor segments (OS), outer limiting membrane (OLM), outer nuclear layer (ONL), outer plexiform layer (OPL), inner nuclear layer (INL), inner plexiform layer (IPL), ganglion cell layer (GLC), nerve fibre layer (NFL), and inner limiting membrane (ILM). Light must penetrate through the thickness of the retina (from the ILM side) to reach and activate the photosensitive cells (rods and cones) in the outer retina to initiate the visual process. The three nuclear layers contain neuronal cell bodies: the ONL contains rods and cones; the INL ON (ON BC) and OFF (OFF BC) bipolar cells, horizontal (HC) and amacrine interneurons (AC) and the GCL contains the retinal ganglion cells (RGCs). Photoreceptors are connected via bipolar cells to RGCs. ON and OFF pathways are separated downstream of rods and cones. Inhibitory HCs and ACs process signals in time and space. Neurons are connected in two plexiform layers: OPL (rods and cones synapse with bipolar cells) and IPL (bipolar cells synapse with RGCs and ACs; ON BC synapse with ON RGCs in sublamina b and OFF BCs synapse with OFF RGCs in sublamina a). RGC axons form the optic nerve and send information to the brain. Muller glia (MC) span the entire length of the retina.

1.1.1. Central versus peripheral retina

There are considerable differences in the thickness of the central (up to 350 μm) compared to the peripheral retina (~250 μm) in humans. This is due to the high packing density of the photoreceptors, especially cones and their associated bipolar and RGCs in the central retina compared to the peripheral retina (Figure 1.3).

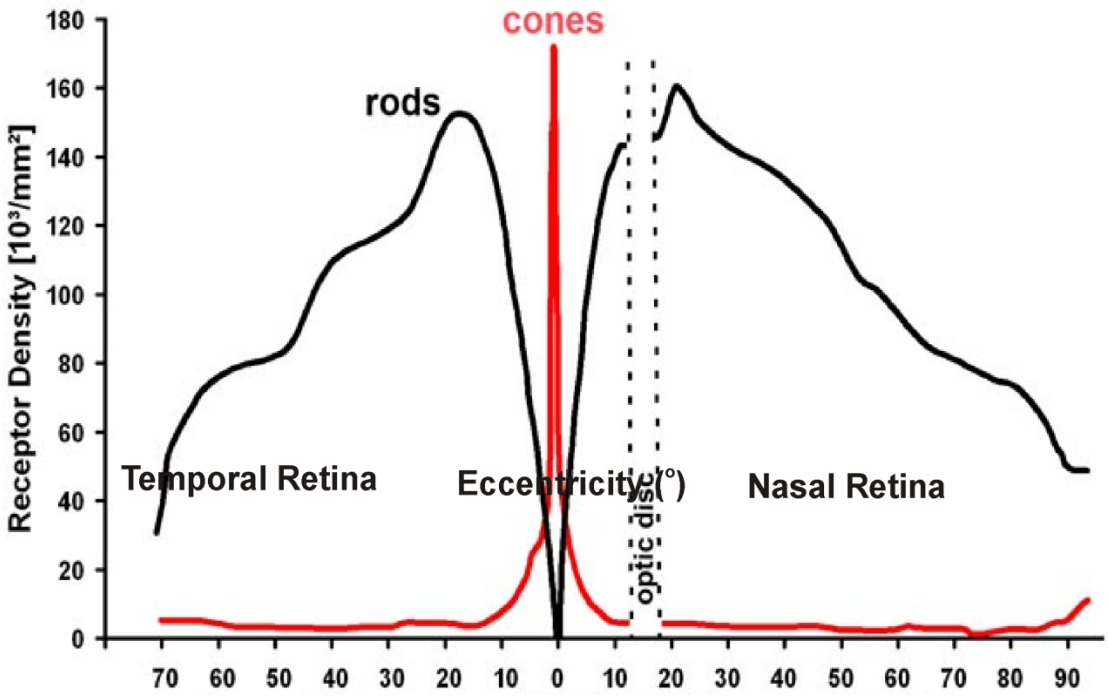

Figure 1.3. Density plot of rods and cones along the horizontal meridian of the human retina. Adapted from webvision.med.utah.edu/imageswv/ Ostergr.jpeg.

This central part of the human retina is called the *macula lutea* (yellow spot), commonly referred to as just the macula, and is responsible for the high acuity vision, unique to humans and higher primates. Histologically, macula is defined as having more than one layer of nuclei in the ganglion cell layer (Orth et al., 1977) and anatomically as the central portion of the retina with approximately 6mm in diameter located within the major vascular arcades (Handa, 2012) (Figure 1.4A). In humans, the central part of the macula is called the fovea, an area where cone photoreceptors are concentrated at maximum density, with exclusion of the rods, and arranged in a hexagonal mosaic at their most efficient packing density (Figure 1.4B). The peripheral

retina in contrast is dominated by the rods. However, in nocturnal species such as the mouse, photoreception is dominated by the rods which remarkably comprise around 97% of outer-retinal photoreceptors (Carter-Dawson and LaVail, 1979).

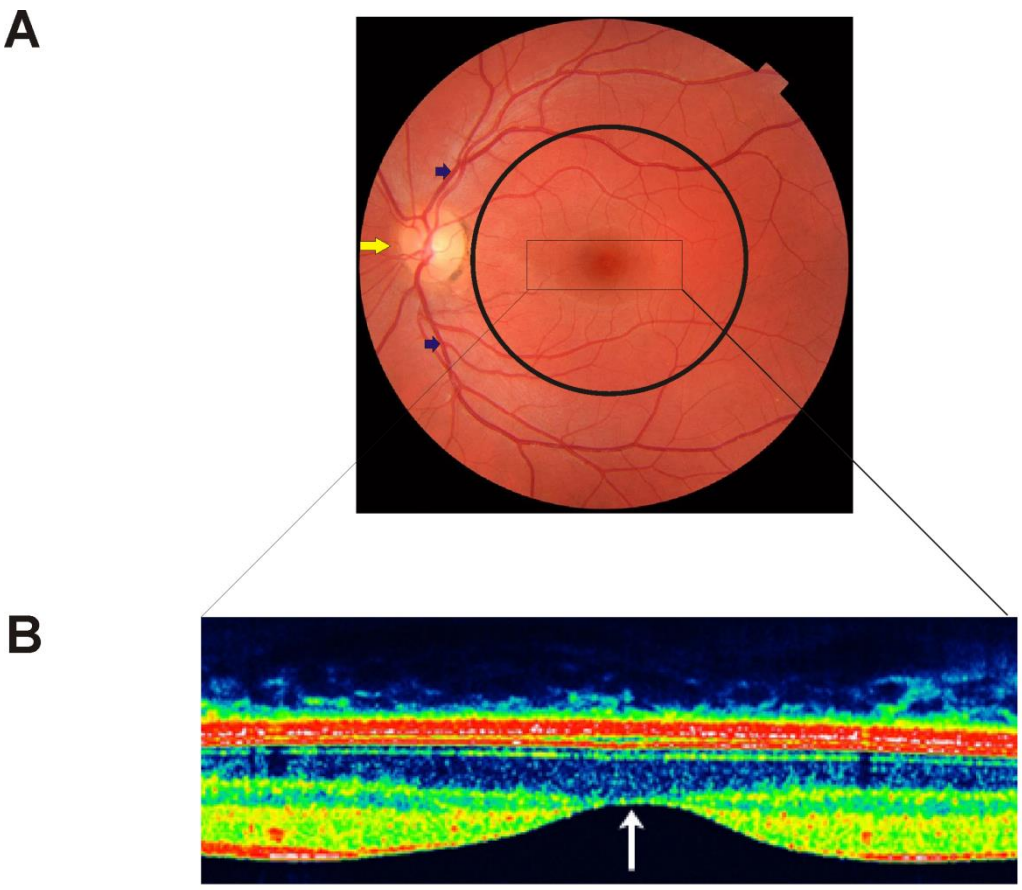

Figure 1.4. The anatomical macula. (A) Fundus photograph of the left human eye depicting the anatomical macula. The macula is shown by the black circle in the central portion of the retina located within the major vascular arcades (blue arrows). Beyond this is the peripheral retina stretching out to the ora serrata. The optic nerve is seen nasal to the macula (yellow arrow). (B) Optical coherence tomography image of the boxed area of the macula in A. Depicted are the foveal pit (white arrow) and the sloping foveal walls with dispelled inner retinal neurons (red and green) and densely packed photoreceptors (mainly cones, blue) above the foveal pit. Adapted from http://webvision.med.utah.edu/wp-content/uploads/2011/01/OCTmacula.jpg.

1.1.2. Rod and cone photoreceptors

There are two types of outer retinal photoreceptors: rods and cones (Figure 1.5A). They differ in their morphological, functional and molecular composition which ultimately enables the retina to respond to an astonishing range of visual stimuli. Due to their exceptional sensitivity (able to detect single photon of light; Hecht et al., 1942) rods are conditioned to operate in dark under low light intensities or 'scotopic' conditions and saturate at bright lights. This high sensitivity comes with reduced spatial acuity, as convergent rod pathways amplify the signal at the cost of high spatial precision. Cones, on the other hand function under bright 'photopic' conditions and although they are less sensitive than rods they are much better able to adapt their sensitivity to respond under a wide range of light intensities.

Structurally, the photoreceptor consists of an outer segment (stacks of bi-lipid membranes densely packed with the visual pigment), an inner segment (containing mitochondria, ribosomes and membranes for assembly of the visual pigment), a cell body (containing the nucleus) and a synaptic terminal (rod pedicles or cone spherules for contact with the bipolar cells in the outer plexiform layer) (Figure 1.5B). Morphologically, rods and cones can easily be distinguished on the basis of their outer segment shape. Cones are conical-shaped structures containing discs that are continuous with the plasma membrane, whereas rods are slim and rod-shaped with detached internalised discs. Apical processes of the retinal pigment epithelium envelop the cone and rod outer segments (Figure 1.2).

1.1.3. Rod and cone opsins

The photoreceptors can respond to light by virtue of their containing a visual pigment embedded in the outer segment discs. The visual pigment consists of a protein moiety called opsin and a chromophore which is a vitamin A derivative

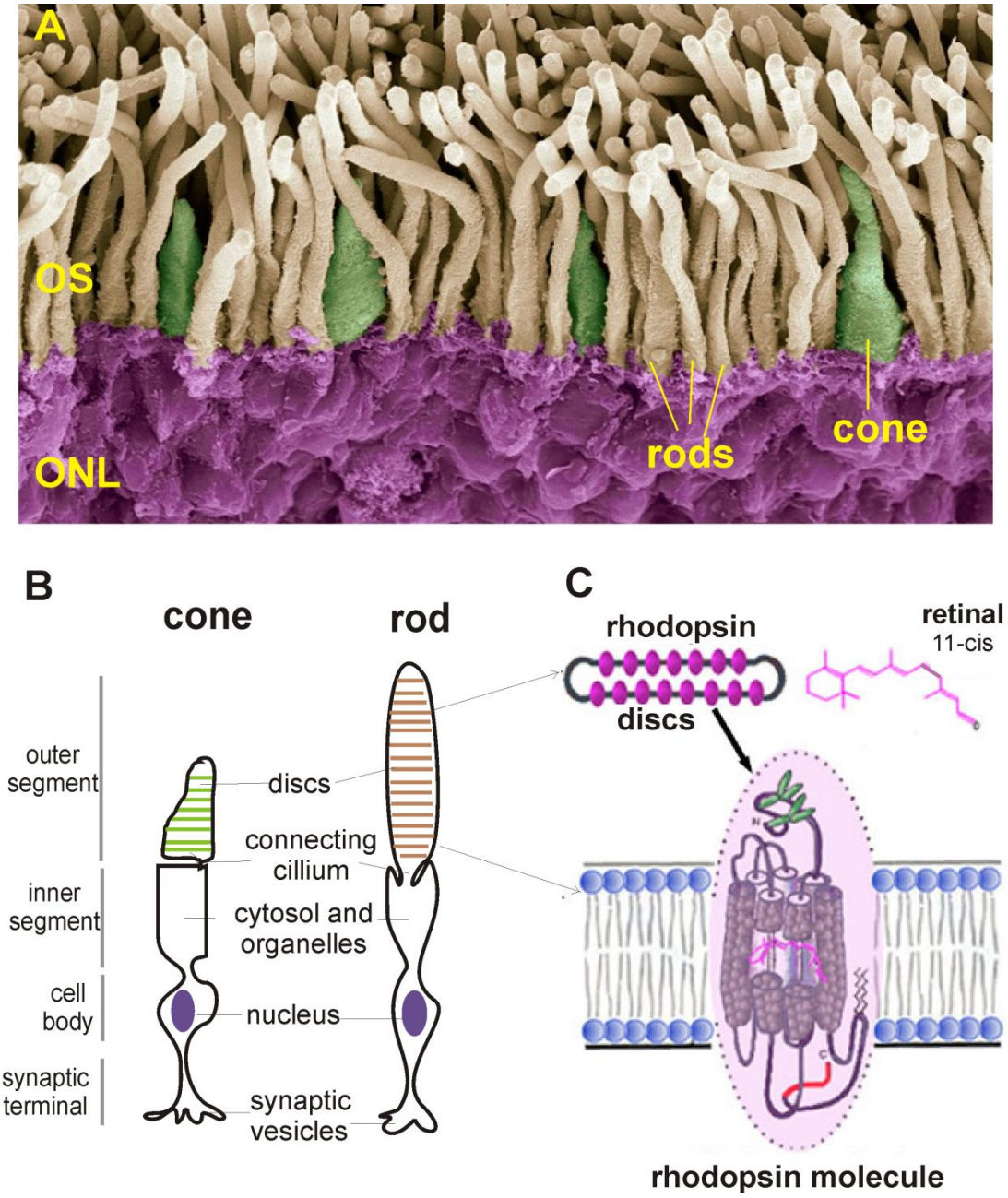

Figure 1.5. Rod and cone photoreceptors. (A) Scanning electron micrograph of the rods and cones in the retina of a human eye. Adapted from www.newscientist.com/article/dn28047-gene-therapy-cures-blindness-by-replacing-vision-cells-in-eyes; Steve Gschmeissner /SPL. (B) Structure of rod and cone photoreceptors. (C) Schematic diagram of the visual pigment: rhodopsin in the outer segment disc. Adapted from http://webvision.med.utah.edu/imageswv/rhodop1.jpeg.

called retinal. The opsin is organised into seven transmembrane domains within the lipid bilayer of the photoreceptor discs (Figure 1.5 C). Mammalian opsins are GTP-binding protein coupled receptors (GPCRs) and belong to a superfamily of naturally occurring and closely related light sensitive pigments which are capable of activating G-proteins. They can be characterised by a light absorption spectra and with opsin specific maximum sensitivity (λ_{max}). In humans, they include three cone opsins (long wavelength sensitive opsin, which absorbs yellowish-green light (λ_{max} of 560nm); middle wavelength sensitive opsin, which absorbs green light (λ_{max} of 530nm); and short wavelength sensitive opsin, which absorbs bluish-violet light (λ_{max} of 430nm) that enable colour discrimination (Merbs and Nathans, 1992) and a rod opsin (RHO) which absorbs red light (λ_{max} of 493nm; Bridges, 1959) and is predominantly used in night vision. Rod and cone opsins signal through the G-protein transducin that belong to a subfamily of G proteins called G_i proteins that signal through the cascade that leads to cell hyperpolarisation.

1.1.4. Phototransduction, signal amplification and deactivation

The outer retinal photoreceptor transduction cascade is summarised in Figure 1.6. This is a series of photo-chemical reactions whereby the light energy is converted into electrical impulses. In the dark a steady current, 'dark current' flows through open cation channels depolarising the photoreceptor cells which in turn release neurotransmitter glutamate. Upon light stimulation the retinal isomerizes from the 11-cis form to an active all-trans form. This causes a conformational change in rhodopsin in the photoreceptor disc membrane, converting rhodopsin into an active form, metarhodopsin II. This is known as photo-bleaching. The activated rhodopsin in turn activates the G-protein transducin, which exchanges guanosine diphosphate (GDP) for guanosine triphosphate (GTP). The activated transducin α-subunit then activates the cyclic guanosine monophosphate (cGMP)- phosphodiesterase (PDE). The activated PDE complex hydrolyses cGMP to 5' GMP closing the cGMP gated cation channels and stopping the dark current. This results in cell membrane hyperpolarisation and cessation of glutamate release. The reducing concentration of neurotransmitter is sensed by the downstream neurons which propagate the electrical impulse through the retina.

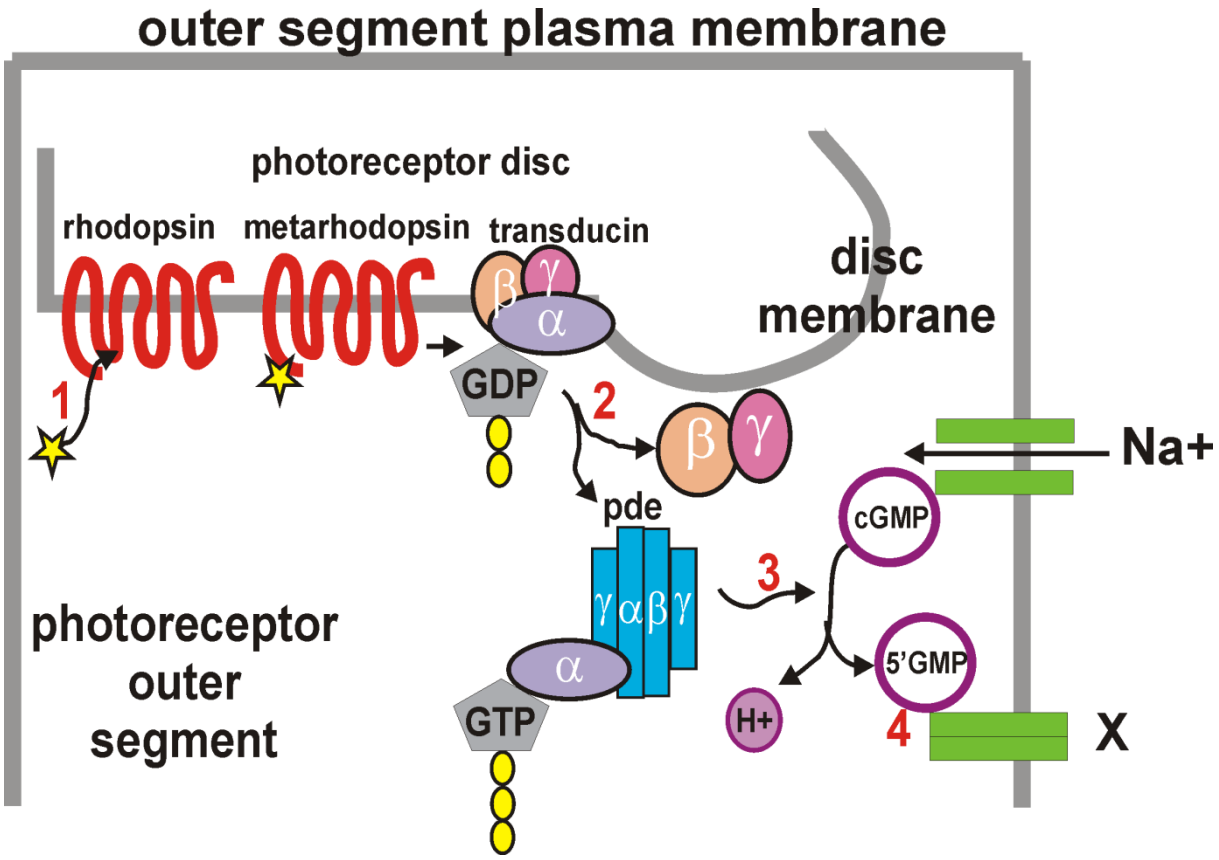

Figure 1.6. The phototransduction cascade. Photon of light transduces the visual pigment via a series of enzymatic reactions: 1. Photons are absorbed by rhodopsin. 2. Activated rhodopsin, metarhodopsin II, activates a GTP binding protein, transducin which exchanges GDP for GTP. The activated transducin α-subunit activates cGMP-phosphodiesterase (PDE). 3. The activated PDE complex GTP complex enzyme hydrolyzes the cGMP closing a membrane bound cGMP-gated cation channel. 4. The resultant reduction in cation influx hyperpolarises the photoreceptor cell resulting in reduction of glutamate release and activation of second order neurons. Adapted from Hargrave and McDowell, 1992).

A significant outcome of phototransduction is the signal amplification which occurs at various points in the cascade. Indeed, the activation of a single rhodopsin molecule in turn activates several hundred transducin molecules. This makes the mammalian photoreceptive system extremely light sensitive to the point of response activation by a single photon of light (Hecht et al., 1942).

The deactivation of phototransduction cascade is greatly accelerated by rhodopsin kinase which phosphorylates metarhodopsin II (Chen et al., 1999) and thereby

allowing subsequent binding of arrestin (Xu et al., 1997), to completely deactivate the opsin. In addition, the activated transducin is deactivated by intrinsic GTPase activity, which replaces the bound GTP with GDP. The deactivated transducin in turn deactivates PDE. Ultimately, cGMP is re-synthesised by guanylate cyclase intermediates causing the re-opening of cGMP-gated cation channels and depolarisation of the photoreceptor membrane.

1.1.5. The visual cycle

The regeneration of the chromophore after photo-bleaching via the retinal pigment epithelium is termed, the visual cycle. The deactivation of metarhodopsin II leads to the dissociation of the opsin to its constitutive parts: an opsin and all-trans retinal which must then be converted back to 11-cis retinal (see Wang and Kefalov, 2011 for review). At first, all-trans retinal is converted to all-trans retinol within the photoreceptor cell. All-trans retinol is then transported to the retinal pigment epithelium (RPE) activating a complex biochemical cascade that utilises the isomerase RPE65 to ultimately convert it back to 11-cis retinal. 11-cis retinal is transported back to the photoreceptor to reform a functional photopigment.

1.1.6. Light adaptation

In order to cope with large changes in ambient levels of light, photoreceptor cell must not simply detect light, but it also has to adapt to different levels of background light intensity (Pugh et al., 1999). For example cone photoreceptors are able to adapt their level of sensitivity in the presence of steady background light, maintaining the ability to detect relative changes in light intensity or contrast. This allows us to see clear images in dusk or in bright sunlight snow, a span of light intensity of 7-9 log units. Rods are less sensitive than cones and are capable of adaptation over a range of 2 log units of background light intensity. However, combined with a network adaptation in rod driven vision this becomes close to 5 log units of background intensity adaptation (Yau, 1994).

1.1.7. Visual processing downstream of rods and cones

The most direct pathway from photoreceptors to the retinal output cells, the RGCs is via retinal bipolar cells. These crucial second order neurons are not only responsible for the propagation of visual information, but are an invaluable source of signal transformation and diversification necessary to cope with everyday visual challenges. Dowling and Werblin (Dowling and Werblin, 1969) were among the first to describe the signalling in bipolar cells through non-spiking membrane currents and the dissection of visual information into ON and OFF pathways through ON (depolarise to light) and OFF (hyperpolarise to light) bipolar cells respectively, downstream of photoreceptors. However, ON-OFF responses (excitation at both light onset and offset) first occur among amacrine cell interneurons which are postsynaptic to bipolar cells. ON and OFF pathways are functionally segregated and capable of independent image processing, have centre-surround organisation and each split into both transient and sustained response-types postsynaptic to bipolar cells.

Each type of ON and OFF bipolar cell can be distinguished on the basis of their morphology, light response and different type of glutamate receptor they express. Modern anatomical and physiological studies indicate that the number of different bipolar cell subtypes is about 12 (11 cone and 1 rod bipolar cell) each responsible for a distinct channel of visual information carried to the brain. A comprehensive classification of the bipolar cells in the mammalian retina is shown on Figure 1.7 (Breuninger et al., 2011). The anatomic diversity comes from differing pre and postsynaptic connectivity and dendritic and axonal stratification patterns as well as differential expression of glutamate receptor subtypes. Some retinal bipolar cells are postsynaptic only to cones, some only to one type of chromatic classes of cones (red, green or blue), some only to rods, whilst others have a non-selective mixed cone-rod input.

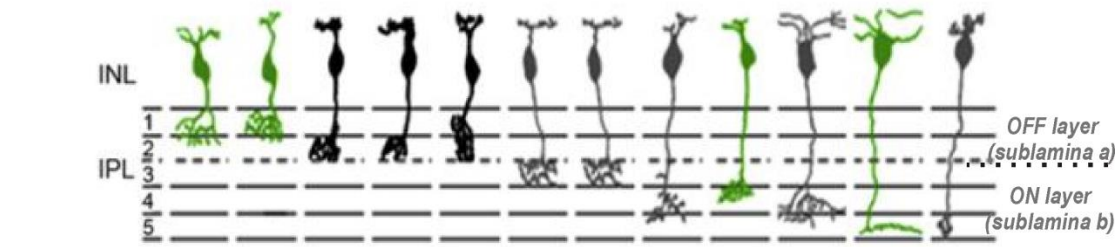

types	1	2	3a	3b	4	5a	5b	6	7	8	9	RBC
markers												
Syt2		++						(+)				
NK3R	++	++										
HCN4			++									
PKARIIβ				++								
Csen					++							
lines												
MitoP	++				(+)							
CLM12		++										
GUS									++			(+)
CLM1	(+)								(+)	(+)	++	
cone contacts	(M)	(S,M)	S,M	(S,M)	S,M				S,M		S	
functional channel	green OFF	non-selective							non-selective		blue ON	
	OFF					ON						

Figure 1.7. The diversity of mammalian retinal bipolar cells. Schematic drawing showing the anatomical classification of mouse bipolar cells based on the different stratifications within the inner plexiform layer (IPL) including types 1,2,3a,3b,4,5a,5b,6,7,8,9 and rod bipolar cell, RBC. INL- inner nuclear layer. The molecular diversity of cells is shown in the table below listing selective immunocytochemical markers; four transgenic mouse lines expressing fluorescent proteins in different subpopulations of bipolar cells; connectivity with the two cone types (S, short wavelength (blue) and M, medium wavelength (green) sensitive cones) and the resulting functional pathways determined by electrophysiological (single-cell patch clamping) light-evoked responses. Mice, like most mammals, feature dichromatic colour vision based on S and M cones provided by antagonistically organized separate chromatic bipolar cell channels (type 1 bipolar cells representing the green OFF pathway, and type 9 bipolar cells displaying blue-ON responses). Brackets indicate weak labelling (under markers and mouse lines) or data statistically not quantified (under cone contacts). For details on individual mouse lines and immunohistological markers please refer to Breuninger et al., 2011. Adapted from Breuninger et al., 2011.

Classically, rods signal through one dedicated rod ON bipolar cell only, whereas cones signal through both ON and OFF bipolar cells, and this ON and OFF signal segregation is maintained on reaching ON and OFF RGCs. ON bipolar cells have their axon terminals in the inner part of the IPL (ON or type b sublamina) where they contact ON RGCs and the OFF bipolar cells have their terminals in the outer part of the IPL (OFF or type a sublamina) where they synapse with OFF RGCs (Famiglietti et al., 1977). In addition, bipolar cells are rendered ON and OFF on the basis of their expression pattern of two classes of glutamate receptor, ionotropic (couple directly to ion channels; including N-methyl-D-aspartate acid, NMDA; kainite; and α-amino-3-hydroxy-5-methylisoxazole-4-propionic acid, AMPA receptors) and metabotropic receptor (mGluR, coupled to G-proteins, which act through intracellular second messengers). AMPA and kainate glutamate receptors are expressed in OFF bipolar cells. These cation channels are opened by glutamate and like photoreceptors hyperpolarise in response to light, in a sign-conserving fashion. By contrast, ON bipolar cells express a metabotropic mGluR6 receptor, which lead to closure of the cation channel TRPM1 (transient receptor potential cation channel subfamily M member 1) in response to glutamate release. Therefore upon light hyperpolarisation of photoreceptors and reduction of glutamate release, TRPM1 channels open and the bipolar cell depolarises in a sign-inverting fashion. (Morgans et al., 2009) (Figure 1.8.).

Activation of ON and OFF bipolar cells release glutamate which drives RGC depolarisation via ionotropic glutamate receptors on RGCs (Lin et al., 2002) which in turn fire action potentials (Diamond and Copenhagen, 1995). The parallel information streams created by bipolar cells (and further modulated by predominantly inhibitory amacrine cell inputs via GABA and glycine neurotransmitters) are connected to specific types of RGCs which roughly transmit 20 different encoding of the visual world to the brain by means of different firing patterns of action potentials.

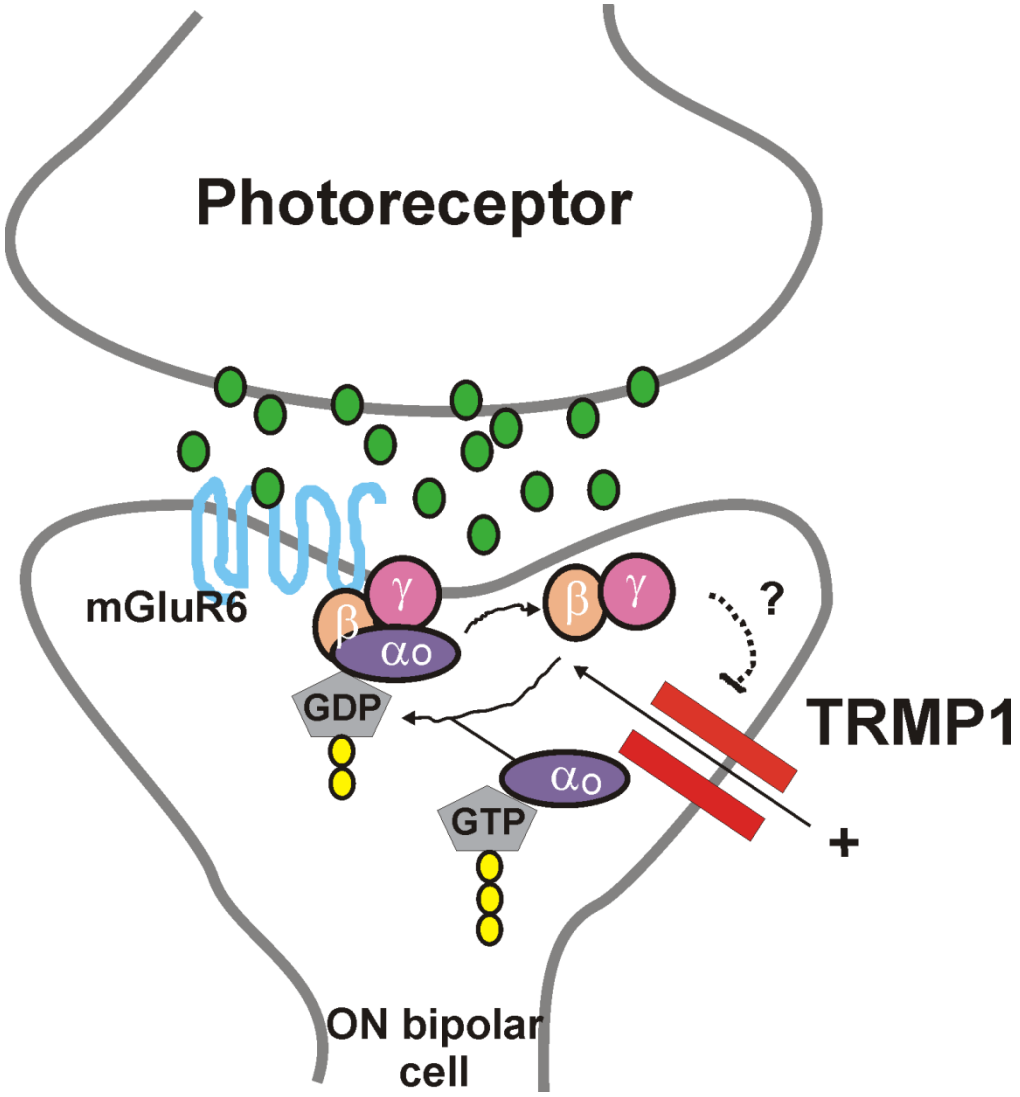

Figure 1.8. A schematic representation of signal transmission at the first visual synapse: rod to ON bipolar cell. Reducing concentrations of glutamate post light stimulated hyperpolarisation of rods are detected by the ON bipolar cells via metabotropic mGluR6 receptor. A series of poorly understood G-protein led secondary cascades ultimately leads to the opening of TRMP1 channels and depolarisation of the bipolar cell. Adapted from www.scripps.edu; image by Kiryll Matremyanov.

1.1.8. Laterally positioned retinal cells

The primary vertical visual pathway of the retina uses excitatory glutamate as its neurotransmitter to propagate visual information from photoreceptors to RGCs. These signals can be modulated by laterally positioned cells: horizontal and amacrine cells (Figure 1.2). These interneurons typically use inhibitory neurotransmitters, GABA and glycine, to regulate information flow through the retina.

Horizontal cells are the interneurons of distal vertebrate retina, with cell bodies in the distal INL. They make connections with the photoreceptors in the IPL laterally and through negative feedback signalling hyperpolarise both local and long-range photoreceptors (Haverkamp et al., 2001). These lateral signalling networks adjust the gain of photoreceptor synaptic output (lateral inhibition) to generate spatial and colour opponency. They form the antagonistic receptive field structure of bipolar cell (and downstream RGCs) by inhibiting input from distal/surround photoreceptors (centre-surround inhibition) in order to facilitate contrast sensitivity and edge detection (Dacey et al., 2000).

Amacrine cells are the interneurons of the proximal retina, with cell bodies in the proximal INL. They modulate synaptic transfer from bipolar cells to RGCs in the IPL in order to interpose a temporal domain to the visual message presented to the RGCs. There are over 30 different types based on neurochemistry and morphology (MacNeil and Masland, 1998). The two main types utilize inhibitory neurotransmitters, glycine and gamma-aminobutryic acid (GABA). Glycinergic amacrine cells, such as AII cell, have important roles in modulating ON and OFF signals (Roska et al., 2006). They receive excitatory input from rod-bipolar cells, but output both excitatory (to cone ON-bipolar cells) and inhibitory (to cone OFF-bipolar cells) signals (Manookin et al., 2008). GABAergic amacrine cells are predominantly concerned with the fine-tuning of lateral inhibition and reduction of centre-surround organisation of bipolar and RGCs signals (Flores et al., 2001).

1.1.9. Glial cells of the retina

There are three main types of human retinal glial cells: Muller cells, astroglia and microglia. They form architectural support for neuronal cells and other components of the retinal tissue.

Muller cells are the principle glial cells of the retina that span all the layers and form the limits of retina at the OLM and ILM (Figure 1.2). The adherens junctions between Muller glia and photoreceptor cell inner segments form OLM, a barrier between the subretinal space and the neurosensory retina. Similarly, laterally connecting Muller cell feet and associated basement membrane constituents, form the ILM, a significant diffusion barrier between the vitreous and the neurosensory retina. Muller cells have multiple roles in regulating and maintaining retinal homeostasis, including removal of toxic waste products, all of which are vital to the health of retinal neurons (for a review see Reichenbach et al., 1995; Biedermann et al., 1995). More recently they have been implicated in an alternative pathway mediating cone opsin regeneration cycle (Wang and Kefalov, 2009).

Astrocytes have cell bodies and processes almost entirely restricted to the NFL of the retina whereas microglia (of mesenchymal origin thus not strictly neuroglia) are ubiquitous cells of the retina, found in almost all retinal layers. Astrocytes envelope RGC axons and blood vessels of the NFL, forming part of the blood-brain barrier, and provide nutrients to the neurons. In addition they have been implicated in K+ homeostasis and metabolism of neurotransmitters (Kettenmann and Verkhratsky, 2011). Microglia can be stimulated into a macrophagic role in trauma and disease where they phagocytose degenerating retinal neurons and become involved in remodelling (Kettenmann and Verkhratsky, 2011).

1.1.10. Melanopsin and ipRGCs

Melanopsin is another photosensitive pigment that belongs to the GPCRs superfamily of opsins (Provencio et al., 1998, Provencio et al., 2000, Terekita, 2005). It is unusual in that it is expressed in vertebrates, but is most homologous to the rhabdomeric pigments found typically in invertebrates (Provencio et al., 1998, Provencio et al., 2000). In mammalian retinas it is normally found in a small subtype of RGCs called intrinsically photosensitive RGCs or ipRGCs (Berson et al., 2002, Hattar et al., 2002, Lucas et al., 2003). Within ipRGCs, melanopsin drives a phototransduction cascade distinguished by its prolonged time course. Thus, a single-photon response of ipRGC transduction integrates over eight seconds, ~100-fold longer than that of mamallian cones and 20-fold longer than that of mamallian rods (Henderson et al., 2000, Do et al., 2009). Melanopsin function in ipRGCs therefore, appears tailored to non-image forming vision and ipRGCs are known to drive pupillary light reflex and circadian rhythm (Lucas et al., 2003 and Panda et al., 2002). However, recent evidence suggests that melanopsin projections form up to 40% of image forming visual thalamus, the lateral geniculate nucleus (LGN) and implicates melanopsin in brightness detection (Brown et al., 2010) contrast signaling (Davis et al., 2015) and in modulation of cone-driven pathways (Allen et al., 2014).

Melanopsin absorbs light in the 'blue' part of the visual spectrum with (λ_{max} of 479nm, Lucas et al., 2001a) and unlike rod and cone opsins, melanopsin signals through a G_q protein cascade (Bailes and Lucas, 2013) and ultimately leads to cell depolarisation and an increase in intracellular Ca^{2+}. In addition, melanopsin demonstrates photopigment bistability in its role of photoregeneration or ability to regenerate chromophore through absorption of an additional photon, rather than through external enzymatic system common to rod and cone opsins. Thus, in heterologous systems, melanopsin can induce cell photosensitivity in the presence of all-*trans* and 11-*cis* retinal (Melyan et al., 2005; Panda et al., 2005; see review by Schmidt et al., 2011). More recently, photoequilibration of melanopsin across three states, two silent and one signaling (melanopsin tristability) has been proposed for sustained and broadband phototransduction (Emanuel and Do, 2015).

The central melanopsin-driven responses are typically sluggish and sustained, peaking only after a few seconds, and elicited at corneal irradiance of $\sim 10^{12}$ photons/cm^2/s, approximately 3 log units less than cone driven responses (Berson 2002, Brown et al., 2010). The relatively low sensitivity of ipRGCs compared to rod and cone photoreceptors is due to poor photon catchment (Do et al., 2009) as a result of significantly lower density of melanopsin molecules compared to rod and cones opsins in outer segment discs (rather than insufficient phototransduction signaling). Remarkably still a single photon can evoke response in ipRGCs due to their near-threshold resting potential.

1.2. Inherited retinal degenerations

Inherited retinal degenerations (IRDs) are a group of genetically and phenotypically heterogeneous conditions that affect the function and viability of photoreceptor cells that eventually leads to severe visual impairment as the retina becomes incapable of detection and/or transmission of light-triggered signals to the brain. IRDs affect approximately one in 2000 – 3000 individuals worldwide (Hartong et al., 2006) and in UK alone cumulative incidence by age 16 is 22/100000 children (Hamblion et al., 2012). In humans, IRDs display an exceptional heterogeneity in their mode of inheritance, underlying genetic defects, age of onset, and phenotypic severity. Currently there is no cure, but recent developments in experimental treatment strategies, including clinical trials, offer some hope for the patients suffering from these debilitating conditions.

1.2.1. Genetics and clinical features of IRDs

IRDs phenotype is a final common clinical pathway that arises from a number of insults that lead to photoreceptor degeneration. Genetic components determine the genesis and health of photoreceptors, and mutations cause structural and/or functional defects that eventually lead to visual loss. Currently there are over 1500 types of inherited diseases with retinal dysfunction (OMIM:

http://www.ncbi.nlm.nih.gov/omim/) associated with over 240 mapped genetic loci and over 200 identified causative genes (RetNet: https://sph.uth.edu/retnet/disease.htm). IRDs can be broadly divided into monogenic (Mendelian) or multifactorial (complex) disorders. Monogenic syndromic (involve multiple tissues in addition to the retina) and non-syndromic forms of retinal dystrophies with autosomal dominant, autosomal recessive, X-linked and mitochondrial inheritance pattern are observed. Some commonly presented phenotypic categories of IRDs are listed in Table 1.1. (for a more comprehensive list see Appendix 1 or RetNet: https://sph.uth.edu/retnet/disease.htm).

Phenotype (disease)	Cell type affected	Mode of inheritance	Genes
Non-syndromic monogenic			
CSNB	Rods more than cones (largely non-progressive)	Dominant	*GNAT1*, *PDE6B*, *RHO*
		Recessive	*GNAT1*, *CABP4*, *GRK1*, *SAG*
		X-linked	*CACNA1F*
LCA	Rods and cones	Dominant	*CRX*
		Recessive	*CRX*, *AIPL1*, *TULP1*, *CABP4*, *RPE65*, *CEP290*
RP	Rods more than cones and/or RPE (progressive)	Dominant	*CRX*, *NRL*, *NR2E3*, *PRPH2*, *RHO*, *ROM1*, *RPE65*
		Recessive	*ABCA4*, *MERTK*, *NRL*, *NR2E3*, *PDE6A*, *PDE6B*, *RHO*, *RPE65*, *SAG*, *TULP1*
		X-linked	*RPGR*, *RP2*
CD-CRD	Cones more than rods	Dominant	*AIPL1*, *CRX*, *PRPH2*
		Recessive	*ABCA4*, *CNGB3*, *RAB28*,
		X-linked	*CACNA1F*, *RPGR*
Macular degeneration	Rods and cones	Dominant	*PRPH2*, *ELOV4*
		Recessive	*ABCA4*
		X-linked	*RPGR*
Synaptic diseases	Rods and cones	Dominant	*UNC119*, *RIMS1*
		Recessive	*CACNA2D4*
		X-linked	*CACNA1F*, *XLRS*
Syndromic			
BBS	Rods and cones	Recessive	*BBS2*, *BBS4*, *BBS6*, *CEP290*
Joubert syndrome	Rods and cones	Recessive	*CEP290*
Senior-Loken syndrome	Rods and cones	Recessive	*CEP290*
Usher syndrome	Rods and cones	Recessive	*MYO7A*, *USH2A*

Table 1.1. A list of some human retinal diseases with monogenic inheritance. Mutations in some of the more commonly observed genes that are listed here (for a complete list see https://sph.uth.edu/retnet/; latest version also listed in Appendix 1) lead to several distinct phenotypic categories: CSNB - Congenital stationary night blindness; LCA – Leber congenital amaurosis; RP - retinitis pigmentosa; CD – cone dystrophy; CRD – cone-rod dystrophy; Macular degeneration; Synaptic diseases and other more complex phenotypes with extraocular involvement, such as BBS- Bardet-Biedl syndrome, Joubert syndrome, Senior-Loken syndrome and Usher syndrome. Adapted from Valeri et al., 2015.

Interestingly, mutations in the same gene (e.g. *Peripherin* can cause a range of clinical phenotypes (Coppieters et al., 2010), whereas similar phenotypes can be the end result of dysfunction in one of many different genes (RetNet). IRDs may affect the entire retina (e.g. retinitis pigmentosa) or be largely or exclusively limited to the macula (macular degeneration e.g. Stargardt disease). Most progressive generalised dystrophies can be classified into two main clinical phenotypes: those that affect the rods followed by the cones (rod-cone dystrophies or retinitis pigmentosa) and those that affect cones first followed by the rods (cone-rod dystrophies).

In early stages, the clinical phenotype generally reflects the primary cell type affected. Thus in retinitis pigmentosa night vision impairment often precedes the loss of visual acuity (rod followed by cone degeneration), whereas in cone-rod dystrophies the loss of visual acuity, impairment of colour vision and photosensitivity are frequently the initial symptoms. However, in advanced cases, distinguishing between these two forms of disease can be difficult. In addition, clinical phenotypes represent a wide spectrum, and the classification of IRDs is continuously being modified as we gain new insights into the genetic causes of the disease. Figure 1.9 illustrates genetic diversity of IRDs and lists selected proteins, mutations in which cause different phenotypes, according to their specific localisation in photoreceptors or RPE.

Important syndromic IRDs are ciliopathies. As the photoreceptor outer segment is modified primary cilia, mutations in genes affecting cilia function often lead to retinal degeneration in addition to dysfunction of cillia in other organs, such as the inner ear. Syndromic ciliopathies with IRDs include Usher syndrome (hearing loss), Bardet-Biedl syndrome (BBS), Joubert syndrome and Senior-Loken syndrome.

Macular degeneration is a specific form of IRDs that is limited to the central region of the human retina, the macula lutea. The most common monogenic MD is Stargardt disease (early age onset), whereas age-related macular degeneration (AMD) is a most common complex multifactorial disease with multiple genetic risk factors with late age onset (Fritsche at al., 2014). The following section focuses on some specific examples of IRDs (and their clinical phenotypes) with most potential for emerging therapies.

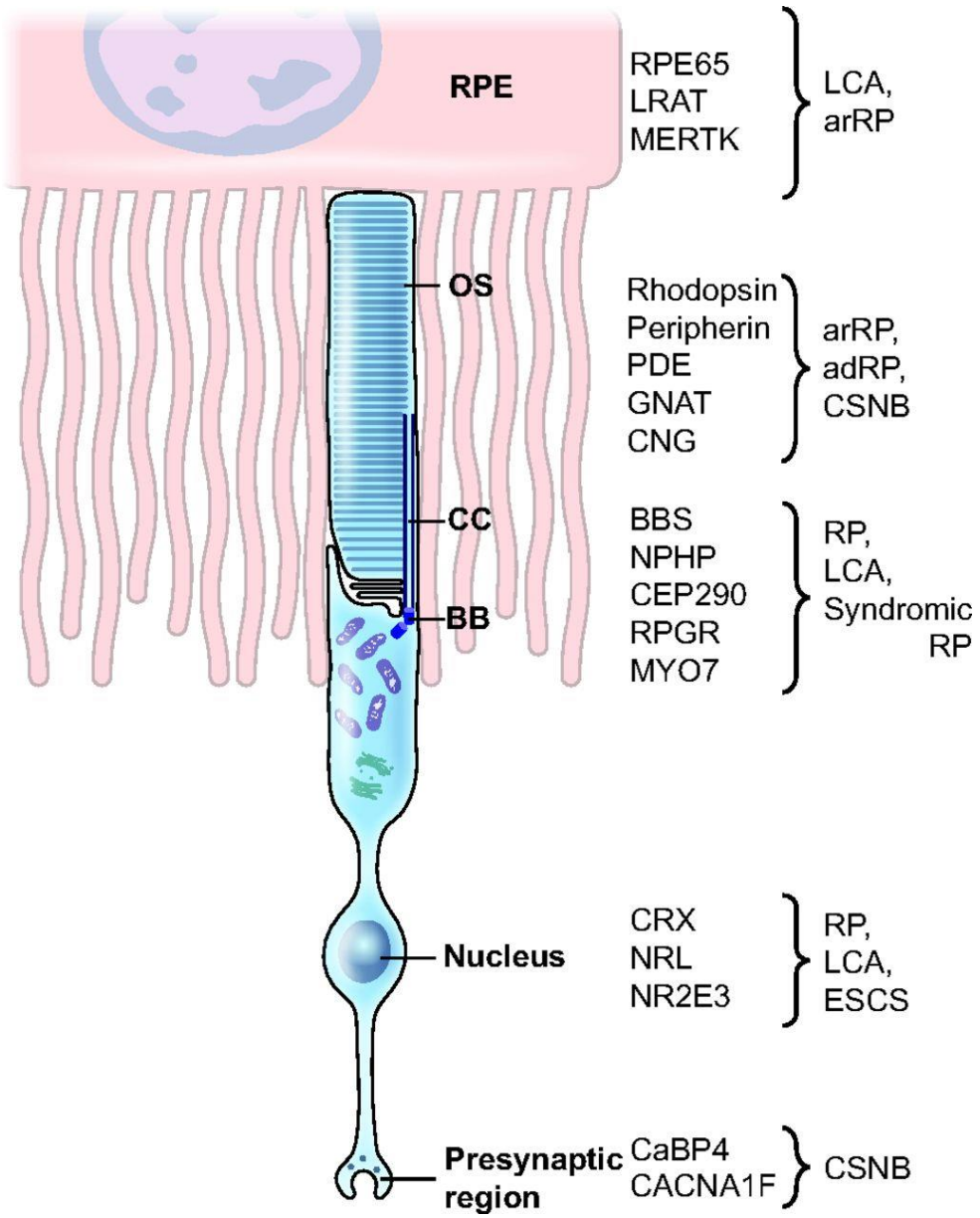

Figure 1.9. Genetic diversity of IRDs. Schematic diagram illustrating a broad classification of proteins associated with IRDs according to their localization or function in photoreceptors and retinal pigment epithelium (RPE). Therefore, RPE65, LRAT and MERTK, which are associated with LCA and arRP, are RPE proteins, whereas CRX, NRL and NR2E3 are photoreceptor-specific transcription factors. The other proteins that are listed localize to the outer segment (OS), connecting cilium (CC) and/or basal body (BB) of the photoreceptor (in this example a rod is represented). RP - retinitis pigmentosa. adRP - autosomal dominant retinitis pigmentosa; arRP - autosomal recessive retinitis pigmentosa; CSNB - congenital stationary night blindness; ESCS - enhanced S-cone syndrome; LCA - Leber congenital amaurosis. Adapted from Valeri et al., 2015.

1.2.1.1. Rod-cone dystrophy

Rod-cone dystrophies, better known as retinitis pigmentosa (RP) are a progressive bilateral degeneration of rod and cone photoreceptors. They can be further divided into non-syndromic or classical (~80% (Ayuso and Millan, 2010), affects eye only) and syndromic (~20%, affects other systems e.g. hearing in Usher's syndrome). In classical RP, there is a progressive loss of function in rods (typically within first two decades, Tsujikawa et al., 2008) followed by secondary degeneration of cones (many years later) in advanced stages. Since rods are responsible for night vision and predominate in the periphery, affected individuals first present with nyctalopia, an impaired dark adaptation and difficulties in seeing in dim lights. With disease advancement there is a progressive loss of peripheral vision with sparing of the central vision, the so-called 'tunnel vision' and majority of patients are registered legally blind by the age of 40 because of the severe loss of visual field. (Hartong et al., 2006). In late stages cones, responsible for high-acuity daylight vision, become affected leading to a progressive loss of central vision.

Clinical assessment of patients includes detailed history and examination as well as a gamut of diagnostic tests which may include psychophysical tests, electrodiagnostics (ERG), spectral domain optical coherence tomography (OCT) and adaptive optics (for a comprehensive review see Hartong et al., 2006). Slit-lamp biomicroscopy examination of the retina can reveal some typical features depending on the stage of the disease. At early stages, there is granularity of the RPE and pigmentary mottling, at mid stages there is patchy loss of RPE and vascular attenuation, and in advances stages there is arteriolar narrowing, optic nerve pallor and bony spicule pigmentation due to RPE intraretinal migration secondary to advanced retinal remodelling and photoreceptor apoptosis. In addition, macular pathology is not uncommon, including cystoid macular oedema (~40%, Adackapara et al., 2008) epimacular membrane and macular atrophy as well as cataract which can affect central vision. Scotopic flash ERG responses (both a and b wave; for details see Chapter 2 Methods) are attenuated in early disease and become negligible in advanced cases when pattern ERG can be used to better assess macular function. Typical features of fundus examination and adaptive optics image are shown in Figure 1.10.

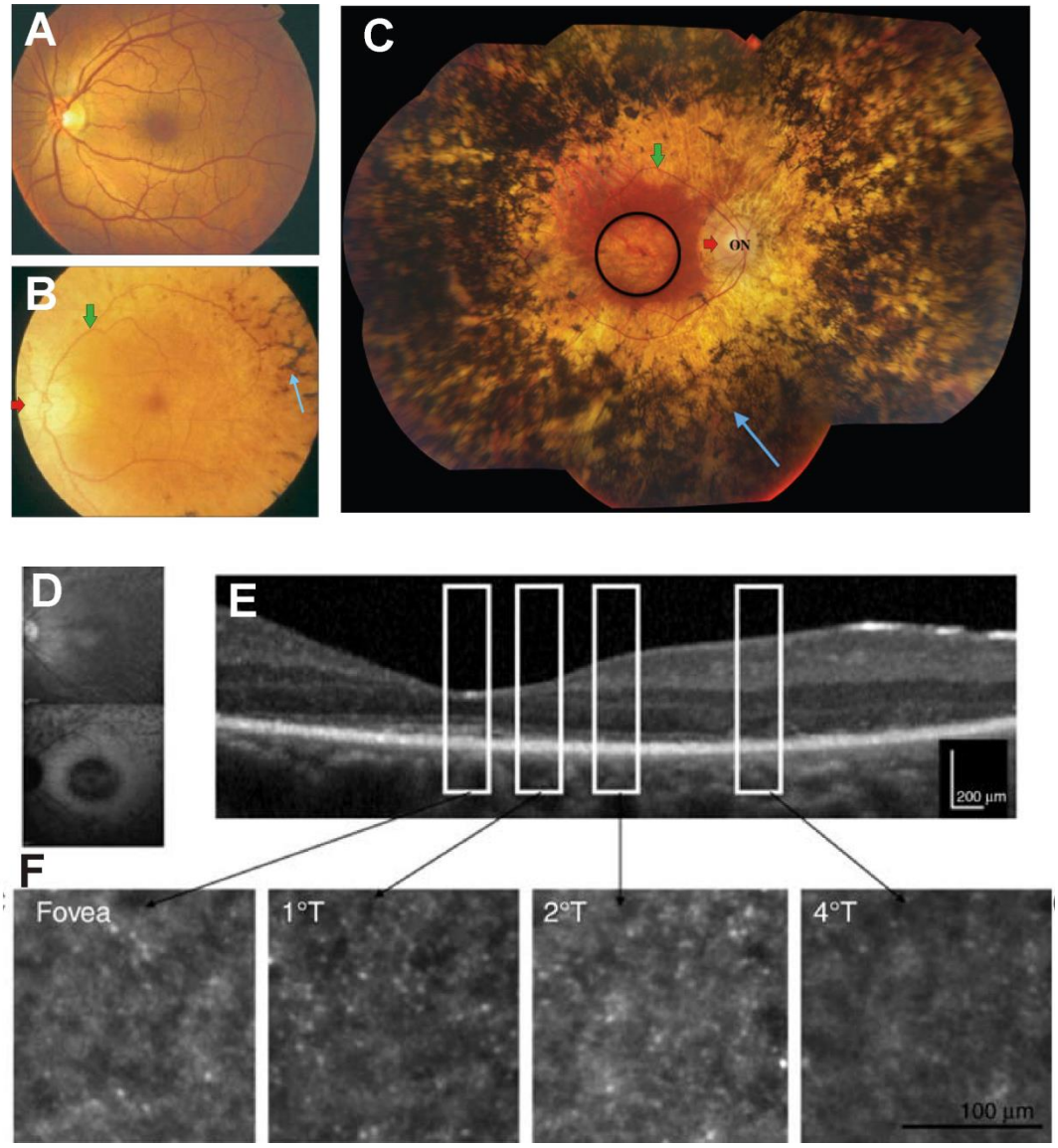

Figure 1.10. Retinal imaging. (A-C) Fundus photograph of a patient with normal retina (A) and of a patient with retinitis pigmentosa (B and C). There is waxy disc pallor (red arrow) arteriolar attenuation (green arrow) and bony spicules from invading retinal pigment epithelial (RPE) cells (blue arrow) dominating the retinal periphery. The widespread bony spicule pigmentation, extensive retinal thinning but relative macular preservation is seen in end-stages (C, adapted from Henriksen et al., 3). ON, optic nerve head; circle, macula. (D-F) Images from a patient with retinitis pigmentosa and peri-foveal macular atrophy: infrared and blue autofluorescence images showing peri-foveal loss of autofluorescence (D); spectral domain optical coherence tomography horizontal scan of the retina showing thinning of the outer retina with relatively preserved foveal lamination with inner segment photoreceptor preservation up to 2º (E); adaptive optics images show presence of cones around the fovea and almost no cones at 4º (F). Adapted from Sahel et al., 2014.

1.2.1.2. Syndromic retinitis pigmentosa

In syndromic RP, ocular RP is associated with other non-ocular disease affecting one or multiple other organs. They include Usher syndrome (RP associated with hearing impairment; Lopez and Williams 2015) and a number of other multisystemic ciliopathies (Novarino et al., 2011) such as Bardet-Biedl syndrome (Forsythe and Beales, 2012), Joubert syndrome (Romani et al., 2013) and Senior-Loken syndrome (Ronquillo et al., 2012) which share are number of overlapping clinical features such as renal cysts, renal and hepatic impairment, polydactlyly, obesity, cognitive impairment and hypogonadism with variable degrees of morbidity and mortality (Waters and Beales, 2011).

The most frequent syndromic RP form is Usher syndrome (combined blindness and deafness, Le Quesne Stabej et al., 2012). There are three major clinical types, Usher syndrome type I, II and III (Petit, 2001) Type I is the most severe form, characterized by congenital, bilateral, severe-to-profound, sensorineural hearing impairment and vestibular dysfunction and progressive vision loss caused by RP by the age of 10. Type II is associated with moderate to-severe hearing impairment from birth, RP onset after puberty and normal vestibular function and type III with variables onsets, progression and severity of vision, hearing and vestibular impairment.

1.2.1.3. Cone-rod dystrophies

Cone-rod dystrophies, CORDs (Michaelides et al., 2004) initially affect cone photoreceptors followed by dysfunction in rod photoreceptors. Early symptoms are thus related to the loss of cone function and include impairment in visual acuity, colour vision and photophobia (increased light sensitivity). This is followed by nyctalopia and loss of peripheral vision. A characteristic feature on retinal examination is the so-called bull's eye maculopathy, with prominent macular pigment deposits and atrophy. Peripheral signs including, bone spicule pigmentation, RPE atrophy, vascular attenuation and optic disc waxy pallor occur in the late stages of the degeneration. CORDs are usually non-syndromic, but have been associated with Bardet-Biedl syndrome or spinocerebellar ataxia type 7 (Michaelides et al., 2004a).

1.2.1.4. Leber congenital amaurosis (LCA)

Leber congenital amaurosis, LCA, is the severest of all retinal dystrophies, accounting for 5% of IRDs (den-Hollander et al., 2008). It can be of either rod-cone or cone-rod type. Affected individuals present in the first year of life with profound blindness, roving nystagmus, sluggish pupils and non-detectable ERG responses. They may also present with an oculo-digital reflex or neurodevelopmental delay. Rare associated ocular manifestations include strabismus, high hyperopia, high myopia, keratoconus/keratoglobus, cataracts, macular pseudocoloboma, pigmentary retinopathy and maculopathy, papilloedema, and retinal arteriolar attenuation. There are occasional systemic associations including ciliopathies.

1.2.1.5. Choroideraemia

Choroideraemia affects 1/50000 individuals with progressive degeneration of choroid, retina pigment epithelium (RPE) as well as the neurosensory retina (rod-cone dystrophy). It typically affects males with early-childhood nyctalopia, progressing to tunnel vision. Reasonable visual acuity can be maintained until 50 or 60 years of age. Phenotypical fundus examination shows large scalloped chorioretinal atrophy with bare sclera in the periphery spreading toward the macula and minimal or no pigment migration. In contrast with RP, there is no disc pallor (until very late stages) or vascular attenuation. ERGs of affected males typically show reduced scotopic responses (low a-wave amplitude). Optical coherence tomography shows thinning of the choroid and outer retina with evidence of retinal tabulation on the atrophic areas (Goldberg et al., 2013).

1.2.1.6. Achromatopsia

Achromatopsia or rod monochromatism affects 1 in 30 000 people (Michaelides et al., 2004a). This usually non-progressive infantile-onset dystrophy affects exclusively cones and is typified by severe impairment in visual acuity, inability to distinguish colours, photophobia, and nystagmus. There is phenotypic variability in terms of visual acuity and residual colour vision ("dysfunction syndrome", Michaelides et al.,

2004a). Fundus examination is generally unremarkable or with some foveal RPE changes. ERG recordings show characteristic normal rod and non-detectable cone responses.

1.2.1.7. Retinoschisis

X-linked retinoschisis accounts for almost all cases of hereditary retinoschisis and is the leading cause of macular dystrophy in young males (Bennett et al., 2016). X-linked retinoschisis is typified by a splitting of the inner layers of the neurosensory retina with characteristic foveal schisis causing visual loss. There is a characteristic "electronegative" response on ERG recordings, with relative loss of the positive, rod-driven b-wave and preservation of the negative a-wave. The age of onset is variable, with individuals presenting in infancy (squint) or at school age (reduced acuity) with variable but usually slow progression until age 40 with steady decline thereafter. Fundoscopy reveals peripheral degeneration in 50% of cases and vitreous haemorrhage and retinal detachment can occur.

1.2.1.8. Stargardt disease

This is the most common macular degenerative disease in individuals under age 50 (Aurrichio et al., 2015). There is juvenile-onset, progressive bilateral macular atrophy with subretinal lipofuscin deposits associated with defects in central vision and reduced acuity and variable colour vision defects (red-green). A phenotypic variant, Fundus Flavimaculatus, is usually diagnosed later with more favourable visual prognosis. Fundus autofluorescence shows typically a loss of foveal autofluorescence, macular patchiness, and peri-papillary sparing. Three functional groups have been described on the basis of ERG: group I, restricted macular dysfunction (pattern ERG) and normal scotopic and photopic flash ERG; group II, generalised cone dysfunction with abnormal photopic and normal scotopic responses and group III, cone and rod dysfunction with abnormalities in both scotopic and photopic flash ERG responses (Lois et al., 2001). Groups II and III show defects in central vison as well as peripheral vision and have overlapping characteristics with earlier described cone-rod dystrophies (linked to ABCA4 mutation).

1.2.1.9. Congenital stationary night blindness

Congenital stationary night blindness (CSNB) is a non-progressive form of IRDs characterized by lifelong night blindness. The most common type is Schubert-Bornschein type with diagnostic flash ERG pattern (reduced scotopic b/a wave ratio). There are two forms, complete and incomplete. The complete form is characterized by severe nyctalopia, nystagmus, high myopia and strabismus, reduced visual acuity. ERG typically shows predominantly decreased b-wave and cone-specific waveform abnormalities. The incomplete form has a more variable clinical picture, and usually presents with photophobia. In addition there may be nystagmus, strabismus, and reduced acuity. ERG shows reduced scotopic b-wave and greatly reduced cone responses.

1.2.2. IRDs and therapeutic strategies

Although rare in the general population, IRDs occupy a central position in global research efforts to develop innovative therapies for blinding diseases. Their complex genetic and phenotypic landscape represents a significant challenge for developing approved therapies. This requires multiple considerations including genetic nature of the disease, mutation prevalence, disease severity, age of onset as well as the type of the intervention (gene, cell or pharmacological) and the potential for clinically quantifiable outcome measures. In addition, treatment options will likely differ for early versus advanced disease. Broadly, for early to mid-stage disease therapies will focus on rescuing retinal cell function and maximising cell survival using pharmaceuticals and gene replacement therapy. For late stage disease, therapies are more likely to be based on optogenetics, cell transplantation, and electronic prosthesis as well as combinatorial therapies involving neuroprotection and optimisation of the host environment for specific interventions. Table 1.2. summarises several IRD phenotypes with their most appropriate therapy/therapies including current clinical trials. Table 1.3. summarises anticipated clinical trials for IRDs.

IRD (gene)	Therapy	Clinical Trials	Location	Key References
LCA2 (*RPE65*)	rAAV2-CBSB-hRPE65	NCT00481546	University of Pennsylvania University of Florida Health Shands Hospital	Bainbridge et al., 2008 Maguire et al., 2008 Cideciyan et al., 2008 Hauswirth et al., 2008
	AAV2-hRPE65v2	NCT00516477	Children's Hospital of Philadelphia, University of Iowa	Simonelli et al., 2010 Cideciyan et al., 2013
	AAV2-hRPE65v2	NCT00999609		
	AAV2-hRPE65v2	NCT01208389		
	rAAV 2/2.hRPE65p.hRPE65	NCT00643747	Moorfields Eye Hospital	
	rAAV2-CB-hRPE65	NCT00749957	Oregon Health and Science University University of Massachusetts-Worcester	
	rAAV2-hRPE65	NCT00821340	Haddasah Medical Organization	
	rAAV2/4.hRPE65	NCT01496040	Nantes Hospital	
RP38 (*MERTK*)	rAAV2-VMD2-hMERTK	NCT01482195	King Khaled Eye Specialist Hospital	Deng et al., 2012 Conlon et al., 2013
Choroideremia (*CHM*)	rAAV2.REP1	NCT01461213 NCT02077361	Moorfields Eye Hospital University of Alberta	Vasireddy et al., 2013 MacLaren et al., 2014
LHON (*ND4*)	rAAV2-ND4	NCT01267422	Tongji Hospital, Huazhong University of Science and Technology	Marella et al., 2010 Yu et al., 2012
	rAAV2/2-ND4 – GS010	NCT02064569	Centre Hospitalier Nationale d'Ophthalmologie des Quinze-Vingts	Chadderton et al., 2013
	scAAV2-P1ND4v2	NCT02161380	Bascom-Palmer Eye Institute	Lam et al., 2014
Stargardt Disease (*ABCA4*)	StarGen (EIAV-ABCA4)	NCT01367444	Oregon Health and Science University	Kong et al., 2008 Binley et al., 2013
		NCT01736592	Centre Hospitalier Nationale d'Ophthalmologie des Quinze-Vingts	
Usher1B (*MYO7A*)	UshStat (EIAV-MYO7A)	NCT01505062	Oregon Health and Science University	Hashimoto et al., 2007 Zallocchi et al., 2014
		NCT02065011	Centre Hospitalier Nationale d'Ophthalmologie des Quinze-Vingts	
Advanced RP	Argus II retinal implant	NCT00407602	Widely in Europe and USA	Zrenner et al., 2011; Humayun et al., 2012
	Retina Implant AG	NCT00515814 NCT01497379	Dresden and Tubigan, Germany University of Hong- Kong	Stingle et al., 2015
AMD	RPE-cell	NCT02563782	Wills Eye Institute Philadelphia	

	transplantation	NCT02463344 NCT01691261 NCT01344993	Widely in USA Moorfields Eye Hospital Widely in USA	Schwartz et al., 2015
Stargardt Disease	RPE-cell transplantation	NCT01345006 NCT01469832	Widely in USA	Schwartz et al., 2015

Table 1.2. Registered clinical trials of gene therapy for IRDs (ClinicalTrials.gov).

IRD (gene)	Therapy	Key references
X-linked retinoschisis (*RS1*)	AAV-RS1	Zeng et al., 2004 Min et al., 2005 Byrne et al., 2014
X-linked RP (*RPGR*)	AAV-RPGR-ORF15	Hong et al., 2005 Beltran et al., 2012
Achromatopsia (*CNGA3*) Achromatopsia (*CNGB3*)	AAV-CNGA3 AAV-CNGB3	Michalakis et al., 2010 Pang et al., 2012 Komaromy et al., 2010 Carvalho et al. 2011
Aautosomal recessive RP (*PDE6B*)	AAV-PDE6B	Petit et al., 2012
Autosomal dominant RP (*RHO*)	AAV-RHO RNA suppression and replacement constructs	O'Reilly et al., 2007 Millington-Ward et al., 2011 Mao et al., 2012
Advanced RP	Optogenetics targeting cone photoreceptor cells: AAV-eNpHR (halorhodopsin)	Busskamp et al., 2010
Advanced RP	Optogenetics targeting rod photoreceptor cells: AAV-RHO (rod opsin)	Gaub et al., 2015 Cehajic-Kapetanovic et al., 2015

Table 1.3. Anticipated clinical trials for IRDs (adapted from Thompson et al., 2015 for the Monaciano Consortium).

Optogenetics, in the first instance, is therefore likely to be suitable for any advanced stage IRD, and in particular retinitis pigmentosa. In addition, macular degeneration including Stargardt disease and end-stage AMD are potential candidates. However,

depending on its successes in future clinical trials, there might also be a shift towards the treatment of mid and early stage diseases. Optogenetics, for example, could be used to treat those conditions where gene replacement therapy might not be an option in the foreseeable future. Such diseases might involve those with unknown mutations or autosomal dominant mutations (where it might not be possible to remove the offending 'gain-of-function' protein and prevent dominant negative interactions). In addition, there are a number of recessive genes with high mutation prevalence that are likely too big for delivery by AAV, including *ABCA4*, which is mutated in Stargardt disease; *CEP290*, which is commonly mutated in LCA; and Usher syndrome genes, including *MYO7A* and *USH2A*.

One way of getting around this is to use dual AAV vectors to deliver partial cDNAs that assemble the full length coding sequence in vivo via trans-splicing (Reich et al., 2003). Alternatively vectors based on lentiviruses, such as equine infectious anaemia virus, EIAV, can accommodate much larger cargo (up to 8 kb), and are being explored as an approach for treating ABCA4-related Stargardt disease (Binley at al., 2013) and Usher 1B (Zallochini et al., 2014). However, EIVA's relative insufficiency to transduce photoreceptors and increasing concerns regarding its integration capacity might limit its clinical applications (Balaggan et al., 2012). Lastly, a high 'cost per dose' of developing treatments that target specific gene mutations in these rare disorders, coupled with high genotypic and phenotypic heterogeneity, means that only a small number of patients might benefit from gene replacement therapy. The appeal of developing mutation independent approaches therefore, such as optogenetics, is becoming more and more apparent.

The following sub-sections focus on gene replacement therapy and some mutation independent approaches for late stage IRDs including electronic implants and optogenetics.

1.2.2.1. Gene therapy and gene replacement trials

Gene replacement therapy involves delivery of healthy genes, by means of a carrying vector, to the target cell where the equivalent gene has been affected by a mutation.

Among monogenic IRDs, X-linked and recessive mutations generally cause an absence of protein or production of functionally null protein. In these cases, replacement of wild-type protein, via vector delivery (gene therapy) has potential to restore or preserve vision. LCA2, choroideraemia, retinoschisis and Stargardt disease are all examples of monogenic recessive diseases and have given rise to a plethora of successful gene replacement trials in animal models of retinal degeneration (Smith et al., 2011).

In these experimental studies recombinant, replication-deficient adeno-associated vectors, rAAVs, have mainly been used with the aim of preventing visual loss or even restoring vision caused by gene mutations (Smith et al., 2003; Dejneka et al., 2004; Pang et al., 2006; Min et al., 2005; Acland et al., 2005; Jacobson et al., 2006; LeMeur et al., 2007; Annear et al., 2011; Komáromy et al., 2010). Among these, the most impressive results were achieved in studies where subretinal AAV vectors (serotype 2) were used to treat RPE specific genetic defects or *RPE65* deficiency in mouse (Dejneka et al., 2004; Pang et al., 2006;) and canine models (Acland et al., 2005; Jacobson et al., 2006; LeMeur et al., 2007; Annear et al., 2011;) of LCA (den Hollander et al., 2008). Following this extraordinary result of restoring vision in the Briard dog model of LCA type 2 (LCA2), four independent human trials were instigated to test the safety and efficacy of subretinal delivery of AAV2 in LCA2 patients (NCT00749957, NCT01496040, NCT00516477, NCT01208389; Bainbridge et al., 2008; Maguire et al., 2008; Hauswirth et al., 2008; Jacobson et al., 2012; Bainbridge et al., 2015). Moreover, gene replacement therapy for choroideraemia has shown promising preliminary results in another recently initiated clinical trial (NCT01461213; MacLaren et al., 2014). These well publicised successes have prompted further development of gene therapy, as one of the most compelling concepts in modern medicine. As a result, clinical trials for Usher type 1B (MYO7A) and Stargardt's (ABCA4) were initiated and a clinical trial for achromatopsia is starting soon (Boye et al., 2013).

1.2.2.2. Lessons learned from clinical trials

Preliminary results from these human trials collectively suggested that (Bainbridge et al., 2008; Maguire et al., 2008; Hauswirth et al., 2008; Bainbridge et al., 2015; Simonelli et al., 2010) (i) among about 20 LCA2 patients included in the trials, the subretinally injected AAV2 vector containing RPE65 cDNA was generally safe (ii) the effect was therapeutic in some patients, leading to improvement in some aspects of sight (iii) in one trial there was evidence that the maximal efficacy with best visual improvement was in the youngest patients, presumably with better retinal preservation (Maguire et al., 2009). Overall, the results were promising and allowed AAV-mediated retinal gene therapy to be safely extended to a whole range of other untreatable eye disorders.

However, the extent and longevity of sight improvement reported in clinical trials to date do not appear to match those observed in animal models (Bainbridge et al., 2015, Testa et al., 2013; Jacobson et al., 2012; Cideciyan et al., 2013). Indeed, *RPE65*-mediated treatment in humans with LCA2 (age 11-30) fails to protect against degeneration despite sustained improvements in retinal function (Cideciyan et al., 2013) and the latest report by Bainbridge et al. (2015), reporting on all 12 participants after 3 years of phase 1-2 trial initiated in 2008, show that the initial modest improvements in retinal sensitivity (rod but not cone function) in some patients start declining after 6-12m after the initial treatment, confirming ongoing degeneration. Contrary to study by Maguire et al. (2009), the authors report no correlation between the treatment effect and the age of the participants, with in fact greatest improvements in older participants. Furthermore, there was no improvement in retinal function (electroretinograms) in any of the participants (in concordance with previous reports, Testa et al., 2013; Jacobson et al., 2012; Cideciyan et al., 2013) and two participants had clinically significant deterioration of vision and macular thinning after subfoveal vector administration. In addition, there were three instances of ocular adverse effects with intraocular inflammation and immune responses to AAV2 indicating dose-limiting toxic effects at higher vector dose (10^{12} gc/ml).

1.2.2.3. Mutation independent therapeutic approaches

Due to the genetic and mechanistic diversity of the retinal diseases, the development of gene therapies tailored to each patient-specific mutation presents enormous challenge. There is therefore a growing interest in treating a larger number of patients through mutation-independent approaches. Several such strategies have made great advances in attempts to protect degenerating neurons (Beltran, 2008; Leveillard and Sahel, 2010; Sahel et al., 2010; Byrne et al., 2015), replace photoreceptor cells (MacLaren et al., 2006; Pearson et al., 2012), or directly stimulate surviving retinal neurons through electrical stimulation (Zrenner et al., 2011; Humayun et al., 2012) or through optogenetics (Bi et al., 2006; Lin et al., 2008; Greenberg et al., 2011; Zhang et al., 2009; Thyagarajan et al., 2010; Doroudchi et al., 2011; Lagali et al., 2008; Cronin et al., 2014; Mace et al., 2015; Busskamp et al., 2010; Polosukhina et al., 2012; Tochitsky et al., 2014; Caporale et al., 2011; Gaub et al., 2014).

Neuroprotection using neurotrophic factors has been an attractive strategy to prolong the lifespan of degenerating neurons and a recent pre-clinical study using a retina specific rod-derived cone viability factor (RdCVF) has been shown to prolong cone survival (Byrne et al., 2015). Transplantation of photoreceptor cells or their progenitor lines is a major approach under pre-clinical study and has been shown to restore vision to blind mice at late stage of degeneration after complete loss of photoreceptors (MacLaren et al., 2006; Pearson et al., 2012). In attempts to stimulate remaining inner retinal neurons, implantable electronic prostheses have been used to trigger retinal ganglion cell (RGC) firing and have provided crude spatial discrimination for at least some patients (Zrenner et al., 2011; Humayun et al., 2012, Rizzo et al., 2014).

1.2.2.4. Electronic retinal implants

Electronic retinal implants are an innovative way of restoring sight in IRDs. In principle they function by directly stimulation surviving cells in the inner retina through externally fitted devices that bring the visual image to the retina. The most

common retinal implants can be classified according to the site of the placement of their microelectrode arrays (Figure 1.11). Thus they include epiretinal, subretinal and suprachoroidal devices (Zrenner, 2013; Chuang et al., 2014). Epiretinal and suprachoroidal arrays use extraocular light sensors. In contrast, newly developed subretinal devices do not require external video cameras but have coupled light sensors with the stimulating electrodes at the position of lost photoreceptors to allow the sensors to exploit natural eye movements. In subretinal and suprachoroidal implants, retinal bipolar cells are targeted in hope to preserve any potential retinal processing. On the other hand, epiretinal implants involve a simpler surgical procedure and directly target the output retinal cells, the RGCs. Perhaps, the simplest surgical approach is the suprachoroidal placement of the implant where a scleral tunnel is used.

Direct electrical stimulation of the surviving cells in the inner retina has proven to be successful in restoring rudimentary greyscale light perception, allowing patients to perform simple visual tasks and navigate independently (Zrenner et al., 2011; Humayun et al., 2012; Mandel et al., 2013; Rizzo et al., 2014). At present, there are seven ongoing retinal prosthesis projects that have either implanted test subjects or have firm aims to do so in the near future. One such approach employs the Argus II device (epiretinal, 60 electrodes, 10x20 degrees of visual angle; developed by Second Sight Medical Products, Inc.) where surgically implanted multielectrode arrays have been used in over 30 patients in both Europe and the USA to stimulate RGCs directly in the degenerate retina (Zrenner et al., 2011; Humayun et al., 2012). Promising results in clinical trials have led to US Food and Drug Administration FDA approval for the Argus II device (Humayun et al., 2012; Rizzo et al., 2014) for commercial sale. Indeed, Argus II is currently the only FDA approved therapy for blindness caused by degeneration of the photoreceptors of the retina. Another device, the Alpha-IMS (subretinal, 1500 electrodes, 11x11 degrees of visual angle; developed by Retina Implant AG) has been implanted in over 40 patients in clinical trials and has recently received the European CE Marketing (Zrenner, 2013). Highest visual acuity of devices tested in humans has reached 20/1262 in Argus II and 20/546 in the Alpha-IMS6 (Humayun et al., 2012 Twyford et al., 2014).

These proof-of-concept studies demonstrated that inner retinal neurons in blind patients can respond to appropriate electrical stimulation and lead to a useful visual percept allowing simple navigation and object recognition. These microelectronic retinal implant devices are under continual development to improve the surgical implantation procedures, to increase the system spatial and temporal resolution, to increase the safety and longevity of these devices and to improve the sophistication of their signal-encoding algorithms (Twyford et al., 2014; Zrenner, 2013).

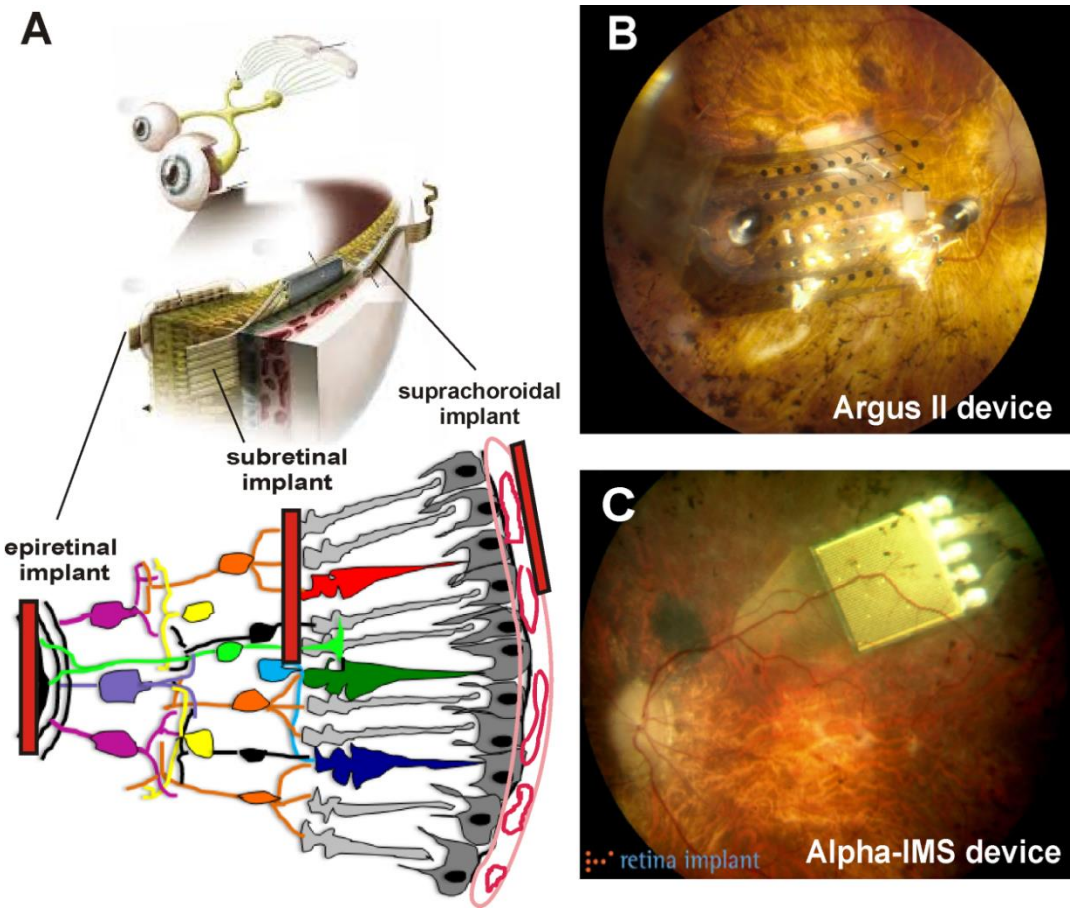

Figure 1.11. General approaches to stimulating the retina via microelectronic devices. (A) Schematic of the visual system and the retina showing three main sites used for retinal implantation, epiretinal, subretinal and suprachoroidal. Adapted from Sahel et al., 2014. (B-C) Fundal images showing the placement of two commercially available implants inside the human eye, the Argus II device (B; adapted from http://www.extremetech.com) and Alpha-IMS device (C; image by Retina Implant).

1.2.2.5. Optogenetic approaches to date

One of the most promising therapeutic strategies for late stage retinal degeneration is optogenetics. Optogenetics is the combined use of genetic material and optical technology to modulate neuronal circuits (Deisseroth et al., 2006; Yizhar et al., 2011; Deisseroth, 2011). For the purpose of treating blindness, optogenetics explores the natural history of the retinal degeneration where despite the loss of outer retinal photoreceptors, inner retinal neurons can survive and retain their ability to send visual information to the brain (Santos et al., 1997; Mazzoni et al., 2008). These neurons therefore, provide a promising niche for emerging optogenetic therapies that aim to convert them into directly visual photoreceptors to recreate the photosensitivity that has been lost with the degeneration (Figure 1.12; Busskamp and Roska, 2011; Busskamp et al., 2012). Optogenetic therapy for an aggressive form of retinal degeneration is explored in Chapters 3 and 4 of this thesis.

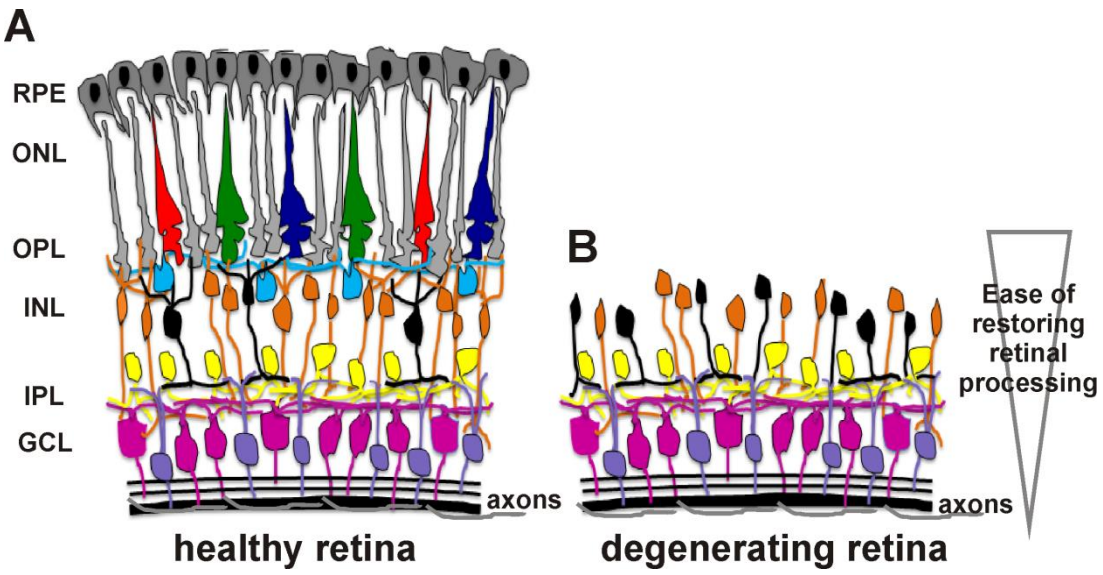

Figure 1.12. Schematic representation of a normal *wild-type* retina and a retina with advanced retinal degeneration. (A) Healthy *wild-type* retina. (B) In advanced retinal degeneration, there is a complete loss of photoreceptors in the outer retina, but cells in the inner retina, INL and GCL can survive making them amenable to optogenetic targeting. Rods- grey; cones- red, dark blue and green; horizontal cells – light blue; ON bipolar cells-orange; OFF bipolar cells – black; amacrine cells – yellow; RGCs – violet and purple.

1.2.2.5.1. Genetic versus chemical approach

Optogenetic strategies can be broadly divided into optogenetics, optopharmacology (photopharmacology) or a combination of both approaches, optogenetic pharmacology (Figure 1.13). The first approach, the optogenetic approach, a genetically encoded light sensor, e.g. an opsin, is targeted to the membrane of a retinal cell and uses endogenous supplies of chromophore, e.g. retinal (Figure 1.13A). Opsin-based light sensors are a family of seven-transmembrane domain proteins that can broadly be divided into two groups: Type I opsins (commonly referred to as microbial opsins) found in prokaryotes, algae and fungi, and used by them for phototaxis or coupling light energy to cellular functions, and Type 2 opsins (commonly referred to as vertebrate opsins) present in higher eukaryotes and involved in higher order functions such as vision and circadian rhythms (Sakmar, 2002). Types 1 and 2 opsins do not share significant homology, but both use retinaldehyde variants as their chromophores; microbial opsins more typically utilize retinal in all-trans configuration whereas vertebrate opsins bind retinal in the dark in 11-cis configuration.

The most widely studied optogenetic tools to date are microbial, Type I opsins such as channelrhodopsins from green algae and light-driven pumps such as halorhodopsin from archaeal species. The microbial opsins capture light energy and use it open channels allowing a passive flow of ions across the cell membrane or to actively pump ions across the cell membrane. As a result, the generated photo-current flows across the cell membrane, depolarising (in case of blue light-gated non-selective cation channel, e.g. channelrhodopsin-2 from *Chlamydomonas reinhardtii,* ChR2; Figure 1.14A) or hyperpolarising (in case of yellow light-activated chloride pump, halorhodopsin from archea *Natronomas pharaoni*, NpHR; Figure 1.14B) that specific cell.

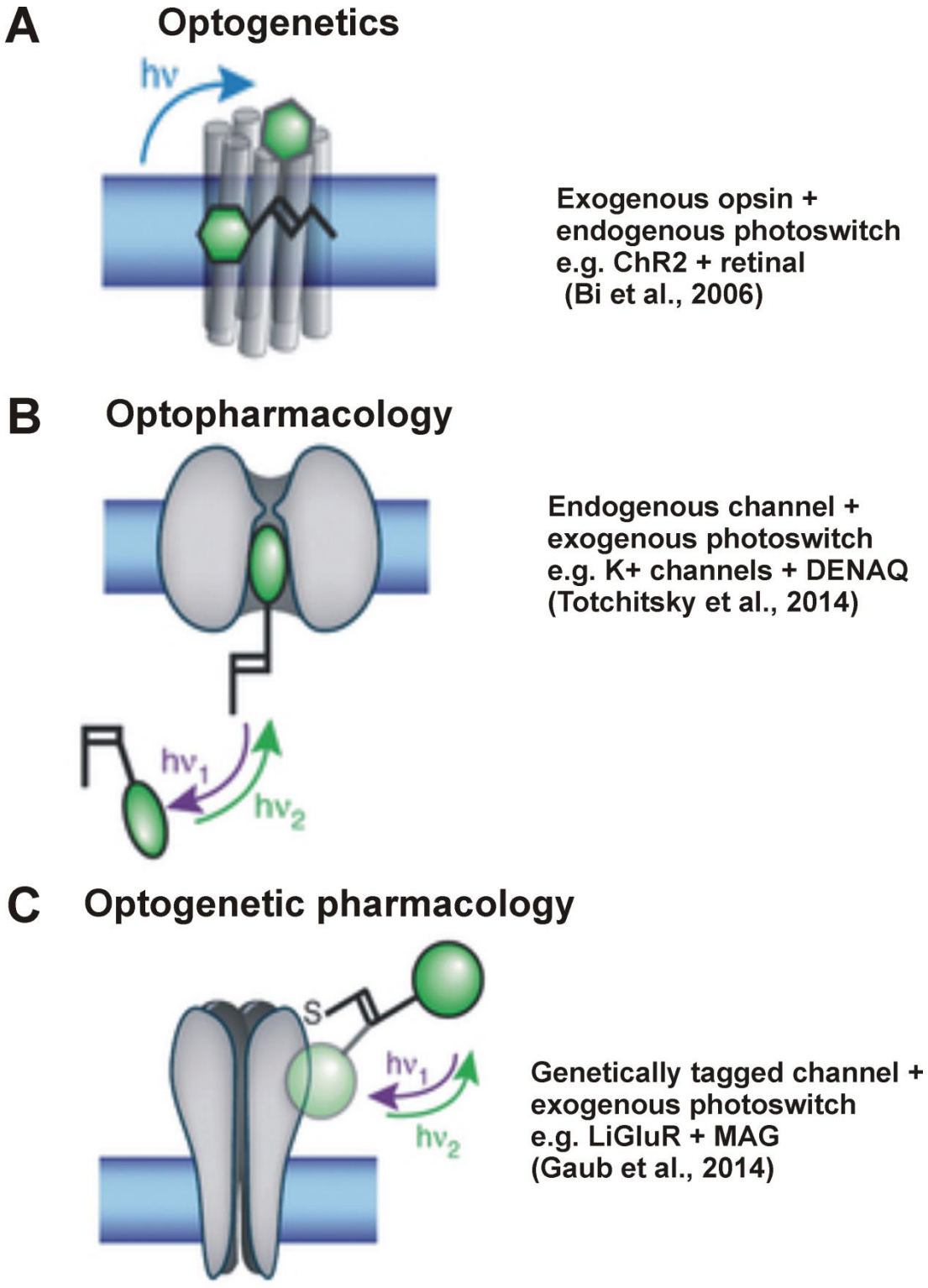

Figure 1.13. Optochemical tools for modulating neuronal function. (A) Optogenetics (B) Optopharmacology (C) Optogenetic pharmacology. Adapted from Kramer et al., 2013.

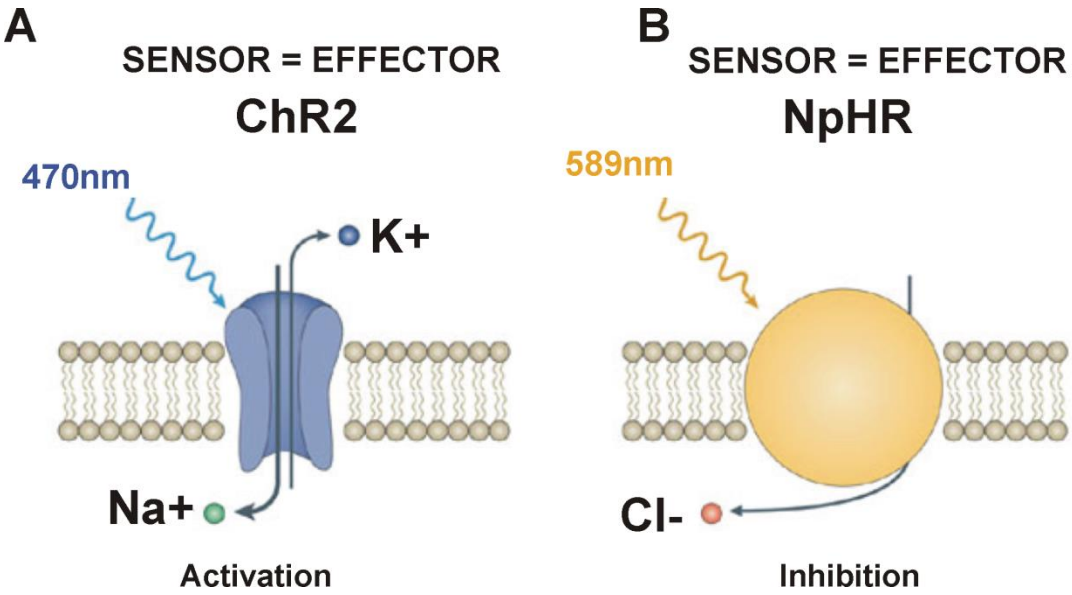

Figure 1.14. Light mediated control of neural activity via microbial opsins. (A) Channelrhodopsin-2 (ChR2) allows entry of sodium ions upon light stimulation to depolarize and activate target neurons. (B) Halorhodopsin (NpHR) allows entry of chloride ions upon light activation to hyperpolarize and silence target neurons. Note that in the case of microbial opsins, the sensor (retinoid-based opsin) is the same as effector (ion channel/pump) with limited potential for adaptation and amplification in the system. Modified from Zhang et al., 2007.

Both of these microbial opsins have been used to elicit light-evoked activity in degenerate retinas (Figure 1.15). To this extent it has been shown that intravitreal injection of an AAV-2 vector carrying the channelrhodopsin-2 gene (ChR2) in the *rd*[1] mouse leads to light activated depolarization or 'ON' responses in RGCs and visually evoked potentials in the cortex (Bi et al., 2006). This study provided the first proof-of-principle that retinal function can be restored using optogenetics. Since then further targeting of RGC (Zhang et al., 2009; Thyagarajan et al., 2010; Doroudchi et al., 2011;) and ON-bipolar cells (Lagali et al., 2008; Cronin et al., 2014; Mace et al., 2015;) with ChR2 as well as cone inner segments with NpHR (Busskamp et al., 2010) has successfully converted them into artificial light-sensors leading to a partial rescue of visual function in blind mice. In addition, on the basis of their different activation maxima, ChR2 and NpHR can be co-expressed in the same cell to activate or silence the cell activity in an independent manner, to recreate antagonistic centre-surround receptive field interactions (Greenberg et al., 2011).

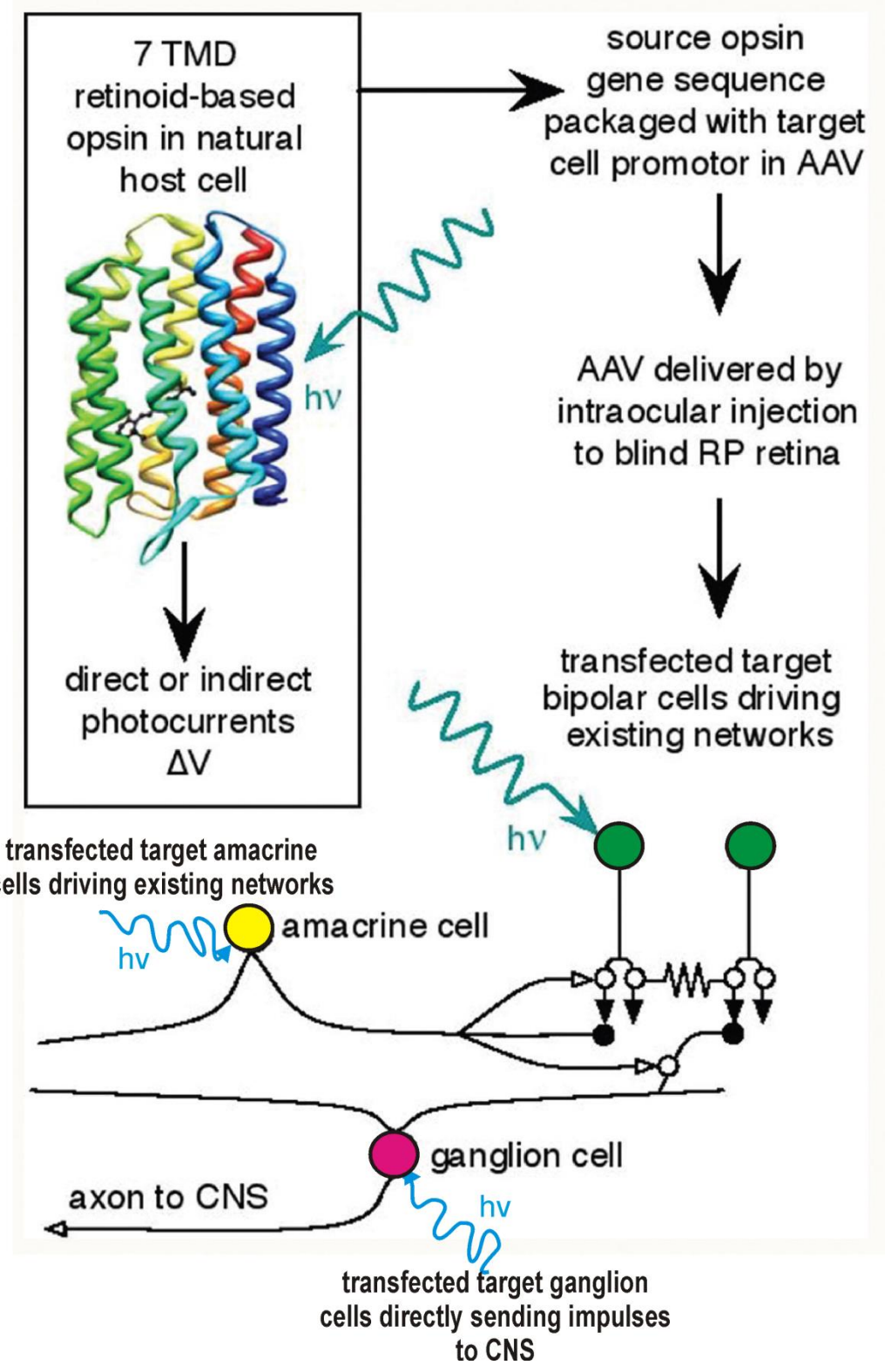

Figure 1.15. A schematic of using opsins as an optogenetic tool for reanimating blind retinas. AAV - adeno-associated virus, TMD -transmembrane domain, ΔV - membrane voltage change, hv – photon, CNS – central nervous system. Rhodopsin image from public domain. Adapted from Henriksen et al., 2014.

The second approach, optopharmacology, uses 'one-component' chemical photoswitches (or photochromic ligands) to directly photosensitise native ion channels and control neuronal activity (Figure 1.13B). These compounds have ligands that are attached to a photoisomerizable group that controls whether the ligand can fit properly into a binding site on a protein, e.g. a K+ channel. Azobenzene-based photoswitch molecules, AAQ (Polosukhina et al., 2012) or DENAQ (Tochitsky et al., 2014), have recently shown to confer light sensitivity on neurons in vitro and in vivo with promising results in rescuing vision in blind mice.

The third system, optogenetic pharmacology, uses 'two-component' photoswitches, e.g. LiGluR/MAG (Caporale et al., 2011; Gaub et al., 2014) where in the first instance there is genetic expression of synthetically engineered light-gated ionotropic glutamate receptor (LiGluR) in retinas and then an exogenous supply of a photoswitch molecule (MAG) for activation (Figure 1.13C). This system has been shown to successfully impart light sensitivity to blind mouse and canine (Gaub et al., 2014) retinas and restore basic visual function in murine models of retinal degeneration.

Each strategy comes with its own opportunities and challenges. Genetically encoded proteins allow for specific cell-targeting and one-time treatment with a long-lasting effect (Bi et al., 2006; Greenberg et al., 2011, Lin et al., 2008, Zhang et al., 2009; Thyagarajan et al., 2010; Doroudchi et al., 2011; Lagali et al., 2008; Cronin et al., 2014; Mace at al., 2015; Busskamp et al., 2010). However, this treatment is irreversible with little control in silencing the system in case of adverse effects. By contrast, the effect of synthetic photoswitches (Polosukhina et al., 2012; Tochitsky et al., 2014; Caporale et al., 2011; Gaub et al., 2014) is non-specific and temporary (days) requiring multiple intraocular injections or administration via sustained-release intra-ocular mechanisms. None-the-less it would be possible to adjust the dose over time for each patient and to discontinue treatment in case of adverse reactions.

1.2.2.5.2. Optogenetics in pre-clinical phase

Despite the recent advances, current optogenetic approaches are still at the phase of pre-clinical studies. There are several important barriers that must be overcome before this technology can be used for clinical applications. In order to work current microbial and chemical-based optogenetic sensors need stimulation with very high intensities of light, well outside the physiological range (Figure 1.16).

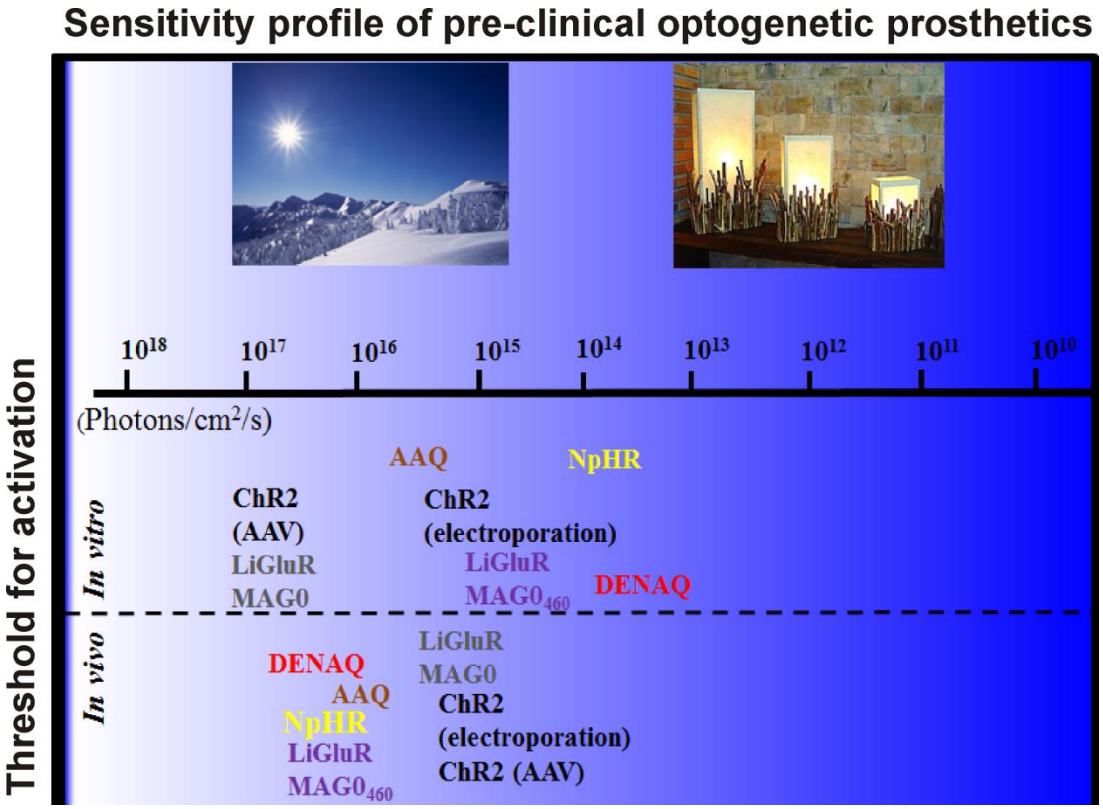

Figure 1.16. Summary of activation thresholds for different experimental optogenetic prosthetics.

These light intensities can only be provided through an externally fitted device and are potentially toxic to the retina. In addition, with the use of microbial opsins there is potential of adverse immune responses raising doubts about their safety profile when used in humans. The temporary effect of single-dose photoswitch molecules and unknown long-term safety effect of possible sustained-release delivery of these ligands precludes these chemical approaches from entering clinical trials at this stage.

1.2.2.5.3. G protein coupled receptors for improved sensitivity

A major advantage of employing GPCRs over currently tested ion channels is that GPCRs operate under physiological light conditions. In directly light-gated ion channels or pumps (ChR2 or NpHR) light sensor (channel or pump) is also an effector (channel or pump) offering 'no gain' in signal processing, with therefore limited adaptation and sensitivity (Figure 1.14 A and B). In contrast, photosensitive GPCRs, the sensor (opsin) is separate from effector (ion channel) with 'built-in-gain' as they process signal through G-protein coupled cascade (Figure 1.6). This results in great signal amplification with major potential for adaptation and enhanced sensitivity. Therefore, harnessing the cell's internal amplification machinery is likely to lower the light intensity needed to drive the optogenetic actuators used as visual prosthetics. We chose to study two human GPCR opsins, melanopsin and rod opsin for the purposes of treating blindness. These studies are presented in Chapters 3 and 4 respectively.

1.2.2.5.4. Mechanisms underlying heterologous activation of downstream pathways

More than 800 human GPCRs with distinct physiological outputs are encoded by 16 $G_{\square}$ genes encoding for 23 different isoforms that belong to 4 major classes of heterotrimeric G proteins, $G_{i/o}$, G_s, G_{12}, and G_q. These heterotrimeric G proteins share a common activation mechanism, but each G protein engages distinct downstream effectors and is therefore able to mediate a variety of biological processes where ultimate outputs are determined by the nature of the cell where signals are elicited as well as signalling connectivity of these cells (Cao et al., 2013). The mammalian opsin family members, rod opsin and melanopsin are photoreceptive GPCRs found in specialised rod cells or ipRGCs respectively, as described in previous sections. Briefly, for visual signal transduction in vivo, rod opsin couples to transducin (G_t, belongs to $G_{i/o}$ subfamily) which in turn activates PDEs to cleave cGMP, thereby reducing levels of cGMP that then lead to closure of cyclic nucleotide-gated channels (CNGs) (Palchewski et al., 2006). In contrast, melanopsin couples to G_q which in turn activates PLCβ for signalling that regulates circadian rhythms and non-image forming vision (Terakita et al., 2005).

Optogenetic targeting of light-sensitive GPCRs to various heterologous systems allows for a new promising approach for studying these proteins and elucidating mechanisms involved in their downstream signalling pathways. Several studies involving expression of GPCRs in heterologous systems (Li et al., 2005; Oh et al., 2010; Gutierrez et al., 2011; Cao et al., 2013, Bailes et al., 2013) have contributed to better understanding of heterologous activation of downstream pathways although many questions remain to be answered in future studies.

Li et al., 2005 demonstrated that vertebrate rat rhodopsin 4 (RO4) and the green algae channelrhodopsin 2 (ChR2) can be used to control neuronal excitability and synaptic transmission in antagonistic light activated fashion in all preparations tested including HEK293 cells (human embryonic kidney cells), cultured hippocampal neurons, and isolated chicken spinal cord. All three heterologous system required exogenous application of all-trans retinal to RO4 or ChR2-expressing cells for light-activation of proteins. However, exogenous retinal was not required for light-mediated activation of RO4 and ChR2 in chicken embryos *in ovo*.

The initial experiments were carried out in HEK cells in order to determine the downstream mechanisms of GPCR light-activation. Vertebrate rod opsin couples to the G protein transducin (Figure 1.6), the α subunit of which belongs to the G_i subfamily. It is therefore possible that mammalian rod opsins would couple to other $G_{i/o}$ family members. In neurons, the pertussis toxin (PTX)-sensitive $G_{i/o}$ pathway activates G protein inward rectifying potassium channels (GIRKs) and inhibits presynaptic voltage-gated Ca^{2+} channels. Authors demonstrated that light-activation of HEK cells co-expressing RO4 and GIRK channels led to increased GIRK-mediated K+ currents and neuronal inhibition. Importantly, this light activation was blocked by PTX, indicating that activation of GIRK channels by vertebrate rod opsin is mediated via PTX-sensitive pathways (G_i pathways). Similarly, co-expressing RO4 and P/Q type Ca^{2+} channels led to light-induced inhibition of Ca^{2+} currents via PTX-sensitive pathways.

In addition, patch-clamp recordings of cultured hippocampal neurons expressing RO4 induced hyperpolarisation within ms comparable to the hyperpolarisation induced by activation of endogenous $GABA_B$ receptors by agonist baclofen and easily reversible upon light termination. Importantly, time-constants of activation and deactivation

were much faster than in HEK cells, presumably because of the effect of endogenous proteins which accelerate the GTPase activity of the G-proteins. Moreover, light-activation of RO4 (localised at synapses) reduced the excitatory post-synaptic current amplitude indicating that RO4 can control neuronal excitability not only through hyperpolarisation of somato-dendritic membranes, but also pre-synaptically via reduction of transmitter release. Lastly, the authors demonstrated that electroporation of CMV-RO4 into the embryonic chick spinal cord *in ovo* led to suppression of spontaneous bursting neuronal activity which was frequency dependent (suction electrode recordings). In summary this landmark study, revealed that heterologously expressed rod opsin promoted modulation of GIRK and P/Q type Ca^{2+} channels via the precise spatio-temporal control of PTX-sensitive $G_{i/o}$ mediated pathway.

The exact mechanism in which $G_{i/o}$ –mediated GPCR modulation may occur within cells and how such modulation may influence the single spike pattern and motor activity is difficult to address in vivo, since other $G_{i/o}$ -coupled receptors including $GABA_B$ receptors are expressed in surrounding cells and can only be activated by slowly diffusing drugs. Thus, a study by Gutierrez et al., 2011, created an optogenetic mouse model for the cell-type specific expression of rod opsin. They showed that in vivo light activation of vertebrate rod opsin, specifically expressed in cerebellar Purkinje cells in a transgenic Cre-dependent mouse model, leads to reduction in spike firing that is comparable to the reduction in firing observed for the activation of endogenous cerebellar $G_{i/o}$ -coupled $GABA_B$ receptors (in vivo neurophysiology recordings after application of baclofen reduce the spontaneous firing rate of Purkinje neurons) indicating that rod opsin and $GABA_B$ receptors activate a similar intracellular signalling pathway to modulate Purkinje cell firing. Furthermore, this light-induced spike modulation was shown to affect motor co-ordination and reduce the capacity of mice to navigate an angled pole. This study therefore confirmed that vertebrate rod opsin also promotes precise spatio-temporal control of the $G_{i/o}$ mediated pathway in vivo. However, further studies are needed to determine which downstream signalling pathway is activated as $G_{i/o}$ -coupled GPCRs have a variety of downstream signalling targets with binding preference to each of their respective targets.

Interestingly, no study so far has implicated rod opsin in activation of other G protein pathways such as G_q or G_s in cellular or neuronal systems. In other words, rod opsin seems to be very specific for activation of inhibitory $G_{i/o}$ pathway. An elegant optogenetic study of light activated rod opsin (9-cis-retinal regenerated bovine opsin) and human melanopsin heterologously expressed these GPCRs in the nervous system of C. *elegans*, which has $G_{i/o}$ and G_q conserved in its transparent body (Cao et al., 2011). The study demonstrated an impressive sudden and transient loss of motility in rod opsin expressing animals and increased locomotor activity in melanopsin expressing worms. Both motor behaviours depended on exogenous supply of 9-cis-retinal and required the presence of endogenous worm $G_{i/o}$ and G_q – signalling components. Thus blocking the endogenous $G_{i/o}$ pathway PTX abolished all light-induced locomotion in rod opsin expressing worms. In addition the rod opsin activated signalling specifically occurred through $G_{i/o}$ pathway. Thus, crossing the worm line with loss-of-function mutants of genes that encode for α subunits of G_o, G_q, G_{12} and G_s, showed as expected, that G_o mutants did not respond to light stimulus, whereas the other three mutants had no change in behaviour and continued to freeze after light pulses. This observation proved that rod opsin in neurons specifically activates $G_{i/o}$ and not the other G proteins.

In addition this study demonstrated that cAMP-specific PDEs are required for $G_{i/o}$ mediated signalling (not cGMP as in human rods). Thus worms carrying loss-of-function mutations in cGMP specific PDEs had no change in light-induced behaviour, whereas mutants of cAMP specific PDEs displayed reduced light responses. Moreover, functional absence of three different genes encoding for CNG channels all led to reduced light-induced loss of motility, indicating that CNG channels play a role in rod opsin coupled $G_{i/o}$ signalling.

By contrast, enhanced light-induced locomotion is mediated by G_q and subsequent activation of PLCβ in worms expressing melanopsin. This was confirmed by melanopsin expression in neurons of *elg-30* ($G_{q\alpha}$), *elg-8* (PLCβ) and *goa-1* ($G_{o\alpha}$) loss-of-function worm mutants and subsequent light-induced behaviour analysis. This showed that light exposure enhanced the locomotion of *goa-1* ($G_{o\alpha}$) mutant worms but not *elg-30* ($G_{q\alpha}$) or *elg-8* (PLCβ) mutant worms, thereby confirming that melanopsin heterologously expressed in C *elegans* neurons directly activates G_q and

subsequently PLCβ in response to light. However, a study by Bailes et al., 2013 revealed that human melanopsin under heterologous expression in HEK cells is able to drive responses via both G_q and $G_{i/o}$ class G-proteins. This study used luminescent reporters for common second messenger systems (luminescent cAMP reporter, (Glosensor) and luminescent calcium reporter (photoprotein aqueorin) which were co-expressed with opsins in HEK cells) to study mechanisms of heterologous activation of downstream pathways of human melanopsin and rod opsin. Thus, a luminescent biosensor assay was used to monitor changes in cAMP production, and reductions in cAMP as a result in $G_{i/o}$ activity were measured by artificially raising cAMP with forskalin, before exposing cells to light. There was a modest reduction in luminescence indicating reduction in cAMP levels ($G_{i/o}$ mediated) In contrast, rod opsin in HEK cells induced a prolonged reduction in cAMP production.

Furthermore, aequorin luminescence (in a 96-well plate reader) was used to analyse levels of intracellular calcium after light pulse. This revealed that light induced significant increase in intracellular calcium (G_q mediated) in HEK cells expressing melanopsin, but no change in luminescence was observed in rod opsin expressing cells. In summary this data implies that melanopsin is able to drive responses via both G_q and $G_{i/o}$ class G-proteins, but that rod opsin driven responses are specific for $G_{i/o}$ downstream pathway/s.

1.3. Adeno-associated vectors

The development of adeno-associated virus (AAV)-mediated gene delivery has allowed ocular gene therapy to gain momentum because the approach has a number of favourable features inherent to the viral biology of AAV (Zinn et al., 2014). AAV is a non-human pathogen that has not been associated with disease; it has wide and promiscuous tropism; it is minimally immunogenic and has the ability to achieve efficient and long-lived gene transfer. In the eye, replication-deficient vectors derived from AAV have been the most promising vehicles for gene delivery, including current clinical trials (Bainbridge et al., 2008; Maguire et al., 2008; Hauswirth et al., 2008; Bainbridge et al., 2015; Simonelli et al., 2010), and they have been shown to elicit minimal viral host response (but see Bainbridge et al., 2015), mediate long-term transgene expression without notable toxicity and infect a variety of non-dividing retinal cell types following a single treatment (Bunning et al., 2008).

Moreover, the eye is an ideal organ in which to test different gene therapy approaches. Its structure and accessibility facilitate the targeted delivery of therapeutic vector to specific tissues under direct visualization. A special system of immune surveillance and modulation limits immune responses directed against vector antigens and transgene expression (Bennett, 2003). Furthermore, the risks of unwanted systemic side effects are minimal as the blood–retinal barrier limits the dissemination of the vector to the rest of the body.

1.3.1. Structure

AAV are one of the smallest viruses and have a non-enveloped icosahedral capsid of approximately 22nm (Figure 1.17A). They contain a linear, single-stranded DNA genome (~4.7 Kilo bases, Kb), with two 145 nucleotide-long inverted terminal repeats (ITR) at the termini that can only replicate in the presence of different helper viruses such as adenovirus, herpes virus or papilloma virus (Goncalves et al., 2005). The virus does not encode a polymerase and therefore relies on cellular polymerases for genome replication. ITRs flank the two viral genes - *rep* (for replication), and *cap* (for capsid), encoding non-structural (Rep78, Rep68, Rep52 and Rep40) and structural (VP1, VP2 and VP3) proteins, respectively.

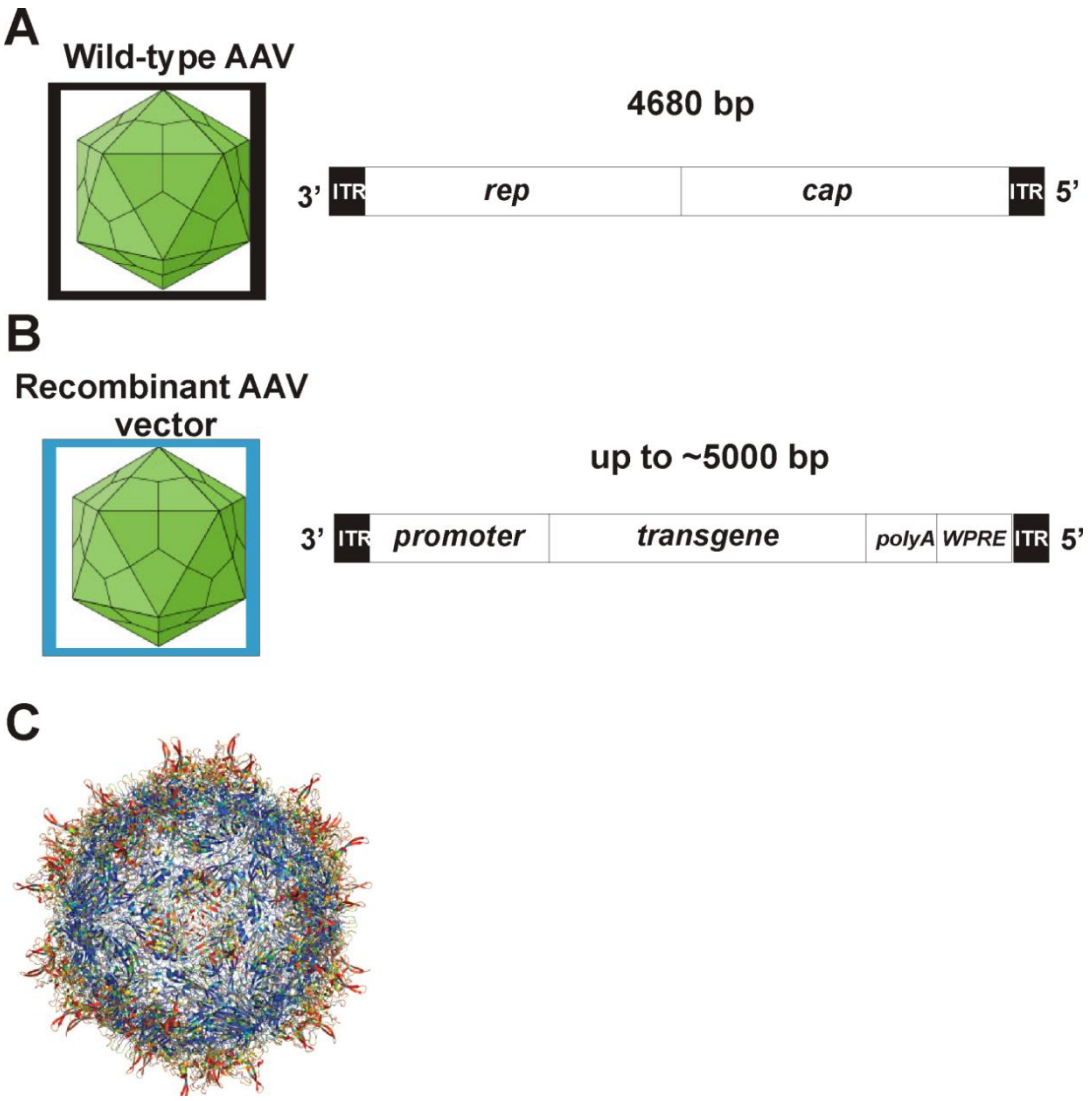

Figure 1.17. The structure and natural diversity of adeno-associated virus capsids (A and B) AAV are small, 20-25 nm in diameter, non-enveloped viruses with a single-stranded DNA genome of 4680 base pairs, bp (~4.7 Kb) encoding *rep* (replication genes) and *cap* (capsid genes). The capsid genes form the 60-mer icosahedral viral capsid. The rep and cap genes are flanked by two inverted terminal repeats (ITRs) that are essential for genome packaging into the capsid. In recombinant AAV vectors, ITRs are the only wild-type sequences retained and rep and cap genes are replaced by the transgene expression cassette typically consisting of the promoter sequence, the gene of interest and a polyadenylation signal sequence (polyA) sequence and a woodchuck hepatitis posttranscriptional regulatory element (WPRE) for stabilisation. (C) Variability between different naturally occurring serotypes plotted on AAV2 capsid. Blue colours represent more conserved positions while red colours represent more variable positions. C – Image adapted from Zinn and Vandenberghe, 2014.

The AAV viral capsid proteins, VP1s = 87kDa, VP2 =73kDa and VP3 = 62kDa assemble into a near-spherical protein shell of 60 subunits (60-mer icosahedral shape, T=1 symmetry) with a stoichiometry 1:1:20 respectively.

In recombinant vectors, rAAVs, genes encoding *rep* and *cap* from the wild-type AAV genome are replaced by a promoter and a therapeutic transgene cassette flanked by the ITRs that are required for packaging genome into viral capsid (Zhou and Muzyczka, 1998) (Figure 1.17B). The ITRs are the only wild-type viral sequences retained in AAV vectors. In addition, most current AAV vectors include polyadenylation signal sequence (polyA) sequence and a woodchuck hepatitis posttranscriptional regulatory element (WPRE) for stabilisation. Typically, therefore, rAAV is generated by transfecting producer cells within a plasmid containing three components: a DNA expression cassette carrying the gene of interest (and flanked by ITRs), a construct expressing the desired viral capsid and the helper factors.

It is important to note that the stability in transgene expression does not arise from foreign DNA insertion into the host cell virus pre-integration site (AAVS1 on Chromosome 19) since the absence of rep gene products prevents DNA targeting to the AAVS1 locus. It is believed that, after the single- to double- stranded DNA conversion, a duplex rAAV genome is formed, through either intra- or inter-molecular recombination at the ITRs. This duplex rAAV, in a circular form, is thought to be responsible for vector persistence and prolonged transgene expression (Buning et al., 2008).

1.3.2. AAV serotypes

AAV belongs to the *Parvoviridae* family, called *Dependoviruses* (Muzyczka, 2001). They display large genetic diversity (Figure 1.17C) and to date a number (~12) of naturally occurring serotypes and over 100 variants have been isolated from adenovirus stocks or from human/non-human primate tissue (Wu et al., 2006). This variability is largely found in their capsids, which are thought to determine their

tissue tropism and transduction efficiency. Viral capsids are known to mediate initial binding to cell surface receptors, cellular entry and intracellular trafficking, thereby determining selectivity for a particular cell type. Structural analysis of AAV serotypes suggests that their capsid surface topology differs, which may account for their unique tropism. For example spikes on the three-fold axis of AAV2 are larger and more pointed than the mounds on the same axis of AAV5 (Walters et al., 2001).

Utilization of alternative AAV serotypes with higher transduction efficiency can potentially lower the vector load and help evade pre-existing neutralizing antibodies generated by prior infection with wild-type AAVs or treatment with AAV-based vectors. Moreover, AAV serotypes and variants can serve as templates for engineering of novel cell-specific vectors with high transduction efficiency.

1.3.3. Hybrid AAV vectors

The first generated recombinant vector was AAV serotype 2, AAV2/2 (for simplicity AAV2/2 is commonly referred to as AAV2; Hermonat and Muzyczka, 1984). Since then researches have adopted a 'cross-packaging' strategy to generate 'hybrid' or 'pseudotyped' vectors based on the fact that expression of AAV2 rep proteins together with cap proteins from an alternative serotype result in formation of viral particles that package AAV2 vector genome but have cellular tropism determined by the capsid of the serotype used (AAV1-AAV12, Figure 1.18; Gao et al., 2004; Schmidt et al., 2008). These hybrid vectors have slight variations in amino-acids exposed on the capsid surface, which can affect cell tropism and transduction efficacy allowing for more targeted, cell-specific gene transfer (Surace and Auricchio, 2008; Auricchio et al., 2001). For instance, if the rAAV2/8 is to be produced, the first plasmid (the genome plasmid) and the third plasmid (the adeno helper plasmid) will be the same as for rAAV production described above. However, the second plasmid (the packaging plasmid, *p/rep/cap*) will be different. Here, the *rep* gene will be derived from AAV2 and the *cap* gene from

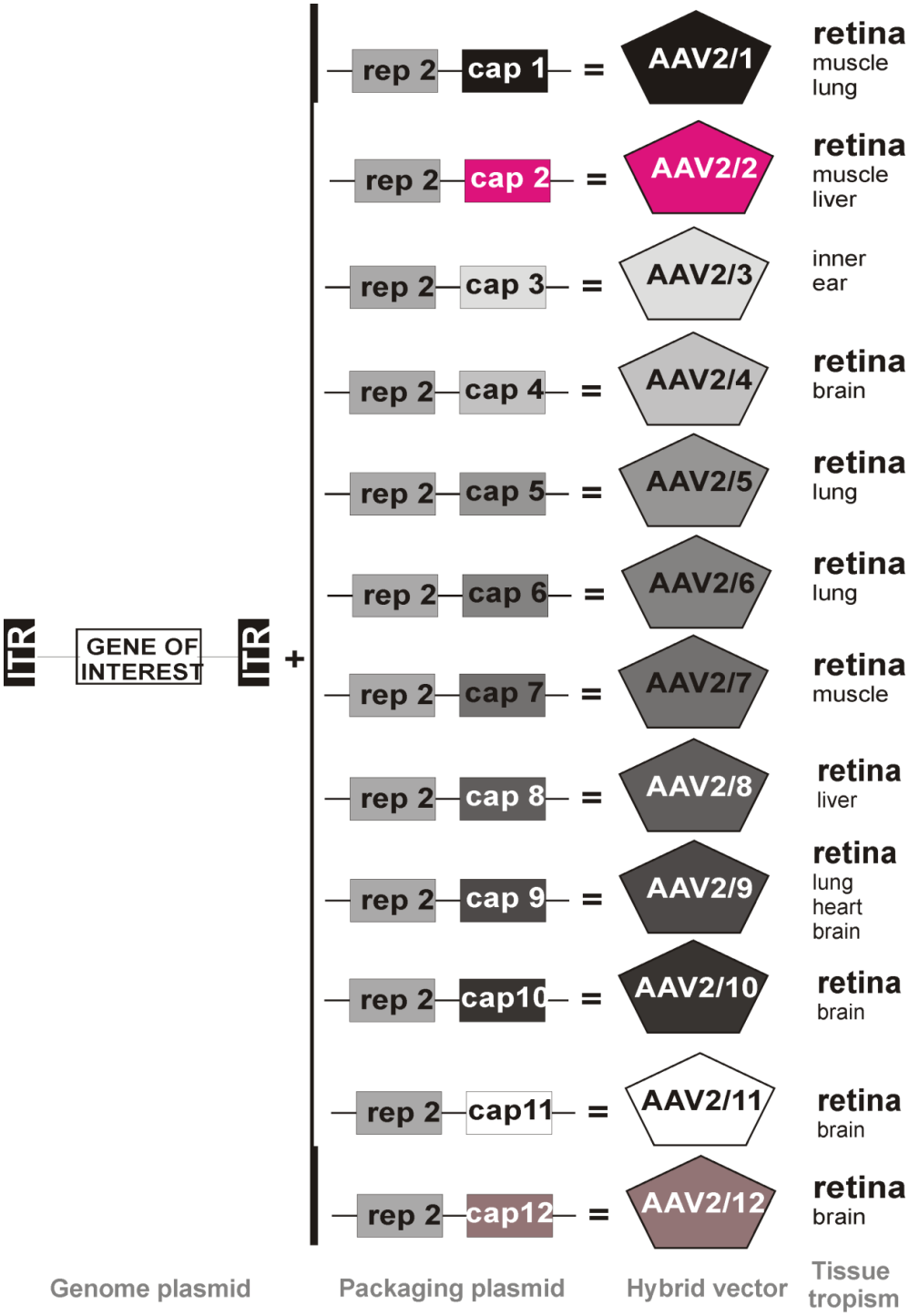

Figure 1.18. Construction of hybrid AAV vectors. The 'cross-packaging' strategy for the production of 'pseudotyped' or 'hybrid' viruses. The plasmids contain the AAV genome with the therapeutic gene contained between the viral inverted terminal repeats, ITRs, and the packaging sequences, the *cap* (encodes capsid proteins) and the *rep* (for replication) which belong to serotype 2. The pseudotyped or hybrid vectors are made from the genome of one serotype (i.e. AAV2) and a capsid from another (i.e. AAV1-9). The tissue and cell tropism of each serotype is determined by the capsid sequence. Adapted from edit.tigem.it/AAV vectors.

AAV8 giving the *p/rep2/cap8* plasmid. The resultant hybrid, rAAV2/8, therefore has a genome based on rAAV2 and capsid based on AAV8. It is assumed the cell tropism displayed by this AAV2/8 hybrid is the same as that of AAV8 (Auricchio et al., 2001). These pseudotyped vectors have enabled the exploration of cellular tropism in various organs, dictated by the capsid properties of the parental serotypes.

1.3.4. Carbohydrate binding and entry into cells

At a cellular level, AAV undergoes five distinct steps in order to achieve gene expression: binding to cell surface receptors, endocytosis, intracellular trafficking to the nucleus, un-coating of the virus to release the genome and conversion of genome single-stranded DNA to double-stranded DNA as a template for gene transcription. Out of these five steps, cell surface-binding specificity is a key determinant of viral tropism.

Somewhat unsurprisingly, naturally occurring AAVs show considerable diversity with regards to the molecular receptors they bind for the entry into a host cell. While many AAVs bind specific glycan motifs there is considerable diversity across and even within clades. In addition, different AAV serotypes do not necessarily use the same parts of the capsid to bind these glycans. Among naturally occurring serotypes, AAV2 is the best characterised and most studied to date. It is now well established that AAV2 uses heparan sulphate proteoglycan (HSPG), a widely-expressed cell surface receptor, as a primary receptor for cell attachment. The HSPGs are the only glycosaminoglycans (GAGs) known to date that AAV2 uses as its primary receptor and its transduction efficiency is thought to be directly proportional to the presence and concentration of HSPG receptors (Summerford et al., 1998). AAV2 also utilizes several co-receptors to assist its internalization: the fibroblast growth factor receptor-1 (Qing et al., 1999), integrin alpha-V-beta-5 (Summerford et al., 1999), and hepatocyte growth factor receptor (Kashiwakura et al., 2005). There is evidence that AAV infection is more efficient when its primary receptor and a co-receptor are co-expressed on the cell surface (e.g. HSPG and fibroblast growth factor receptor-1; Qing et al., 1998).

For most other serotypes, cellular receptors remain largely undetermined. None-theless, current evidence suggests that AAV4 and AAV5 bind to sialic acid as their primary receptor (Kaludov et al., 2001, Walters et al., 2001) and AAV5 also utilises a platelet-derived growth factor receptor as its co-receptor (Di Pasquale et al., 2003). It has recently been suggested that AAV serotypes 1 and 6 may also depend on sialic acid for initial binding (Wu et al., 2006). Other studies have found that AAV9 binds to N-linked galactose (Bell et al., 2011, Shen et al., 2011) but in a region of the AAV9 capsid (Bell et al., 2012) that is distinct from the HSPG binding region of AAV2 (Kern et al., 2003). AAV2, 8, and 9 may also bind to the laminin receptor, likely as their secondary receptor (Akache et al., 2006). It is possible that the retinal distribution and accessibility of these cell surface receptors to various AAV serotypes determines the degree of gene expression in different layers of the retina.

1.3.5. Current limitations of naturally occurring serotypes

Whilst naturally occurring vectors have evolved to offer many desirable characteristics for therapeutic gene transfer, they have some important limitations. For example the carrying capacity of AVV (~5 Kb) excludes many therapeutic genes form being utilised via this approach. For example, Usher type 1B causing gene, MYO7A is 6.7 Kb, and Stargardt's disease causing gene ABCA4 is 6.8 Kb, exceeding the AAV carrying capacity. Another significant limitation is the fact that despite their great diversity most naturally occurring AAV serotypes have very limited transduction efficiency of specific retinal cell types (in particular bipolar cells and photoreceptors) when injected into the vitreous of the eye (Schmidt et al., 2008; Surace and Auricccchio et al., 2008; Lebherz et al., 2008; Rabinowitz et al., 2002; Surace et al., 2003) especially if delivered in higher order animals, such as non-human primates (Dalkara et al., 2013). Thus, modern molecular biology techniques have been used creatively to engineer novel AAV variants that address these limitations.

1.3.6. Retinal transduction by AAV serotypes

Development of AAV vectors with ability to transduce outer retinal photoreceptors or indeed retinal bipolar cells with high efficiency by less invasive approaches than the currently used subretinal injection (see Chapter 2 Methods) would present a major advancement in the field of ocular gene therapy. The intravitreal route exposes the inner retina to the therapeutic agent, targeting directly RGCs (see Figure 2.1). This method may therefore be effective for rescuing these neurons in degenerative conditions such as glaucoma or optic neuropathy (Qi et al., 2007; Martin and Quigley, 2004; Zhou et al., 2005) or in optogenetic targeting of RGC (Bi et al., 2006; Line et al., 2008; Greenberg et al., 2011). However, to date, intravitreal injection of naturally occurring AAVs, such as AAV2, results in RGC transduction only. The transduction pattern is relatively widespread and dose-dependent in rodents (Martin et al., 2002; Ali et al., 1998) but it is present only in a ring around the fovea in primates (Yin et al., 2011). No other AAV serotypes appear to transduce the retina following intravitreal injection (Schmidt et al., 2008; Surace and Auricchio, 2008; Lebherz et al., 2008; Rabinowitz et al., 2002; Surace et al., 2003).

Some of the first serotype comparison studies indicated that AAV2, but not AAV1 or AAV5 can transduce the retina following the intravitreal delivery (Surace and Auricccchio, 2008; Simonelli et al., 2010). Another study including the more novel serotypes, AAV7, 8, and 9 has shown that only AAV2 and AAV8 would transduce some RGCs after intravitreal injection, with occasional Muller cells transduction by AAV2, 8 and 9 (Lebherz et al., 2008). In a quantitative study in the rat, intravitreal AAV6 transduced cells, in the inner nuclear layer, including amacrine, bipolar and some Muller cells, albeit at a low level (Hellstrom et al., 2009).

Animal studies that have used subretinal approach to deliver transgenes to photoreceptors can provide important information on the serotypes with native tropism for these cells. Thus several AAV serotypes have successfully transduced photoreceptors following subretinal injection, including AAV2, AAV5 and AAV8 with all three vectors demonstrating efficacy in proof of concept studies across multiple

species (mouse, rat, dog, pig and non-human primate; Ali et al., 1996; Auricchio et al., 2001; Weber et al., 2003; Acland et al, 2001; Vanrenberhge et al., 2011; Bennett et al., 1999; Petersen-Jones et al., 2009; Boye et al., 2012; Stieger et al., 2008; Mussolino et al., 2011). Several studies have compared relative efficiency of AAV serotypes following subretinal delivery in murine models and show that both AAV5 and AAV8 transduce photoreceptors more efficiently than AAV2, with AAV8 being the most efficient (Yang et al., 2002; Allocca et al., 2007; Rabinowitz et al., 2002; Boye et al., 2011; Pang et al., 2011).

1.3.7. Engineering AAV variants and manipulating intracellular barriers to optimise retinal transduction

In order to improve retinal transduction efficiency by naturally occurring AAV serotypes via the vitreous, two novel techniques have been developed that attempt to overcome barriers to vector transduction, rational mutagenesis and directed evolution. Rational mutagenesis is an *in vitro* knowledge-based approach to interfering with the viral capsid to develop novel variants with desirable phenotypes. Directed evolution, selects AAV variants with desirable phenotypes from large combinatorial libraries *in vivo* without a priori knowledge of the vector properties. Both approaches have led to the engineering of novel vectors with improved transduction efficiency (Petrs-Silva et al., 2009) altered tropism (Petrs-Silva et al., 2011, Klimczak et al., 2009) and the ability to evade immune responses (Li et al., 2012).

Tyrosine phosphorylation serves as a signal for ubiquitination and proteasome-degradation of wild-type AAV particles before they reach the nucleus. Therefore, mutating vector capsids through rational mutagenesis (e.g. by mutating tyrosines to other amino acids) allows the vectors to escape the proteasome degradation pathway so that more copies of vector genome are delivered to the nucleus. Recent experiments in which surface exposed tyrosine residues on AAV capsids were mutated show increased transduction efficiency as well as altered tropism for some of the novel variants tested (Petrs-Silva et al., 2009; Petrs-Silva et al., 2011).

Specifically, both mutants of AAV2 (Y444F and Y730F) AAV8 mutant (Y733F) and AAV9 mutant (Y446F) in were found to enhance the efficiency of transduction in the retinal ganglion cell layer after intravitreal injection compared with their wild-type counterparts. In addition, AAV2 mutant Y444F (quad Y-F) exhibited a novel property (at the highest titre) in the ability to transduce photoreceptors after intravitreal injection (Petrs-Silva et al., 2011).

In addition to mutations of surface exposed tyrosine (Y) residues, transduction efficiency can further be improved via directed mutagenesis of surface exposed threonine (T) residues to either valine (V) or alanine (A). Both tyrosine (Y−F) and threonine (T−V/T−A) mutations increase transduction efficiency by reducing capsid phosphorylation and subsequent ubiquitination (Zhong et al., 2008; Gabriel et al., 2013). A further study, compared AAV2, AAV5 and AAV8-based vectors containing a combination of Y and T mutations for their transduction ability after intravitreal delivery and identified AAV2 containing four Y to F mutations combined with a single T to V mutation ('quad' Y−F+T−V) as the most efficient vector for transduction of photoreceptors (Kay et al., 2013). Proof of concept studies have shown that incorporation of these mutations can lead to more pronounced rescue in animal models of inherited retinal disease (Boye et al., 2011; Pang et al., 2012) and in one instance, an AAV mutant was able to treat a particularly aggressive form of degeneration that was refractory to treatment using an unmodified parent serotype (Pang et al., 2011). Nonetheless, interfering with the intracellular trafficking poses a risk of viral miss-expression or over-expression, which may have negative effects on tissue survival.

In parallel with directed mutagenesis, a novel technique called directed evolution has been developed to enhance AAV-mediated delivery from the vitreous (Bartel et al., 2012). Thus, through multiple cycles of evolution, large AAV-based libraries are screened in vivo to select for variants of specific cell tropism (Sh10 variant for Muller cells; Klimczak et al., 2009) or improved pan-retinal transduction after intravitreal delivery (7m8 variant, Dalkara et al., 2013) in murine models. Interestingly, the 7m8

variant (parent AAV is AAV2) which reaches outer retina after intravitreal delivery, has lower affinity for the AAV2 primary binding receptor, heparin sulphate. However, with translational studies in mind, it is of note that 7m8 only transduces cells in a small peri-foveal ring in primates with their thicker ILM (Dalkara et al., 2013).

1.4. Extracellular matrix

1.4.1. What is extracellular matrix?

Extracellular matrix is an interlocking mesh of extracellular molecules that provides structural and biochemical support to the surrounding cells and plays a significant role in cell adhesion, cell-to-cell communication and cell differentiation (Abedin and King, 2010). In animals, extracellular matrix is composed of the interstitial matrix and the basement membrane. Interstitial matrix is made of gels of polysaccharides and proteins to act as a compression buffer against the stress placed on the extracellular matrix Basement membrane is a sheet-like deposition of extracellular matrix providing resting support for various epithelial and endothelial cells. Molecular components of the extracellular matrix, fibrous proteins and GAGs are secreted by resident cells into the extracellular matrix via exocytosis and aggregate within the existing matrix.

1.4.2. Glycosaminoglycans and proteoglycans

GAGs are long unbranched polysaccharides typically composed of ~200 repeating diasaccharide units: an uronic acid, followed by an amino sugar. There are five main classes of GAGs which differ in their disaccharide composition, their linkage with the core protein and their degree of sulphation: heparan sulphate (HS; and the related highly sulphated heparin), dermatan sulphate (DS), chondroitin sulphate (CS), hyaluronan (HA) and keratan sulphate (KS) (Figure 1.19). HA is the only GAG that is not bound to a core protein, it typically has more than 200 repeating diasaccharide units and in mammals it is completely unsulphated and ubiquitously expressed in the ECM (Murano et al., 2011). Generally, within the disaccharide unit the uronic acid is

either D-glucuronic or L-iduronic acid and the amino sugar is either D-galactosamine or D-glusosamine, except in keratan sulphate which has galactose instead of the uronic acid (Couchman and Pataki, 2012).

Proteoglycans, PGs, consist of a core protein covalently bound to one or more GAG chains (Heinegard, 2009; Couchman and Pataki, 2012). They are commonly classified according to their associated GAG chains (e.g. HSPGs or CSPGs). PGs can be found in association with the cell membrane (cell surface PGs) or located in the extracellular matrix. Extracellular matrix PGs can be sub-divided into three main families: the basement membrane PGs (e.g. agrin, bamacan, collagen XVIII and perlecan), the hylectans (or lecticans whose core protein usually consists of three domains; e.g. aggrecan, brevican, neurocan and versican) and the small leucine-rich repeat proteoglycan family of PGs whose core proteins are characterised by leucine-rich repeats flanked by cysteine clusters (e.g. decorin, lumican and opticin).

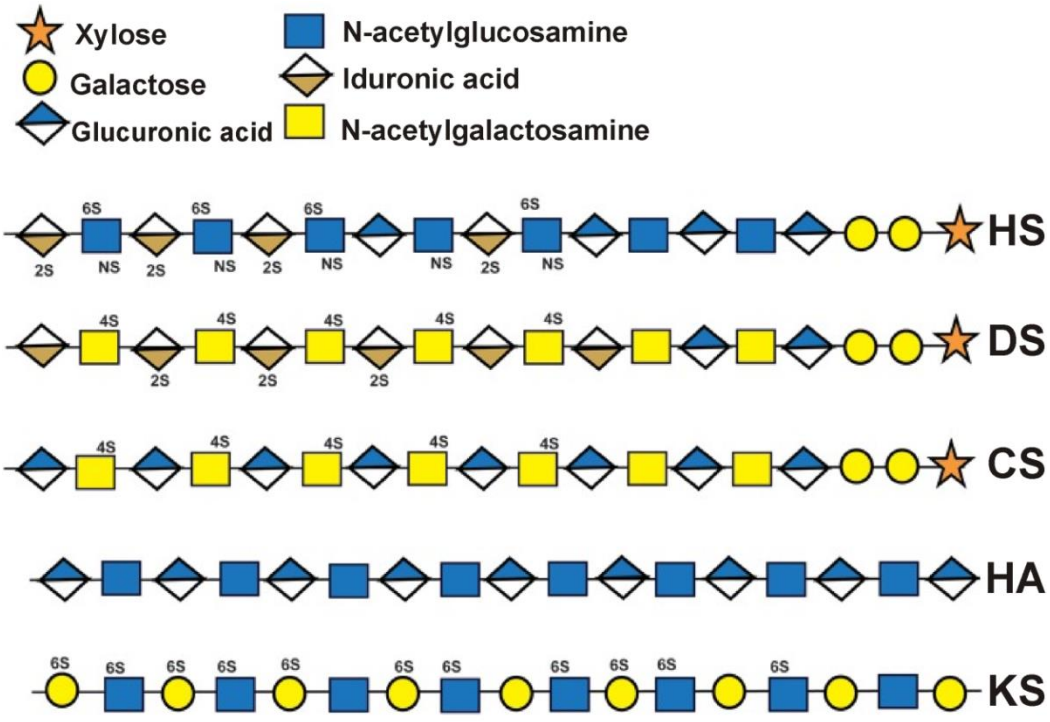

Figure 1.19. Schematic of the typical composition of the mammalian glycosaminoglycans. Heparan sulphate (HS), chondroitin sulphate (CS), dermatan sulphate (DS), hyaluronan (HA) and keratan sulphate (KS). HS, DS, CS and KS contain various degrees of sulphation: 2-O (2S), 4-O (4S), 6-O (6S) and rarely 3-O (3S) sulphation. NS refer to domains of high sulphation. Adapted from Couchman and Pataki, 2012.

PGs have multifunctional roles and may interact with different biologically active molecules (through their core proteins or GAGs) and play important roles in the interactions between cells and the extracellular matrix including the regulation of cell differentiation, proliferation, adhesion, migration and microbial recognition (Iozzo and Schaefer, 2015). In addition, 'sugar code' consisting of region-specific PG modifications holds spatial information required for neurodevelopment (Holt and Dickson, 2005). In the mammalian eye PGs and GAGs are critical in embryological development of the eye and determining the axonal guidance from the retina (Ichijo, 2004). In addition, PGs can contribute to the filtration properties of the Bruch's membrane in the human eye (Booij et al., 2010) and CSPGs are critical in the maintenance of adhesions between RPE and the neurosensory retina (Lazarus and Hageman, 1992).

1.4.3. Extracellular matrix - barrier to AAV transduction from the vitreous

In addition to their roles described above, PGs and GAGs that are found in the intact vitreous, the ILM and the retinal extracellular matrix, could act as barriers to the movement of exogenous particles such as viral vectors from the vitreous, into and through the retina. Each of these extracellular barriers has a different PG and GAG content and concentration (Clark et al., 2011; Keenan et al., 2012) and can therefore lead to a variable level of viral entrapment. For example, HA and CSPGs in the vitreous; HA, CSPGs and HSPGs in the ILM; CSPGs, HSPGs and HA in the retinal matrix, HSPGs and CSPGs in OLM and in interphotoreceptor matrix (IPM, surrounds the rod and cone photoreceptor inner and outer segments) can all trap viral particles and hamper transduction (Figure 1.20). This impedance at the molecular level could be a result of limitation of diffusion and entrapment through electrostatic interactions. The following section gives a brief discussion on how these extracellular barriers (the vitreous, ILM and extracellular matrix of the retina) could inhibit the passage of AAV particles into the retina after they have been injected into the vitreous.

The vitreous contains a network of collagen fibrils and HA. It can act as a diffusional barrier to particles travelling through and out of the vitreous as demonstrated using different sized polymeric nanospheres, 2-µm, 200-nm, and 50-nm, which were able to diffuse out of the rabbit vitreous at variable rates resulting in half-lives of 10.1 ± 1.8, 8.6 ± 0.7 and 5.4± 0.8 days, respectively (Sukurai et al., 2001). Furthermore, nanoparticles of 2-µm diameter, we able to diffuse through the vitreal matrix and were subsequently observed in the trabecular meshwork, whereas those smaller than 200nm, were also observed in the retina and other tissues. In addition, the vitreous can also impede the movement of particles due to charge interactions. An in-vitro study in bovine eyes by Peeters et al (Peeters et al., 2005) showed that the negatively charged vitreal GAGs can interact with polystyrene nanospheres and therapeutic DNA complexed to non-viral carriers – cationic liposomes (LPXs) and cause aggregation. Furthermore, by decreasing the zeta potential of liposomes to become anionic, the researchers showed that binding of the liposome to the GAGs in the vitreous decreased with more homogeneous diffusion. A further in vivo study demonstrated that intravitreally administered anionic human serum albumin nanoparticles (HSA-NPs, zeta potential =-33.3±6.1 mV) diffused freely in the posterior direction from the vitreous to the retina in rat eyes, whereas most of the cationic HSA-NPs (zeta potential = 11.7 ± 7.2mV) were bound and aggregated to the vitreous (Hyuncheol et al., 2009).

A second barrier that can limit movement of particles from the vitreous into the retina is the inner limiting membrane (ILM). ILM is located between retinal Müller cell end feet and the vitreous cortex, and the inner limiting lamina (ILL), found within the ILM, is a true basement membrane of Müller cells. The ultrastructural detail of the ILL reveals a fine 3-D meshwork structure with numerous pores (Nishihara et al., 1989). The diameter of the pores in rabbit's ILM varies from 10 to 25nm with mean diameter of the pores being 13.43nm in the visual streak, 13.59nm in the medullary ray and 13.40nm in the peripheral retina.

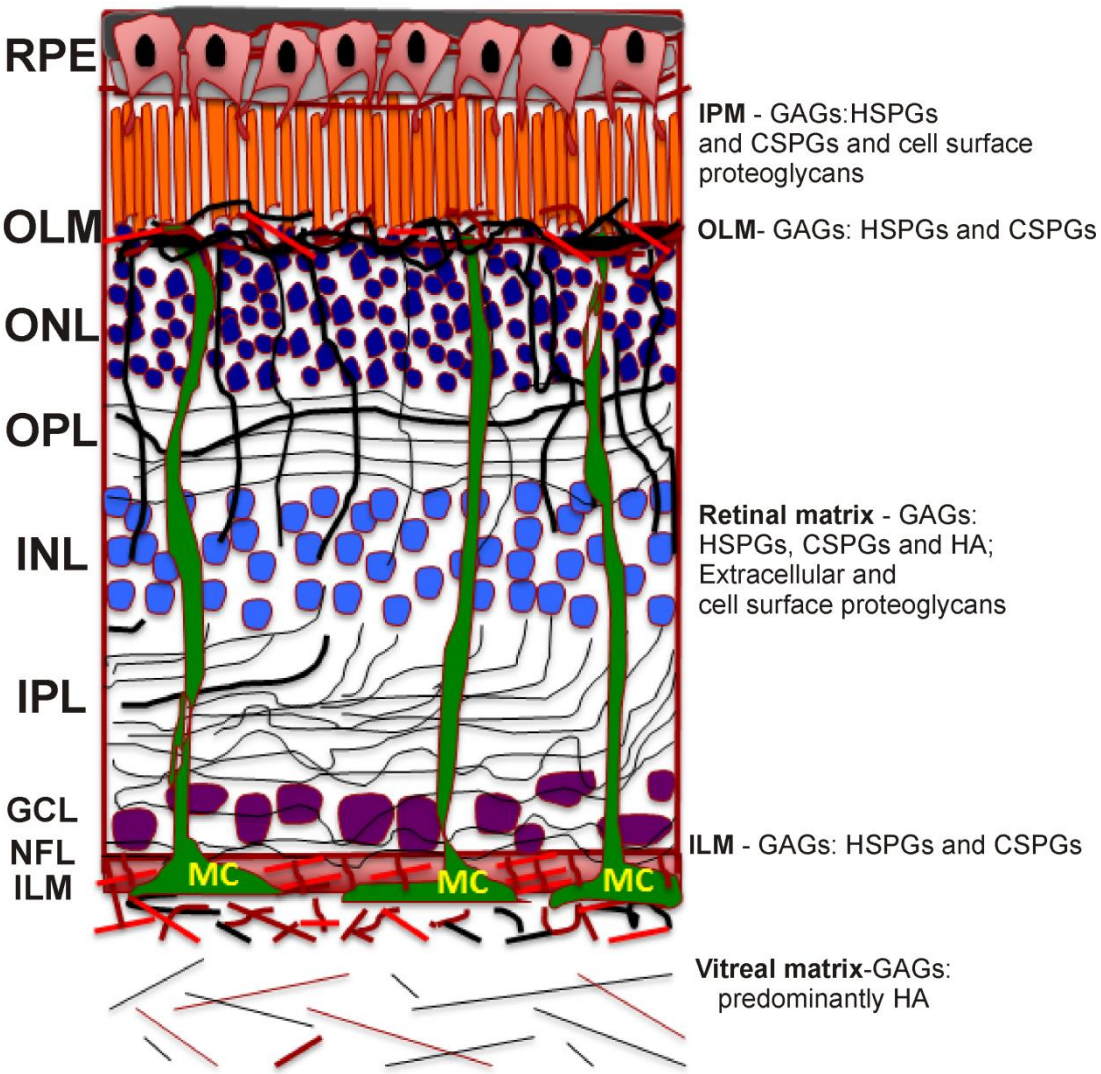

Figure 1.20. Extracellular matrices and cell surface proteoglycans in the retina. These layers form both electrostatic and diffusional barriers that can limit the movement of viral vectors into and through the retina. Each barrier has a different GAG content and concentration and therefore leads to a variable level of viral entrapment. Therefore, HA and CSPGs in the vitreous; HA, CSPGs and HSPGs in the ILM; and CSPGs, HSPGs, extracellular and cell surface proteoglycans in the retina including the interphotoreceptor matrix can all inhibit viral transduction. Glycosaminoglycan (GAG), hyaluronic acid (HA), chondroitin sulphate proteoglycan (CSPG), heparan sulphate proteoglycans (HSPG), inner limiting membrane (ILM), ganglion cell layer (GLC), inner nuclear layer (INL), outer nuclear layer (ONL), outer limiting membrane (OLM), retinal pigment epithelium (RPE), interphotoreceptor matrix (IPM), Muller cell (MC).

In the peripheral retina the pore's shape is different from that in the posterior pole and vitreous fibrils lay densely on it. It is supposed that the bulk of substances must be transported through the ILM of the posterior pole, because dense vitreous fibrils seen in the peripheral retina could make this transport very difficult (Nishihara et al., 1989).

Interestingly, a study by Bourges et al (Bourges et al., 2003) investigated effects of different size and electric charge on kinetics of polylactide nanoparticle localization within the intraocular tissues after single intravitreal injection in rat's eyes and found that for the movement of nanoparticles, the charge and size have little influence on the intraocular tissue distribution of particles smaller than 350nm. Post intravitreal injection, most particles rapidly settle on the ILM with gradual transretinal movement and a later localization in the RPE cells. However, it is likely that the behaviour of the nanoparticles is quite different to that of proteins or viral particles. Moreover, in the above study the researchers discuss a possible rupture of the ILM and modification of vitreo-retinal interface by polylactides, the presence of inflammatory reaction and the activation of the microglial cells which could all affect the permeability of the ILM and contribute to the ease of transretinal movement of the nanoparticles.

The intraocular movement of particles was investigated by Kamei et al. (Kamei et al., 1999) who demonstrated that intravitreally injected 70 kDa tissue plasminogen activator could not diffuse across the ILM in rabbits. Another study of antibodies delivered into the vitreous cavity of rhesus monkey found that Fab antibody fragments (48 kDa) diffused across the retina, but full-length antibodies (148 kDa) did not (Mordenti et al., 1999). However, clinical experience shows that the full-length humanized monoclonal antibody bevacizumab does cross the human retina after intravitreal delivery as it provides an effective treatment for choroidal neovascularisation in age-related macular degeneration. A further in-vitro study by Jackson et al (Jackson et al., 2003) have looked at the maximum size of molecule capable of freely diffusing across human retina, or the retinal exclusion limit (REL) and found this to be 76.5+/-1.5 kDa (6.11+/-0.04 nm). There was only moderate interspecies variation in animal studies including pig, cattle and rabbits (60+/-11.5, 78.5+/-20.5, and 86+/-30 kDa, respectively). Interestingly, they found that the inner

and outer plexiform layers formed the sites of highest resistance to diffusion, even greater than the ILM. Molecules of larger size were capable of crossing the retina although the rate of diffusion was much reduced.

The AAV viral capsid has a total radius between 20-25nm. This would suggest that the size of the pores of the ILM is the main filtration barrier between the retina and the vitreous in rabbit eyes. Furthermore, several negatively charged GAGs (hyaluronan, heparin sulphate, chondroitin sulphate, dermatan sulphate) are abundant in the ILM and these anionic sites make the ILM not only a physical barrier but also an electrostatic barrier between retina and vitreous (Russell et al., 1991). GAGs are also found throughout the retinal and interphotoreceptor matrices. The isoelectric point of the AAV ranges from 5-7 depending on the serotype, indicating an overall negative net charge above pH 7 and an overall positive net charge below neutral pH (Chai et al., 1994). This would suggest that at a physiological intraocular pH of 7.35, AAV would have an overall negative charge and would be repelled in all directions once surrounded by negatively charged GAGs. However, despite the overall negative charge there are positively charged regions on viral capsid surface that would bind GAGs. Indeed once some AAV particles have found their way through the matrices and reached the cell targets they binds GAGs in order to gain entry into the cell (e.g. AAV2 binds heparan sulphate proteoglycan to enter a variety of retinal cells; Summerford and Samulski, 1998).

1.4.4. AAV transduction beyond the ILM

A notable advance in the field of AAV-mediated retinal transduction from the vitreous was made in a recent study by Dalkara et al (Dalkara et al., 2009) where authors identified the ILM as the main barrier for AAV in a serotype-specific manner. AAV serotype capsids were fluorescently labelled with Cy3 and followed their retinal distribution after intravitreal injection in rats. Authors demonstrated that AAV2, 8, and 9 accumulate at the vitreo-retinal junction (Figure 1.20). AAV1 and 5 showed no accumulation – the researchers proposed that they stay dispersed in the vitreous. Furthermore, digestion of the ILM with Pronase E (0.0002%), a nonspecific protease, leads to an improvement in retinal transduction by AAV5. Interestingly, in some degenerate retinas (TgS334ter-3 rat model of ADRP) these barriers seem to be less

critical, leading to better transduction of outer retina and RPE following intravitreal delivery (Kolstad et al., 2010). However, this does not apply to all types of retinal degeneration as in a mouse *rd*^{10} model of less aggressive RP outer retinal targeting by intravitreal injection is very poor (Allocca et al., 2011).

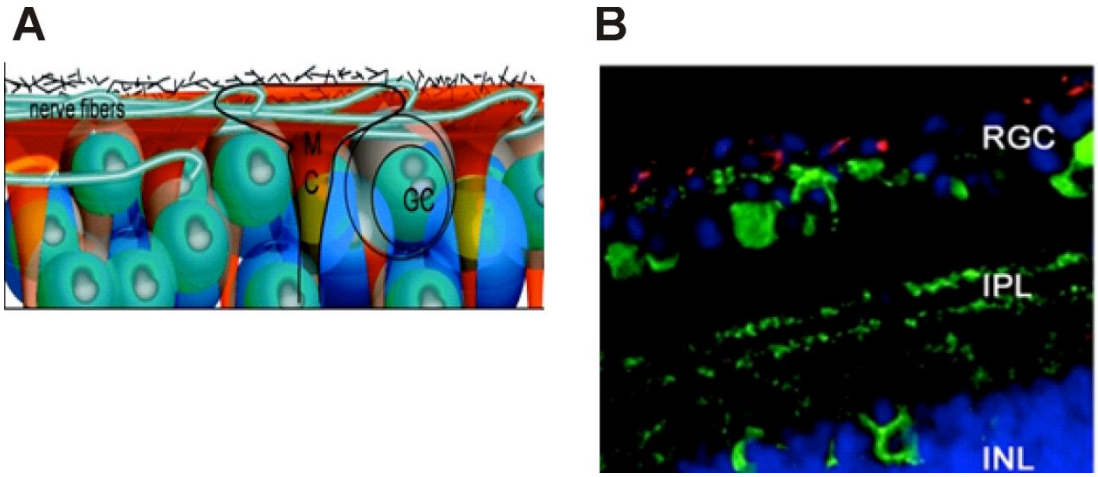

Figure 1.21. AAV particle localisation at the vitreo-retinal junction (A) Schematic representation of the inner limiting lamina (ILM) and overlapping structures at the vitreo-retinal junction. Muller cell (MC), Ganglion cell (GC). (B) Confocal images of AAV2-Cy3 (red) showing accumulation at the ILM following intravitreal delivery. Retinal ganglion cells (RGC), Inner plexiform layer (IPL), Inner nuclear layer (INL). Nuclei are stained with DAPI (blue) and retinal neurons with antibody against calbindin (green) (Adapted from Dalkara et al., 2009).

Interestingly, the lack of retinoschisin (*RS1*) causes a striking change in the properties of the retina and its permeability to AAV vectors. The wild-type murine retinas are not permeable to AAV vectors delivered intravitreally. However, all serotypes tested so far including 2, 5 and 8 are able to penetrate all retinal layers of *RS1*-KO mice and will even transduce the RPE from the vitreous (Park et al., 2009). The absence of *RS1* seems to significantly alter the extracellular matrix properties increasing the porosity of the retina to particles that are at least 25 nm in diameter.

1.4.5. Glycosidic enzymes

Glycosidic enzymes catalyse the hydrolysis of glycosidic bonds in complex sugars. They are a diverse group of enzymes that are found in essentially all domains of life with multifactorial roles and have been implicated in cancer, angiogenesis and neuronal plasticity. They are typically named after the substrate that they act upon, including many constituents of the ECM, and include commercially available enzymes such as heparinase (E.C. 4.2.2.8), chondroitin ABC lyase (E.C. 4.2.2.4) and hyaluronan lyase (E.C. 4.2.2.1), which are commonly used for the study of complex carbohydrates (http://www.sigmaaldrich.com).

1.4.5.1. Actions of glycosidic enzymes

Heparinases and chondroitin ABC lyase are eliminases and so, on cleavage of their respective GAGs they create an unsaturated uronic acid residue (Couchman and Pataki, 2012). Heparinase catalyses elimination of sulphate by acting on linkages between N-acetyl-D-glucosamine and uronate. There are three bacterial heparinases, I, II, and III, each of which has particular substrate specificity in terms of the HS structure it will cleave. For example, heparinase III will cleave at unsulphated domains, and since the domain proximal to the core protein is usually of low sulphation, this enzyme will cleave the polysaccharide close to the core protein.

Chondroitin ABC lyase catalyzes the eliminative degradation of polysaccharides containing (1-4)-b-D-hexosaminyl and (1-3)-b-D-glucuronosyl or (1-3)-a-L-iduronosyl linkages to disaccharides containing 4-deoxy-b-D-gluc-4-enuronosyl groups. It will cleave chondroitin 4-sulfate (CS-A), DS (CS-B), and chondroitin 6-sulfate (CS-C) and it acts slowly on hyaluronate (Enzyme Nomenclature, Academic Press, San Diego, California, 1992).

Hyaluronan lyase catalyses the hydrolysis of HA, lowering its viscosity, and thereby increasing tissue permeability. Its common application is in ophthalmic surgery to speed up dispersion of local anaesthetic (Cehajic-Kapetanovic et al., 2011).

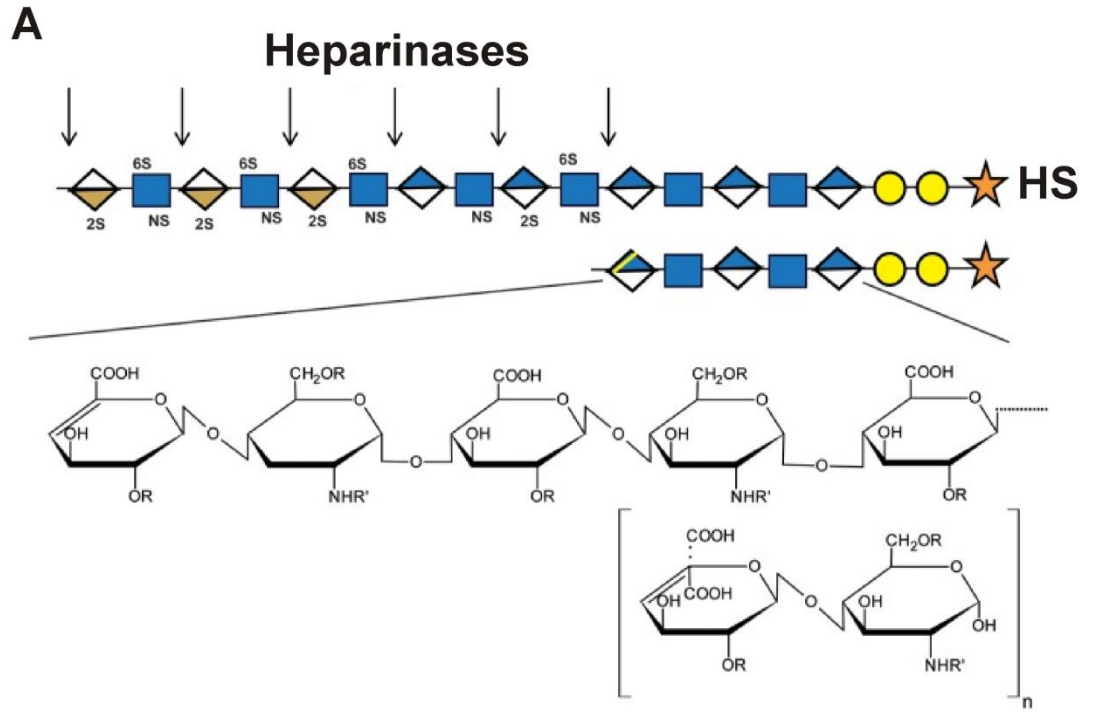
A
Heparinases
HS
6S
NS
2S
COOH
CH2OR
OH
OR
NHR'
n

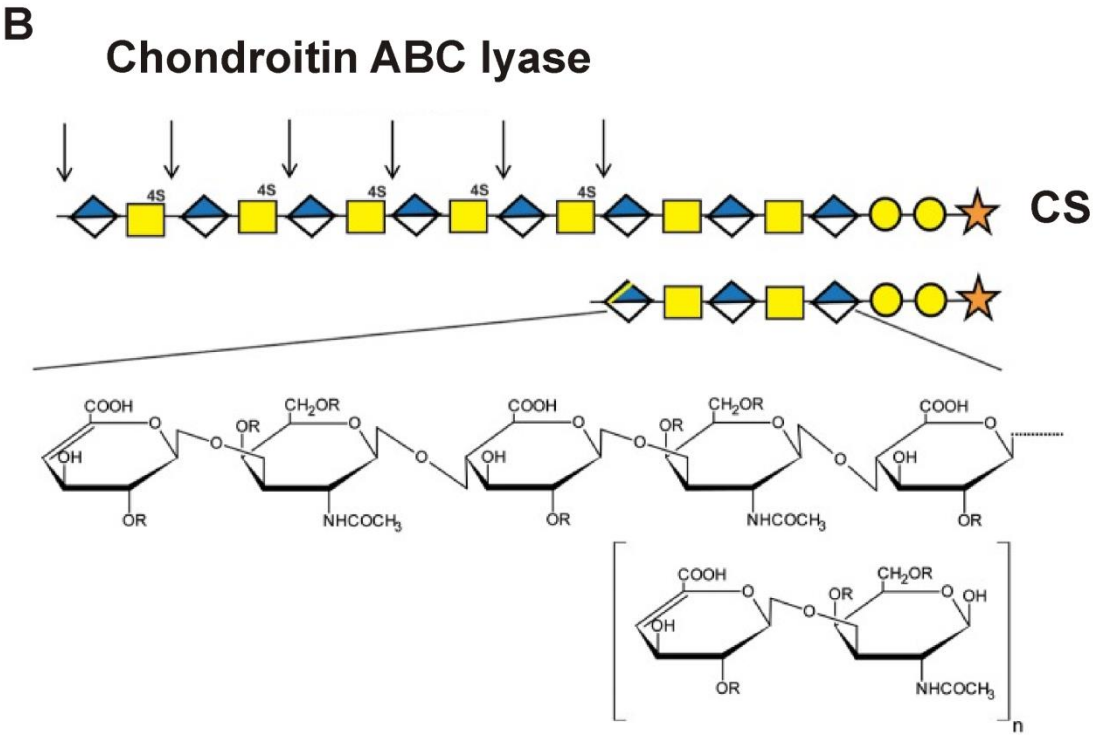
B
Chondroitin ABC lyase
CS
4S
COOH
CH2OR
OH
OR
NHCOCH3
n

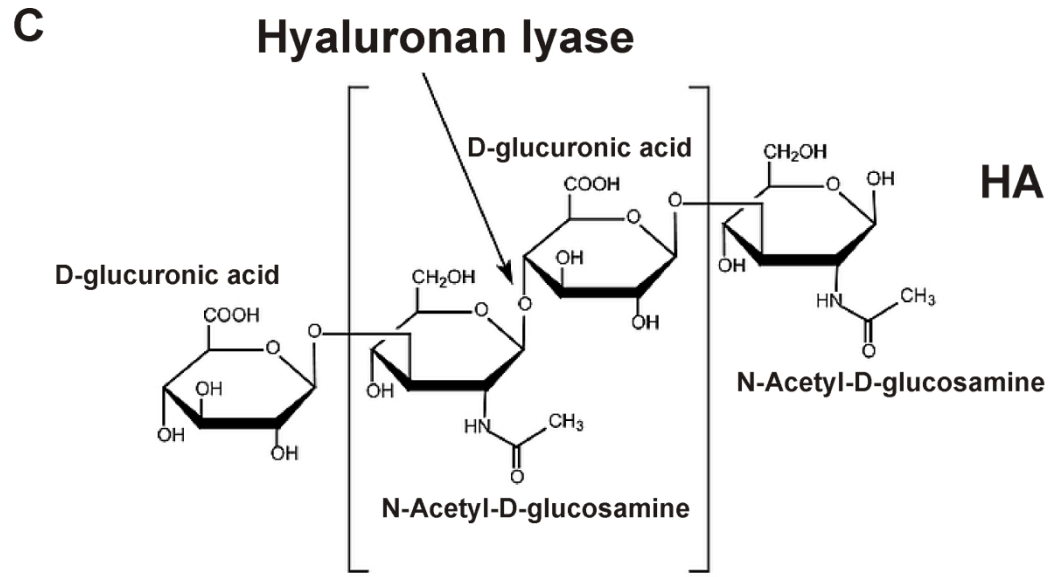

Figure 1.22. Action of heparinises, chondroitin ABC lyase and hyaluronan lyase on their respective GAGs. Action of heparinases on heparan sulphate (HS) is shown in A; action of chondroitin ABC lyase on chondroitin sulphate (CS) is shown in B and action of and hyaluronan lyase on hyaluronan (HA) is shown in C. A and B are adapted from Couchman and Pataki, 2012 and C is adapted from www.sigmaaldrich.com).

1.4.5.2. Glycosidic enzymes enhance retinal gene therapy

In our recent work we showed that ECM degrading glycosidic enzymes markedly improved the efficiency of retinal transduction following intravitreal gene delivery (Cehajic-Kapetanovic et al., 2011). Thus, intravitreal co-injection of AAV2 vector containing cDNA encoding green fluorescent protein (GFP) and heparinase III or chondroitin ABC lyase in adult mice led to marked improvement of retinal transgene expression compared to AAV2 alone. These enzymes not only increased the expression in the GCL, proximal to the vitreous, but in addition they led to an improved penetration of the vector deeper into the retinal tissue. Assessment of retinal function by electroretinograms (ERGs) indicated that ERGs survived with much higher doses of enzymes than were used to achieve enhanced retinal transduction.

1.5. Hypothesis and aims

1.5.1. Hypothesis

1. The photosensitive human G protein coupled receptors, melanopsin and rod opsin, can restore optogenetic visual responses in retinal degeneration with enhanced sensitivity compared to current optogenetic tools.

2. Optogenetic targeting of retinal ON bipolar cells improves spatio-temporal vision compared to non-specific targeting of all surviving cells in the degenerate retina.

1.5.2. Aims

1. To optimise and evaluate safety of AAV2 based gene delivery to the retina following intravitreal injection with glycosidic enzymes.

2. To investigate whether retinal transduction with the optimised vector delivery system carrying melanopsin or rod opsin can restore visual function in mice with an advanced retinal degeneration.

1.6. Appendix 1

RetNet: https://sph.uth.edu/retnet/

Gene and Locus Symbols by Disease Category (One or More Diseases per Gene/Locus)

Disease Category	Mapped Loci (not Identified)	Mapped and Identified Genes
Bardet-Biedl syndrome, autosomal recessive	none	ARL6, BBIP1, BBS1, BBS2, BBS4, BBS5, BBS7, BBS9, BBS10, BBS12, CEP290, IFT172, IFT27, INPP5E, KCNJ13, LZTFL1, MKKS, MKS1, NPHP1, SDCCAG8, TRIM32, TTC8
Chorioretinal atrophy or degeneration, autosomal dominant	none	PRDM13, RGR, TEAD1
Cone or cone-rod dystrophy, autosomal dominant	(- - -), CORD4, CORD17, RCD1	AIPL1, CRX, GUCA1A, GUCY2D, PITPNM3, PROM1, PRPH2, RIMS1, SEMA4A, UNC119
Cone or cone-rod dystrophy, autosomal recessive	CORD8	ABCA4, ADAM9, ATF6, C21orf2, C8orf37, CACNA2D4, CDHR1, CERKL, CNGA3, CNGB3, CNNM4, GNAT2, KCNV2, PDE6C, PDE6H, POC1B, RAB28, RAX2, RDH5, RPGRIP1, TTLL5
Cone or cone-rod dystrophy, X-linked	COD2	CACNA1F, RPGR
Congenital stationary night blindness, autosomal dominant	none	GNAT1, PDE6B, RHO
Congenital stationary night blindness, autosomal recessive	none	CABP4, GNAT1, GPR179, GRK1, GRM6, LRIT3, RDH5, SAG, SLC24A1, TRPM1
Congenital stationary night blindness, X-linked	none	CACNA1F, NYX
Deafness alone or syndromic, autosomal dominant	none	WFS1

Deafness alone or syndromic, autosomal recessive	none	CDH23, CIB2, DFNB31, MYO7A, PCDH15, PDZD7, USH1C
Leber congenital amaurosis, autosomal dominant	none	CRX, IMPDH1, OTX2
Leber congenital amaurosis, autosomal recessive	none	AIPL1, CABP4, CEP290, CRB1, CRX, DTHD1, GDF6, GUCY2D, IFT140, IQCB1, KCNJ13, LCA5, LRAT, NMNAT1, PRPH2, RD3, RDH12, RPE65, RPGRIP1, SPATA7, TULP1
Macular degeneration, autosomal dominant	BCAMD, BSMD, MCDR3, MCDR4, MCDR5, MDDC	BEST1, C1QTNF5, EFEMP1, ELOVL4, FSCN2, GUCA1B, HMCN1, IMPG1, PRDM13, PROM1, PRPH2, RP1L1, TIMP3
Macular degeneration, autosomal recessive	none	ABCA4, CFH, DRAM2, IMPG1
Macular degeneration, X-linked	none	RPGR
Ocular-retinal developmental disease, autosomal dominant	none	VCAN
Optic atrophy, autosomal dominant	OPA4, OPA5, OPA8	MFN2, NR2F1, OPA1
Optic atrophy, autosomal recessive	OPA6	TMEM126A
Optic atrophy, X-linked	OPA2	TIMM8A
Retinitis pigmentosa, autosomal dominant	RP63	BEST1, CA4, CRX, FSCN2, GUCA1B, HK1, IMPDH1, KLHL7, NR2E3, NRL, OR2W3, PRPF3, PRPF4, PRPF6, PRPF8, PRPF31, PRPH2, RDH12, RHO, ROM1, RP1, RP9, RPE65, SEMA4A, SNRNP200, SPP2, TOPORS
Retinitis pigmentosa, autosomal recessive	RP22, RP29, RP32	ABCA4, ARL6, ARL2BP, BBS1, BBS2, BEST1, C2orf71, C8orf37, CERKL, CLRN1, CNGA1, CNGB1, CRB1, CYP4V2, DHDDS, DHX38, EMC1, EYS, FAM161A, GPR125, HGSNAT, IDH3B, IFT140, IFT172, IMPG2, KIAA1549, KIZ, LRAT, MAK, MERTK, MVK, NEK2, NEUROD1, NR2E3, NRL, PDE6A, PDE6B, PDE6G,

		PRCD, PROM1, RBP3, RGR, RHO, RLBP1, RP1, RP1L1, RPE65, SAG, SLC7A14, SPATA7, TTC8, TULP1, USH2A, ZNF408, ZNF513
Retinitis pigmentosa, X-linked	RP6, RP24, RP34	OFD1, RP2, RPGR
Syndromic/systemic diseases with retinopathy, autosomal dominant	CORD1	ABCC6, ATXN7, COL11A1, COL2A1, JAG1, KCNJ13, KIF11, MFN2, OPA3, PAX2, TREX1, VCAN
Syndromic/systemic diseases with retinopathy, autosomal recessive	CORS2, FHASD, MRST, WFS2	ABCC6, ABHD12, ACBD5, ADAMTS18, AHI1, ALMS1, CC2D2A, CEP164, CEP290, CLN3, COL9A1, CSPP1, ELOVL4, FLVCR1, GNPTG, HARS, HGSNAT, HMX1, IFT140, INPP5E, INVS, IQCB1, LAMA1, LRP5, MKS1, MTTP, NPHP1, NPHP3, NPHP4, OPA3, PANK2, PCYT1A, PEX1, PEX2, PEX7, PHYH, PLK4, PNPLA6, POC1B, PRPS1, RDH11, RPGRIP1L, SDCCAG8, TMEM237, TTPA, TUB, TUBGCP4, TUBGCP6, WDPCP, WDR19, WFS1, ZNF423
Syndromic/systemic diseases with retinopathy, X-linked	(- - -)	OFD1, TIMM8A
Usher syndrome, autosomal recessive	USH1E, USH1H, USH1K	ABHD12, CDH23, CEP250, CIB2, CLRN1, DFNB31, GPR98, HARS, MYO7A, PCDH15, USH1C, USH1G, USH2A
Other retinopathy, autosomal dominant	CACD, CODA1, EVR3, MCDR4	BEST1, CAPN5, CRB1, FZD4, ITM2B, LRP5, MIR204, OPN1SW, RB1, TSPAN12, ZNF408
Other retinopathy, autosomal recessive	RNANC, VRD1	BEST1, C12orf65, CDH3, CNGA3, CNGB3, CNNM4, CYP4V2, LRP5, MFRP, MVK, NR2E3, OAT, PLA2G5, PROM1, RBP4, RGS9, RGS9BP, RLBP1
Other retinopathy, mitochondrial	none	KSS, LHON, MT-ATP6, MT-TH, MT-TL1, MT-TP, MT-TS2
Other retinopathy, X-linked	PRD	CACNA1F, CHM, DMD, NDP, OPN1LW, OPN1MW, PGK1, RS1

Appendix 1. A comprehensive list of gene and locus symbols by disease category (One or More Diseases per Gene/Locus)**.** Adapted from **RetNet:** https://sph.uth.edu/retnet/.

Chapter 2: Materials and methods

See also methods sections of individual papers/results chapters

2.1. Animals

Adult C57BL/6J (*wild-type*) and homozygous C3H/HeJ (*rd*^{1}) mice were used in experimental procedures. *Wild-type* and *rd*^{1} mice were used in vector optimisation studies (Chapter 3) and *rd*^{1} mice were used in subsequent vision recovery studies (Chapters 4 and 5). All animal experiments were conducted in accordance with the UK Home Office regulations for the care and use of laboratory animals, the UK Animals (Scientific Procedures) Act (1986) and the Animal Welfare Body of the University of Manchester. Animals were kept under a 12-hour light-dark cycle and supplied with food and water *ad libitum.*

Figure 2.1. The *rd*^{1} mouse model of retinal degeneration.

Take from http://www.thetimes.co.uk/tto/science/article4525577.ece

2.1.1. Critical analysis: Why *rd¹* mouse model?

The exceptional genetic diversity of RP in humans described earlier in Chapter 1 is reflected in the large collection of retinal degeneration (rd) mutations available in RP mouse models (Chang et al., 2002). We chose to study the *retinal degeneration 1* (*rd¹,* rodless, Pde6b^{rd1}) mouse, with a homozygous nonsense mutation in exon 7 (codon 347) of the *Pde6b* gene (Pittler et al., 1991; Bowes C et al., 1993). This results in a deficient activity of the rod-specific cGMP-phosphodiesterase and leads to early onset, rapidly progressing photoreceptor degeneration. Degeneration starts with fast onset rod photoreceptor dystrophy at postnatal day 8 (P8) (Carter-Dawson et al., 1978; Farber et al., 1994; Barabas et al., 2010). The vast majority of rod photoreceptors are lost soon after their terminal differentiation and essentially absent by P30 (Sancho-Pelluz et al., 2008). A single layer of cone photoreceptors remains that subsequently degenerate, through unknown mechanisms, and only a small subset in the peripheral retina remains by P90 (Faber et al., 1974; Faber et al., 1976; Carter-Dawson et al., 1978; García-Fernández et al., 1995; Farber et al., 1994; Hart et al., 2005). The cone outer segments are misshaped and presumed dysfunctional, which manifests in an undetectable ERG at P21 (Gibson et al., 2013) and a total loss of image-forming vision by P40 (Carter-Dawson et al., 1978).

During this early developmental period when photoreceptors are being lost, inner retinal circuits are being established (Coombs et al., 2007). In *rd¹* mice RGC activity is normal in early post-natal period before eye opening (~P12) after which ensues a critical period of active synaptogenesis and significant remodelling of inner retinal circuits (~P12-P30). During this time RGC signalling to brain exhibit hyperactivity, firing spontaneously at higher rates than normal. In addition, OFF responses are preferentially preserved in a brief period before light-evoked RGC activity is completely lost (Stasheff, 2008; Stasheff et al., 2011).

We chose to study *rd¹* mice for several important reasons: (1) due to early and rapid loss of photoresponses, these mice become essentially blind, and any recorded light-evoked responses or observed visual behaviour should be secondary to therapeutic

interventions; (2) despite the photoreceptor loss, inner retinal neurons survive and remain electrically active and amenable to optogenetic therapy (Strettoi and Pignatelli, 2000; Mazzoni et al., 2008); (3) higher than normal RGC baseline firing rates should allow for the detection of both light evoked increases and decreases in firing rates driven by ectopic expression of depolarising (melanopsin; see Chapter 4) and hyperpolarising (rod opsin; see Chapter 5) optogenetic sensors; (4) importantly, the disease causing mutation does not directly affect our choice of a replacement optogenetic sensor (rod opsin); (5) its phenotype resembles that of human patients with RP carrying mutation in *Pde6b* gene (McLaughlin et al., 1995) (6) it has become a standard in most vision recovery studies, making comparisons between studies possible, and (7) it is a relatively inexpensive and accessible model amongst laboratory mice.

Chapter 6 discusses the limitations of this mouse model with a reference to alternative rodent and other animal models and their suitability for the study of therapeutic approaches in retinal degeneration.

2.2. Gene delivery via AAV vectors

In order to determine the optimum combination of AAV2 vector and glycosidic enzymes for enhanced retinal transduction efficiency following intravitreal delivery, AAV2 vector constructs were injected into healthy *wild-type* eyes as well as into *rd*[1] eyes. All vectors were obtained from Vector Biolabs, Philadelphia, USA. The vectors contained the enhanced green fluorescent protein (GFP) gene under the control of a strong ubiquitous pan-neuronal promoter (CAG, a fusion of CMV early enhancer and chicken β-actin promoter, called AAV2-CAG-GFP) or a cell specific ON-bipolar cells promoter (grm6; 36), a fusion of 200-base pair enhancer sequence of the mouse grm6 gene encoding for ON-bipolar cell specific metabotropic glutamate receptor, mGluR6, and an SV40 eukaryotic promoter, called AAV2-grm6-GFP. The gene-promoter sequence was flanked by inverted terminal repeat (ITR) domains and stabilised by

polyadenylation signal sequence (polyA) and a woodchuck hepatitis posttranscriptional regulatory element (WPRE) (Figure 2.2 A-B).

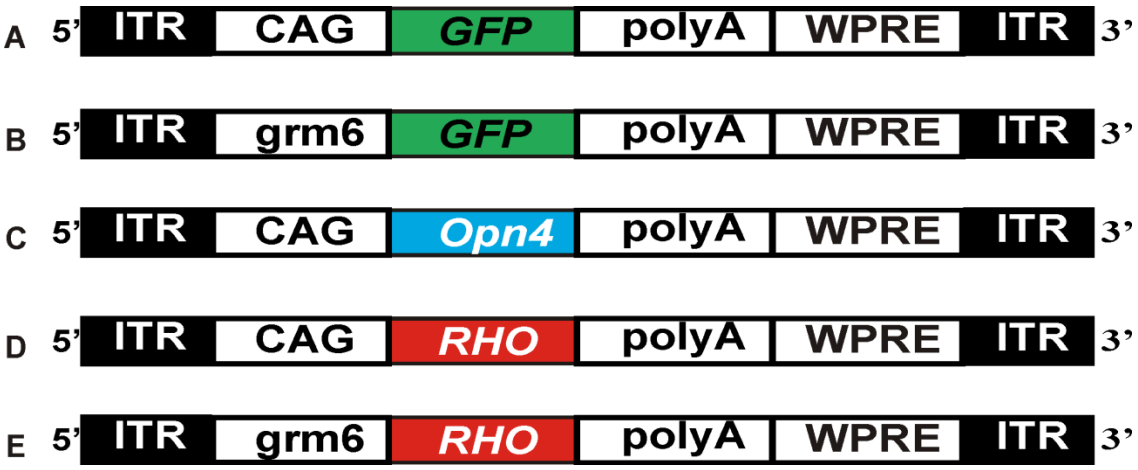

Figure 2.2. Schematic diagram of cDNA constructs carried by AAV2 vector. Transgenes of interest (enhanced green fluorescent protein, *GFP*, melanopsin, *Opn4* and rod opsin, *RHO*) are driven by either a ubiquitous, CAG promoter (a hybrid of CMV enhancer/chickenβ-actin promoter) or by ON-bipolar cells specific promoter, grm6 (a fusion of 200-base pair enhancer sequence of the mouse grm6 gene encoding for ON-bipolar cell specific metabotropic glutamate receptor, mGluR6, and an SV40 eukaryotic promoter). The gene-promoter sequences are flanked by inverted terminal repeats (ITRs) and stabilised by a polyadenylation signal sequence (polyA) and a woodchuck hepatitis posttranscriptional regulatory element (WPRE).

Vectors were injected intravitreally in isofluorane anaesthetised mice at >8 weeks of age. In addition, for vision recovery studies in *rd*[1] mice three further constructs were used, carrying optogenetic sensor genes, melanopsin (*Opn4*) gene under the control of a ubiquitous CAG promoter (see Chapter 4) and rod opsin (*RHO*) gene under the control of CAG or the ON bipolar cell specific grm6 promoter (see Chapter 5) (Figure 2.2 C-E). Prior to injections, pupils were dilated with tropicamide (1%; Chauvin Pharmaceuticals, UK) and phenylephrine (2.5%; Chauvin Pharmaceuticals, UK). A custom made ultra-fine needle (Hamilton RN needle 34 gauge, supplied by ESSLAB) was attached to a 5μl Hamilton glass syringe and was passed at 45 degrees through the pars plana into the vitreous cavity without retinal perforation. The injection was

performed under a direct visualisation of the needle tip through cover-slipped eyes under an operating microscope (Microscopes Inc., USA) carefully avoiding lenticular contact and blood vessels.

In vector optimisation studies (see Chapter 3) AAV2-CAG-GFP was injected at a low or high dose and AAV2-grm6-GFP at a high dose only. Eyes that were injected with low dose vector received 1 µl of 2x 10^{11} genomic counts (gc)/ml (i.e. 2 x 108 gc/eye) and those that were injected with high dose vector received 3µl of 1x10^{13} gc/ml (i.e. 3 x 1010 gc/eye). Each eye that was injected with enzymes, received 0.5µl of solution containing 0.125 units of chondroitin ABC lyase from Proteus vulgaris (E.C. 4.2.2.4), heparinase III from Flavobacterium heparinum (E.C. 4.2.2.8) or hyaluronan lyase from Streptomyces hyalurolyticus (E.C. 4.2.2.1) singly or in different combinations (all from Sigma-Aldrich, Dorset, UK). The chondroitin ABC lyase digests chondroitin sulphate, dermatan sulphate and hyaluronan to some extent, heparinase III specifically digests heparan sulphate (and heparin), and the hyaluronan lyase specifically digests hyaluronan. The enzyme solutions were made fresh on the day of injection by dissolving the enzymes in sterile phosphate-buffered saline (PBS). The vector and enzymes were mixed in a syringe immediately before an eye injection and were given in a single combined injection.

In vision recovery studies, optimised vector-enzyme combination was used. Therefore AAV2 carrying 'optogenes' (*Opn4* or *RHO*) was injected so that each eye received 3µl of viral construct containing 1x10^{13} genomic counts, in combination with 0.5µl of glycosidic enzyme solution containing 0.125 units of heparinise III and hyaluronan lyase.

2.3. Tissue processing, immunohistochemistry, bioimaging and transduction efficiency studies

2.3.1. Tissue processing

Retrieved eyecups (>6 weeks post injections) were fixed in 4% paraformaldehyde (PFA) in PBS for 24 hours at 4^{o} C after the cornea and lens had been removed anteriorly under a light microscope. The tissue was then washed in PBS prior to incubating in in PBS containing 30% sucrose overnight at 4^{o} C. For whole-mounts (AAV2-GFP injected eyes) fixed eyes were washed in PBS and whole retinas were carefully dissected under a light microscope. Retinas were then flat-mounted with fluorescent mounting media containing DAPI (Vectashield, Vector Laboratories Ltd., Peterborough, UK) to stain cell nuclei. For cryosections, fixed eyes were cryo-protected in optimal-cutting temperature medium (Raymond A Lamb Ltd., Eastbourne, UK) and frozen at -80^{o} C until further processing. The cryo-protected retina was sectioned (8-10µm thickness) on a cryostat (Leica, Microsystems) horizontally through the eyecup from ventral to dorsal sides, so that each section contained a complete nasal to temporal cross-section of the retina. For quantification of GFP expressing cells six-eight sections were collected on each slide containing sections representative of the entire retina; for immunostaining analysis slides contained ~12 sections covering the entire retina. Slides were stored at -80^{o} C.

2.3.2. Immunohistochemistry

Prior to analysis slides were removed from the freezer and allowed to air-dry at room temperature for 1 hour. AAV2-GFP injected eyes were mounted directly onto slides with fluorescent mounting media containing DAPI (Vectashield, Vector Laboratories Ltd., Peterborough, UK) to stain cell nuclei. For immunohistochemistry, sections were permeabilised by immersing slides in PBS with 0.2% Triton for 20 minutes at room temperature. Following this, sections were background blocked with PBS with 0.2% Triton X-100 containing 10% donkey serum (D9663; Sigma, UK) for 1 hour at room temperature. Primary antibodies (Polyclonal Rabbit Anti-Human Melanopsin, Abcam, Ab65641 or Rabbit Anti-Human Rhodopsin, Abcam, Ab112576) were applied to

AAV2-*Opn4* or *RHO* injected eyes respectively, at 1:200 dilutions in blocking buffer (PBS with 0.2% Triton X-100 and 2.5% donkey serum) for 3 hours at room temperature. After washing in tween 0.05% PBS, four times for 10 minutes, sections were incubated with secondary antibody (Alexa Fluor® 546 Donkey Anti-Rabbit IgG (H+L) Antibody, Life Technologies, lot: 1504518) diluted 1:200 in PBS with 0.2% Triton X-100 and 2.5% donkey serum for 2 hours at room temperature. Slides were then washed four times for 10 minutes in 0.05% tween PBS followed by one final wash with dH_20. After removing excess fluid, slides were mounted with fluorescent mounting media containing DAPI (Vectashield, Vector Laboratories Ltd., Peterborough, UK) to stain cell nuclei.

2.3.3. Bioimaging

Imaging was performed under fluorescent upright microscope (Olympus BX51) using several objectives (4x, 10x or 20x/ 0.30 Plan Fln) and images were captured using a Coolsnap ES camera (Photometrics) and processed through MetaVue Software (Molecular Devices). Images were then analysed using ImageJ software (http://rsb.info.nih.gov/ij).

2.3.4. Quantitative analysis of vector transduction efficiency (see Chapter 3)

For quantification of GFP+ cells in retinal sections one slide per eye (containing 6-8 sections) for each treatment group (n=4) was taken for analysis and all retinal sections were examined on these selected slides. Sections were photographed at x4 using the fluorescent microscope and the length of each section measured along the retinal surface in Image J. All sections were then re-photographed at x10 in order to count GFP+ cells. Transduced GFP+ cells were identified on the basis of their laminar location and morphology. GFP+ cells were counted and documented according to the retinal layer in which they were found including the GCL, INL and ONL. The quantification was performed with examiner being blind to the treatment group. The total number of GFP+ cells per eye was divided by the total retinal length for that eye.

Data for each group is presented in scatter plots with mean cell count per mm retinal section ± SEM. Differences between groups were evaluated using ordinary one-way ANOVA followed by Turkey's multiple comparison's test in Graph Pad Prism (V6; Graph Pad, USA). Significance was set at $p<0.05$.

2.3.5. Critical analysis of vector optimisation studies

One of the main limiting factors in gene therapy studies is the large variability in retinal transgene expression following vector delivery. Thus, the same vector dose can lead to varying degrees of patchy expression between different retinas, making quantitative comparisons between different treatment groups rather challenging. Several important advances in the vector optimisation studies were made from our previous published work on enhancing retinal gene therapy with glycosidic enzymes (Cehajic-Kapetanovic et al., 2011) in order to minimise expression variability. These optimisation studies included refinements in intravitreal injection technique, doses of vector-enzyme combinations injected (see Chapter 3 for details) timing of transgene expression (6 weeks compared to 2 weeks used previously) tissue processing (expression examined in cryosections compared to previously used whole-mounts) and quantification analysis (based on quantifying GFP+ cells in cryo-sections compared to overall retinal fluorescence used previously). Improving the intravitreal injection technique was one of the most significant factors that contributed to the reduction in expression variability. Thus, intravitreal injections were performed under direct visualisation of the needle tip (custom made) under the operating microscope to ensure delivery of the vector into the correct space with minimal regurgitation and trauma to the surrounding tissue, including retinal perforation, that could lead to the deposition of the vector into the subretinal space and further confound the efficacy of the intravitreal treatment.

2.4. Electroretinography

2.4.1. The electroretinogram (ERG)

Retinal neurons except for RGCs (which signal via action potentials) signal through graded changes in membrane potentials in order to propagate visual information through the retina. This variation in the electrical field potential of retinal neurons is measurable at the corneal surface of the eye and is called the electroretinogram (ERG). Figure 2.3 depicts the basic ERG components, attributed to specific neuronal events, which are derived after light stimulation of the retina.

The ERG has become an essential tool for evaluation of retinal function and sensitivity, providing a non-invasive and repeatable measurement of retinal activity. It can be recorded in both dark-adapted (scotopic) and light-adapted (photopic) conditions in order to isolate specific rod- or cone-driven responses respectively (Peachey et al., 1993). Thus under low light intensities in scotopic conditions primed for rod sensitivity, rod-specific responses can be isolated. In contrast, ERG recorded under rod-saturating, photopic, light background, gives a cone-dominant ERG following a bright flash of light. Photopic responses result in small b-wave amplitudes with a short latency (~30-32 ms), whereas scotopic responses give much larger b-wave amplitudes with a longer latency (~60 ms).

2.4.2. Types of ERG

In addition to the full-field ERG described above there are several other ERG types that complement the assessment of retinal function. With full-field flash ERG that produces the massed retinal electrical potential response, the small isolated retinal lesions may not be revealed. Thus, the focal ERG (also referred to as the foveal ERG) exists to measure the functional integrity of the central retina including the fovea. In addition, localised retinal abnormalities can be detected by multifocal ERG which simultaneously measures focal retinal responses from up to 250 different retinal locations within the central 30 degrees mapped topographically. The pattern ERG

uses pattern-reversal stimuli to record RGC activity (N95 waveform component) and detect optic neuropathies.

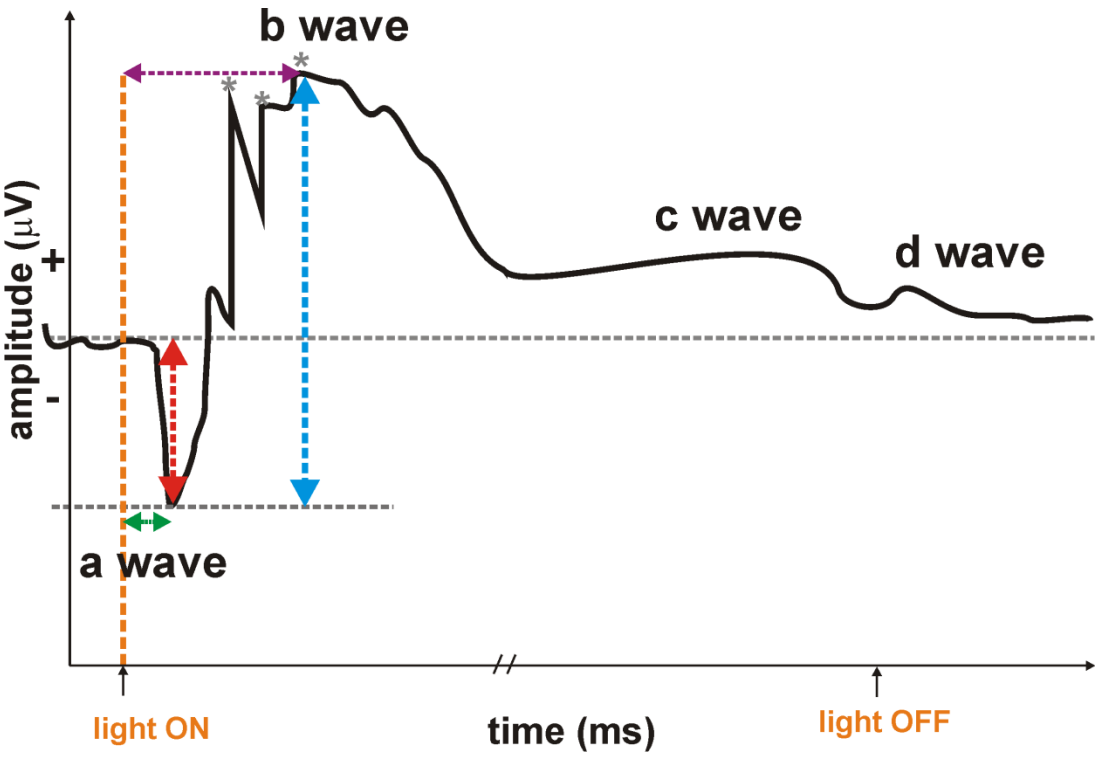

Figure 2.3. The ERG waveform. Typical ERG components are shown following full-field light onset: **the a-wave** – initial fast (<20ms) corneal-negative deflection, derived from hyperpolarisation of outer retinal photoreceptors, rods and cones; **the b-wave** – corneal positive deflection derived from the inner retina, predominantly originating from depolarising ON-bipolar cells and bipolar cell dependent K+ currents affecting Muller cells (occurs ~60-100ms); **the c wave** – a slow positive wave at ~500ms after light onset (peaks >2s) derived from the 'trans epithelial' RPE potential in response to the reduction in extracellular (K+) and hyperpolarisation of the apical RPE cell membrane (and of distal portion of the Muller cells) which is driven by hyperpolarisation of photoreceptors; **the oscillatory potentials** – fast, high frequency (~100-160 Hz) deflections on the rising edge of a b-wave (asterisks) most likely to originate within the IPL from different neuronal subtypes including amacrine cells; **the d wave** – a positive deflection observed with longer stimulus duration (not a flash) upon light offset and derived from hyperpolarisation of OFF bipolar cells. Typical measurements used in the analysis of ERGs are also shown: the implicit time of a-wave- time from flash onset to the peak of a-wave (green); the implicit time of b-wave- time from flash onset to the peak of b-wave (purple); a-wave amplitude –

measured from baseline to the trough of the a-wave (red); b-wave amplitude – measured from trough of the a-wave to the peak of the b-wave (blue).

2.4.3. The experimental protocol (see also Chapter 3)

In order to evaluate the safety of newly developed vector-enzyme combinations for gene delivery, retinal function was tested in *wild-type* mice at one week, six weeks and twelve months after intravitreal injections. Mice were dark adapted overnight (>12 hours) and prepared for full-field ERG recordings under dim red light (at 0.6 $\log_{10}$ cd/m^2 at 650 nm). Anaesthesia was induced with an intraperitoneal injection of a mixture of ketamine (75 mg/ml, 10%) and xylazine (13.6 mg/ml, 20%). Pupils were dilated with topical mydriatics (tropicamide 1% and phenylephrine 2.5%; Chauvin Pharmaceuticals, UK) prior to placement of a corneal contact-lens type electrode, held in place by a drop of hydroxypropyl methylcellulose solution (0.5%; Alcon Laboratories, Ltd., UK). The mice were placed onto a silver wire bite bar which provided head support and it acted as a ground. A needle reference electrode (Ambu, Neuroline) was inserted subcutaneously into the left cheek. Electrodes were connected to a Windows PC via a signal conditioner (Model 1902 Mark III, CED, UK), which differentially amplified (×3000) and filtered (band-pass filter cut-off 0.5 to 200 Hz) the signal, and a digitizer (Model 1401, CED). ERG signals were averaged three to six times to reduce noise. Core body temperature was maintained throughout the procedure with a homeothermic heat mat (Harvard Apparatus).

Both dark-adapted (scotopic) and light-adapted (photopic) ERGs were recorded. Scotopic ERGs were performed in dark and elicited by 15ms full-field flashes produced by a light source (Cold White LED, 800 mW Thorlabs) fitted with neutral density (ND) filters in an ascending intensity series (retinal irradiances in the range 14.6-6.6 log photons/cm^2/s). Average response waveforms for each individual were produced from between 30 and 6 stimulus repeats applied at inter-stimulus intervals ranging from 1500 ms at dimmest intensities to 30s at brightest intensities to avoid significant bleaching of the visual pigment. Photopic ERGs were performed under room illumination and elicited by bright white flashes (10 μs duration at ND0; peak retinal irradiance 14.6 log photons/cm^2/s) recorded over 20 min at a frequency of

0.75 Hz, presented against a rod-saturating background white light. The amplitude of the a-wave was measured from the baseline prior to stimulus onset to the primary trough of negative polarity voltage. The amplitude of b-wave was determined from the a-wave trough to the maximum of the secondary positive peak. Data for each group is presented in scatter plots with mean amplitude ± SEM. Irradiance response curves (IRCs) were fitted with sigmoidal function. Statistical differences between groups were evaluated in Graph Pad Prism (V6; Graph Pad, USA) using ordinary one-way ANOVA followed by Dunnett's post-test (comparing group means to control PBS or AAV2 group), Turkey's post-test (multiple comparisons of group means between all groups) or in instances when only 2 groups were compared, two-tailed paired t-tests were used to compare response between enzyme and PBS-injected eyes. Significance was set at $p<0.05$.

2.4.4. Limitation of ERG studies

The main limitation of ERG functional studies is the large variability in recorded ERG amplitudes between different eyes. This can be due to naturally occurring range that is observed for a particular strain of mice but can also be influenced by the length of dark adaptation and the position of electrodes on the cornea. Importantly, the length of dark adaptation was minimised as much as possible and corneal electrodes were carefully positioned in order to minimise noise and artefacts. In addition, experiments were designed so that one particular treatment group had an equal representation of left and right eyes, in order to minimise any differences originating from 'noisy' or 'faulty' left or right electrodes in any one experiment.

Another important limitation of the ERG technique is that it requires integrity of the eye optics in order to get meaningful recordings. Careful intraocular injection technique is necessary to prevent any lenticular touch and cataract formation which may lead to differences in recorded amplitudes. Although no obvious cataracts were observed at the time of recordings, small lenticular opacities cannot be excluded. Moreover, some eyes had persistent vitreous haemorrhage (noted at the time of injections), at recordings performed at week 1 post treatment significantly reducing

the ERG amplitudes, so experiments had to be repeated at week 6 in order to draw firm conclusions about the effect of treatment on the retinal function.

Since only full-field flash ERG (but not pattern ERG) was established in our laboratory, RGC activity could not be directly tested using the ERG studies. In addition, pattern ERGs require more involved procedures and stimulus presentation and give relatively small signals compared to full-field ERGs requiring more complex analysis. However, since RGCs are the first neurons that intravitreally injected enzymes come into contact, it was imperative to evaluate RGC function. The pupillometry, described below, was therefore used in order to assess RGC function.

2.5. Pupillometry

2.5.1. The pupillary light reflex (PLR)

The pupillary light reflex, PLR, is a physiological response that allows a regulation in pupil size relative to ambient light intensity, through a well characterised PLR pathway (Figure 2.4). Its main function is to protect the photoreceptors from high light intensities (hence, pupil constricts in response to bright lights to reduce the amount of light reaching the retina) and to act as an aperture and control the depth of field. The inner (ipRGCs) and outer retina (rods and cones) make unique contributions to the PLR. The PLR is retained in mice lacking rods and cones (*rd/rd cl*, Lucas et al., 2001a) but only at relatively high light intensities. In mice lacking melanopsin (*Opn4 -/-)* the pupil only constricts to ~20% of the *wild-type* area (Lucas et al., 2003; Panda et al., 2003) indicating that melanopsin is necessary for the maximum pupil constriction, whereas rods and cones define the sensitivity and the speed of evoked PLR.

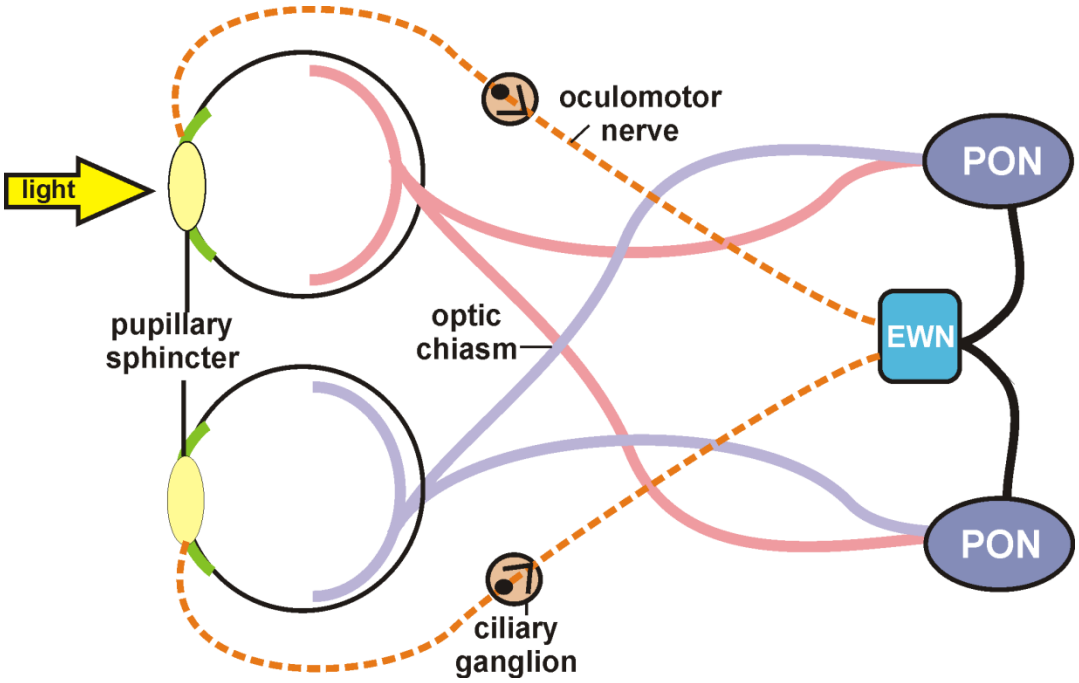

Figure 2.4. The pupillary light reflex (PLR).

2.5.2. Measuring PLR

Pupillometry is a technique used to measure the evoked response of the pupil to light. Since it is dependent on the input from photoreceptors and the ipRGCs as well as the intact PLR pathway involving retinal output from RGC, it allows an objective measure of the health of the retina (Gooley et al., 2012). The PLR is significantly reduced in patients with retinal degenerations (Park et al., 2011; Skaat et al., 2013) as well as in rodent models of IRDs (Lucas et al., 2001a). In this thesis, pupillomety was used for two main purposes: (1) to evaluate the retinal function and sensitivity in vector optimisation safety studies; (2) in order to assess any recovered retinal photosensitivity following the ectopic expression of melanopsin.

2.5.3. The experimental protocol

In vector optimisation studies, the PLR was measured in wild-type mice at six weeks and six months post injections. Mice were dark-adapted overnight (>12 hours) before the recordings. Light stimuli were provided by a 150W metal halide lamp, Phillips, USA and were transmitted along a fibre-optic bundle to an integrating reflective sphere, which provided uniform light at the mouse cornea, similar to previously described by Enezi et al., 2011) (Figure 2.5). Consensual PLR was recorded in un-anaesthetised, lightly scruffed mice, under infra-red conditions with an infra-red sensitive CCD camera fitted with 10x macro lens and an infra-red filter (Rolera-XR High Performance, Near Infrared IEEE 1394 FirewireTM Digital CCD Camera, QImaging). An intervening shutter (Cairn UniBlitz) controlled stimulus timing. A single trial lasted 20 seconds: 5 seconds light OFF, 10 seconds light ON, 5 seconds light OFF. The intensity of the light was controlled by neutral density (ND) filters and mice were subjected to white light exposures in an ascending intensity series, with individual trials being separated by at least 5 minutes. Retinal irradiance values ranged from 13.8 (ND0) to 10.01 (ND5) log photons/cm^2/s. Pupillary responses were quantified from the video images using ImageJ software. Data were normalised to pupil area immediately preceding the light onset and reported as maximum pupillary constriction, mean ± SEM. Irradiance response curves (IRCs) were fitted with sigmoidal function. Statistical differences between groups were evaluated in Graph Pad Prism (V6; Graph Pad, USA) using a two-tailed paired t-tests to compare response between enzyme and PBS-injected eyes. Significance was set at $p<0.05$.

In melanopsin-driven functional recovery studies, PLR was measured in *wild-types* (n = 6) and *rd*^{1} mice treated with AAV2-CAG-GFP (n = 5) or AAV2-CAG-hOPN4 (n = 5) at >12 weeks post injections as described above.

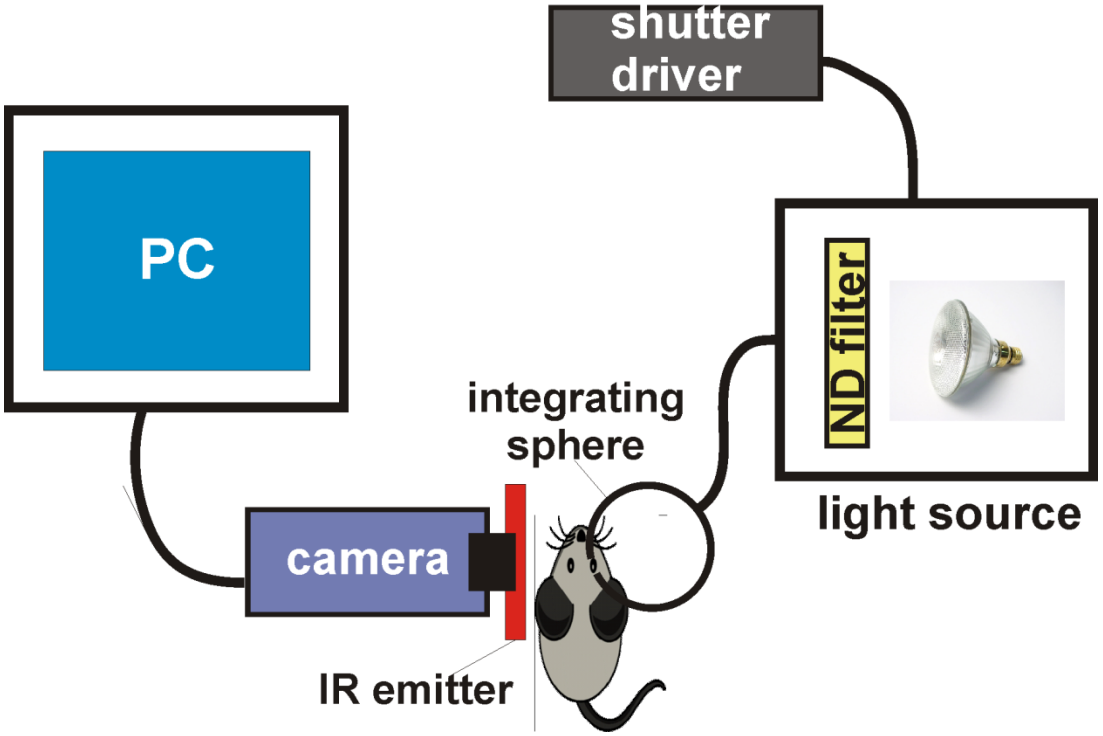

Figure 2.5. The experimental set up of pupillometry for the measurement of PLR. A light source was attached to both a shutter supply and an integrating sphere. When the trigger was manually engaged, a shutter was opened, allowing light from the light source into the integrating sphere via a fibre optic cable. An infra-red CCD camera was used to capture real time infrared recordings from a consensual pupil response. An infra-red emitting block was used to maximise the amount of contrast in the image.

2.6. Electrophysiology (Neurophysiology)

Upon activation, neurons create depolarising or hyperpolarising ion currents through their cell membranes, causing a change in voltage between the inside and the outside of the cell. As a result, changes in extracellular currents mirror the activity of individual neurons, both temporally and spatially. Thus, recording extracellular activity can be used to assay neuronal activity. When recording, the electrodes transduce the change in voltage from the extracellular activity, carried by ions, into currents carried by electrons (electronic currents) that can be measured.

In the retina, photoreceptor responses ultimately result in the depolarisation of RGCs and firing of action potentials, encoding sensory information. This activity can be evoked *in vitro* in retinal explants and be used to measure the retinal function in response to different light stimuli via multi-electrode array (MEA) (Figure 2.6). In addition, this light-evoked activity can readily be observed in areas downstream of the retina, as action potentials are propagated down RGC axons and the optic nerve to the retro-recipient regions where they modulate their activity. A major retro-recipient region concerned with image-forming vision is the lateral geniculate nucleus (LGN) in the thalamus. Thus, recording neuronal activity in the LGN provides invaluable information about retinal responses that are transmitted to the brain, in an intact *in vivo* system (Figure 2.7).

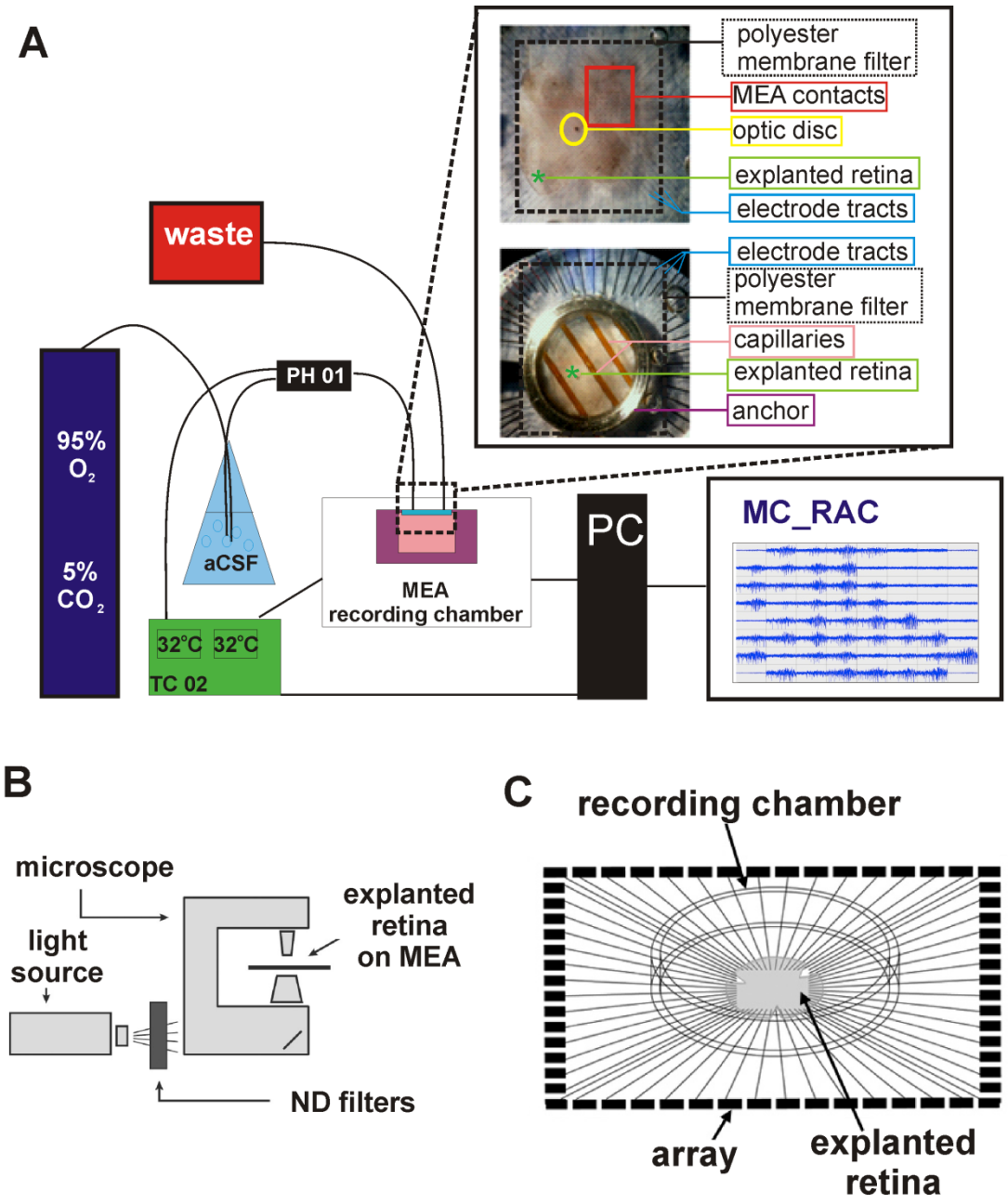

Figure 2.6. Experimental setup and apparatus used in MEA recordings. (A) Schematic diagram of experimental setup used for the maintenance of explanted retinas and MEA recordings. Retinas are maintained under physiological conditions with a constant flow of heated oxygenated aCSF and kept at 32˚C by heating a copper plate below the recording chamber and an inline heater (PH01). Insert on the top right shows images of a retina positioned on an MEA (top) and held down by a stainless steel anchor (bottom). (B) Apparatus used for MEA recordings. Adapted from http://www.scientifica.uk.com/. (C) Schematic of an MEA (Multichannel Systems) showing a central recording chamber surrounding a planar electrode array of 60 electrodes. Adapted from webvision.med.utah.edu.

2.6.1. *In vitro* electrophysiology: multi-electrode array (MEA) recordings

Enucleated eyes were placed in a petri dish filled with carboxygenated (95% CO2/5%CO_2) aCSF (artificial cerebro-spinal fluid, concentration in mM: 118 NaCl, 25 $NaHCO_3$, 1 NaH_2PO_4, 3 KCl, 1 $MgCl_2$, 2 $CaCl_2$, 10 $C_6H_{12}O_6$, and 0.5 L-Glutamine). Retinas were then carefully isolated in diffuse red light under a dissecting microscope and mounted, ganglion cell side down, onto a 60- or 256-channel multi-electrode array (Multi Channel Systems, Reutlingen, Germany). Retinal explants were coupled in place with a weighted dialysis membrane, and continuously perfused with carboxygenated aCSF at 2.2 ml per minute using a peristaltic pump (SCI400, Watson Marlow, UK), and maintained at 32˚C using a Universal Serial Bus temperature controller regulating an inline heater for the inflow of aCSF.

Light stimuli (white light) were presented by a customised light engine source (Lumencor, USA or Thorlab LEDs). At brightest intensity (ND0) LEDs were $1x10^{15}$ total photons/cm^2/s for Lumencore and $8x10^{14}$ total photons/cm^2/s for Thorlab LEDs. An Arduino Due card (Italy) controlled by programmes written in LabVIEW (Version 8.6, National Instruments, TX, USA) was used to control stimulus duration and intensity by altering LED output and adjusting a filter wheel containing neutral-density filters (ThorLabs, UK) which reduced intensity by x10. Stimuli were delivered at 2-second pulses of light (20s inter-stimulus interval) for 20-30 repeats at ND0, ND1 (10x dimmer) and ND2 (100x dimmer). Data were sampled at 25 kHz during the acquisition of both spontaneous and evoked activity and recorded for off-line sorting using Offline Sorter (Plexon). After removing clear artefacts common to all channels, principal component analyses were used to discriminate single units, identified as distinct clusters of spikes within the principal component space, with a clear refractory period in the interspike interval distribution. Spike-sorted, single-unit data were then further analysed using Neuroexplorer (Nex Technologies) and MATLAB R2010a (The Mathworks Inc.).

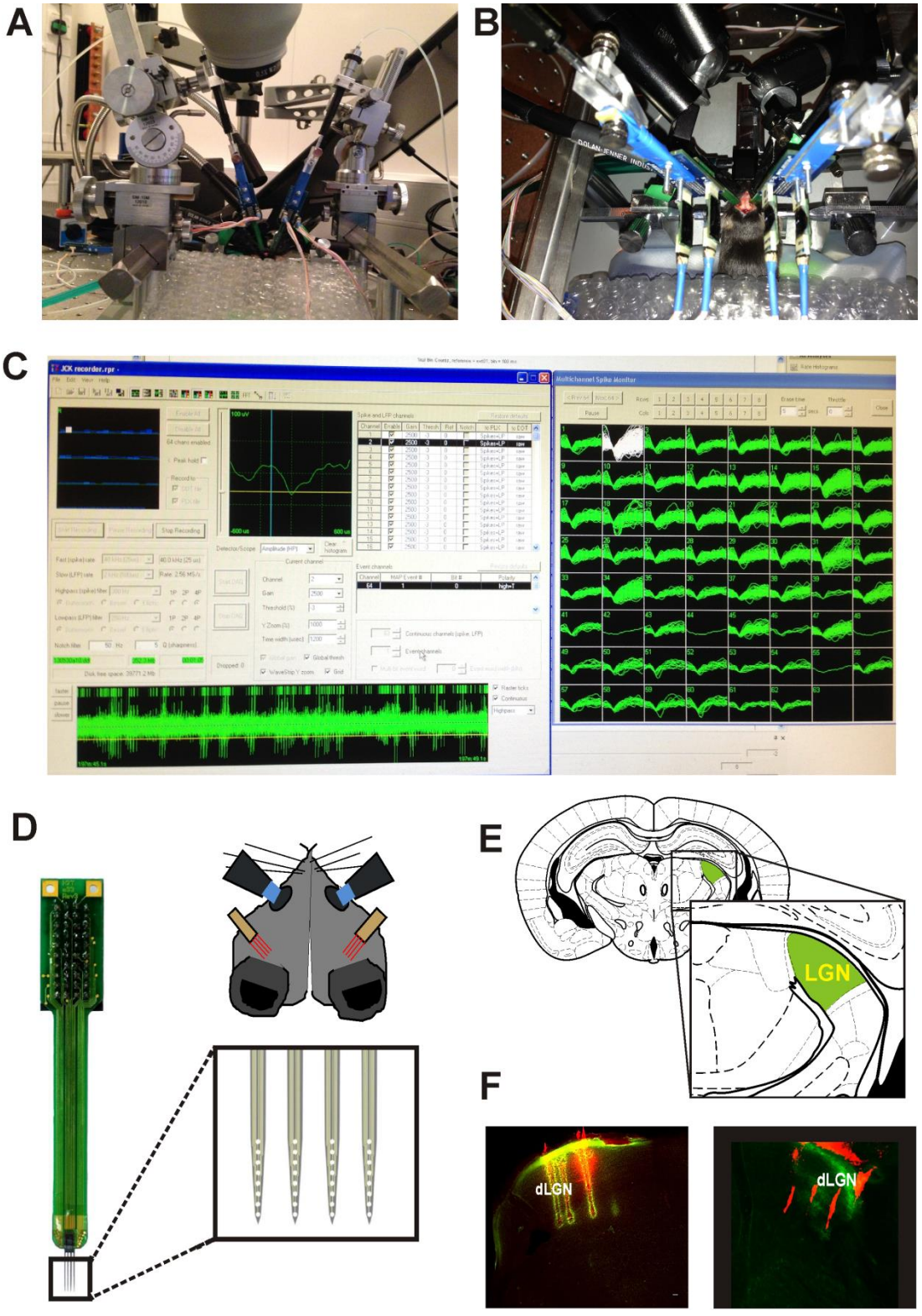

Figure 2.7. Experimental setup used in LGN recordings. (A-B) Images of the experimental setup used in LGN recordings. (C) Typical multichannel neuronal activity recorded from bilateral LGNs using a Recorder64 system (Plexon, TX, USA) (D) Multi-channel recording electrode (NeuroNexus Technologies Inc., MI, USA) used in recordings. An insert shows magnified electrode shanks showing the distribution of 32 recording sites. (E) A schematic taken from mouse atlas (Paxinos and Franklin,

2001) depicting the position of LGN. (F) Histological brain sections showing electrode sites (fluorescence DiI tracks) within the dorsal LGN (dLGN).

2.6.2. In-vivo electrophysiology: LGN recordings

Recordings were performed on two groups of *rd1* mice: group 1 (n = 7), one eye injected with AAV2-CAG-*RHO* and the other with AAV2-CAG-*GFP*; and group 2 (n = 5), one eye injected with AAV2-grm6-*RHO* and the other with AAV2-grm6-GFP. Mice were anaesthetised with urethane (intraperitoneal injection 1.55g/kg; 20% w/v; Sigma Aldrich, Poole, UK), ketamine and xylazine (100mg/kg ketamine and 10mg/kg xylazine; intraperitoneally) or isofluorane (initial dose of 2-3% and maintenance dose of 0.6-1.0% administered via a nose cone; GM-4, Narishige, Japan). Animals were mounted in a stereotaxic frame (SR-15M; Narishige International Ltd, London, UK) and core body temperature was maintained at 37 °C via a homeothermic heat mat (Harvard Apparatus, Edenbridge, UK). Pupils were dilated with atropine and mineral oil (Sigma Aldrich) was applied to retain corneal moisture.

A small craniotomy and durotomy (~1 mm^2) was performed directly above each lateral geniculate nucleus (LGN) using stereotaxic coordinates according to mouse atlas (Paxinos and Franklin, 2001; hole centre= bregma: −2.46 mm; midline: −2.8). A 32-channel electrode (NeuroNexus Technologies Inc., MI, USA) was introduced to each LGN in the centre of the hole (medial shank: -2.5 mm relative to midline; depth: −2.6 mm relative to brain surface at 18 degrees angle) for simultaneous recording from both LGNs. A second recording was performed where electrodes were re-positioned and advanced 250µm dorsally with respect to bregma (at -2.71mm). Following electrode insertion mice were dark adapted for 30 minutes to allow neuronal activity to stabilize.

Data were acquired using a Recorder64 system (Plexon, TX, USA) with signal amplification by a 20x gain AC-coupled head stage (Plexon, TX) followed by preamplifier conditioning providing a total gain of 3500x. Data were high-pass

(300Hz) filtered and time-stamped neural waveforms were digitized simultaneously from all channels at a rate of 40 kHz. Multiunit data was then stored for offline sorting and analysis as for the MEA data described above. To confirm the location of recording sites, the recording electrode was dipped in fluorescent dye (Cell Tracker CM-DiI; Invitrogen) prior to insertion into the brain. After in-vivo recordings, the mouse's brain was removed and post-fixed overnight in 4% paraformaldehyde, prior to cryoprotection for 24 hours in 30% sucrose. 100µm coronal sections were then cut using a sledge microtome, mounted onto glass slides and cover slipped using Vectashield (Vector Laboratories, Inc.).

Visual stimuli were provided by LEDs (Thorlab λmax: 410 nm) and delivered via fibre optic to purpose-made eye cones tightly positioned onto each eye to minimise any potential light leak. A National Instruments card (USB-6229) controlled by programmes written in LabVIEW (Version 8.6, National Instruments, TX, USA) was used to control stimulus duration and intensity by altering LED output and adjusting filter wheel containing neutral-density (ND) filters (ThorLabs, UK). At brightest intensity (ND0) LEDs gave a corneal irradiance of 47 W/m^2 or $4x10^{15}$ of effective flux for rod opsin; estimated retinal irradiance is $4.5x10^{14}$ log photons/cm^2/s based upon the method (Lyubarsky et al., 2004). Light was measured using a spectroradiometer (Bentham Instruments Ltd., UK or Cambridge Research Systems Ltd., UK), which measured the relative power in mW/cm^2 at wavelengths between 350-700nm. The effective quantal flux (in photons/cm^2/s) for each opsin was then estimated by weighting spectral irradiance according to pigment spectral efficiency using the formula: effective photon flux = $\int P(\lambda).s(\lambda).l(\lambda)d\lambda$ where $P(\lambda)$ is spectral irradiance in photons/cm^2/s/nm; $s(\lambda)$ is pigment spectral sensitivity approximated by the Govardovskii visual template (Govardovskii et al., 2000) and $l(\lambda)$ is mouse lens transmission as measured by Jacobs and Williams (Jacobs et al., 2007).

Light flashes were delivered according to a light protocol consisting of 2 parts. Part 1 included flashes from darkness: 2s light ON, 20s light OFF with 10s offset between each eye. This paradigm was repeated at least 10x at each ND filter. Retinal irradiance

ranged from $4.5x10^{12}$ photons/cm^2/s at ND2 to $4.5x10^{14}$ photons/cm^2/s at ND0. Part 2 of the light protocol involved recording in light adapted conditions where 5-second steps of light were applied to a steady background illumination at Michelson contrast of 96%. There was a 20-second inter-stimulus interval and a 10-second offset between two eyes. This paradigm was repeated ten times.

Naturalistic movies were presented with a digital mirror device projector (DLP® LightCommanderTM; Logic PD Inc.), whose intrinsic light engine had been replaced with our own multispectral LED light source containing four independently controlled LEDs (λmax at 405nm, 455nm, 525nm and 630nm; Phlatlight PT-120 Series (Luminus Devices). Light from the LEDs was combined by a series of dichroic mirrors (ThorLabs), and directed onto the mirror device. The movie was presented using Python running PsychoPy Version 1.70.00 software. It featured mice moving around a behavioural arena including movement and looming of different sized objects (subtending visual angles ranging from 0.5° to 36°) at a range of orientations, speeds and contrasts (maximum Michelson contrast at 96%). The movie was presented at irradiance 0.81 W/m^2 with estimated retinal irradiance of $1x10^{13}$ rod equivalent photons/cm^2/s). The movie lacked differences in colour, and changes in irradiance across time were minimal (standard deviation of irradiance = 5.94%). Previous validations in wild-type mice have shown undetectable responses for presentations of de-focussed versions, indicating that most activity was elicited by changes in spatial patterns and object motion.

2.6.3. Critical analysis of electrophysiology techniques

The use of multi-channel electrodes greatly extends the scope of extracellular recordings. The activity of one or many neurons can be detected with an individual channel, so using an MEA (*in vitro*) or a multi-channel electrode (*in vivo*) allows the acquisition of concurrent recordings from a large body of neurons within a particular area of the retina (*in vitro* MEA) or within a particular brain nucleus (*in vivo* LGN recordings) in any one experiment. These techniques also reduce and refine

experimental procedures, significantly decreasing the number of animals necessary for research studies.

One of the main shortcomings of the *in vitro* retinal preparations is that they do not fully mimic the intact *in vivo* systems. Thus, in this case, ectopically expressed rod opsin bleaches upon light exposure and restored RGC responses dissipate over multiple repeats of a light stimulus, unless the culture medium is supplemented with its chromophore, *9-cis* retinal, when responses become robustly repeatable. However, bleaching was not a problem for *in vivo* LGN recordings, where endogenous levels of *cis*-retinal were sufficient to allow ectopic rod opsin to function over multiple repeats.

All *in vivo* electrophysiology recordings were made in anaesthetised mice, resulting in stable preparations in which recordings could be made for a relatively long duration (>6hrs) and from several electrode placements. However, we cannot exclude the possibility that anaesthesia may have had some influence on the neuronal response properties. In addition, electrophysiology does not provide information on the conscious visual percepts, important for the evaluation of any visual prosthetic to be used in humans. An attractive alternative would be to use chronically implanted electrodes in freely moving animals which would overcome the shortcomings of recordings in anaesthetised animals and also enable correlations to be made between neuronal activity and behavioural outputs.

2.7. Behavioural assessment of vision

2.7.1. Critical analysis of a novel behavioural paradigm to assess restored visual function

There are several standards used in vision research to assess visual discrimination in murine models. Commonly, these tasks involve stressful environments, extensive training or are based on reflexes rather than goal oriented behaviour. They include tests based on operant schemes; reward based learning, or innate vision-guided reflexes. Reinforcement-based tasks rely on deprivation, for example water is used as a reward for correct reporting of visual stimuli (Histed at al., 2012). 'Shock-box' tests

utilize painful electric stimuli to re-enforce learning. Visual water maze tasks involve stressful environments and long training periods where mice have to learn to associate an escape platform with visual stimuli (Prusky et al., 2000; Brown et al., 2012). Optokinetic reflex (Prusky and Douglas, 2004) tests are quicker and less stressful than water maze tasks, but they rely on sub-cortical processing and thus do not truly assess the cortical vision.

To address these deficits, we developed a simple, high-throughput and less-stressful method of assessing vision based on spontaneous behaviour. Motivated by classical open-field light-dark box tests (Bourin and Hascoët 2003) and other reports of behavioural responses to simple visual stimuli (Lagali et al., 2008; Tochitsky et al., 2014), we measured the locomotor behaviour in response to various artificial and natural light stimuli. Monitoring the animals' spontaneous behaviour alone reduces the stress of the task for these animals and allows for rapid assessment of vision. We hypothesized that abrupt alterations in the visual scene might induce changes in spontaneous locomotor activity (either increases or decreases) that could be measured objectively with available image analysis software.

We validated this methodology in fully-sighted wild-type animals as a viable and preferable alternative to the existing methodologies, and went on to assess the efficacy of optogenetic therapy in blind mice. This data is presented in Chapter 4.

Our estimates of spatial acuity thresholds in *wild type* mice are consistent with values generated from water maze tasks (Prusky et al., 2000) and optokinetic responses (Prusky and Douglas, 2004) albeit on the more conservative end of the values likely due to the lower light intensities and lower contrasts (75%) used in our study. These lower parameters were used in order to reduce the possibility of any photophobic aversion from very bright stimuli and condition the assay for the assessment of lower light intensities suitable for responses driven by ectopic rod opsin. The reactions of the mice in the arena suggested that they became interested in certain stimuli and increased their exploratory behaviour, or indeed tried to escape from a predator (when presented with a rendition of an owl movie) as they increase their activity. This highlights a particular strength of this assay in the adaptability that it provides, allowing assessment of multiple aspects of vision including flicker response, contrast detection or response to a natural movie.

This novel method does not require any training and multiple test trials do not lead to habituation to the stimulus, so long as the 'novelty' is maintained by interleaving stimulus presentations. The assay is thus suitable for longitudinal studies of visual acuity in rodents. This would be particularly useful for the studies of the long-term effects of optogenetic treatments or any progression of retinal degeneration. Importantly, a similar open field assay has recently been shown to be dependent on cortical processing lending support to this paradigm as a better alternative to the traditional assessments of mouse vision (Prusky and Douglas, 2004; Prusky et al., 2000).

2.7.2. Experimental protocol for behavioural assessment of vision

The modified light/dark box (dimensions: length=40cm width=40cm and height=30cm, open top) was made of Perspex and its walls painted white except for the two long sides of each arena, which were kept clear. Two identical infra-red lamps were placed centrally above each arena, to allow visualisation of mouse movement under dark conditions (Figure 2.8)

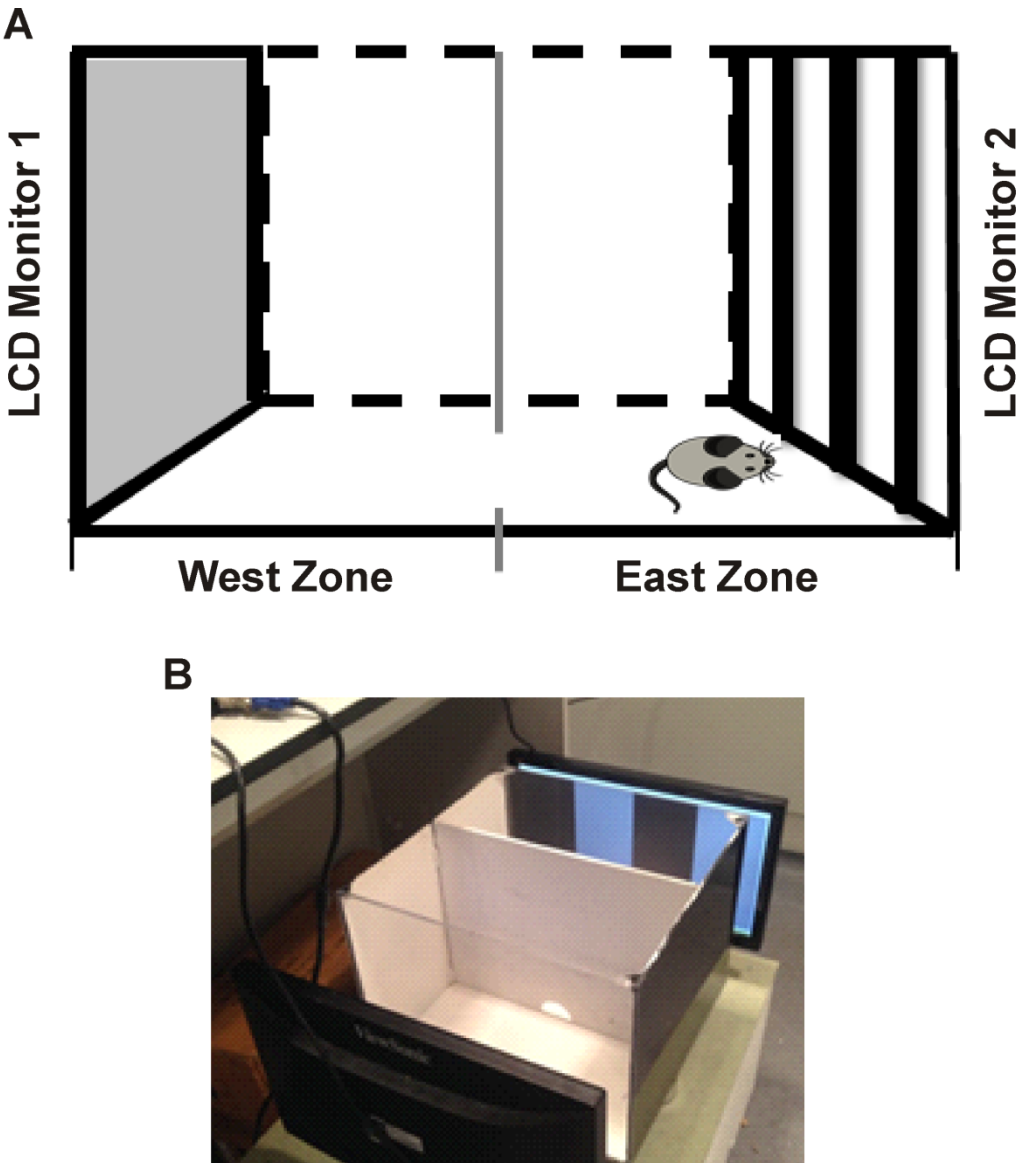

Figure 2.8. Experimental setup for the novel behavioural paradigm. (A) Schematic of the apparatus used. (B) Image of the experimental setup for the behavioural assay of visual function in mice.

The visual stimuli were displayed from two 17-inch flat screen computer monitors (Acer V173b or Dell E173FP and ViewSonic matched for power by adjusting screen brightness) facing clear walls of each arena, using a DualHead2Go Digital Edition external multi-display adapter (Matrox Graphics Inc.). A variety of visual stimuli were generated using a custom written program and displayed on one monitor at a time. Stimuli included switching from 'black' (minimum brightness) to 'white', from steady grey to full screen flicker (see Chapter 5 Figures S4B to S4E) or square-wave gratings without an associated change in irradiance. The stimuli were presented when the

mouse was in the middle of one half of the arena and the spatial frequency of gratings is reported for this viewing distance. Spatial frequency would become lower (by up to 2x) if the mouse moved towards the monitor and higher if it moved away. In addition a natural movie (colour rendition of an owl swooping in slow motion; see Chapter 5 Figure S4F) was presented. Light intensity from 400-700nm was measured using a spectroradiometer (Bentham Instruments Ltd., UK or Cambridge Research Systems Ltd., UK). For full screen modulations, corneal irradiance for a mouse looking directly at the screen was measured (for ease of comparison with other studies) by using a cosine diffuser light placed in the appropriate location in the arena.

Before the experimental period, mice were handled and habituated to their novel environment over 5 days, at the same time each day, by leaving them in the experimental box with their cagemates for 30 min. Following the habituation period, behaviour experiments were conducted over several weeks at the same time each day. Each group of mice was allowed to undergo only one testing condition per day. On each test day, mice were brought into the testing room in their home cages, allowed to acclimatise to the testing room conditions for 30 minutes and then each mouse was tested individually. Mice were placed into the open field box (randomly to east or west half) and allowed to move freely between two arenas. All test trials were recorded under infra-red conditions through a camcorder fitted with an infra-red filter (λ=665nm). The box was thoroughly cleaned with 70% ethanol after each test trial and allowed to air-dry before next mouse was placed into the box.

A recording trial began after 3 minutes of habituation. Each trial run consisted of 5 minutes of control stimulus, following which a test stimulus was presented on a screen facing an arena that contained a mouse at this time point. The recorded trials were stored for off-line analysis using a video tracking software device (EthoVision® XT 10.1 Noldus, Tracksys Ltd., UK). We analysed distance travelled by each mouse in the entire box and outputted results in 30 second bins. The mouse's ability to detect the visual stimuli was assessed as a change in distance travelled in the 30s either side of test stimulus appearance. As we had no strong a priori expectation that stimuli would increase vs. decrease activity, we used a two-tailed paired t test to detect changes in locomotion. To account for habituation to the novel stimulus, we tested for statistically significant responses across the group of treated mice in a single

presentation for most tests. The exception was the drifting grating, in which we explored the robustness of responses over repeated presentations in *wild-type* and *rd1* (treated and control) mice. We found that responses were retained over multiple presentations, but that high repeat numbers did not necessarily maximise the likelihood of detecting small effect sizes, as mouse behaviour appeared to change as they became increasingly accustomed to the task. Thus, for example, we found that baseline activity progressively increased in both *rd1*-grm6-*RHO* and *rd1*-grm6-*GFP* animals, but the magnitude of the increased activity declined beyond 10 repeats (data not shown).

2.8. Critical analysis of functional assessment of vision for evaluation of optogenetic treatments

In order to determine the effect of optogenetic strategies in restoring vision in blind animals, appropriate tests of visual function must be used. In summary, *in vitro* and *in vivo* electrophysiological approaches are widely used in visual neuroscience to assess neuronal function. ERGs assess retinal function in terms of electrical potential but provide no information on downstream visual pathways. Pupillometry can be used to assay RGC function and provide information on retinal photosensitivity. However, this reflex behaviour does not provide any information on conscious image forming vision. MEA measures direct activity from RGCs, but *in vitro* preparations do not closely mimic intact *in vivo* systems. CNS recordings, such as recordings from the LGN, provide critical information on the quality of the restored visual code. In particular, LGN recordings (first central synapse of RGCs) provide information that is closest to that found in the retina, without a significant influence from the cortex. Cortical recordings or visual evoked potentials can provide information on direct cortical vision, but the signals encoded remain largely undefined in mice. The use of anaesthesia in neurophysiology may influence the quality of information recorded which may be different in awake animals and it inhibits its suitability for long-term monitoring and repeated studies. Lastly, behavioural tests are the ultimate ways of assessing visual discrimination and can provide information on the quality of perceived vision. Using a combination of the above techniques, provides the best evaluation of the efficacy and the clinical feasibility of optogenetic strategies in animal models.

Chapter 3: Paper 1

Efficacy and safety of glycosidic enzymes for improved gene delivery to the retina following intravitreal injection

Authors: Jasmina Cehajic-Kapetanovic[1], Nina Milosavljevic[2], Robert A. Bedford[2], Robert J. Lucas[2], Paul N. Bishop[1]

Affiliations:

[1]Centre for Ophthalmology & Vision Sciences, Institute of Human Development, University of Manchester and Manchester Royal Eye Hospital, CMFT, Manchester Academic Health Sciences Centre, Manchester, UK.

[2]Faculty of Life Sciences, University of Manchester, Oxford Road, Manchester M13 9PT, UK

Efficacy and safety of glycosidic enzymes for improved gene delivery to the retina following intravitreal injection

Authors: Jasmina Cehajic-Kapetanovic[1], Nina Milosavljevic[2], Robert A. Bedford[2], Robert J. Lucas[2], Paul N. Bishop[1]

Affiliations:

[1]Centre for Ophthalmology & Vision Sciences, Institute of Human Development, University of Manchester and Manchester Royal Eye Hospital, CMFT, Manchester Academic Health Sciences Centre, Manchester, UK.

[2]Faculty of Life Sciences, University of Manchester, Oxford Road, Manchester M13 9PT, UK

Summary:

Adeno-associated virus (AAV)-mediated gene therapy has shown great promise in treating inherited retinal degenerations and other retinal conditions. Reaching adequate levels of transgene expression following intravitreal delivery represents a major challenge for ocular gene therapy studies, so current clinical trials rely on a more complex delivery approach via subretinal injection. We have previously reported that the extent of transgene expression in the mouse retina following intravitreal injection of AAV serotype 2 (AAV2) can be enhanced by co-injection of glycosidic enzymes targeting the extracellular matrix. Here we set out to determine the optimal combination of enzymes for this approach. To this end we assessed the transduction efficiency of AAV2 (carrying a reporter gene, enhanced green fluorescent protein, GFP, driven by a ubiquitous promoter) in conjunction with chondroitin ABC lyase, hyaluronan lyase, heparinase III and combinations thereof by qualitative and quantitative analysis of GFP positive cells in the treated *wild-type* retinas. In addition, using an optimised AAV2-enzyme combination, we qualitatively analysed GFP expression in degenerate retinas from *rd*^{1} mice, a model of advanced retinal degeneration, after both untargeted delivery and when GFP was selectively targeted to ON-bipolar cells. Lastly, we performed a functional analysis of the retina by flash electoretinography and pupillometry to determine if glycosidic enzymes had any effects on the retinal function.

We report that a combination of heparinase III and hyaluronan lyase produced the greatest enhancement of gene delivery to the healthy wild-type retinas. This optimised AAV2-enzyme combination also led to a marked improvement in transduction of retinas from *rd*^{1} mice compared to AAV2 injected without the enzymes. Safety studies measuring retinal function by flash electroretinography in both scotopic and photopic conditions and pupillometry indicated that retinal function was unaffected in acute period and up to at least 12 months post enzymatic treatment. Collectively these data confirmed that this approach enhances retinal transduction efficiency by AAV, potentially allowing the development of intravitreal injection of gene therapy vectors for clinical applications.

Introduction

Inherited retinal degenerations (retinal dystrophies) are a major cause of blindness affecting approximately 1:2500 people worldwide. In most forms, genetic mutations affect the cells in the outer retina, i.e. the photoreceptors and retinal pigment epithelium (RPE), making these cells primary targets for emerging gene-based therapies. The landmark ocular gene therapy clinical trials for Leber congenital amaurosis (LCA2, a rare form of inherited retinal degeneration; 1-5) have demonstrated safety and efficacy of delivering therapeutic transgene via adeno-associated viral (AAV) vector to the retinal pigment epithelium (RPE) by subretinal injection. However, unlike in LCA2 where retinal architecture remains intact for many years (6), other more common retinal dystrophies (especially advanced cases; 7) have thin and fragile retinas, making subretinal delivery of AAV vectors challenging and prone to complications (5, 8-10). An alternative approach is via intravitreal injection, a technically less challenging, safer and therefore more broadly applicable approach compared to subretinal injection. However, reaching therapeutic levels of transduction in the retina from the vitreous presents challenges and has been a focus of a number of recent preclinical gene therapy studies (11-21).

AAV-based vectors are currently being developed that are capable of transducing the outer retina following intravitreal injection using rational mutagenesis (13-20) or *in-vivo* directed evolution (21-23). Rational mutagenesis manipulates viral capsids (surface-exposed tyrosine, threonine and lysine residues) to decrease intracellular ubiquitination and proteosomal degradation of the vector resulting in increased retinal transduction. Directed evolution selects AAV variants from combinatorial libraries with desirable cellular tropism *in-vivo*. Thus, through multiple cycles of evolution it enriches for AAV variants with specific cell tropism (e.g. the Sh10 variant for Muller cells; 21) or those capable of reaching the outer retina from the vitreous through altered receptor-binding properties such as the 7m8 variant (23). These novel AAV variants have been shown to produce a more effective functional rescue of disease phenotype in animal models of retinal degeneration (23, 24).

An alternative strategy for increasing retinal transduction following intravitreal delivery is to tackle the physical barriers to vector penetration of the retina. Naturally occurring AAV serotypes produce limited inner retinal transduction and are ineffective in transducing outer retina via intravitreal delivery because the vitreous, inner limiting membrane (ILM), retinal extracellular matrix (ECM) and cell surface proteoglycans form substantial barriers and binding sites that immobilise the AAV particles (11-12, 25). We demonstrated previously that enzymatic lysis of these barriers, using glycosidic enzymes, improved the depth and efficiency of vector penetration leading to more efficient retinal transduction (11). Enzymatic digestion of the ILM with the non-specific protease, Pronase E, (12) also enhanced retinal transduction, suggesting that the ILM forms the greatest barrier to vector penetration.

Here, we describe an optimised approach to increasing retinal transduction of intravitreally-delivered unaltered AAV2 in conjunction with glycosidic enzymes. We performed quantitative and qualitative analysis of transduction efficiency of AAV2 (carrying a reporter gene, GFP) in conjunction with several glycosidic enzymes, chondroitin ABC lyase, hyaluronan lyase, heparinase III and combinations thereof, and found that a combination of heparinase III and hyaluronan lyase produced the greatest improvement in retinal penetration by the AAV2 vector (including modest expression in photoreceptors), and overall the highest level of transduction in intact *wild-type* retina. Robust transgene expression was also observed using these enzymes with intravitreal AAV2 in the degenerate retina of *rd*^{1} mice, a model of advanced retinal degeneration, after both untargeted delivery and when GFP was selectively targeted to ON-bipolar cells. Safety studies demonstrated that that retinal function was unaffected in the short, intermediate and long-term phase post enzyme treatment.

Results

Glycosidic enzymes increase in-vivo transduction efficiency of AAV2 from the vitreous

To characterise expression of reporter gene (GFP) mediated via low dose AAV2 vector we injected $2x10^8$ genomic counts (gc)/eye of AAV2-CAG-GFP vector (which contains a ubiquitous promotor, Figure 1A) into the vitreous of adult *wild-type* mice alone or in combination with glycosidic enzymes. As expected with the AAV2-CAG-GFP alone (11-12, 25) there was weak gene expression and this was restricted to the inner retina (Figure 1B and S1A). By contrast, when AAV2-CAG-GFP was injected in conjunction with the glycosidic enzymes chondroitin ABC lyase (CH; Figure 1C), hyaluronan lyase (HYL; Figure 1D and S1B) or heparinase III (HEP; Figure 1E and S1C) there was a marked increase in GFP expression in retinal ganglion cell layer (GCL) and in inner nuclear layer (INL) confirming our previous findings (11). Next we tested various combinations of enzymes including chondroitin ABC lyase and heparinase III (CH+HEP; Figure 1F), chondroitin ABC lyase and hyaluronan lyase (CH+HYL; Figure 1G) and heparinase III and hyaluronan lyase (HEP+HYL; Figure 1H) and found that they further enhanced GFP expression. The strongest transduction was achieved with a combination of heparinase III and hyaluronan lyase (Figure 1H) which produced robust GFP expression throughout the GCL and INL (Figure 1J) with some regions also having modest outer retinal transduction (Figure 1I). Quantitative assessment of transduction efficiency of AAV2-CAG-GFP in combination with glycosidic enzymes showed a significant increase in the number of GFP+ cell bodies per mm retinal section with addition of glycosidic enzymes (or their combinations) compared to AAV2 alone (Figure 1K). In particular, heparinase III and hyaluronan lyase resulted in the highest count of GFP+ cells with a ~17-fold increase compared to unenhanced AAV2-CAG-GFP mediated transduction ($p<0.0001$). This increase was significant in both GCL (Figure 1L; $p<0.001$) and INL (Figure 1M; $p<0.0001$) cells, but not in ONL cell bodies (Figure 1N).

High dose AAV2 vector in conjunction with the heparinase III and hyaluronan lyase enzymes in *wild-type* mice

For these experiments we injected *wild-type* mice with the combination of heparinase III and hyaluronan lyase along with a higher dose of AAV2-CAG-GFP ($3x10^{10}$ gc/eye). Increasing the vector dose in the presence of the glycosidic enzymes resulted in a strong pan-retinal transduction of cells in the GCL and INL (Figure 2A-D) including Muller cells (Figure 2D). In addition, outer retinal transduction (ONL) was observed, albeit at a lower level (Figure 2A, lower image) with longer stretches of modest GFP expression (Figure 2F) and some areas of relatively high expression (Figure 2E). This patchy expression is potentially due to a non-homogeneous diffusion of the enzymes and vector through the vitreous leading to more efficient retinal transduction near the injection site.

AAV2 vector in conjunction with glycosidic enzymes leads to robust expression of reporter gene in *rd1* retinas

In addition to assessing transduction efficiency of enzyme-enhanced gene delivery in *wild-type* retinas we evaluated its effects in disease-state retinas. For these experiments we investigated AAV2 transduction in *rd1* retinas – a model of advanced retinal degeneration. We injected AAV2-CAG-GFP vector ($3x10^{10}$ gc/eye) with heparinase III and hyaluronan lyase into the vitreous of adult *rd1* mice (> 8 weeks of age). When retinas were harvested ~6 weeks post injections, robust reporter gene expression was observed in cells of GCL and in INL (Figures 3A, C and D) compared to AAV2-CAG-GFP alone (Figure 3B). The expression in GCL was uniform, whereas INL expression, although pan-retinal, displayed more varied density and depth of transgene expression (Figure S2A). In further experiments we injected AAV2 with an ON-bipolar specific promoter driving GFP expression (AAV2-grm6-GFP, Figure 3E) in conjunction with the AAV2-CAG-GFP and found, as expected, expression restricted to cells in the INL layer (Figures 3F-H and Figure S2B).

Short, intermediate and long-term effect of glycosidic enzymes on retinal function

We evaluated the safety of enzyme treatments by examining their short-, intermediate and long-term effect on retinal function in *wild-type* animals. All histological sections appeared morphologically intact (Figures 1-3), so the enzymes did not produce an obvious disruption of retinal architecture. We investigated whether the glycosidic enzymes had any effect upon retinal function as assessed by electroretinograms (ERGs) elicited by flash stimuli one week after injection (Figure 4A-D). We observed no significant differences in the mean amplitude of a-wave (assessing photoreceptor function; Figure 4A, B) or b-wave (assessing bipolar-cell function; Figure 4C, D) under scotopic (Figure 4A, C) or photopic (Figure 4B, D) conditions in enzyme treated (hyaluronan lyase, heparinase III or heparinase III combined with hyaluronan lyase) compared to controls (PBS or AAV2-CAG-GFP without enzymes) eyes at 1 week post intravitreal injections (Ordinary one-way ANOVA with Dunnett's multiple comparisons test comparing differences in mean between control and treated groups; $p>0.05$ for each condition, Figures 4A-D). These findings confirm that retinal function, specifically photoreceptor and bipolar functions, remain unchanged shortly (1 week) after treatment.

Next we assessed retinal function 6 weeks after treatment. As with week 1, we found no significant differences in the mean amplitude of scotopic a-wave (Figure 4E), photopic a-wave (Figure 4F), scotopic b-wave (Figure 4G) or photopic b-wave (Figure 4G) in enzyme treated compared to control (PBS or AAV2-CAG-GFP treated without enzymes) eyes (Ordinary one-way ANOVA with Dunnett's multiple comparisons test comparing differences in mean between control and treated groups; $p>0.05$ for each condition at 6 weeks, Figures 4E-H; paired t-test $p>0.05$ also for comparison between week 1 and week data 6 for each group). Notably, a few eyes (11/82, marked with stars across enzyme treated and control groups; Figures 4E-H) with lower a- and b-wave amplitudes had persistent intravitreal haemorrhage at 1-week that was caused by the

injection procedure. In majority of cases (8/11), this completely resolved by week 6, with a resultant recovery in ERG amplitudes.

We examined retinal function in terms of photosensitivity and recorded scotopic ERG not only at the brightest light level of 13.85 log photons/cm^2/s but also at lower retinal irradiances, spanning 9 log units (from ND0-ND8) for enzyme treated (HEP+HYL) and control (PBS) eyes. We found no differences in irradiance-response curves between enzymes treated and PBS injected eyes at week 1 or 6 post treatment (Figure 4I; $p>0.05$ ordinary one-way ANOVA with Turkey's multiple comparisons test comparing differences in mean between groups at each irradiance).

As ganglion cell activity is not directly assessed by the ERG, we recorded the pupillary light reflex (PLR) at a range of retinal irradiances (spanning 6 log units) in *wild-type* animals where one eye was treated with enzymes and the other with PBS (internal control) 6 weeks after intravitreal injection. No change in PLR function was observed at any irradiance in enzyme treated compared to control eyes ($p>0.05$, paired t-test between enzyme and PBS treated eyes at each irradiance) demonstrating unaltered function of retinal ganglion cells in the presence of the glycosidic enzymes.

Lastly, we examined long-term effects of combined heparinase III and hyaluronan lyase on retinal function by repeating our safety assessments after intravitreal injections in *wild-type* mice; ERGs at 12 months (using a separate cohort of mice; Figures 5A-E) and PLR at 6 months using the same cohort of mice as for 6 week data (Figure 5F). As for the week 1 and week 6 data, there were no significant differences in the mean amplitude of scotopic and photopic a-waves (Figure 5A and B) or scotopic and photopic b-waves (Figure 5C and D) between enzyme treated and control eyes at 12 months post injections (Figures 5A-D, $p>0.05$; ordinary one-way ANOVA with Turkey's multiple comparisons

test comparing differences in mean between groups at 6 weeks and 12 months). In addition, we compared the irradiance-response curve (IRC) for scotopic ERG between enzyme and PBS treated eyes at 12 months post injections and found no significant differences in maximum b-wave amplitude at a range of irradiances tested (Figure 5E, $p>0.05$; ordinary one-way ANOVA with Turkey's multiple comparisons test comparing differences in mean between groups at 6 weeks and 12 months). To assess any detrimental long-term effects of enzymes on RGC function, we re-recorded the PLR at 6 months post treatment. We observed no significant shift in the irradiance response curves between enzyme and PBS treated eyes at a range of irradiances tested (Figure 5F, $p>0.05$; paired-t test comparing mean pupillary constriction between enzyme and PBS treated eyes at each irradiance at 6 months). Interestingly, we observed a small decrease in retinal photosensitivity from both enzyme and PBS curves at 6 month compared to 6 week data (Figure 5F, two-tailed paired t-test shows significance at higher irradiances: for enzyme curves at 13.8 ($p=0.02$), 13.0 ($p=0.01$) and 11.5 ($p=0.04$) and for PBS curves at 13.8 ($p=0.007$), 13.0 ($p=0.01$) log photons/cm^2/s). This shift in sensitivity could be explained by age-related changes (lens opacification, reduction in rod sensitivity). However, a direct effect from the intravitreal injection procedure (although unlikely) cannot be completely ruled out.

Discussion

We have demonstrated that intravitreal injection of glycosidic enzymes is an effective method of increasing AAV2-mediated transduction of the retina. We obtained the largest effect using a combination of heparinase III and hyaluronan lyase which produced robust expression in wild type and degenerate retina of the GFP reporter gene. We observed a diverse population of transduced cells and penetration of deeper layers of the retina, including outer retinal layer, and when we used an ON-bipolar cell specific promoter we confined this expression to the inner nuclear layer. Short and long-term safety studies, assessing retinal function *in vivo,* demonstrated that retinas can tolerate this enzymatic

treatment and that their function and sensitivity remain unchanged for at least nine months after the intraocular injection.

The approach described here advances on our previous work where we compared enzyme activity based on relative fluorescence in retinal whole-mounts at two weeks post AAV2-GFP injections. In these experiments we observed an increase in retinal fluorescence compared to controls (without enzyme) after intravitreal injection of CAG-AAV2-GFP in conjunction with chondroitin ABC lyase or heparinase III and a weak effect form hyaluronan lyase at 2 weeks post injections. Here we show that a higher dose of hyaluronan lyase (0.125 compared to 0.05 units per eye used in earlier study) led to a significant increase in retinal transduction (as determined by the number of GFP+ cells) at 6 weeks post injections. The increase was even greater than that produced by chondroitin ABC lyase alone, although a combination of two enzymes led to an additive increase in overall transduction rate. We observed a considerable improvement from our earlier study in terms of spread and uniformity of transduction across the retina and in variability in transduction between the eyes and this may be due to using higher viral titres; in our early studies we used $5x10^7$ gc/eye, whereas in this study we used $2x10^8$ gc/ml and $3x10^{10}$ gc/eye.

In order to reach photoreceptors from the vitreous, AAV needs to diffuse through the vitreous away from the site of injection, pass through the ILM and move through the retinal matrix into the outer retina. Hyaluronan lyase, by its specific ability to cleave the hyaluronan which is present in all these barriers, could facilitate this AAV journey. The highest concentration of hyaluronan is in the vitreous, degrading the vitreous hyaluronan may facilitate movement of the AAV through the vitreous cavity thereby allowing widespread delivery to the ILM at the vitreo-retinal junction. Heparinase III, by its action on heparan sulphate chains of heparan sulphate proteoglycans (HSPGs), abundant in ILM as well as other retinal layers (including the nerve fibre layer, the inner and outer

plexiform layers, and in the interphotoreceptor matrix; 26), could make these retinal layers more porous and thus improve the trans-retinal penetration of the viral vector. In addition, AAV2 can bind heparan sulfate, so heparan sulfate in extracellular structures such as the ILM could sequester AAV2 and prevent its movement through the retina. However, whilst heparan sulphate is thought to be a cell surface receptor for AAV2, digestion with heparinase III does not prevent entry of the AAV into retinal cells. This increased tissue penetration may also enable the use of relatively low vector doses (e.g. $3x10^{10}$ gc/eye) thereby reducing the chance of adverse immune response (27). Interestingly, the 7m8 variant of AAV2, which produces outer nuclear transduction following intravitreal injection, has lower affinity for binding to its primary cell-surface receptor, heparan sulfate (28, 29) and may therefore also have lower affinity for heparan sulfate in the ILM.

The safety profiles of glycosidic enzymes shown here are very encouraging. Electroretinography confirmed unaltered a, and b waves (which specifically tested photoreceptor and bipolar cell function respectively) short-, intermediate- and long-term after the treatment, while pupillometry confirmed that retinal ganglion cell activity was retained. Retinal photosensitivity remained unchanged as determined by electroretinograms and pupillometry at a range of irradiances tested. Glycosidic enzymes (hyaluronidases and a chondroitinase) have previously been tested in animal models for pharmacological vitreolysis without reported adverse effects (30-32) and a highly purified ovine hyaluronidase, Vitrase™ (ISTA Pharmaceuticals, Calif., USA) has been used in clinical trial to aid the dispersion of vitreous haemorrhage (33). On a molecular level, using electron microscopy of monkey ILM digests, chondroitin ABC lyase was shown to have no effect on the morphology of the retina, whereas testicular hyaluronidase had a mild effect on the ILM causing the fibrillar meshwork to assume a more irregular pattern (34).

In this study we have developed an AAV-mediated treatment with improved retinal transduction by intravitreal injection. We have recently used this approach to deliver rod opsin to RGC and ON-bipolar cells and successfully rescue vision in an advanced model of retinal degeneration (35). In addition, it has the potential to effectively deliver AAV to the outer retina following intravitreal injection, and perhaps further improvements could be made combining engineered vectors with these glycosidic enzymes.

In summary, our data suggests that heparinase III and hyaluronan lyase in combination greatly enhance AAV2-mediated gene delivery from the vitreous. Given the simplicity of this approach and its excellent safety profile in rodents, glycosidic enzymes offer therapeutic potential for a broad range of retinal degenerative diseases involving inner, mid and outer retina.

References:

1. Bainbridge, J.W., Smith, A.J., Barker, S.S., Robbie, S., Henderson, R., Balaggan, K., Viswanathan, A., Holder, G.E., Stockman, A., Tyler, N.*, et al.* (2008). Effect of gene therapy on visual function in Leber's congenital amaurosis. N Engl J Med *358*, 2231-2239.

2. Maguire, A.M., Simonelli, F., Pierce, E.A., Pugh, E.N., Jr., Mingozzi, F., Bennicelli, J., Banfi, S., Marshall, K.A., Testa, F., Surace, E.M.*, et al.* (2008). Safety and efficacy of gene transfer for Leber's congenital amaurosis. N Engl J Med *358*, 2240-2248.

3. Hauswirth, W.W., Aleman, T.S., Kaushal, S., Cideciyan, A.V., Schwartz, S.B., Wang, L., Conlon, T.J., Boye, S.L., Flotte, T.R., Byrne, B.J.*, et al.* (2008). Treatment of leber congenital amaurosis due to RPE65 mutations by ocular subretinal injection of adeno-associated virus gene vector: short-term results of a phase I trial. Hum Gene Ther *19*, 979-990.

4. Maguire, A.M., High, K.A., Auricchio, A., Wright, J.F., Pierce, E.A., Testa, F., Mingozzi, F., Bennicelli, J.L., Ying, G.S., Rossi, S.*, et al.* (2009). Age-dependent effects of RPE65 gene therapy for Leber's congenital amaurosis: a phase 1 dose-escalation trial. Lancet *374*, 1597-1605.

5. Bainbridge, J.W., Mehat, M.S., Sundaram, V., Robbie, S.J., Barker, S.E., Ripamonti, C., Georgiadis, A., Mowat, F.M., Beattie, S.G., Gardner, P.J.*, et al.* (2015). Long-term effect of gene therapy on Leber's congenital amaurosis. N Engl J Med *372*, 1887-1897.

6. Jacobson, S.G., Aleman, T.S., Cideciyan, A.V., Sumaroka, A., Schwartz, S.B., Windsor, E.A., Traboulsi, E.I., Heon, E., Pittler, S.J., Milam, A.H.*, et al.* (2005). Identifying photoreceptors in blind eyes caused by RPE65 mutations: Prerequisite for human gene therapy success. Proc Natl Acad Sci U S A *102*, 6177-6182.

7. Wright, A.F., Chakarova, C.F., Abd El-Aziz, M.M., and Bhattacharya, S.S. (2010). Photoreceptor degeneration: genetic and mechanistic dissection of a complex trait. Nat Rev Genet *11*, 273-284.

8. Jacobson, S.G., Cideciyan, A.V., Ratnakaram, R., Heon, E., Schwartz, S.B., Roman, A.J., Peden, M.C., Aleman, T.S., Boye, S.L., Sumaroka, A.*, et al.* (2012). Gene therapy for leber congenital amaurosis caused by RPE65 mutations: safety and efficacy in 15 children and adults followed up to 3 years. Arch Ophthalmol *130*, 9-24.

9. Jacobson, S.G., Acland, G.M., Aguirre, G.D., Aleman, T.S., Schwartz, S.B., Cideciyan, A.V., Zeiss, C.J., Komaromy, A.M., Kaushal, S., Roman, A.J.*, et al.* (2006). Safety of recombinant adeno-associated virus type 2-RPE65 vector delivered by ocular subretinal injection. Mol Ther *13*, 1074-1084.

10. Nork, T.M., Murphy, C.J., Kim, C.B., Ver Hoeve, J.N., Rasmussen, C.A., Miller, P.E., Wabers, H.D., Neider, M.W., Dubielzig, R.R., McCulloh, R.J.*, et al.* (2012). Functional and anatomic consequences of subretinal dosing in the cynomolgus macaque. Arch Ophthalmol *130*, 65-75.

11. Cehajic-Kapetanovic, J., Le Goff, M.M., Allen, A., Lucas, R.J., and Bishop, P.N. (2011). Glycosidic enzymes enhance retinal transduction following intravitreal delivery of AAV2. Mol Vis *17*, 1771-1783.

12. Dalkara, D., Kolstad, K.D., Caporale, N., Visel, M., Klimczak, R.R., Schaffer, D.V., and Flannery, J.G. (2009). Inner limiting membrane barriers to AAV-mediated retinal transduction from the vitreous. Mol Ther *17*, 2096-2102.

13. Zhong, L., Li, B., Mah, C.S., Govindasamy, L., Agbandje-McKenna, M., Cooper, M., Herzog, R.W., Zolotukhin, I., Warrington, K.H., Jr., Weigel-Van Aken, K.A.*, et al.*

(2008). Next generation of adeno-associated virus 2 vectors: point mutations in tyrosines lead to high-efficiency transduction at lower doses. Proc Natl Acad Sci U S A *105*, 7827-7832.

14. Petrs-Silva, H., Dinculescu, A., Li, Q., Min, S.H., Chiodo, V., Pang, J.J., Zhong, L., Zolotukhin, S., Srivastava, A., Lewin, A.S.*, et al.* (2009). High-efficiency transduction of the mouse retina by tyrosine-mutant AAV serotype vectors. Mol Ther *17*, 463-471.

15. Petrs-Silva, H., Dinculescu, A., Li, Q., Deng, W.T., Pang, J.J., Min, S.H., Chiodo, V., Neeley, A.W., Govindasamy, L., Bennett, A.*, et al.* (2011). Novel properties of tyrosine-mutant AAV2 vectors in the mouse retina. Mol Ther *19*, 293-301.

16. Yin, L., Greenberg, K., Hunter, J.J., Dalkara, D., Kolstad, K.D., Masella, B.D., Wolfe, R., Visel, M., Stone, D., Libby, R.T.*, et al.* (2011). Intravitreal injection of AAV2 transduces macaque inner retina. Invest Ophthalmol Vis Sci *52*, 2775-2783.

17. Vandenberghe, L.H., and Auricchio, A. (2012). Novel adeno-associated viral vectors for retinal gene therapy. Gene Ther *19*, 162-168.

18. Gabriel, N., Hareendran, S., Sen, D., Gadkari, R.A., Sudha, G., Selot, R., Hussain, M., Dhaksnamoorthy, R., Samuel, R., Srinivasan, N.*, et al.* (2013). Bioengineering of AAV2 capsid at specific serine, threonine, or lysine residues improves its transduction efficiency in vitro and in vivo. Hum Gene Ther Methods *24*, 80-93.

19. Kay, C.N., Ryals, R.C., Aslanidi, G.V., Min, S.H., Ruan, Q., Sun, J., Dyka, F.M., Kasuga, D., Ayala, A.E., Van Vliet, K.*, et al.* (2013). Targeting photoreceptors via intravitreal delivery using novel, capsid-mutated AAV vectors. PLoS One *8*, e62097.

20. Aslanidi, G.V., Rivers, A.E., Ortiz, L., Song, L., Ling, C., Govindasamy, L., Van Vliet, K., Tan, M., Agbandje-McKenna, M., and Srivastava, A. (2013). Optimization of the capsid of recombinant adeno-associated virus 2 (AAV2) vectors: the final threshold? PLoS One *8*, e59142.

21. Klimczak, R.R., Koerber, J.T., Dalkara, D., Flannery, J.G., and Schaffer, D.V. (2009). A novel adeno-associated viral variant for efficient and selective intravitreal transduction of rat Muller cells. PLoS One *4*, e7467.

22. Bartel, M.A., Weinstein, J.R., and Schaffer, D.V. (2012). Directed evolution of novel adeno-associated viruses for therapeutic gene delivery. Gene Ther *19*, 694-700.

23. Dalkara, D., Byrne, L.C., Klimczak, R.R., Visel, M., Yin, L., Merigan, W.H., Flannery, J.G., and Schaffer, D.V. (2013). In vivo-directed evolution of a new adeno-associated virus for therapeutic outer retinal gene delivery from the vitreous. Sci Transl Med *5*, 189ra176.

24. Pang, J.J., Dai, X., Boye, S.E., Barone, I., Boye, S.L., Mao, S., Everhart, D., Dinculescu, A., Liu, L., Umino, Y.*, et al.* (2011). Long-term retinal function and structure rescue using capsid mutant AAV8 vector in the rd10 mouse, a model of recessive retinitis pigmentosa. Mol Ther *19*, 234-242.

25. Hellstrom, M., Ruitenberg, M.J., Pollett, M.A., Ehlert, E.M., Twisk, J., Verhaagen, J., and Harvey, A.R. (2009). Cellular tropism and transduction properties of seven adeno-associated viral vector serotypes in adult retina after intravitreal injection. Gene Ther *16*, 521-532.

26. Clark, S.J., Keenan, T.D., Fielder, H.L., Collinson, L.J., Holley, R.J., Merry, C.L., van Kuppevelt, T.H., Day, A.J., and Bishop, P.N. (2011). Mapping the differential distribution of glycosaminoglycans in the adult human retina, choroid, and sclera. Invest Ophthalmol Vis Sci *52*, 6511-6521.

27. Li, Q., Miller, R., Han, P.Y., Pang, J., Dinculescu, A., Chiodo, V., and Hauswirth, W.W. (2008). Intraocular route of AAV2 vector administration defines humoral immune response and therapeutic potential. Mol Vis *14*, 1760-1769.

28. Summerford, C., and Samulski, R.J. (1998). Membrane-associated heparan sulfate proteoglycan is a receptor for adeno-associated virus type 2 virions. J Virol *72*, 1438-1445.

29. Kern, A., Schmidt, K., Leder, C., Muller, O.J., Wobus, C.E., Bettinger, K., Von der Lieth, C.W., King, J.A., and Kleinschmidt, J.A. (2003). Identification of a heparin-binding motif on adeno-associated virus type 2 capsids. J Virol *77*, 11072-11081.

30. Bishop, P.N. (2009). Vitreous as a substrate for vitreolysis. Dev Ophthalmol *44*, 7-19.

31. Gottlieb, J.L., Antoszyk, A.N., Hatchell, D.L., and Saloupis, P. (1990). The safety of intravitreal hyaluronidase. A clinical and histologic study. Invest Ophthalmol Vis Sci *31*, 2345-2352.

32. Staubach, F., Nober, V., and Janknecht, P. (2004). Enzyme-assisted vitrectomy in enucleated pig eyes: a comparison of hyaluronidase, chondroitinase, and plasmin. Curr Eye Res *29*, 261-268.

33. Kuppermann, B.D., Thomas, E.L., de Smet, M.D., Grillone, L.R., and Vitrase for Vitreous Hemorrhage Study, G. (2005). Safety results of two phase III trials of an intravitreous injection of highly purified ovine hyaluronidase (Vitrase) for the management of vitreous hemorrhage. Am J Ophthalmol *140*, 585-597.

34. Heegaard, S., Jensen, O.A., and Prause, J.U. (1986). Structure and composition of the inner limiting membrane of the retina. SEM on frozen resin-cracked and enzyme-digested retinas of Macaca mulatta. Graefes Arch Clin Exp Ophthalmol *224*, 355-360.

35. Cehajic-Kapetanovic, J., Eleftheriou, C., Allen, A.E., Milosavljevic, N., Pienaar, A., Bedford, R., Davis, K.E., Bishop, P.N., and Lucas, R.J. (2015). Restoration of Vision with Ectopic Expression of Human Rod Opsin. Curr Biol *25*, 2111-2122.

36. Kim, D.S., Matsuda, T., and Cepko, C.L. (2008). A core paired-type and POU homeodomain-containing transcription factor program drives retinal bipolar cell gene expression. J Neurosci *28*, 7748-7764.

37. Enezi, J., Revell, V., Brown, T., Wynne, J., Schlangen, L., and Lucas, R. (2011). A "melanopic" spectral efficiency function predicts the sensitivity of melanopsin photoreceptors to polychromatic lights. J Biol Rhythms *26*, 314-323.

Materials and Methods

Animals

Adult C57BL/6J (*wild-type*) and C3H/HeJ (rd^1) mice were used in this study. All animal experiments were conducted in accordance with the UK Home Office regulations for the care and use of laboratory animals, the UK Animals (Scientific Procedures) Act (1986) and the Animal Welfare Body of the

University of Manchester. Animals were kept under a 12-hour light-dark cycle and supplied with food and water *ad libitum.*

Gene delivery via AAV

AAV2 vectors used in this study were obtained from Vector Biolabs, Philadelphia, USA. The vectors contained the enhanced green fluorescent protein (GFP) gene which was under the control of a strong ubiquitous pan-neuronal promoter (CAG, a fusion of CMV early enhancer and chicken β-actin promoter, called AAV2-CAG-GFP; Figure 1A) or a cell specific ON-bipolar cells promoter (grm6; 36), a fusion of 200-base pair enhancer sequence of the mouse grm6 gene encoding for ON-bipolar cell specific metabotropic glutamate receptor, mGluR6, and an SV40 eukaryotic promoter, called AAV2-grm6-GFP; Figure 3F) was flanked by inverted terminal repeat (ITR) domains and stabilised by polyadenylation signal sequence (polyA) and a woodchuck hepatitis posttranscriptional regulatory element (WPRE). Vectors were injected intravitreally in isofluorane anaesthetised mice at >8 weeks of age.

Prior to injections, pupils were dilated with tropicamide (1%; Chauvin Pharmaceuticals, UK) and phenylephrine (2.5%; Chauvin Pharmaceuticals, UK). A custom made ultra-fine needle (Hamilton RN needle 34 gauge, supplied by ESSLAB) was attached to a 5µl Hamilton glass syringe and was passed at 45 degrees through the pars plana into the vitreous cavity without retinal perforation. The injection was performed under a direct visualisation of the needle tip through cover-slipped eyes under an operating microscope (Microscopes Inc., USA) carefully avoiding lenticular contact and blood vessels. AAV2-CAG-GFP was injected at a low or high dose and AAV2-grm6-GFP at a high dose only. Eyes that were injected with low dose vector received 1 µl of $2x\ 10^{11}$ genomic counts (gc)/ml (i.e. 2×10^8 gc/eye) and those that were injected with high dose vector received 3µl of $1x10^{13}$ gc/ml (i.e. 3×10^{10} gc/eye). Each eye that was injected with enzymes, received 0.5µl of solution containing 0.125 units of chondroitin ABC lyase from *Proteus vulgaris* (E.C. 4.2.2.4), heparinase III from *Flavobacterium heparinum* (E.C. 4.2.2.8) or hyaluronan lyase from *Streptomyces hyalurolyticus* (E.C. 4.2.2.1) singly or in different combinations (all

from Sigma-Aldrich, Dorset, UK). The chondroitin ABC lyase digests chondroitin sulphate, dermatan sulphate and hyaluronan to some extent, heparinase III specifically digests heparan sulfate (and heparin), and the hyaluronan lyase specifically digests hyaluronan. The enzyme solutions were made fresh on the day of injection by dissolving the enzymes in sterile phosphate-buffered saline (PBS). The vector and enzymes were mixed in a syringe immediately before an eye injection and were given in a single combined injection.

Histology

Retrieved eyecups (>6 weeks post injections) were fixed in 4% paraformaldehyde (PFA) in PBS for 24 hours at 4^{o} C after the cornea and lens had been removed anteriorly under a light microscope. The tissue was then washed in PBS prior to incubating in in PBS containing 30% sucrose overnight at 4^{o} C. For whole-mounts fixed eyes were washed in PBS and whole retinas were carefully dissected under a light microscope. Retinas were then flat-mounted with fluorescent mounting media containing DAPI (Vectashield, Vector Laboratories Ltd., Peterborough, UK) to stain cell nuclei. For cryosections, fixed eyes were cryo-protected in optimal-cutting temperature medium (Raymond A Lamb Ltd., Eastbourne, UK) and frozen at -80^{o} C until further processing. The cryo-protected retina was sectioned (8-10µm thickness) on a cryostat (Leica, Microsystems) horizontally through the eyecup from ventral to dorsal sides, so that each section contained a complete nasal to temporal cross-section of the retina. Six-eight sections were collected on each slide containing sections representative of the entire retina. Slides were stored at -80^{o} C. Prior to analysis slides were removed from the freezer and allowed to air-dry at room temperature for 1 hour and mounted with fluorescent mounting media containing DAPI (Vectashield, Vector Laboratories Ltd., Peterborough, UK) to stain cell nuclei.

Bioimaging

Imaging was performed under fluorescent upright microscope (Olympus BX51) using several objectives (4x, 10x or 20x/ 0.30 Plan Fln) and images were

captured using a Coolsnap ES camera (Photometrics) and processed through MetaVue Software (Molecular Devices). Images were then analysed using ImageJ software (http://rsb.info.nih.gov/ij).

Quantitative analysis of vector transduction

For quantification of GFP+ cells in retinal sections one slide per eye (6-8 sections) for each treatment group (n=4) was taken for analysis and all retinal sections were examined on these selected slides. Sections were photographed at x4 using the fluorescent microscope and the length of each section measured along the mid retinal surface in Image J. All sections were then re-photographed at x10 in order to count GFP+ cells. Transduced GFP+ cells were identified on the basis of their laminar location and morphology. GFP+ cells were counted and documented according to the retinal layer in which they were found including the ganglion cell layer (GCL) inner nuclear layer (INL) and outer nuclear layer (ONL). The quantification was performed with examiner being blind to the treatment group. The total number of GFP+ cells per eye was divided by the total retinal length for that eye. Data for each group is presented in scatter plots with mean cell count per mm retinal section ± SEM. Differences between groups were evaluated using ordinary one-way ANOVA followed by Turkey's multiple comparison's test in GraphPad Prism (V6; GraphPad, USA). Significance was set at $p<0.05$.

Electroretinography

Retinal function was evaluated in *wild-type* mice at one week, six weeks and twelve months after intravitreal injections. Mice were dark adapted overnight (>12 hours) and prepared for electroretinogram (ERG) recordings under dim red light (< 0.6 $\log_{10}cd/m^2$ >650 nm). Anaesthesia was induced with an intraperitoneal injection of a mixture of ketamine (75 mg/ml, 10%) and xylazine (13.6 mg/ml, 20%). Pupils were dilated with topical mydriatics (tropicamide 1% and phenylephrine 2.5%; Chauvin Pharmaceuticals, UK) prior to placement of a corneal contact-lens type electrode, held in place by a drop of hydroxypropyl methylcellulose solution (0.5%; Alcon Laboratories, Ltd., UK). The mice were placed onto a silver wire bite bar which provided head support

and it acted as a ground. A needle reference electrode (Ambu, Neuroline) was inserted subcutaneously into the left cheek. Electrodes were connected to a Windows PC via a signal conditioner (Model 1902 Mark III, CED, UK), which differentially amplified (×3000) and filtered (band-pass filter cut-off 0.5 to 200 Hz) the signal, and a digitizer (Model 1401, CED). ERG signals were averaged three to six times to reduce noise. Core body temperature was maintained throughout the procedure with a homeothermic heat mat (Harvard Apparatus).

Light protocol

Both dark-adapted (scotopic) and light-adapted (photopic) ERGs were recorded. Scotopic ERGs were performed in dark and elicited by 15ms full-field flashes produced by a light source (Cold White LED, 800 mW Thorlabs) fitted with neutral density (ND) filters in an ascending intensity series (retinal irradiances in the range 13.85-5.85 log photons/cm^2/s). Average response waveforms for each individual were produced from between 30 and 6 stimulus repeats applied at inter-stimulus intervals ranging from 1500 ms at dimmest intensities to 30s at brightest intensities to avoid significant bleaching of the visual pigment. Photopic ERGs were performed under room illumination and elicited by bright white flashes (10 μs duration at ND0; peak retinal irradiance 13.85 log photons/cm^2/s) recorded over 20 min at a frequency of 0.75 Hz, presented against a rod-saturating background white light. The amplitude of the a-wave was measured from the baseline prior to stimulus onset to the primary trough of negative polarity voltage. The amplitude of b-wave was determined from the a-wave trough to the maximum of the secondary positive peak. Data for each group is presented in scatter plots with mean amplitude ± SEM. Irradiance response curves (IRCs) were fitted with sigmoidal function. Statistical differences between groups were evaluated in GraphPad Prism (V6; GraphPad, USA) using ordinary one-way ANOVA followed by Dunnett's post-test (comparing group means to control PBS or AAV2 group), Turkey's post-test (multiple comparisons of group means between all groups) or in instances when only 2 groups were compared, a two-tailed paired t-tests was used to

compare response between enzyme and PBS-injected eyes. Significance was set at $p<0.05$.

Pupillometry

Pupillary light reflex (PLR) was measured in *wild-type* mice at six weeks and six months post injections. Mice were dark-adapted overnight (>12 hours) before the recordings. Light stimuli were provided by a 150W metal halide lamp, Phillips, USA and were transmitted along a fibre-optic bundle to an integrating reflective sphere, which provided uniform light at the mouse cornea (similar to previously described by Enezi et al., 37). Consensual PLR was recorded in un-anaesthetised, lightly scruffed mice, under infra-red conditions with an infra-red sensitive CCD camera fitted with 10x macro lens and an infra-red filter. An intervening shutter controlled stimulus timing. A single trial lasted 20 seconds: 5 seconds light OFF, 10 seconds light ON, 5 seconds light OFF. The intensity of the light was controlled by neutral density (ND) filters and mice were subjected to white light exposures in an ascending intensity series, with individual trials being separated by at least 5 minutes. Retinal irradiance values ranged from 13.8 (ND0) to 10.01 (ND5) log photons/cm^2/s. Pupillary responses were quantified from the video images using ImageJ software. Data were normalised to pupil area immediately preceding the light onset and reported as maximum pupillary constriction, mean ± SEM. Irradiance response curves (IRCs) were fitted with sigmoidal function. Statistical differences between groups were evaluated in GraphPad Prism (V6; GraphPad, USA) using a two-tailed paired t-tests to compare response between enzyme and PBS-injected eyes. Significance was set at $p<0.05$.

Author contributions

JCK, PNB and RJL designed the research; JCK performed intraocular injections, ERGs, pupillometry, and retinal histology. JCK performed all data processing and analysis. RAB assisted with pupillometry. NM performed ERG recordings at 12 months post treatment with assistance from RAB. JCK wrote and revised the manuscript with comments from all authors. PNB and RJL supervised research.

Acknowledgements

We thank Jonathan Wynne for technical assistance. JCK was supported by a Medical Research Council Clinical Research Training Fellowship (G1000268/1). The project was supported by a grant from the ERC to RJL.

Figures:

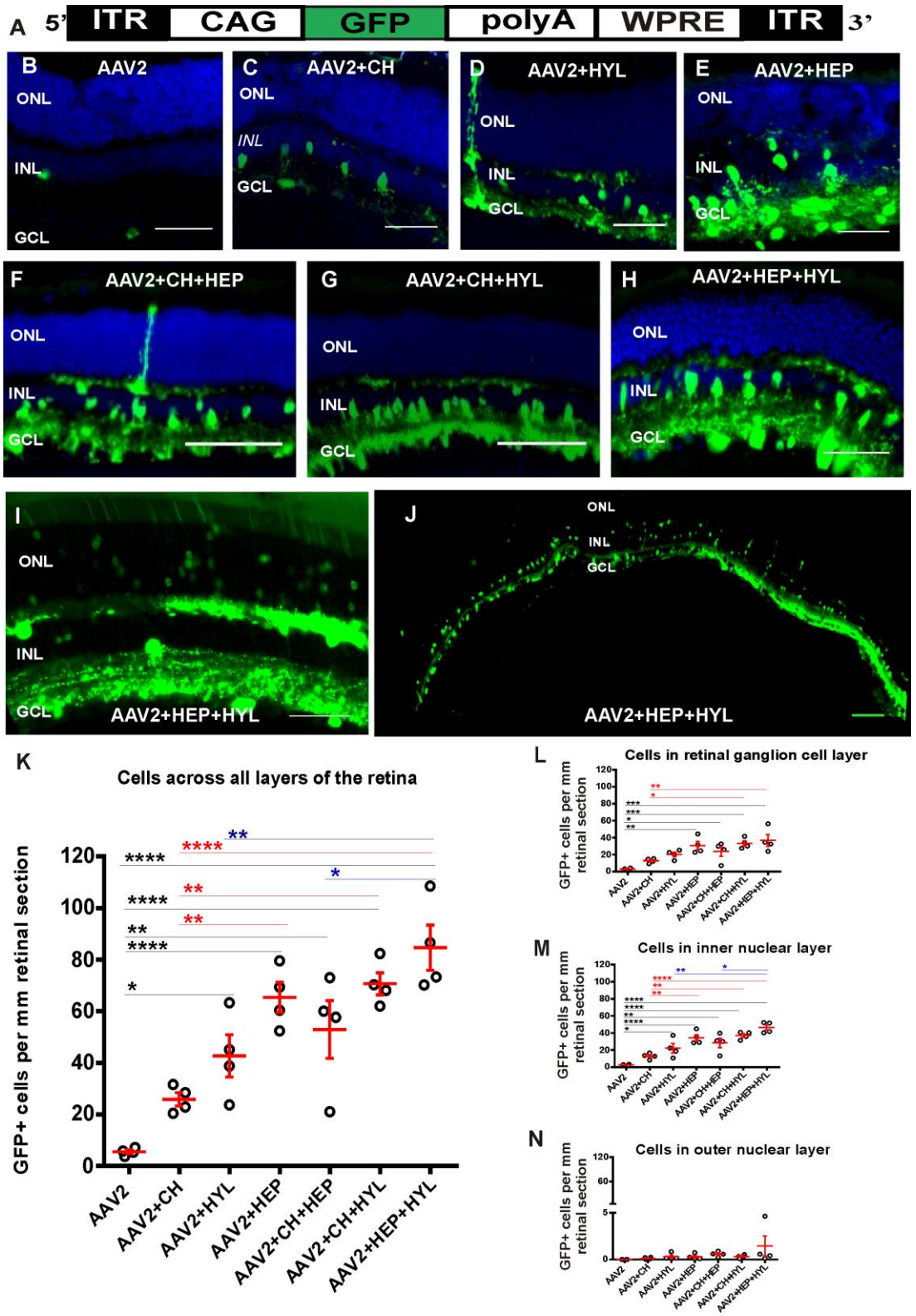
A
5'
ITR
CAG
GFP
polyA
WPRE
ITR
3'
B AAV2
C AAV2+CH
D AAV2+HYL
E AAV2+HEP
F AAV2+CH+HEP
G AAV2+CH+HYL
H AAV2+HEP+HYL
I AAV2+HEP+HYL
J AAV2+HEP+HYL
ONL
INL
GCL
K
Cells across all layers of the retina
GFP+ cells per mm retinal section
AAV2
AAV2+CH
AAV2+HYL
AAV2+HEP
AAV2+CH+HEP
AAV2+CH+HYL
AAV2+HEP+HYL
L
Cells in retinal ganglion cell layer
M
Cells in inner nuclear layer
N
Cells in outer nuclear layer

Figure 1. Transduction efficiency in *wild-type* retinas of low dose AAV2-CAG-GFP vector in combination with glycosidic enzymes.

(A) Schematic diagram of the AAV2-CAG-GFP vector. An enhanced green fluorescent protein (GFP) sequence is driven by a hybrid CMV enhancer/chickenβ-actin (CAG) promoter. The sequences are flanked by inverted terminal repeats (ITRs) and stabilised by a polyadenylation signal sequence (polyA) and a woodchuck hepatitis posttranscriptional regulatory element (WPRE). (B-H) Exemplar images of transverse sections through a *wild-type* mouse retina >6 weeks after intravitreal delivery of AAV2-CAG-GFP ($2x10^8$ gc/eye) without glycosidic enzymes (B) or in conjunction with glycosidic enzymes: chondroitin ABC lyase (CH; C), hyaluronan lyase (HYL; D), heparinase III (HEP; E) and their combinations (CH+HEP; F), (CH+HYL; G) and (HEP+HYL; H). Nuclei are counterstained with DAPI (blue). (I, J) Exemplar images of sections through a *wild-type* mouse retina >6 weeks after intravitreal delivery of $2x10^8$ gc/eye AAV2-CAG-GFP in conjunction with heparinase III and hyaluronan lyase combined demonstrating part of a retina where GFP expression in present in outer nuclear layer ONL (high magnification image: x20 objective; I) and the extent of transgene expression in a cryosection across the entire retina (low magnification image: x4 objective; J). Calibration bar = 50μm. (K-N) Quantitative analysis of transduction efficiency of vector in A showing GFP+ cell counts per mm of retinal section: across all retinal layers (K), in GCL (L), in INL (M) and in ONL (N). Ordinary one-way ANOVA with Turkey's multiple comparison's test comparing counts between groups (* $p<0.05$, ** $p<0.01$, *** $p<0.001$, **** $p<0.0001$).

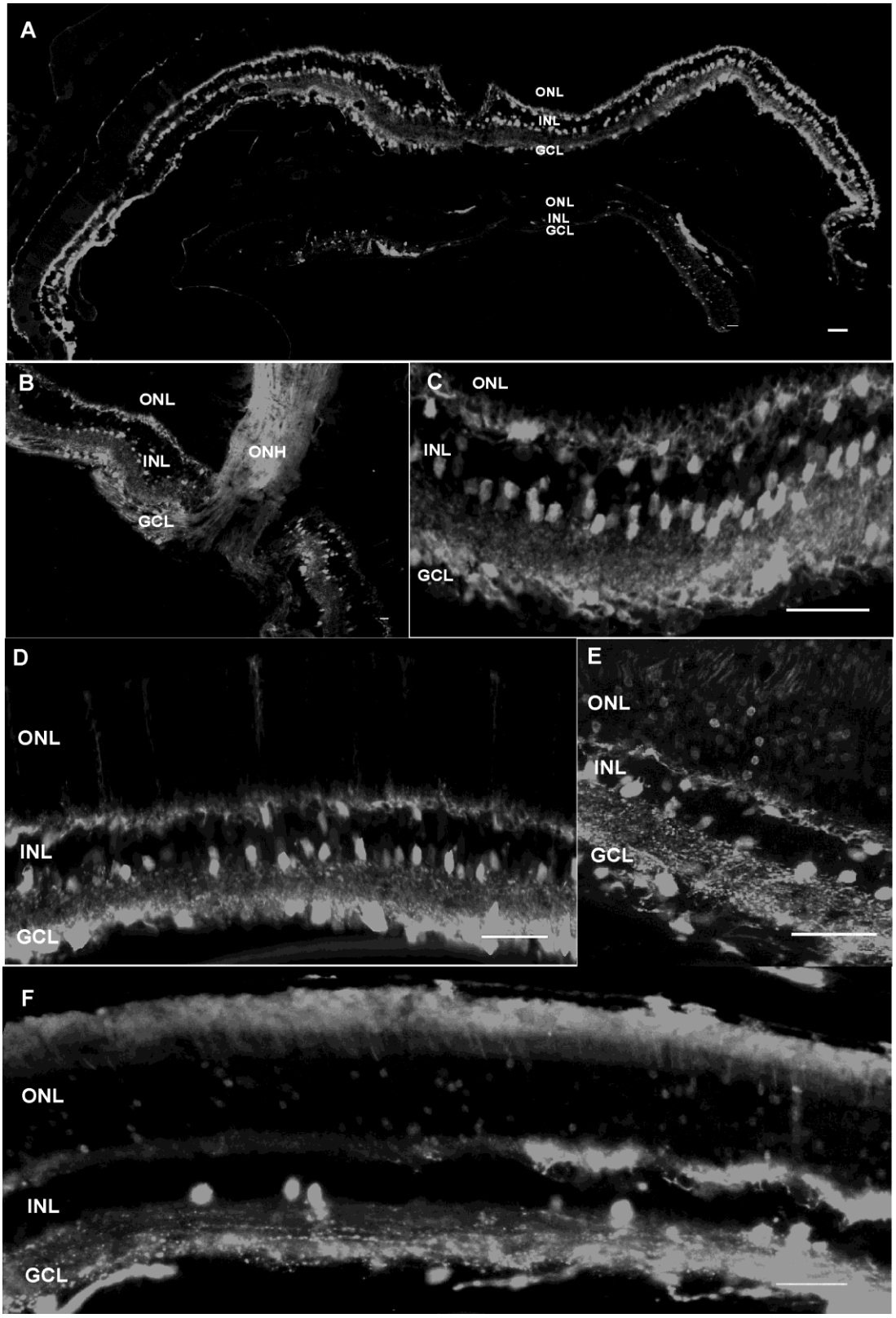
A
ONL
INL
GCL
ONL
INL
GCL
B
ONL
INL
ONH
GCL
C
ONL
INL
GCL
D
ONL
INL
GCL
E
ONL
INL
GCL
F
ONL
INL
GCL

Figure 2. Transduction efficiency in *wild-type* retinas of high dose AAV2-CAG-GFP vector in combination with heparinase III and hyaluronan lyase.

(A-F) Exemplar images of transverse sections through an adult *wild-type* mouse retina >6 weeks after intravitreal delivery of AAV2-CAG-GFP vector (3 $x10^{10}$ gc/eye) in conjunction with heparinase III (HEP) and hyaluronan lyase (HYL). Two cryosections are shown in A depicting the extent of unamplified enhanced green fluorescent protein (GFP) expression (grey) along the ganglion cell layer (GCL) and inner nuclear layer (INL; upper image) and a more patchy expression in outer nuclear layer (ONL; lower image). Robust GFP expression is observed in GCL and INL (B-D), with some areas of particularly high expression in Muller cells (D), whereas more variable expression is found in ONL (E, F), with some patches of strong expression (E).

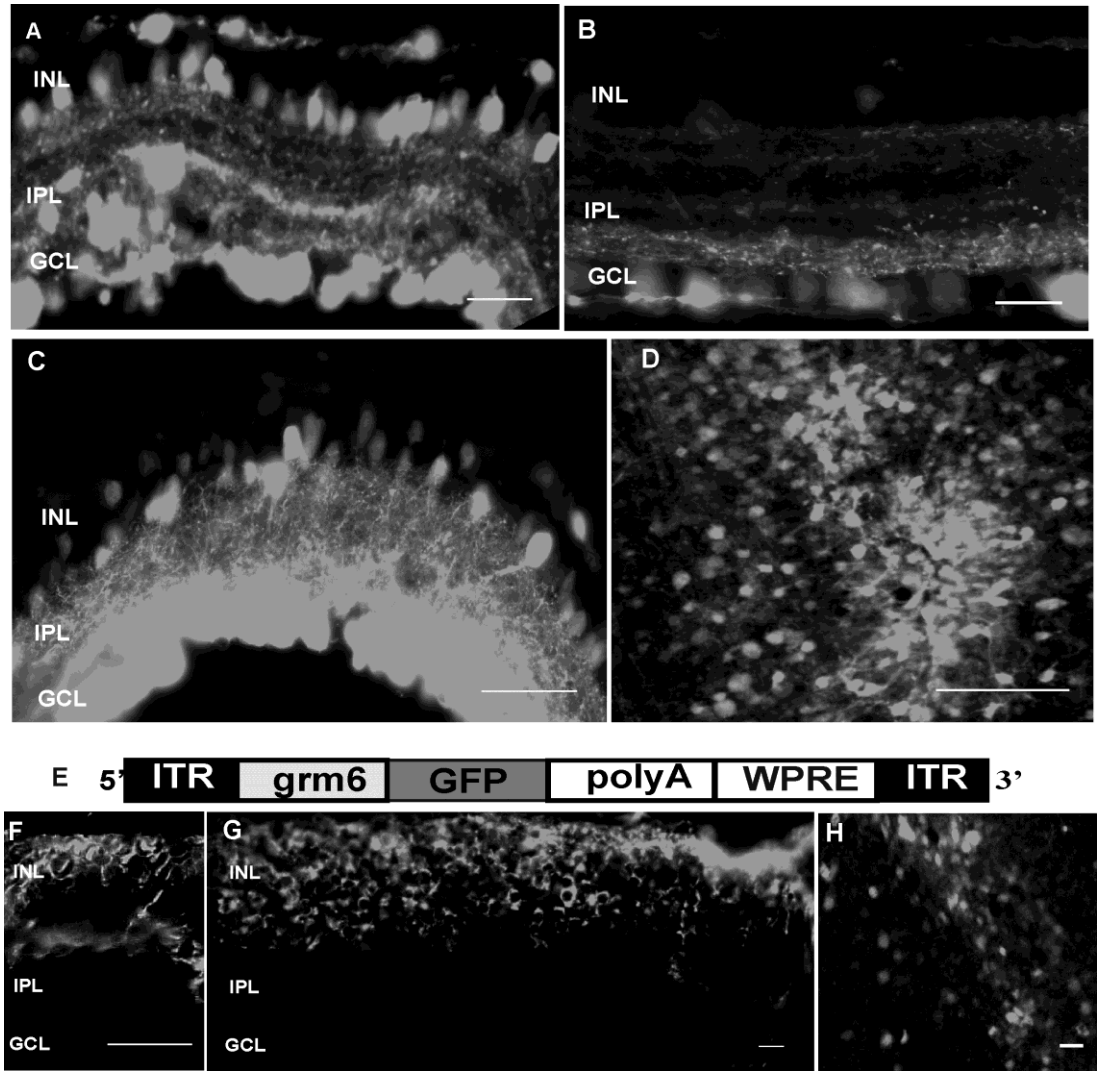
A
INL
IPL
GCL
B
INL
IPL
GCL
C
INL
IPL
GCL
D
E
5'
ITR
grm6
GFP
polyA
WPRE
ITR
3'
F
INL
IPL
GCL
G
INL
IPL
GCL
H

Figure 3. Transduction efficiency profile of in *rd1* retinas of high dose AAV2-CAG-GFP and AAV2-grm6-CAG vectors in combination with heparinase III and hyaluronan lyase.

(A-D) Exemplar images of transverse sections through an *rd1* mouse retina >6 weeks after intravitreal delivery of AAV2-CAG-GFP vector (3 x10^{10} gc/eye) in conjunction with heparinase III (HEP) and hyaluronan lyase (HYL) (A ~8μm thick section, as are other sections in image apart from C which is ~50μm in thickness) or AAV2 alone (B). Strong GFP expression (grey) is observed in the cells of ganglion cell layer (GCL) and inner nuclear layer (INL). Exemplar image of an area from a retinal whole-mount (oriented with the GCL facing upward) showing robust GFP expression (D). (E-H) Schematic of the AAV2-grm6-GFP vector with the ON-bipolar cell specific promoter grm6 (E) which as delivered intravitreally to *rd1* mice at 3 x10^{10} gc/eye. (F, G) Exemplar images of transverse sections (F ~8μm in thickness and G ~30μm in thickness) through an *rd1* mouse retina >6 weeks after intravitreal delivery of AAV2-grm6-GFP vector in conjunction with heparinase III (HEP) and hyaluronan lyase (HYL). Robust GFP expression (grey) is observed in the cells of inner nuclear layer (INL). Exemplar image of an area from a retinal whole-mount (oriented with the INL facing upward) showing strong GFP expression (H).

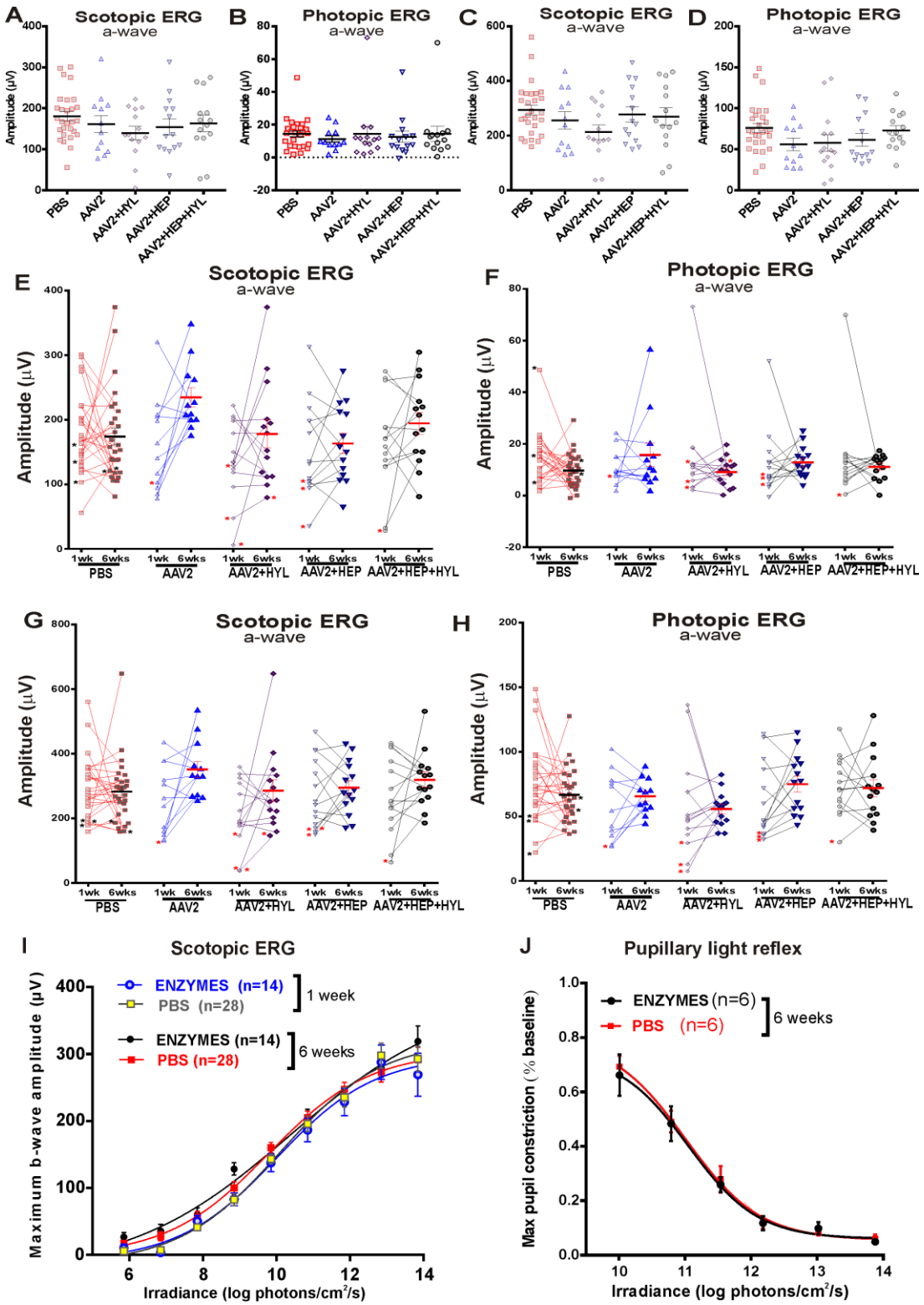
A
Scotopic ERG
a-wave
B
Photopic ERG
a-wave
C
Scotopic ERG
a-wave
D
Photopic ERG
a-wave
Amplitude (μV)
PBS
AAV2
AAV2+HYL
AAV2+HEP
AAV2+HEP+HYL
E
Scotopic ERG
a-wave
F
Photopic ERG
a-wave
1wk 6wks
G
Scotopic ERG
a-wave
H
Photopic ERG
a-wave
I
Scotopic ERG
ENZYMES (n=14)
PBS (n=28)
1 week
6 weeks
Maximum b-wave amplitude (μV)
Irradiance (log photons/cm²/s)
J
Pupillary light reflex
ENZYMES (n=6)
PBS (n=6)
6 weeks
Max pupil constriction (% baseline)
Irradiance (log photons/cm²/s)

Figure 4. Short- and intermediate-term effects of glycosidic enzymes on retinal function in *wild-type* animals

(A-H) Electroretinograms following intravitreal injections of PBS, AAV2-CAG-GFP (AAV) alone and AAV2-CAG-GFP (3 x10^{10} gc/eye) in combination with hyaluronan lyase, heparinase III (HEP + HYL). Dark-adapted (scotopic; A, C) and light-adapted (photopic; B, D) electroretinogram (ERG) recordings showing distribution of maximum a-wave (mean±SEM; A, B) and b-wave (mean±SEM; C, D) amplitude at 1 week after intravitreal injection. Following injection of the glycosidic enzymes there was no significant change in a-wave or b-wave amplitude compared to vector only or PBS injected eyes ($p>0.05$, ordinary one-way ANOVA with Dunnett's multiple comparisons test). (E-H) Dark-adapted (scotopic; E, G) and light-adapted (photopic; F, H) electroretinogram (ERG) recordings showing paired comparison of maximum a-wave (E, F) and b-wave (G, H) amplitude at 1 and 6 weeks after intravitreal injection. Stars signify presence of an intravitreal haemorrhage. Horizontal bars/error = mean±SEM. Glycosidic enzyme injections did not significantly change a-wave or b-wave amplitude compared to vector alone or PBS injected eyes at 6 weeks post treatment ($p>0.05$, ordinary one-way ANOVA with Turkey's multiple comparisons test for comparing means between all groups at 1 and 6 weeks). (I, J) Retinal photosensitivity after intravitreal delivery of hyaluronan lyase and heparinase III (ENZYMES) or PBS alone as measured by irradiance-response curve for maximum b-wave amplitude in scotopic ERG (I; 1 and 6 weeks post treatment) or maximum pupillary constriction in pupillary light reflex ((PLR) J; 6 weeks post treatment) at a range of retinal irradiances. There is no significant difference in scotopic-ERGs (I; 1 or 6 weeks post treatment) or in the PLR (J; 6 weeks post treatment) in eyes that with treated with enzymes and those that were not. Data for PLR are normalised to pupil size immediately preceding light onset (10s white light). Values are mean ± SEM, with n indicating the number of mice examined. The data are fitted with a sigmoidal function. (I; $p>0.05$, ordinary one-way ANOVA with Turkey's multiple comparisons test comparing differences in mean between groups at each irradiance for scotopic ERG and J; $p>0.05$, paired t-test between eyes that were and were not treated with the enzymes at each irradiance for PLR).

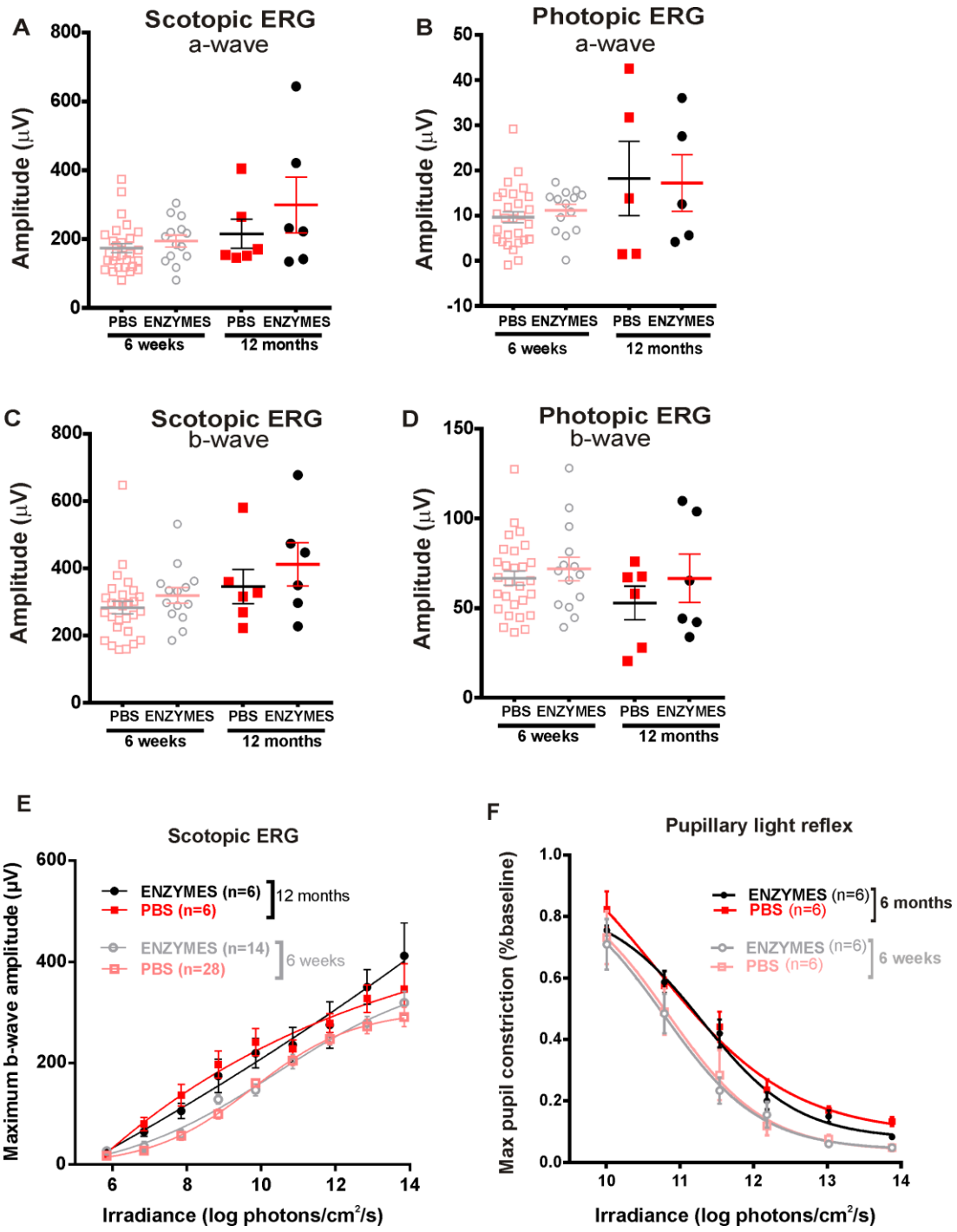
A
Scotopic ERG
a-wave
Amplitude (μV)
800
600
400
200
0
PBS ENZYMES PBS ENZYMES
6 weeks
12 months
B
Photopic ERG
a-wave
Amplitude (μV)
50
40
30
20
10
0
-10
PBS ENZYMES PBS ENZYMES
6 weeks
12 months
C
Scotopic ERG
b-wave
Amplitude (μV)
800
600
400
200
0
PBS ENZYMES PBS ENZYMES
6 weeks
12 months
D
Photopic ERG
b-wave
Amplitude (μV)
150
100
50
0
PBS ENZYMES PBS ENZYMES
6 weeks
12 months
E
Scotopic ERG
Maximum b-wave amplitude (μV)
600
400
200
0
ENZYMES (n=6)
PBS (n=6)
12 months
ENZYMES (n=14)
PBS (n=28)
6 weeks
6
8
10
12
14
Irradiance (log photons/cm²/s)
F
Pupillary light reflex
Max pupil constriction (%baseline)
1.0
0.8
0.6
0.4
0.2
0.0
ENZYMES (n=6)
PBS (n=6)
6 months
ENZYMES (n=6)
PBS (n=6)
6 weeks
10
11
12
13
14
Irradiance (log photons/cm²/s)

Figure 5. Long-term effects of glycosidic enzymes on retinal function in *wild-type* animals

(A-D) Dark-adapted (scotopic; A, C) and light-adapted (photopic; B, D) electroretinogram (ERG) recordings showing distribution of maximum a-wave (A, B) and b-wave (C, D) amplitude (mean±SEM) after intravitreal delivery of heparinase III and hyaluronan lyase (ENZYMES) or PBS alone 9 months post treatment. Data at 6 weeks post treatment are shown for comparison. Glycosidic enzyme injection showed no significant change in a-wave (need to see photopic data at 9m) or b-wave amplitude compared to control (PBS) eyes at 9 months post treatment. Two-tailed paired t-tests comparing response between enzyme and PBS treated eyes at each time point or one-way ANOVA with Turkey's multiple comparison test for comparison between all groups. (E, F) Retinal photosensitivity after intravitreal delivery of heparinase III and hyaluronan lyase (ENZYMES) or PBS alone as measured by irradiance-response curve for maximum b-wave amplitude in scotopic ERG (E; at 9 months post treatment) or maximum pupillary constriction in pupillary light reflex ((PLR) F; 6 months post treatment) at a range of retinal irradiances. Data at 6 weeks post treatment is shown for comparison. There is no significant change in scotopic-ERG (E) or in PLR (F) between the enzyme or PBS treated eyes at 9 months post treatment. A small decrease in sensitivity is observed for both curves (PBS and ENZYMES) at 6 months compared to 6 weeks (significant at high irradiances; for enzyme curves at 13.8 ($p=0.02$), 13.0 ($p=0.01$) and 11.5 ($p=0.04$) and for PBS curves at 13.8 ($p=0.007$), 13.0 ($p=0.01$) log photons/cm^2/s. Data for PLR are normalised to pupil size immediately preceding light onset (10s white light). Values are mean ± SEM, with n indicating the number of mice examined. The data are fitted with a sigmoidal function. Two-tailed paired t-test was used to compare response between ENZYME and PBS-injected eyes at each irradiance.

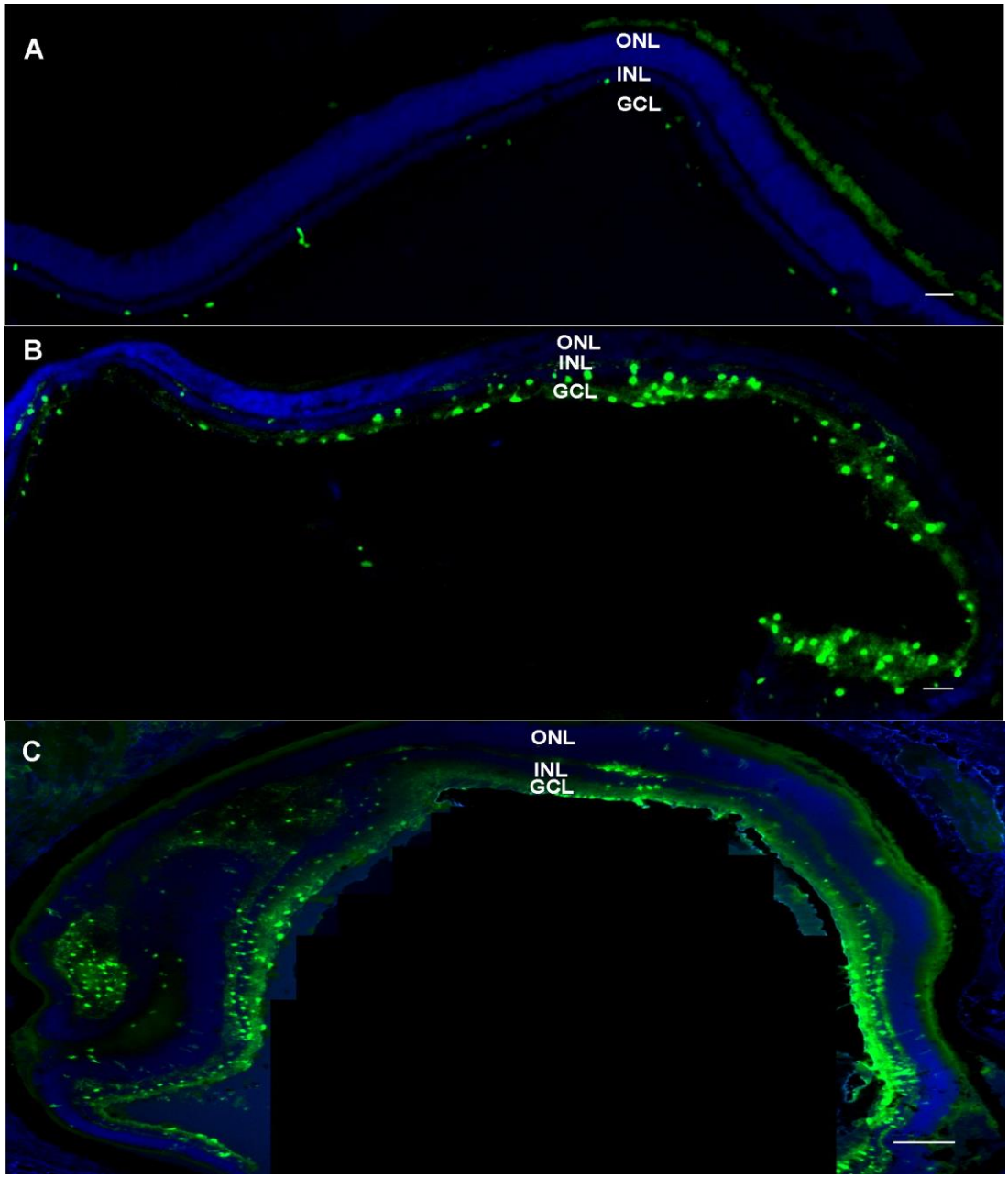

Supplemental Figure 1

Transgene expression in *wild-type* retina using low dose AAV2-CAG-GFP in conjunction with glycosidic enzymes

(A-C) Exemplar images of transverse sections through a *wild-type* mouse retina >6 weeks after intravitreal delivery of AAV2-CAG-GFP ($2x10^8$ gc/eye) alone (A) or in conjunction with heparinase III (B) and hyaluronan lyase (C). Unamplified expression of GFP in cells of the ganglion cell layer (GCL) and inner nuclear layer (INL) is shown in green. Nuclei are counterstained with DAPI (blue).

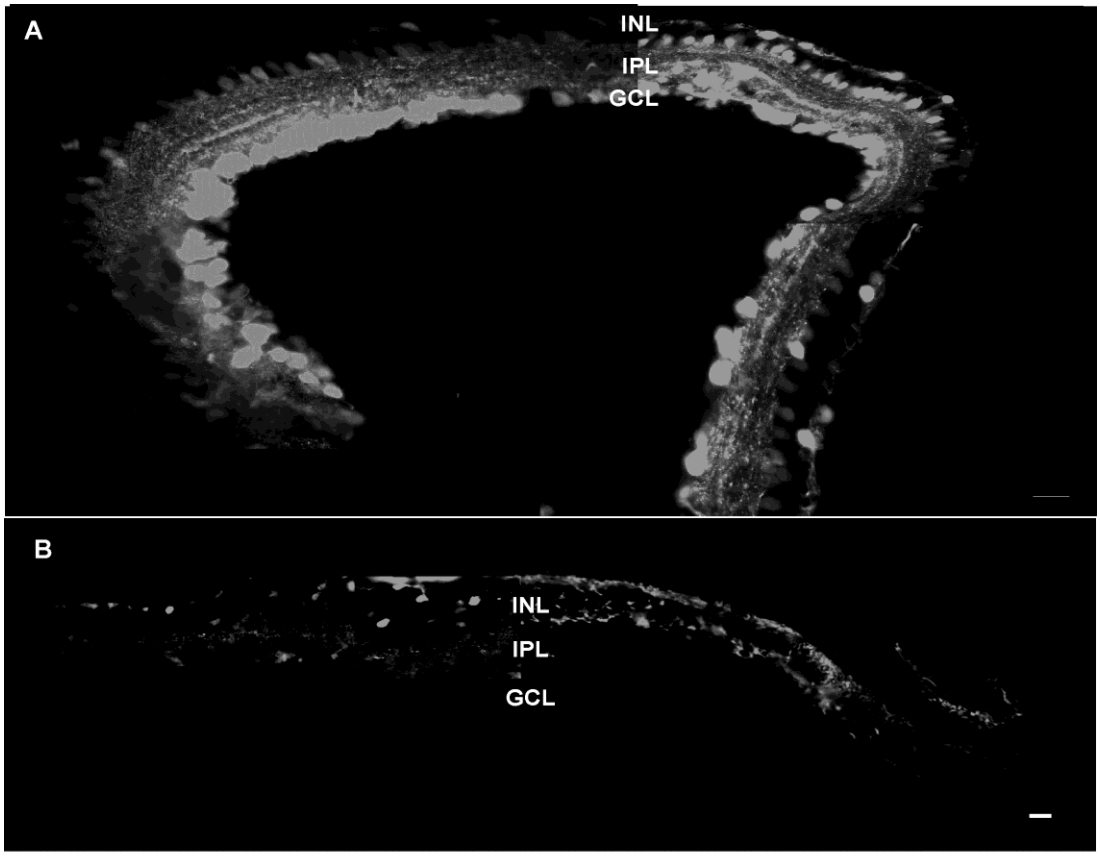

Supplemental Figure 2

Transgene expression in *rd1* retina using high dose AAV2-GFP in conjunction with glycosidic enzymes

(A, B) Montage of several high magnification images from an exemplar transverse section through an *rd1* mouse retina >6 weeks after intravitreal delivery of (A) AAV2-CAG-GFP (3 x10^{10} gc/eye) or (B) AAV2-grm6-GFP (3x10^{10} gc/eye) in conjunction with heparinase III and hyaluronan lyase combined. Expression of enhanced green fluorescent protein in cells of the ganglion cell layer (GCL) and inner nuclear layer (INL) is seen in (A) and in cells of the INL only in (B).

Chapter 4: Paper 2

Enhancing visual responses in retinal degeneration with human melanopsin

Authors: Jasmina Cehajic-Kapetanovic[1], Annette E. Allen[2], Nina Milosavljevic[2], Timothy M. Brown[2], Paul N. Bishop[1], Robert J. Lucas[2].

Affiliations:

[1]Centre for Ophthalmology & Vision Sciences, Institute of Human Development, University of Manchester and Manchester Royal Eye Hospital, CMFT, Manchester Academic Health Sciences Centre, Manchester, UK.

[2]Faculty of Life Sciences, University of Manchester, Oxford Road, Manchester M13 9PT, UK

Enhancing visual responses in retinal degeneration with human melanopsin

Authors: Jasmina Cehajic-Kapetanovic[1], Annette E. Allen[2], Nina Milosavljevic[2], Timothy M. Brown[2], Paul N. Bishop[1], Robert J. Lucas[2].

Affiliations:

[1]Centre for Ophthalmology & Vision Sciences, Institute of Human Development, University of Manchester and Manchester Royal Eye Hospital, CMFT, Manchester Academic Health Sciences Centre, Manchester, UK.

[2]Faculty of Life Sciences, University of Manchester, Oxford Road, Manchester M13 9PT, UK

Highlights:

Ectopic melanopsin restores *in vivo* visual responses in retinal degeneration

Ectopic melanopsin functions at a range of irradiances under physiological light conditions

Ectopic melanopsin functions under light adapted conditions

Summary:

Optogenetic therapies show promise for the treatment of degenerative retinal conditions, in particular advanced retinal dystrophies. Melanopsin is a native retinal photopigment normally expressed in a subset of (intrinsically photosensitive) retinal ganglion cells (ipRGCs). Here, we expressed human melanopsin ectopically in both RGCs and inner nuclear layer (INL) cells of *rd*^{1} mice, a model of advanced retinal degeneration. This was achieved by intravitreal injection of AAV2 containing melanopsin cDNA under the control of a generalised promoter, in conjunction with glycosidic enzymes. Control eyes were injected with AAV2 containing enhanced green fluorescent protein (GFP) cDNA. Melanopsin treated mice showed enhanced pupil light reflex, as previously reported for over-expression of melanopsin in the degenerate retina. *In vivo* electrophysiology recordings were made from the dorsal lateral geniculate nucleus (LGN). Light pulses

presented to eyes expressing human melanopsin drove excitatory responses in both the ipsi- and contralateral LGN that were more numerous, larger, and of higher sensitivity and shorter latency than those elicited in control, GFP-expressing eyes. Moreover, we found that ectopic human melanopsin expression could result in the detection of changes in irradiance under light adapted conditions, a function which was absent in control *rd*[1] mice. These responses could be elicited at moderate light intensities, ~2-3 orders of magnitude lower than necessary for current microbial-based optogenetic and photopharmacological strategies.

Introduction

Retinal dystrophies, such as retinitis pigmentosa, are a major cause of untreatable blindness in which visual loss is caused by the loss of rod and cone photoreceptors. Whilst considerable advances have been made in preventing or slowing down this visual loss using gene replacement therapies [1-5], restoration of vision once lost presents major challenges. Some progress has been made using electrical stimulation of retinal ganglion cells (RGCs) through external devices which provides crude spatial discrimination for at least some patients [6-7]. Another promising strategy is using optogenetic approaches to impart photoreception to non-light sensing neurons which remain viable after the native rod and cone photoreceptors have been lost [8-10].

A variety of optogenetic sensors have been introduced into the surviving inner retina of animal models of retinal dystrophies, including microbial channels/pumps [11-16] and synthetic photoswitches [17-20] that have restored visual responses in these models. However, the light levels necessary to operate these actuators are often very high and synthetic photoswitches require frequent supplementation with 'photoswitch' molecules. Native mammalian light-sensitive proteins [21-23] and a mammalian based chimeric protein [24] have also been introduced into inner retinal neurons and shown to restore visual function with improved light sensitivity. In our most recent work, we introduced the G-protein coupled receptor (GPCR) rod opsin to blind *rd*^{1} retinas and demonstrated that this restored useful spatiotemporal discrimination under natural viewing conditions [22].

Here, we used melanopsin, the GPCR opsin photopigment normally present in the small subset of photosensitive ganglion cells (ipRGCs). Melanopsin, with its bi-stable properties confers bleach resistance without the need for chromophore recycling [25], so a supply of chromophore is not required. This would be particularly advantageous in end-stage retinal degeneration and conditions with primary retinal pigment epithelium RPE defects where long-term chromophore

supplies might be limited [26, 27]. In a previous study melanopsin was ectopically expressed in the inner retina (mainly RGCs) of *rd*^{1} mice with an advanced degeneration [21]. *In vitro* single cell recordings from these transduced cells showed that they were light sensitive, pupillary reflex was largely restored and the mice could distinguish light from dark.

Here, we set out to determine the extent of restored visual responses *in vivo* and to characterise the sensitivity and kinetic properties of augmented (versus native) melanopsin responses using the same mouse model. We delivered human melanopsin via intravitreal gene therapy to inner retinal neurons in combination with glycosidic enzymes to improve retinal penetration. More numerous light responses were observed in the dorsal lateral geniculate nucleus (dLGN) in mice downstream of ectopically expressing melanopsin retinas compared to controls. In addition, light responses driven by ectopic melanopsin were superior in terms of sensitivity, amplitude and latency of response compared to native melanopsin responses. Moreover, restored responses could be elicited under moderate light intensities, typical of indoor lighting levels and were present under light adapted conditions.

Results

Gene delivery to *rd*^{1} retina

We used intravitreal injection of viral vector (AAV2) to deliver human melanopsin under control of a ubiquitous CAG promoter (CAG-hOPN4; Figure 1A). Control eyes were injected with the same vector coding for the green fluorescent protein, GFP (CAG-GFP; Figure 1B). To enhance vector transduction and increase the depth of retinal penetration we co-injected glycosidic enzymes with both vectors [28]. Immunolabelling with an antibody against human melanopsin (anti-hOPN4) at ~12 weeks post injections showed widespread ectopic expression of melanopsin in

both the ganglion cell and inner nuclear layers (GCL; INL) of all treated *rd1* mice (Figures 1C and E) confirming previous findings that melanopsin can express outside native ipRGCs [21]. A similar expression pattern was observed for GFP in eyes injected with CAG-GFP (Figures 1D and F). Expression pattern was variable across the retina and was generally higher in GCL than INL (Figures S1A-C). Staining was absent from a control PBS injected group (Figure S1D and E) and the retina of *wild-type* mice (Figure S1F and G) showing that the anti-body against hOPN4 did not cross-react with endogenous murine melanopsin in the ipRGCs.

Ectopic melanopsin enhances *in vivo* visual responses in *rd1* mice

We measured the pupillary light reflex (PLR) to investigate whether the ectopically-expressed melanopsin enhanced photosensitivity in *rd1* retinas. The PLR is mediated in part by endogenous melanopsin [29] and so a residual response remains in the *rd1* mice after photoreceptor degeneration [30]. We recorded stimulus-response curves for maximum pupillary constriction during ten seconds of white light at a range of irradiances (Figure 2A). We found impaired PLR in mice injected with the control GFP virus, confirming previous reports of the impact of retinal degeneration on this reflex [31], whereas ectopic melanopsin expression restored the PLR to levels approaching that of wild type mice at high irradiances. We detected an improvement in pupil response down to at least ~10^{11} photons/cm^2/s (Figures 2A and 2B), well within normal ambient lighting conditions.

Next we wished to determine whether ectopic melanopsin expression in the degenerate *rd1* retinas restores responses in the cortical visual pathway. To do this we focused on the lateral geniculate nucleus (LGN), a major retino-recipient region concerned with pattern vision. We used GFP expression to trace the axonal projections of the transduced RGCs. Significant contralateral (and to a lesser extent ipsilateral) axonal projections of the GFP transduced RGCs were observed in both

ventral and dorsal aspects of the LGN (Figure 2C). Therefore we undertook *in vivo* electrophysiological recording from the dLGN of anaesthetised mice using silicon multielectrode probes. For these experiments we used animals in which one eye had been injected with the hOPN4 virus and the other with a control GFP virus (Figure 2D). This enabled us to compare responses to stimuli (10 sec full-field 410nm flash; estimated retinal irradiance ~$6x10^{14}$ melanopsin) presented to treated and control retinas in the same individual (Figure 2E). Of 729 single units from 6 mice recorded from the two LGN (ipsi- and contra- to the melanopsin injected eye), 41 showed a significant change in firing (see methods) associated with light presentation to the hOPN4-treated eye and 23 a response to light presented to the control GFP-treated eye (Figure 2F&G).

Characterisation of enhanced *in vivo* responses in *rd[1]* mice

Examination of the dLGN units downstream of *rd[1]*-CAG-hOPN4 eyes showed a heterogeneous group of light-induced responses with robust increases in firing across many repeats of a visual stimulus (Figure 3A). Responses were excitatory and either sustained or transient (Figure 3A). When presented with 10s pulses of white light 7/41 (17%) units showed transient increase in firing rate (duration of response <1s), 11/41 (27%) units had more sustained response (duration 1-10s), and 23/41 (56%) maintained elevated firing beyond light exposure (duration >10s). By contrast, responses found in the control group were more uniform with very weak light evoked modulations in firing rate that were poorly reproducible over repeated stimulus presentations (Figure 3B). Many responses were very brief (11/23; 48%, response duration of <1s) and more persistent activation was found in the remainder of units (duration 1-10s in 2/23; 9%, and duration >10s in 10/23; 43%).

Light responses from hOPN4 treated eyes could be detected for stimuli at estimated retinal irradiance of $6x10^{14}$, $6x10^{13}$ and $6x10^{12}$ melanopsin photons/cm^2/s but responses were not recorded when the irradiance was reduced to $6x10^{11}$ melanopsin photons/cm^2/s (Figures 3A and 3C). This sensitivity is comparable to that recently reported for human rod opsin [22-23] and Opto-mgluR6 [24] optogenetic actuators, but superior to that we observed for endogenous melanopsin responses in degenerate *rd1* eyes (Figures 3B and 3D) or to that reported for microbial photopigments and synthetic light switches, which generally require threshold irradiances in the range 10^{14}-10^{17} photons/cm^2/s [11-20].

Furthermore, recorded dLGN responses varied substantially between treated and control groups in response amplitude at a range of irradiances (Figure 3E) with significant difference in mean amplitude at maximum irradiance $6x10^{14}$ photons/cm^2/s (mean firing rate ±SD in treated group was 11.09±16.67 spikes/s, n=41 units and for control group 3.00±2.85 spikes/s; n=23 units; unpaired t-test p=0.02; Figure 3F). In addition, the total number of units showing a significant response was higher for stimuli presented to hOPN4- than GFP-expressing eyes at each of the lower irradiances (n=22 vs 11 at $6x10^{13}$ photons/cm^2/s; n=7 vs 2 at $6x10^{12}$ photons/cm^2/s; n=3 vs 1 at $6x10^{11}$ photons/cm^2/s). In addition, we observed a range of response latencies in the melanopsin treated and control groups at different irradiances (melanopsin treated, 0.8 to 15.8s at $6x10^{14}$ photons/cm^2/s; Figure 3G and control group, 0.8 to 19.8s at $6x10^{14}$ photons/cm^2/s; Figure 3H) with importantly a significant improvement in mean latency in melanopsin treated compared to endogenous *rd1* melanopic responses at maximum tested intensity (melanopsin treated = 6.67±4.9s mean±SD; control = 10.83±5.65s mean±SD; unpaired t-test p=0.003).

Ectopic melanopsin restores *in vivo* visual responses under light adapted conditions

To determine whether ectopic melanopsin expression can induce responses under light adapted conditions, we adapted the treated *rd*[1] mice to a background light (estimated retinal irradiance $6x10^{14}$ melanopsin photons/cm^2/s) and applied a light step at three levels of contrast (Michelson contrast 33%, 66% and 96%; Figure 4A). We found a number of units whose firing rate was increased by this stimulus when presented to CAG-hOPN4 treated eyes (Figure 4B and 4C; n=12/590 units from 4 mice that met our objective criterion for light responsiveness; Michelson contrast 96%) but none of the units met the response criterion in the control eyes. Examination of individual response profiles showed units with both transient and more sustained firing patterns that were repeatable over multiple stimulus presentations (Figure 4D). We observed a range of response latencies (1.3 to 9.9s) with mean latency±SD of 5.31±2.57s (Figure 4E). Duration of response was also variable with 5/12 (42%) units lasting <1s, 1/12 (8%) units lasting 1-5s and 6/12 (50%) having more persistent activation (>5s). In addition, we observed a few units whose firing rate was modulated at lower levels of contrast (n=4 units met objective criterion for light responsiveness at Michelson contrast 66% and n=2 units met this criterion at Michelson contrast 33%) (Figures 4F and 4G).

Discussion

In this study, we demonstrated that ectopically expressed human melanopsin can enhance *in vivo* visual responses in retinal degeneration mice. We delivered melanopsin to degenerate *rd*[1] retina in therapeutically relevant manner using an intravitreal injection of clinically approved AAV2 vector. As previously reported [21], we found that over-expression of melanopsin leads to an increase in sensitivity of the PLR. Thus, once ectopically expressed in the inner retina, melanopsin enhanced retinal photosensitivity capable of driving non-image forming vision (PLR). In addition, we found that transduced retinal neurons

projected their axons to the lateral geniculate nucleus (LGN), a brain region implicated in form vision. Using *in vivo* electrophysiological recordings in the LGN, we found that ectopic melanopsin enhances responses to light stimuli over a range of irradiances typical of our everyday experience. We observed a heterogeneous collection of excitatory responses that were either sustained or transient at a single unit level. The restored responses were superior to those driven by native melanopsin in ipRGCs in terms of mean sensitivity, amplitude and latency of response and the CAG-hOPN4 treated mice could detect changes in contrast under light adapted conditions at moderate illumination.

This study provides new information on the quality of the recreated visual code for ectopic human melanopsin. It responds over a range of light intensities spanning ~3 log units of irradiances encountered in normal everyday scenes. Responses were found at retinal irradiances as low as $6x10^{12}$ photons/cm^2/s comparable to previously reported for ectopic rod opsin [$\sim10^{12}$ photons/cm^2/s; 22-23] and a synthetic Opto-mgluR6 receptor [$6x10^{12}$ photons/cm^2/s; 24], but significantly lower intensities than required for microbial opsins [thresholds between 10^{14}-10^{17} photons/cm^2/s; 11-16] and synthetic photoswitches [thresholds between 10^{13}-10^{16}; 17-20]. However, as melanopsin is a Gq coupled protein [32-33], its primary activation was excitatory and we did not observe any convincing inhibitory responses driven by the ectopic melanopsin expression. It is possible that the melanopsin expression was insufficient to drive significant lateral inhibition via amacrine circuitry and produce detectable OFF responses. In addition, OFF excitatory responses could have been hidden by some long-lasting ON excitations. It is also conceivable that we are augmenting pre-existing ipRGC responses, driven by endogenous melanopsin, as would be suggested by enhanced PLR and that improved response properties (in terms of amplitude and kinetics) are originating from over-expression of melanopsin in ipRGCs.

Although the responses in the LGN were improved from those of the endogenous melanopsin in ipRGCs of the *rd1* mice in terms of latency, most still had long latencies and long duration of activation limiting their potential for high spatial vision. However, when the light-sensing portion of melanopsin is combined with an mGluR6 receptor, as in Opto-mgluR6, and targeted to ON bipolar cells [24], melanopsin is capable of driving fast responses with latencies matching those mediated through photoreceptors, indicating that melanopsin activation is intrinsically fast and that slow melanopsin responses from ipRGCs are likely to be a result of slow kinetics of intracellular signalling cascades. We did observe some relatively fast responses (15% units had onset within 1.5s; recorded in anaesthetised animals) in a range similar to those driven by ectopic rod opsin and shown to be capable of driving more complex spatiotemporal visual discrimination in awake freely moving animals [22-23]. It is possible that some of the faster responses we observed might originate from melanopsin expressed in ON bipolar cells, coupling to a pre-existing fast secondary messaging cascade in a light-dependent manner.

We have previously reported that melanopsin is capable of driving responses under light adapted states in *wild-type* mice and Cnga3-/- mice (a model lacking cone function but having more intact system compared to degeneration models), whereas such responses were much more difficult to elicit (less reliable and very sluggish) in *rd/rd cl* mice (a model of retinal degeneration) [34-36]. Here, we have found a subset of dLGN neurons downstream of CAG-hOPN4 treated eyes with advanced *rd1* mediated retinal degeneration that elicited reliable responses when presented with pulses of light over a moderate steady background illumination, but these were absent in the control CAG-GFP treated mice. Response latencies for these restored photopic responses were in the order of several seconds (mean latency ~5s), although we did find a few units (25%) that responded within 2s of stimulus onset. Restoring this ability to detect dynamic changes in light intensity under photopic conditions is an important step in providing richer information about patterns encountered in everyday natural scenes.

In summary, the LGN studies presented here provide a detailed description of the visual responses driven by ectopic human melanopsin. For consideration as a therapy for retinal degenerations, ectopic melanopsin (in its unaltered, native form) drives responses at modest intensities but inferior temporal fidelity compared to responses driven by rod opsin or Opto-mGluR6, although in the latter case the use of a transgenic mouse model prevents direct comparison to the gene therapy approach presented here which, although more clinically relevant, will inevitably give inferior ectopic gene expression.

Experimental Procedures:

Animals

Homozygous adult C3H/HeJ (*rd*^{1}) mice were used in this study. All animal experiments were conducted in accordance with the UK Home Office regulations for the care and use of laboratory animals, the UK Animals (Scientific Procedures) Act (1986) and the Animal Welfare Body of the University of Manchester. Animals were kept under a 12-hour light-dark cycle and supplied with food and water *ad libitum.*

Gene delivery via AAV

AAV2 vectors used in this study were obtained from Vector Biolabs, Philadelphia, USA. In each case the gene of interest (human melanopsin, hOPN4, Figure 1A; or green fluorescent protein, GFP; Figure 1B) under the control of a strong ubiquitous pan-neuronal promoter (CAG; a fusion of CMV early enhancer and chicken β-actin promoter) was flanked by inverted terminal repeat (ITR) domains and stabilised by polyadenylation signal sequence (polyA) and a woodchuck hepatitis posttranscriptional regulatory element (WPRE). Vectors were injected intravitreally in isofluorane anaesthetised mice at >8 weeks of age.

Prior to injections, pupils were dilated with tropicamide and phenylephrine. A custom made ultra-fine needle (Hamilton RN needle 34 gauge, supplied by ESSLAB) was attached to a 5µl Hamilton glass syringe and was passed at 45 degrees through the pars plana into the vitreous cavity, carefully avoiding the lens and blood vessels. The injection was performed under a direct visualisation of the needle tip through cover-slipped eyes under an operating microscope (Microscopes Inc., USA). For each mouse, one eye was injected with CAG-hOPN4 and the other with control CAG-GFP vector (3µl of 10^{13} genomic counts of AAV2 for each vector) in combination with 0.5µl of glycosidic enzyme solution containing 0.125 units each of heparinase III and hyaluronan lyase (E.C. 4.2.2.8 & E.C. 4.2.2.1; Sigma-Aldrich, Dorset, UK). The enzyme solutions were made fresh on the day of injection by dissolving the enzymes in sterile phosphate-buffered saline (PBS). The vector and enzymes were mixed in a syringe immediately before an eye injection and were given in a single combined injection.

Histology

Retrieved eyecups (>12 weeks post vector injection) were fixed in 4% paraformaldehyde (PFA) in PBS for 24 hours at 4^{o} C. The tissue was then washed in PBS and further fixed in 30% sucrose in PBS overnight at 4^{o} C. Fixed eyes were cryo-protected in optimal-cutting temperature medium (Raymond A Lamb Ltd., Eastbourne, UK) and frozen at -80^{o} C until further processing. Cryo-protected retinal section were sectioned on a cryostat (Leica, Microsystems) horizontally through the eyecup at 8-10µm thickness from ventral to dorsal side, so that each section contained a complete nasal to temporal cross-section of the retina. Ten-twelve sections were collected on each slide containing sections representative of the entire retina. Slides were stored at -80^{o} C.

For immunohistochemistry, slides were removed from the freezer and allowed to air-dry at room temperature for 1 hour. Sections were permeabilised by immersing slides in PBS with 0.2% Triton for 20 minutes at room temperature. Following this,

sections were background blocked with PBS with 0.2% Triton X-100 containing 10% donkey serum (D9663; Sigma, UK) for 1 hour at room temperature. Primary antibody (Polyclonal Rabbit Anti-Human Melanopsin, Abcam, Ab65641) was applied at 1:200 dilution in blocking buffer (PBS with 0.2% Triton X-100 and 2.5% donkey serum) for 3 hours at room temperature. After washing in tween 0.05% PBS, four times for 10 minutes, sections were incubated with secondary antibody (Alexa Fluor® 546 Donkey Anti-Rabbit IgG (H+L) Antibody, Life technologies, lot: 1504518) diluted 1:200 in PBS with 0.2% Triton X-100 and 2.5% donkey serum for 2 hours at room temperature. Slides were then washed four times for 10 minutes in 0.05% tween PBS followed by one final wash with dH_20. After removing excess fluid, slides were mounted with fluorescent mounting media containing DAPI (Vectashield, Vector Laboratories Ltd., Peterborough, UK) to stain cell nuclei.

For bio-imaging, sections were analysed under an Olympus BX51 upright microscope using x4, x10 and x20 Plan Fln objectives and captured using a Coolsnap ES camera (Photometrics, Tucson, AZ) through MetaVue Software (Molecular Devices Ltd. Wokingham, UK). Images were taken under specific band pass filter sets and colour-combined images were used for further processing using ImageJ.

Pupillometry

Pupillary light reflex (PLR) was measured in *wild-types* (n = 6) and *rd*[1] mice treated with AAV2-CAG-GFP (n = 5), AAV2-CAG-hOPN4 (n = 5) at >12 weeks post injections. Mice were dark-adapted for 1 hour before the recordings. 10s full field white light stimuli were provided by a light source (150W metal halide lamp; Phillips, USA), intensity controlled using neutral density filters, and consensual pupil responses measured as previously described [31, 37].

In vivo electrophysiology

In vivo electrophysiology recordings were performed in isofluorane anaesthetised mice (initial dose of 2-3% and maintenance dose of 0.6-1.0% administered via a nose cone; GM-4, Narishige, Japan) where one eye was injected with CAG-hOPN4 and the other with CAG-GFP gene therapy vector (Figure 2D) at >12 weeks post injections. Animals were mounted in a stereotaxic frame (SR-15M; Narishige International Ltd, London, UK) and core body temperature was maintained at 37 °C via a homeothermic heat mat (Harvard Apparatus, Edenbridge, UK). Pupils were dilated with atropine and mineral oil (Sigma Aldrich) was applied topically to the cornea to keep it moist. A small craniotomy and durotomy (~1 mm^2) was performed directly above each lateral geniculate nucleus (dLGN) using stereotaxic coordinates according to mouse atlas (Paxinos and Franklin, 2001; hole centre= bregma: −2.46 mm; midline: −2.8). A 32-channel electrode (NeuroNexus Technologies Inc., MI, USA) was introduced to each dLGN in the centre of the hole (medial shank: -2.5 mm relative to midline; depth: -2.6 mm relative to brain surface at 18 degrees angle) for simultaneous recording from both LGNs. A second recording was performed where electrodes were re-positioned and advanced 250μm dorsally with respect to bregma (at -2.71mm). Following electrode insertion mice were dark adapted for 30 minutes to allow neuronal activity to stabilize. Data were acquired using a Recorder64 system (Plexon, TX, USA) with signal amplification by a 20x gain AC-coupled head stage (Plexon, TX) followed by preamplifier conditioning providing a total gain of 3500x. Data were high-pass (300Hz) filtered and time-stamped neural waveforms were digitized simultaneously from all channels at a rate of 40 kHz.

To confirm the location of recording sites, the recording electrode was dipped in fluorescent dye (Cell Tracker CM-DiI; Invitrogen) prior to insertion into the brain. After *in vivo* recordings, the mouse's brain was removed and post-fixed overnight in 4% paraformaldehyde, prior to cryoprotection for 24 hours in 30% sucrose.

100µm coronal sections were then cut using a sledge microtome, mounted onto glass slides and cover slipped using Vectashield (Vector Laboratories, Inc.).

Visual stimuli

Visual stimuli were provided by LEDs (Thorlab λmax: 410 nm; based on the fact that all mouse photoreceptors display similar photosensitivity in this part of the spectrum) and delivered via fibre optic to purpose-made eye cones tightly positioned onto each eye to minimise any potential light leak. A National Instruments card (USB-6229) controlled by programmes written in LabVIEW (Version 8.6, National Instruments, TX, USA) was used to control stimulus duration and intensity by altering LED output and adjusting filter wheel containing neutral-density (ND) filters (ThorLabs, UK). At brightest intensity (ND0) LEDs gave a corneal irradiance of 47 W/m^2 or 15.5 log effective photon flux for melanopsin; estimated retinal irradiance is $6x10^{14}$ melanopsin photons/cm^2/s based upon the method [38] (assuming fully dilated pupil area of 3.2mm and retinal area of 18mm). Light was measured using a spectroradiometer (Bentham Instruments Ltd., UK or Cambridge Research Systems Ltd., UK), which measured the relative power in mW/cm^2 at wavelengths between 350-700nm. The effective quantal flux (in photons/cm^2/s) for each opsin was then estimated by weighting spectral irradiance according to pigment spectral efficiency using the formula: effective photon flux = $\int P(\lambda).s(\lambda).l(\lambda)d\lambda$ where $P(\lambda)$ is spectral irradiance in photons/cm^2/s/nm; $s(\lambda)$ is pigment spectral sensitivity approximated by the Govardovskii visual template [39]; and $l(\lambda)$ is mouse lens transmission as measured by Jacobs and Williams [40].

Light flashes were delivered according to a light protocol consisting of 2 parts. For most studies flashes from darkness: 10s light ON, 120s light OFF with 60s offset between each eye were used. This paradigm was repeated at least 10x at each ND filter. Retinal irradiance ranged from $6x10^{10}$ melanopsin photons/cm^2/s at ND4 to $6x10^{14}$ melanopsin photons/cm^2/s at ND0 (Figure 2E). For recording in light

adapted conditions 5-second steps of light were applied to a steady background illumination at Michelson contrast of 96%, 66% and 33% (retinal irradiance $6x10^{14}$ melanopsin photons/cm^2/s). There was a 20-second inter-stimulus interval and a 10-second offset between two eyes. This paradigm was repeated ten times (Figure 4A).

Data analysis

Multiunit data from the dLGN recordings was sorted offline using Offline Sorter (v3; Plexon, USA). After removing clear artefacts common to all channels, principal component analyses were used to discriminate single units, identified as distinct clusters of spikes within the principal component space, with a clear refractory period in the interspike interval distribution. Spike sorted, single unit data were then further analysed using Neuroexplorer (v4; Nex Technologies, USA) and MATLAB (R2013a, The Mathworks Inc. UK). Group data was then further analysed statistically using Prism (v6; Graphpad; USA). We used an objective criterion to identify all light responsive units. Units were classed as light responsive if their mean firing rate (0-10s) fell >2 standard deviations outside mean of baseline firing (-10-0s) prior to exposure of 10s of light starting at time 0s. Applying this criterion to recordings from control *rd*^{1} eyes provides confidence that it returns few false positives, the rate of false negatives is harder to determine. The latency of the response was determined as the time at which the PSTH crossed confidence intervals (>2 SDs) and the duration as the time when it dropped back below confidence intervals.

Author contributions

JCK, AEA, TB, PNB and RJL designed the research; JCK performed intraocular injections, pupillometry, LGN recordings and retinal histology. JCK performed all data processing and analysis with assistance from AEA. NM assisted with pupillometry. JCK wrote and revised the manuscript with comments from all authors. PNB and RJL supervised research.

Acknowledgements

We thank Jonathan Wynne and Michael Howarth for technical assistance. JCK was supported by a Medical Research Council Clinical Research Training Fellowship (G1000268/1). Project was supported by grant from the ERC to RJL.

References

1. Bainbridge, J.W., Smith, A.J., Barker, S.S., Robbie, S., Henderson, R., Balaggan, K., Viswanathan, A., Holder, G.E., Stockman, A., Tyler, N.*, et al.* (2008). Effect of gene therapy on visual function in Leber's congenital amaurosis. N Engl J Med *358*, 2231-2239.

2. Maguire, A.M., Simonelli, F., Pierce, E.A., Pugh, E.N., Jr., Mingozzi, F., Bennicelli, J., Banfi, S., Marshall, K.A., Testa, F., Surace, E.M.*, et al.* (2008). Safety and efficacy of gene transfer for Leber's congenital amaurosis. N Engl J Med *358*, 2240-2248.

3. Cideciyan, A.V., Aleman, T.S., Boye, S.L., Schwartz, S.B., Kaushal, S., Roman, A.J., Pang, J.J., Sumaroka, A., Windsor, E.A., Wilson, J.M.*, et al.* (2008). Human gene therapy for RPE65 isomerase deficiency activates the retinoid cycle of vision but with slow rod kinetics. Proc Natl Acad Sci U S A *105*, 15112-15117.

4. MacLaren, R.E., Groppe, M., Barnard, A.R., Cottriall, C.L., Tolmachova, T., Seymour, L., Clark, K.R., During, M.J., Cremers, F.P., Black, G.C.*, et al.* (2014). Retinal gene therapy in patients with choroideremia: initial findings from a phase 1/2 clinical trial. Lancet *383*, 1129-1137.

5. Bainbridge, J.W., Mehat, M.S., Sundaram, V., Robbie, S.J., Barker, S.E., Ripamonti, C., Georgiadis, A., Mowat, F.M., Beattie, S.G., Gardner, P.J.*, et al.* (2015). Long-term effect of gene therapy on Leber's congenital amaurosis. N Engl J Med *372*, 1887-1897.

6. Zrenner, E., Bartz-Schmidt, K.U., Benav, H., Besch, D., Bruckmann, A., Gabel, V.P., Gekeler, F., Greppmaier, U., Harscher, A., Kibbel, S.*, et al.* (2011). Subretinal electronic chips allow blind patients to read letters and combine them to words. Proc Biol Sci *278*, 1489-1497.

7. Humayun, M.S., Dorn, J.D., da Cruz, L., Dagnelie, G., Sahel, J.A., Stanga, P.E., Cideciyan, A.V., Duncan, J.L., Eliott, D., Filley, E.*, et al.* (2012). Interim results from the international trial of Second Sight's visual prosthesis. Ophthalmology *119*, 779-788.

8. Busskamp, V., Picaud, S., Sahel, J.A., and Roska, B. (2012). Optogenetic therapy for retinitis pigmentosa. Gene Ther *19*, 169-175.

9. Mazzoni, F., Novelli, E., and Strettoi, E. (2008). Retinal ganglion cells survive and maintain normal dendritic morphology in a mouse model of inherited photoreceptor degeneration. J Neurosci *28*, 14282-14292.

10. Santos, A., Humayun, M.S., de Juan, E., Jr., Greenburg, R.J., Marsh, M.J., Klock, I.B., and Milam, A.H. (1997). Preservation of the inner retina in retinitis pigmentosa. A morphometric analysis. Arch Ophthalmol *115*, 511-515.

11. Bi, A., Cui, J., Ma, Y.P., Olshevskaya, E., Pu, M., Dizhoor, A.M., and Pan, Z.H. (2006). Ectopic expression of a microbial-type rhodopsin restores visual responses in mice with photoreceptor degeneration. Neuron *50*, 23-33.

12. Doroudchi, M.M., Greenberg, K.P., Liu, J., Silka, K.A., Boyden, E.S., Lockridge, J.A., Arman, A.C., Janani, R., Boye, S.E., Boye, S.L.*, et al.* (2011). Virally delivered channelrhodopsin-2 safely and effectively restores visual function in multiple mouse models of blindness. Mol Ther *19*, 1220-1229.

13. Cronin, T., Vandenberghe, L.H., Hantz, P., Juttner, J., Reimann, A., Kacso, A.E., Huckfeldt, R.M., Busskamp, V., Kohler, H., Lagali, P.S.*, et al.* (2014). Efficient transduction and optogenetic stimulation of retinal bipolar cells by a synthetic adeno-associated virus capsid and promoter. EMBO Mol Med *6*, 1175-1190.

14. Lagali, P.S., Balya, D., Awatramani, G.B., Munch, T.A., Kim, D.S., Busskamp, V., Cepko, C.L., and Roska, B. (2008). Light-activated channels targeted to ON bipolar cells restore visual function in retinal degeneration. Nat Neurosci *11*, 667-675.

15. Mace, E., Caplette, R., Marre, O., Sengupta, A., Chaffiol, A., Barbe, P., Desrosiers, M., Bamberg, E., Sahel, J.A., Picaud, S.*, et al.* (2015). Targeting channelrhodopsin-2 to ON-bipolar cells with vitreally administered AAV Restores ON and OFF visual responses in blind mice. Mol Ther *23*, 7-16

16. Busskamp, V., Duebel, J., Balya, D., Fradot, M., Viney, T.J., Siegert, S., Groner, A.C., Cabuy, E., Forster, V., Seeliger, M.*, et al.* (2010). Genetic reactivation of cone

photoreceptors restores visual responses in retinitis pigmentosa. Science *329*, 413-417.

17. Caporale, N., Kolstad, K.D., Lee, T., Tochitsky, I., Dalkara, D., Trauner, D., Kramer, R., Dan, Y., Isacoff, E.Y., and Flannery, J.G. (2011). LiGluR restores visual responses in rodent models of inherited blindness. Mol Ther *19*, 1212-1219.

18. Gaub, B.M., Berry, M.H., Holt, A.E., Reiner, A., Kienzler, M.A., Dolgova, N., Nikonov, S., Aguirre, G.D., Beltran, W.A., Flannery, J.G.*, et al.* (2014). Restoration of visual function by expression of a light-gated mammalian ion channel in retinal ganglion cells or ON-bipolar cells. Proc Natl Acad Sci U S A *111*, E5574-5583.

19. Polosukhina, A., Litt, J., Tochitsky, I., Nemargut, J., Sychev, Y., De Kouchkovsky, I., Huang, T., Borges, K., Trauner, D., Van Gelder, R.N.*, et al.* (2012). Photochemical restoration of visual responses in blind mice. Neuron *75*, 271-282.

20. Tochitsky, I., Polosukhina, A., Degtyar, V.E., Gallerani, N., Smith, C.M., Friedman, A., Van Gelder, R.N., Trauner, D., Kaufer, D., and Kramer, R.H. (2014). Restoring visual function to blind mice with a photoswitch that exploits electrophysiological remodeling of retinal ganglion cells. Neuron *81*, 800-813.

21. Lin, B., Koizumi, A., Tanaka, N., Panda, S., and Masland, R.H. (2008). Restoration of visual function in retinal degeneration mice by ectopic expression of melanopsin. Proc Natl Acad Sci U S A *105*, 16009-16014.

22 Cehajic-Kapetanovic, J., Eleftheriou, C., Allen, A.E., Milosavljevic, N., Pienaar, A., Bedford, R., Davis, K.E., Bishop, P.N., and Lucas, R.J. (2015). Restoration of Vision with Ectopic Expression of Human Rod Opsin. Curr Biol *25*, 2111-2122.

23. Gaub, B.M., Berry, M.H., Holt, A.E., Isacoff, E.Y., and Flannery, J.G. (2015). Optogenetic Vision Restoration Using Rhodopsin for Enhanced Sensitivity. Mol Ther.

24. van Wyk, M., Pielecka-Fortuna, J., Lowel, S., and Kleinlogel, S. (2015). Restoring the ON Switch in Blind Retinas: Opto-mGluR6, a Next-Generation, Cell-Tailored Optogenetic Tool. PLoS Biol *13*, e1002143

25. Sexton, T.J., Golczak, M., Palczewski, K., and Van Gelder, R.N. (2012). Melanopsin is highly resistant to light and chemical bleaching in vivo. J Biol Chem *287*, 20888-20897.

26. Van Hooser, J.P., Aleman, T.S., He, Y.G., Cideciyan, A.V., Kuksa, V., Pittler, S.J., Stone, E.M., Jacobson, S.G., and Palczewski, K. (2000). Rapid restoration of visual pigment and function with oral retinoid in a mouse model of childhood blindness. Proc Natl Acad Sci U S A *97*, 8623-8628.

27. Ablonczy, Z., Crouch, R.K., Goletz, P.W., Redmond, T.M., Knapp, D.R., Ma, J.X., and Rohrer, B. (2002). 11-cis-retinal reduces constitutive opsin phosphorylation and improves quantum catch in retinoid-deficient mouse rod photoreceptors. J Biol Chem *277*, 40491-40498.

28. Cehajic-Kapetanovic, J., Le Goff, M.M., Allen, A., Lucas, R.J., and Bishop, P.N. (2011). Glycosidic enzymes enhance retinal transduction following intravitreal delivery of AAV2. Mol Vis *17*, 1771-1783.

29. Guler, A.D., Ecker, J.L., Lall, G.S., Haq, S., Altimus, C.M., Liao, H.W., Barnard, A.R., Cahill, H., Badea, T.C., Zhao, H*., et al.* (2008). Melanopsin cells are the principal conduits for rod-cone input to non-image-forming vision. Nature *453*, 102-105.

30. Lucas, R.J., Hattar, S., Takao, M., Berson, D.M., Foster, R.G., and Yau, K.W. (2003). Diminished pupillary light reflex at high irradiances in melanopsin-knockout mice. Science *299*, 245-247.

31. Lucas, R.J., Douglas, R.H., and Foster, R.G. (2001). Characterization of an ocular photopigment capable of driving pupillary constriction in mice. Nat Neurosci *4*, 621-626.

32. Cao, P., Sun, W., Kramp, K., Zheng, M., Salom, D., Jastrzebska, B., Jin, H., Palczewski, K., and Feng, Z. (2012). Light-sensitive coupling of rhodopsin and melanopsin to G(i/o) and G(q) signal transduction in Caenorhabditis elegans. FASEB J *26*, 480-491.

33. Bailes, H.J., and Lucas, R.J. (2013). Human melanopsin forms a pigment maximally sensitive to blue light (lambdamax approximately 479 nm) supporting activation of G(q/11) and G(i/o) signalling cascades. Proc Biol Sci *280*, 20122987.

34. Brown, T.M., Tsujimura, S., Allen, A.E., Wynne, J., Bedford, R., Vickery, G., Vugler, A., and Lucas, R.J. (2012). Melanopsin-based brightness discrimination in mice and humans. Curr Biol *22*, 1134-1141.

35. Brown, T.M., Gias, C., Hatori, M., Keding, S.R., Semo, M., Coffey, P.J., Gigg, J., Piggins, H.D., Panda, S., and Lucas, R.J. (2010). Melanopsin contributions to irradiance coding in the thalamo-cortical visual system. PLoS Biol *8*, e1000558.

36. Davis, K.E., Eleftheriou, C.G., Allen, A.E., Procyk, C.A., and Lucas, R.J. (2015). Melanopsin-derived visual responses under light adapted conditions in the mouse dLGN. PLoS One *10*, e0123424.

37. Enezi, J., Revell, V., Brown, T., Wynne, J., Schlangen, L., and Lucas, R. (2011). A "melanopic" spectral efficiency function predicts the sensitivity of melanopsin photoreceptors to polychromatic lights. J Biol Rhythms *26*, 314-323.

38. Lyubarsky, A.L., Daniele, L.L., and Pugh, E.N., Jr. (2004). From candelas to photoisomerizations in the mouse eye by rhodopsin bleaching in situ and the light-rearing dependence of the major components of the mouse ERG. Vision Res *44*, 3235-3251..

39. Govardovskii, V.I., Fyhrquist, N., Reuter, T., Kuzmin, D.G., and Donner, K. (2000). In search of the visual pigment template. Vis Neurosci *17*, 509-528.

40. Jacobs, G.H., and Williams, G.A. (2007). Contributions of the mouse UV photopigment to the ERG and to vision. Doc Ophthalmol *115*, 137-144.

Figures:

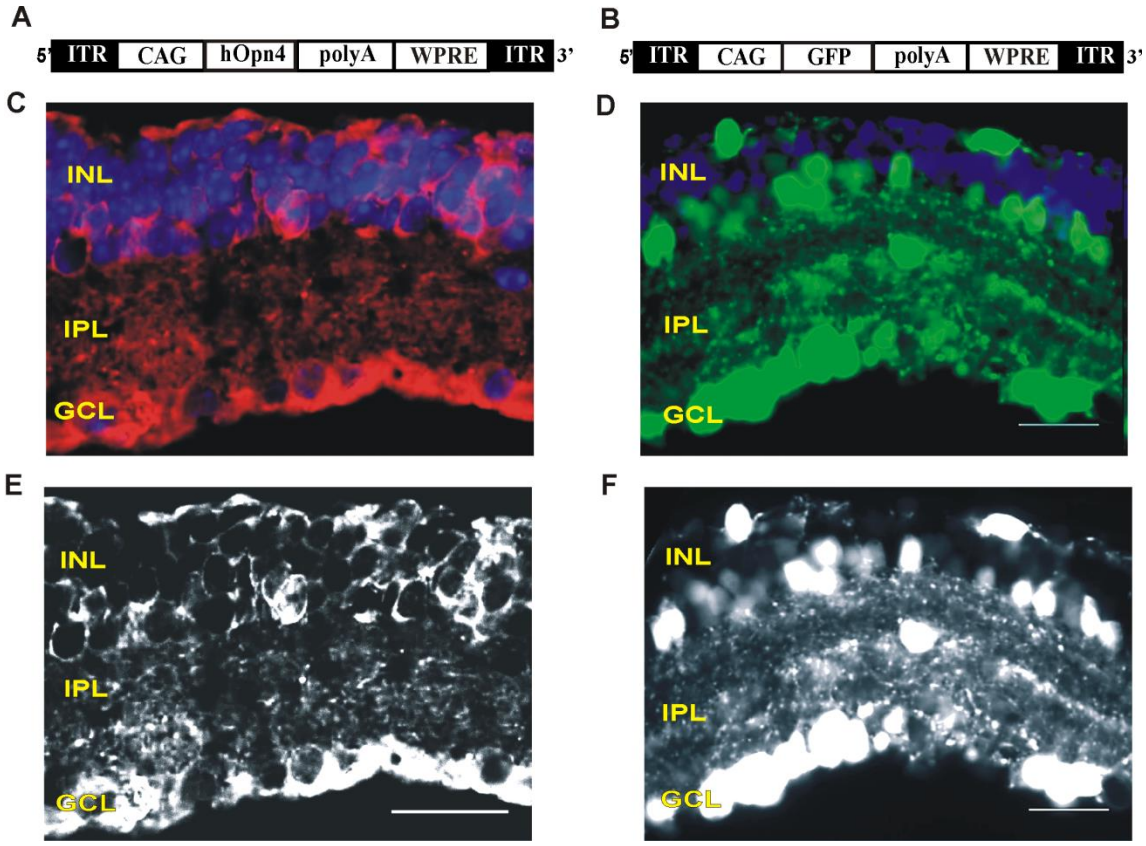

Figure 1. Ectopic expression of human melanopsin and green fluorescent protein in the *rd*[1] retina

(A and B) Schematic of DNA expression cassettes delivered by AAV2 vector to the *rd*[1] retina. A human melanopsin coding sequence (hOPN4; A) or control green fluorescent protein sequence (GFP; B) are driven by a hybrid CMV enhancer/chickenβ-actin (CAG) promoter. The sequences are flanked by inverted terminal repeats (ITRs) and stabilised by a polyadenylation signal sequence (polyA) and a woodchuck hepatitis posttranscriptional regulatory element (WPRE). Expression vectors are referred to as CAG-hOPN4 and CAG-GFP. (C and D) Exemplar images of sections through an *rd*[1] mouse retina >12 weeks after intravitreal delivery of CAG-hOPN4 (C) and CAG-GFP (D) in conjunction with glycosidic enzymes. Expression of human melanopsin in cells of the ganglion cell layer (GCL) and inner nuclear layer (INL) and processes in the inner plexiform layer (IPL) is revealed by labelling with an α-hOPN4 antibody (red) and counterstain of nuclei with DAPI (blue) (C). A similar expression pattern is observed with GFP delivered using CAG-GFP (D). Calibration bar = 50μm. (E and F) Monochrome images showing anti-hOPN4 antibody staining in C (E) and GFP expression in D (F).

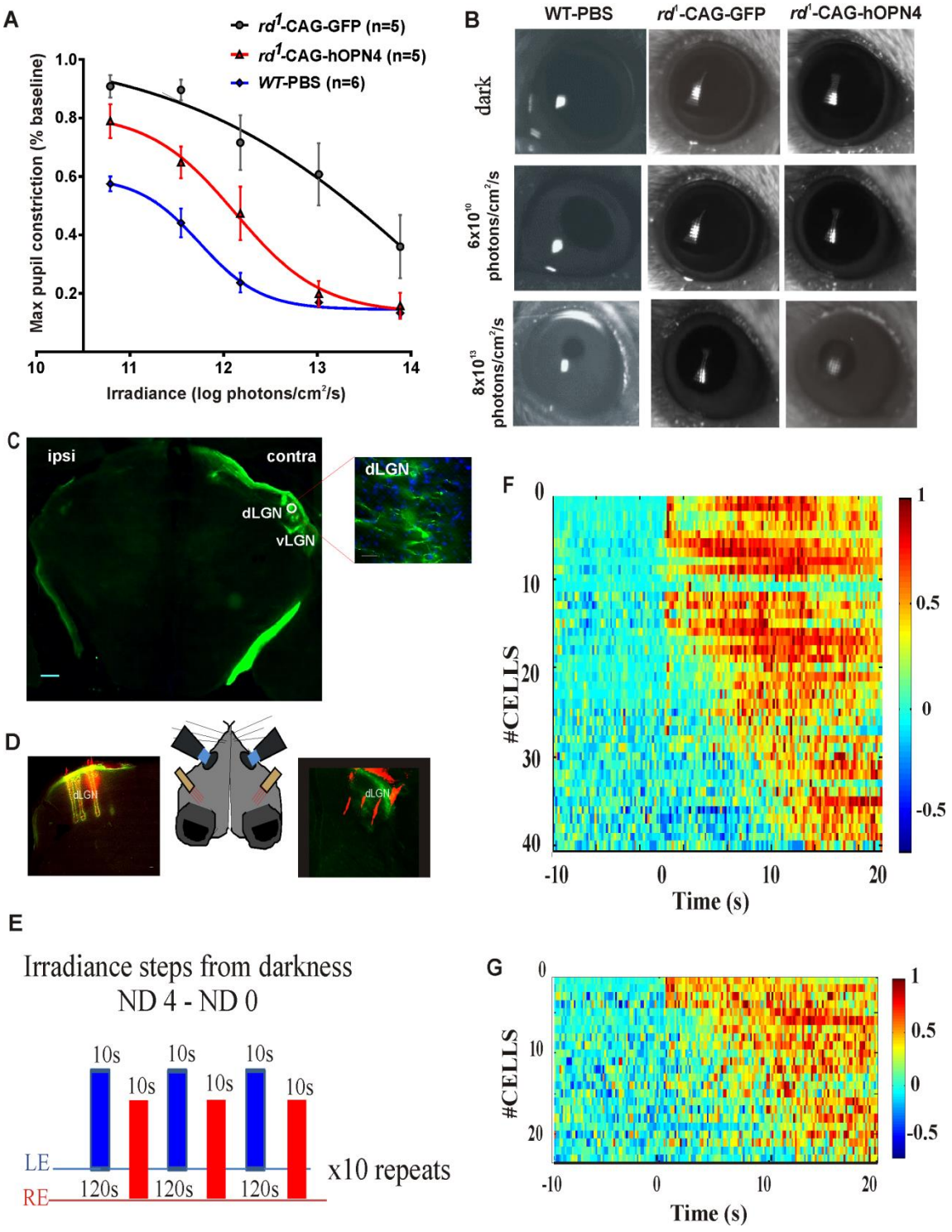
A
rd1-CAG-GFP (n=5)
rd1-CAG-hOPN4 (n=5)
WT-PBS (n=6)
Max pupil constriction (% baseline)
1.0
0.8
0.6
0.4
0.2
10
11
12
13
14
Irradiance (log photons/cm²/s)
B
WT-PBS
rd1-CAG-GFP
rd1-CAG-hOPN4
dark
6x10¹⁰ photons/cm²/s
8x10¹³ photons/cm²/s
C
ipsi
contra
dLGN
vLGN
dLGN
D
dLGN
dLGN
E
Irradiance steps from darkness
ND 4 - ND 0
10s
10s
10s
10s
10s
10s
LE
RE
120s
120s
120s
x10 repeats
F
#CELLS
0
10
20
30
40
-10
0
10
20
Time (s)
1
0.5
0
-0.5
G
#CELLS
0
10
20
-10
0
10
20
Time (s)
1
0.5
0
-0.5

Figure 2. Ectopic melanopsin expression restores *in vivo* visual responses in *rd1* mouse

(A) Stimulus-response curves for maximum pupillary constriction over a range of retinal irradiances. Melanopsin treated *rd1*-CAG-hOPN4 eyes (red) demonstrate a marked improvement in visual sensitivity compared to control (*rd1*-CAG-GFP) injected eyes (black). Data for wild-type PBS injected mice are shown for comparison (blue). Data are normalised to pupil size immediately preceding light onset (10s white light). Values are mean ± SEM, with n indicating the number of mice examined. The data are fitted with a sigmoidal function. (B) Representative infrared images of pupil area measured in the dark (baseline), at $6x10^{10}$ total photons/cm^2/s and at $8x10^{13}$ total photons/cm^2/s for *WT*, *rd1*-CAG-GFP *and rd1*-CAG-hOPN4 mice. (C) Exemplar image of a coronal section through an *rd1* mouse brain at the level of visual thalamus (dorsal and ventral lateral geniculate nucleus, dLGN and vLGN respectively) at >8 weeks after intravitreal delivery of CAG-GFP (shown in 1B) to the contralateral eye showing innervation of the LGN by GFP-expressing axons. Ipsi and contra denote hemispheres ipsilateral and contralateral to the injected eye. Insert shows a magnified image of the dLGN with GFP expressing axon terminals. Nuclei are stained with DAPI (blue). (D) Schematic of recording apparatus allowing presentation of separate light stimuli to each eye and insertion of silicone multi-channel recording electrode probes to the dLGNs in either hemisphere. Representative histological sections through the left and right dLGN with DiI tracks (in red) showing path of insertion for recording probes at stereotactic co-ordinates: -2.46 mm (from bregma) and -2.8 mm (from midline). (E) Schematic of light protocol used to characterise light responses in the dLGN in dark adapted conditions. (F and G) Heat maps of mean firing rate across 10 presentations of 10s of light (on at time 0) at $6x10^{14}$ melanopsin photons/cm^2/s to CAG-hOPN4 (F) and CAG-GFP (G) treated eyes of *rd1* mice. Each line in a map represents a single unit that met our objective criterion for light responsiveness (41 units downstream of 6 treated and 23 units downstream of 6 control eyes met an objective criterion of stimulus associated change in firing). Colour code represents normalized firing rate (-1 and 1 being minimum and maximum firing rate for that unit respectively). Traces are ordered according to response latency.

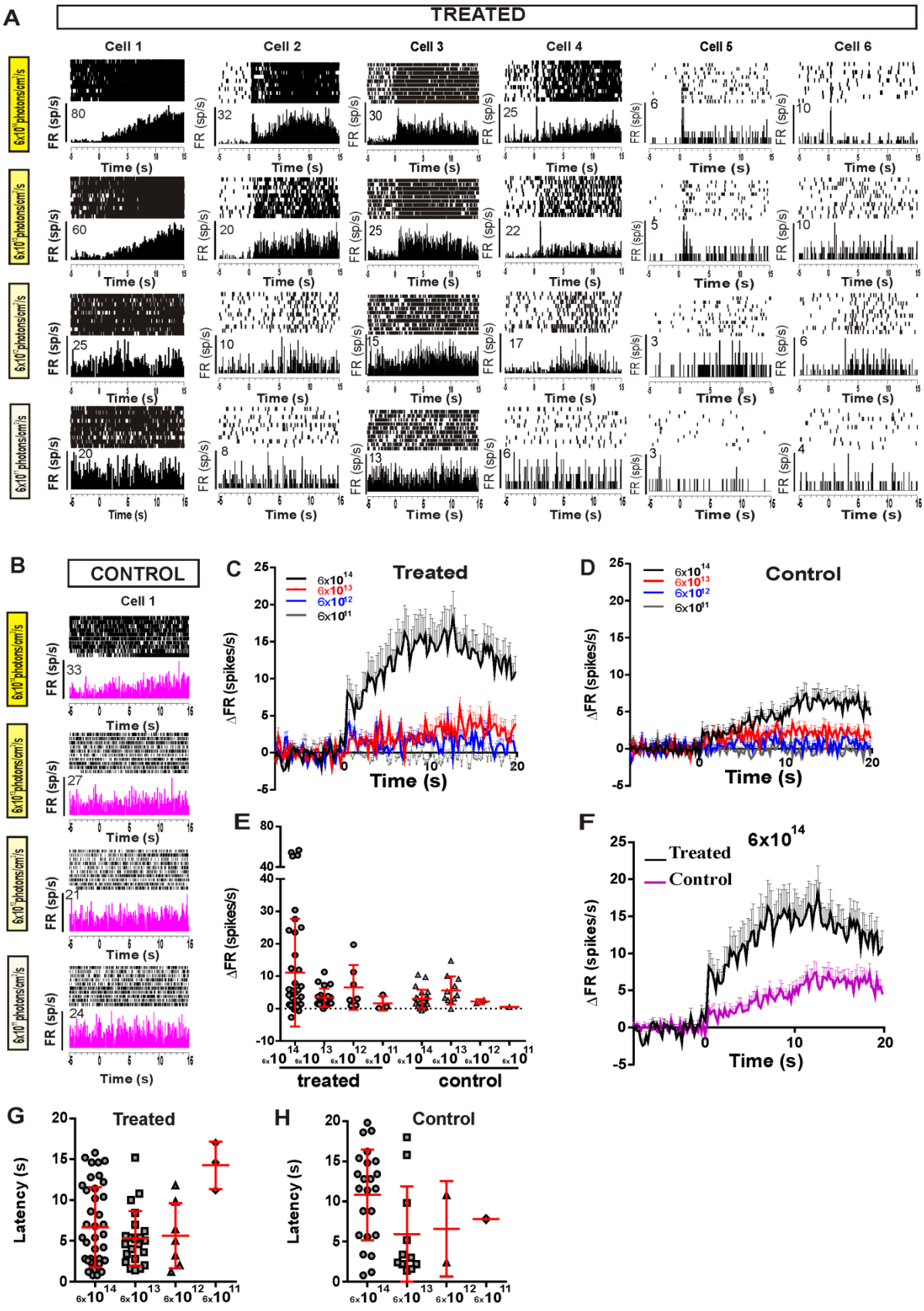
A
TREATED
Cell 1
Cell 2
Cell 3
Cell 4
Cell 5
Cell 6
FR (sp/s)
Time (s)
B
CONTROL
C
Treated
D
Control
ΔFR (spikes/s)
E
treated
control
F
Treated
Control
G
Treated
Latency (s)
H
Control

Figure 3. Characteristics of restored in vivo visual responses in *rd*^{1} mouse

(A and B) Sensitivity response profile (perievent rasters and associated perievent firing rate histograms) for six representative dLGN single units isolated from the CAG-hOPN4 treated group (A) and one representative dLGN single units isolated from the CAG-GFP treated (control) group (B) at four different retinal irradiances: $6x10^{14}$, $6x10^{13}$, $6x10^{12}$ and $6x10^{11}$ photons/cm^2/s. Each set of rasters depicts spiking activity for 10 sequential presentations of a 10s light flash (inter-stimulus interval 120s) starting at time 0. PSTHs below depict mean firing rate in 200ms epochs across all 10 repeats. (C and D) Mean±SEM firing rate (mean firing rate from 0 to 10s with subtracted pre-stimulus firing rate -10 to 0s) for all light responsive units exposed to 10s pulses of light (starting at 0s) at $6x10^{14}$, $6x10^{13}$, $6x10^{12}$ and $6x10^{11}$ melanopsin photons/cm^2/s in treated (C; n=41 units) compared to control (D; n=23 units) group. (E) Distribution of response amplitudes (mean change in firing rate±SD) for units responding to 10s of light stimulus at $6x10^{14}$, $6x10^{13}$, $6x10^{12}$ and $6x10^{11}$ melanopsin photons/cm^2/s for treated and control groups. (F) Mean±SEM firing rate for light responsive units exposed to 10s pulses (starting at 0s) at $6x10^{14}$ melanopsin photons/cm^2/s for treated (black) compared to control (purple) group. Only units that crossed our objective criterion for light responsiveness were included (n=41 units in treated and n=23 units in control group. (G and H) Distribution of response latencies (time at which mean firing rate first fell outside 2 SDs of baseline) at $6x10^{14}$, $6x10^{13}$, $6x10^{12}$ and $6x10^{11}$ photons/cm^2/s for treated (G) versus control (H) group.

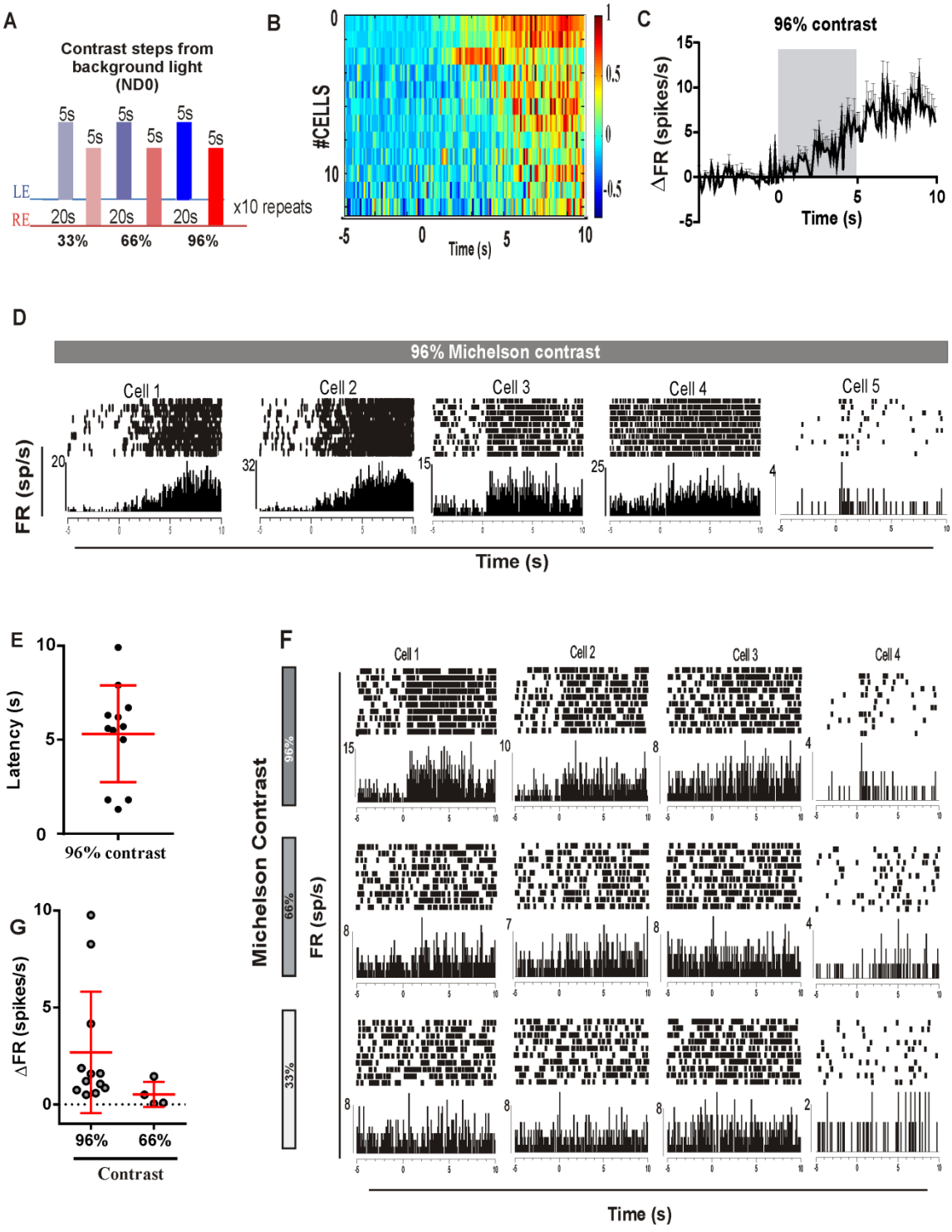
A
Contrast steps from background light (ND0)
5s
20s
LE
RE
x10 repeats
33%
66%
96%
B
#CELLS
Time (s)
C
96% contrast
ΔFR (spikes/s)
Time (s)
D
96% Michelson contrast
Cell 1
Cell 2
Cell 3
Cell 4
Cell 5
FR (sp/s)
Time (s)
E
Latency (s)
96% contrast
G
ΔFR (spikes/s)
96%
66%
Contrast
F
Michelson Contrast
96%
66%
33%
FR (sp/s)
Time (s)

Figure 4. Ectopic melanopsin drives visual responses under light adapted conditions in *rd1* mouse

(A) Schematic of light protocol used to characterise light responses in the dLGN under light adapted conditions: (retinal irradiance $6x10^{14}$ melanopsin photons/cm^2/s and different levels of Michelson contrast: 96%, 66% and 33%). (B) Heat map representations of mean firing rate across 10 presentations of 5s of light (on at time 0) to *rd1*-CAG-hOPN4 eyes. Each line in a map shows a single unit that met our objective criterion for light responsiveness (n = 12 units downstream of 5 treated eyes; no units met the criterion downstream of 5 control eyes). Colour code represents normalized firing rate (-1 and 1 being minimum and maximum firing rate for that unit respectively). Traces are ordered according to response latency. (C) Population mean (±SEM) firing rate profile for light responsive units (Michelson contrast 96%). (D) Light adapted responses (perievent rasters and associated perievent firing rate histograms) for 5 representative dLGN units from *rd1*-CAG-hOPN4 eyes (Michelson contrast 96%). Each set of rasters depicts spiking activity for 10 sequential presentations of a 5s light flash (inter-stimulus interval 20s) starting at time 0. PSTHs below depict mean firing rate in 100ms epochs across all 10 repeats. (E) Distribution of response latencies (time at which mean firing rate first fell outside 2 SDs of baseline) for dLGN units from *rd1*-CAG-hOPN4 eyes responding under light adapted conditions (Michelson contrast 96%). (F) Light adapted responses for four representative dLGN units recorded at three levels of Michelson contrast: 96%, 66% and 33%. (G) Distribution of response amplitudes (mean change in firing rate) for dLGN units from *rd1*-CAG-hOPN4 treated eyes at Michelson contrast 96% and 66%.

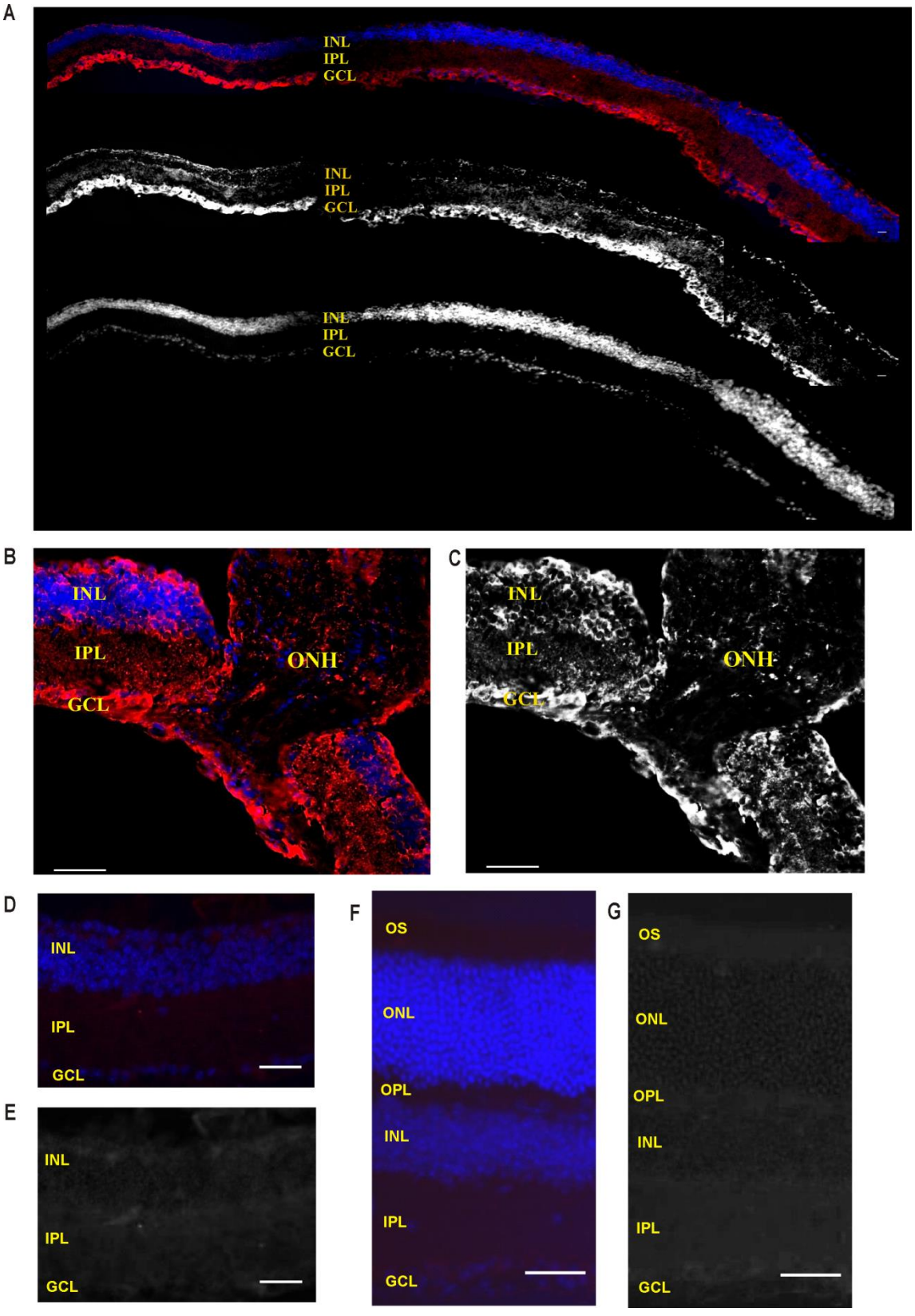
A
INL
IPL
GCL
INL
IPL
GCL
INL
IPL
GCL
B
INL
IPL
GCL
ONH
C
INL
IPL
GCL
ONH
D
INL
IPL
GCL
E
INL
IPL
GCL
F
OS
ONL
OPL
INL
IPL
GCL
G
OS
ONL
OPL
INL
IPL
GCL

Figure S1. Melanopsin expression in *rd1* retinas and control *rd1* and *wild-type* stains. Relating to Figure 1.

(A) Exemplar images of a section through an *rd1* mouse retina >12 weeks after intravitreal injection of the CAG-hOPN4 vector in conjunction with glycosidic enzymes. Variable melanopsin expression along the retinal section is shown after staining with α-hOPN4 antibody (upper image in red; middle image a monochrome version showing antibody labelling). Nuclei are stained with DAPI (upper image in blue; lower image showing DAPI staining in monochrome). The image was produced by splicing together several high magnification images of smaller portions of the retina. (B and C) Exemplar image of a section through an *rd1* mouse retina >12 weeks after intravitreal delivery of CAG-hOPN4 in conjunction with glycosidic enzymes showing melanopsin expression after staining with α-hOPN4 antibody (red) around the optic nerve head (ONH) (B). Nuclei are stained with DAPI (blue). C is a monochrome version of antibody labelling in B. (D to G) Exemplar images of sections through PBS injected *rd1* (D and E) and *wild-type* (F and G) mouse retina showing no staining after treatment with α-hOPN4 antibody; nuclei are stained with DAPI (blue); E and G are monochrome versions of antibody labelling in D and F respectively. INL – inner nuclear layer, IPL- inner plexiform layer, GCL – ganglion cell layer, ONL – outer nuclear layer. OPL – outer plexiform layer. CAG - a hybrid CMV enhancer/chickenβ-actin promoter. hOPN4 - human melanopsin. Calibration bar = 50μm.

Chapter 5: Paper 3

Restoration of vision with ectopic expression of human rod opsin

Authors: Jasmina Cehajic-Kapetanovic[1], Cyril Eleftheriou[2], Annette E. Allen[2], Nina Milosavljevic[2], Abigail Pienaar[2], Robert A. Bedford[2], Katherine E. Davis[2], Paul N. Bishop[1], and Robert J. Lucas[2].

Affiliations:

[1]Centre for Ophthalmology & Vision Sciences, Institute of Human Development, University of Manchester and Manchester Royal Eye Hospital, CMFT, Manchester Academic Health Sciences Centre, Manchester, UK.

[2]Faculty of Life Sciences, University of Manchester, Oxford Road, Manchester M13 9PT, UK

Article

Current Biology

Restoration of Vision with Ectopic Expression of Human Rod Opsin

Highlights

- Ectopic human rod opsin restores visual functions in advanced retinal degeneration
- Rod opsin has greater sensitivity than current optogenetic strategies
- Rod opsin-treated animals respond to spatial stimuli, flicker, and natural scenes
- As a human protein ordinarily found in retinal tissue, barriers to clinic are minimized

Authors

Jasmina Cehajic-Kapetanovic, Cyril Eleftheriou, Annette E. Allen, ..., Katherine E. Davis, Paul N. Bishop, Robert J. Lucas

Correspondence

paul.bishop@manchester.ac.uk (P.N.B.), robert.lucas@manchester.ac.uk (R.J.L.)

In Brief

Cehajic-Kapetanovic at al. show that ectopically expressed human rod opsin restores vision in a mouse model of advanced retinal degeneration. The quality of the restored vision compares favorably, especially in terms of sensitivity, with alternative approaches, and using a native human protein reduces barriers to future clinical trials.

Cehajic-Kapetanovic et al., 2015, Current Biology 25, 2111–2122
August 17, 2015 ª2015 The Authors
http://dx.doi.org/10.1016/j.cub.2015.07.029

Current Biology
Article

Restoration of Vision with Ectopic Expression of Human Rod Opsin

Jasmina Cehajic-Kapetanovic,[1,2] Cyril Eleftheriou,[3] Annette E. Allen,[3] Nina Milosavljevic,[3] Abigail Pienaar,[3] Robert Bedford,[3] Katherine E. Davis,[3] Paul N. Bishop,[1,2,*] and Robert J. Lucas[3,*]
[1]Centre for Ophthalmology and Vision Sciences, Institute of Human Development, University of Manchester, Manchester M13 9PT, UK
[2]Manchester Royal Eye Hospital, CMFT, Manchester Academic Health Sciences Centre, Manchester M13 9NT, UK
[3]Faculty of Life Sciences, University of Manchester, Oxford Road, Manchester M13 9PT, UK
*Correspondence: paul.bishop@manchester.ac.uk (P.N.B.), robert.lucas@manchester.ac.uk (R.J.L.)
http://dx.doi.org/10.1016/j.cub.2015.07.029

SUMMARY

Many retinal dystrophies result in photoreceptor loss, but the inner retinal neurons can survive, making them potentially amenable to emerging optogenetic therapies. Here, we show that ectopically expressed human rod opsin, driven by either a non-selective or ON-bipolar cell-specific promoter, can function outside native photoreceptors and restore visual function in a mouse model of advanced retinal degeneration. Electrophysiological recordings from retinal explants and the visual thalamus revealed changes in firing (increases and decreases) induced by simple light pulses, luminance increases, and naturalistic movies in treated mice. These responses could be elicited at light intensities within the physiological range and substantially below those required by other optogenetic strategies. Mice with rod opsin expression driven by the ON-bipolar specific promoter displayed behavioral responses to increases in luminance, flicker, coarse spatial patterns, and elements of a natural movie at levels of contrast and illuminance (z50–100 lux) typical of natural indoor environments. These data reveal that virally mediated ectopic expression of human rod opsin can restore vision under natural viewing conditions and at moderate light intensities. Given the inherent advantages in employing a human protein, the simplicity of this intervention, and the quality of vision restored, we suggest that rod opsin merits consideration as an optogenetic actuator for treating patients with advanced retinal degeneration.

INTRODUCTION

Inherited retinal degenerations (retinal dystrophies), such as retinitis pigmentosa, affect 1:2,500 people worldwide. Irrespective of etiology, most affect the outer retina and lead to progressive and permanent loss of photoreception. Severe visual impairment is common in advanced stages of the degeneration, and these conditions are currently incurable. However, despite the loss of outer retinal photoreceptors, inner retinal neurons, including bipolar and ganglion cells, can survive and retain their ability to send visual information to the brain [1, 2]. These neurons therefore, represent promising targets for emerging optogenetic therapies that aim to convert them into photoreceptors and recreate the photosensitivity that has been lost during degeneration [3].

Pioneering work has shown that electrophysiological responses to light can be restored to animal models of retinal degeneration by introducing a variety of optogenetic actuators to the surviving inner retina, including the mammalian photopigment melanopsin [4], prokaryotic photoactivated ion channels or pumps [5–10], synthetic light switches [11–14], and a synthetic photopigment (Opto-mGluR6) [15]. These interventions can also support behavioral light responses including, in some cases, maze navigation or optokinetic reflexes reliant upon detection of spatial patterns or fast temporal modulations (flicker). However, in most cases, these actuators function only under very bright light, and, to date, no clinically achievable optogenetic intervention has recreated spatiotemporal discrimination at commonly encountered light levels.

Here, we set out to determine whether it is possible to recreate vision in blind mice using ectopic expression of a natural human protein, rod opsin. Mammalian rod opsins are readily produced under heterologous expression and can couple to native signaling cascades in several cell types in a light-dependent manner [16–19]. We reasoned that if they did this also in neurons of the inner retina, they could restore photosensitivity, and that several features of this approach could be beneficial for clinical application. First, the use of a human protein, and indeed one ordinarily found in the retina, would minimize the potential for immunogenic adverse effects when applied to patients. Second, as a G protein-coupled receptor, rod opsin has access to mechanisms of signal amplification not available to directly light-gated ion channels and thus could have much higher light sensitivity. Finally, rod opsin has the potential to address the need for sensitivity normalization in vision. Detecting objects in our environment relies upon distinguishing local differences in relative luminance across the huge variation in background light intensity. That is only possible because photoreceptors adjust their sensitivity according to the background light intensity. Achieving that goal for optogenetic photoactivators is challenging, but ectopically expressed rod opsin could theoretically do so via two mechanisms. On the one hand, its G protein signaling cascade could show dynamic desensitization. On the

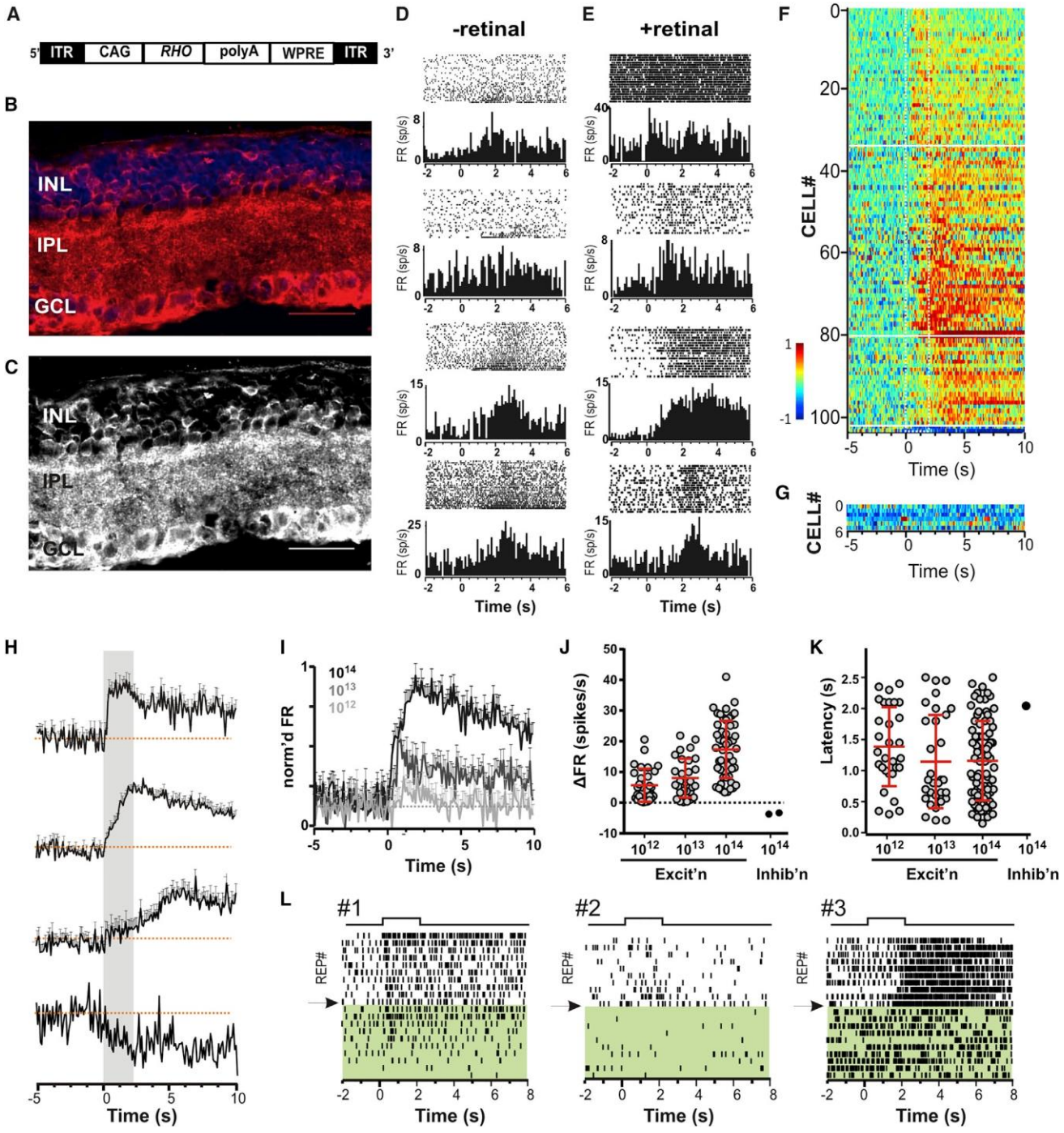

Figure 1. Ectopic Expression of Human Rod Opsin Restores Light Responses in *rd*[1] Mouse Retina

(A) Schematic of the DNA expression cassette delivered by AAV2/2 vector to the retina. A human rod opsin coding sequence (*RHO*) is driven by a hybrid CMV enhancer/chickenb-actin (CAG) promoter. The sequence is flanked by inverted terminal repeats (ITRs) and stabilized by a polyadenylation signal sequence (polyA) and a woodchuck hepatitis posttranscriptional regulatory element (WPRE).

(B and C) Exemplar images of a section through an *rd*[1] mouse retina >4 months after intravitreal delivery of vector in (A) in conjunction with glycosidic enzymes. Expression of human rod opsin in cells of the ganglion cell layer (GCL) and inner nuclear layer (INL) and processes in the inner plexiform layer (IPL) are revealed by staining with an a-hRho antibody (red) and counterstaining of nuclei with DAPI (blue) to aid orientation (B). A monochrome version of a-hRho antibody staining in (B) in which rod opsin expression appears in white is shown in (C). Calibration bar = 50 mm.

(D and E) Perievent rasters and associated perievent firing rate histograms (PSTHs) for eight representative single units isolated from multi-electrode array (MEA) recordings of *rd*[1]-CAG-*RHO* retinas without (D) and with (E) exogenous 9-*cis*-retinal. Each set of rasters depicts spiking activity for 20 sequential presentations of a 2-s white light flash (4 3 10^{14} rod photons/cm^2/s; interstimulus interval 20 s) starting at time 0. PSTHs below depict mean firing rate in 100-ms epochs across all

(legend continued on next page)

other, because rod opsin bleaches upon light exposure, the effective concentration of pigment should be inversely proportional to the background irradiance. The associated reduction in sensitivity is well described for cone photoreceptors where it is termed ''bleaching adaptation'' [20, 21].

We expressed human rod opsin in surviving inner retinal neurons of a mouse model of aggressive retinal degeneration with near complete loss of rod and cone photoreceptors (*rd*^{1}) by intravitreal administration of clinically approved adeno-associated virus (AAV) vector, AAV2/2. Widespread light-evoked changes in firing were observed in neurons of the retina and dorsal lateral geniculate nucleus (dLGN) in treated mice. These responses could be elicited using physiologically encountered light levels and under natural light-adapted conditions. Behavioral studies indicated that the treated mice had regained the ability to detect modest changes in brightness, relatively fast flickers, spatial patterns, and naturalistic movie scenes.

RESULTS

Gene Delivery to *rd*^{1} Retina

We injected a viral vector (AAV2/2) containing a human rod opsin coding sequence under control of a CAG promoter (CAG-*RHO*; Figure 1A) into the vitreous of *rd*^{1} mice in conjunction with glycosidic enzymes that increase vector transduction [22]. As predicted for this promoter, when retinas were harvested 4–6 months later, immunolabelling revealed rod opsin in both the ganglion cell layer (GCL) and inner nuclear layer (INL) of all treated *rd*^{1} mice (Figures 1B and 1C). Expression was found at uneven density across the retina and was generally higher in GCL than INL (Figure S1A). Staining was absent from a control PBS-injected group (Figures S1B and S1C) and the inner retina of wild-type mice (Figures S1D and S1E). Patchy expression was also confirmed in retinal whole mounts for a reporter gene (GFP) delivered via a control AAV2-CAG-GFP vector (Figure S3A).

Restoring Light-Evoked Activity in Retinal Ganglion Cells

We tested for restored photosensitivity in CAG-*RHO*-transduced retinas by recording spiking activity from the GCL in vitro using a multi-electrode array. 2-s full-field flashes (interstimulus interval 20 s) of broad-spectrum white light increased spiking in numerous units (Figures 1D and 1E). Rod opsin bleaches upon light exposure, and, as might be expected, these responses dissipated over multiple repeats (Figure 1D) unless the culture medium was supplemented with 9-*cis*-retinal, when they became robustly repeatable (Figure 1E). We applied an objective criterion (see Experimental Procedures) to identify light-dependent changes in firing in these retinal explants. This returned 104 out of 671 single units as ''light responsive'' in CAG-*RHO*-treated retinas (Figure 1F) but only 6 out of 132 units in untreated *rd*^{1} mice (Figure 1G). Closer examination of firing patterns in the six light-responsive units in control retinas provides little confidence that they did indeed respond to the stimulus, suggesting that these rather provide an indication of the false-positive rate of our objective test.

Restored ganglion cell light responses varied substantially in response latency (range 0.15 to 2.5 s at rv4 3 10^{14} rod-effective photons/cm^{2}/s) and amplitude (1.21 to 46.51 spikes/s at rv4 3 10^{14} rod-effective photons/cm^{2}/s; Figures 1H–1K). One-third of light-responsive units (n = 34) increased firing within 500 ms of the appearance of light, with a further 46 units responding between 500 ms and 1 s. However, longer delays were also observed (n = 24), including some units being excited after stimulus termination. A very small number of units decreased firing. Responses were obtained not only at maximum intensity (rv4 3 10^{14} rod-effective photons/cm^{2}/s) but also when irradiance was reduced by 310 or 3100 (Figures 1I and 1J), with 31 and 30 units meeting our objective criterion of responsiveness at the two dimmer irradiances. This sensitivity is equivalent to that reported for Opto-mgluR6 [15] but superior to that of microbial photopigments and synthetic light switches, which generally require irradiances in the range 10^{14}–10^{17} photons/cm^{2}/s [5–14].

One interesting feature of restored light responses is that stimulus-induced increases in firing were much more numerous than decreases (Figure 1F). Rod opsin shows selectivity for $Ga_{i/o}$ class G proteins in heterologous expression [16–19], and one would therefore expect its primary light response to be inhibitory. Nevertheless, this could produce excitatory responses from retinal ganglion cells if it were to reduce the activity of inhibitory amacrine-cell synapses. Previous studies confirm that such sign inversions can occur in the degenerate retina [9, 15]. To test this possibility, we applied GABAa and GABAc receptor antagonists (TPMP 25 mM and picrotoxin 50 mM) to two retinal preparations. We found that excitatory responses were abolished by this treatment (Figure 1L, right-hand records) with the exception of one unit (Figure 1L, left-hand record). These data imply that the excitatory responses we observe originate primarily with light-dependent disinhibition of ganglion cell firing.

20 repeats. In both conditions, units show increases in firing associated with light presentation (from 0 to 2 s), but these are most pronounced for the first few trials (lower traces in raster) in (D), indicating bleaching, while inclusion of *9-cis*-retinal (E) renders them repeatable across many trials.

(F and G) Heatmap representations of mean firing rate across at least 20 presentations of 2-s stimulus (ON at time 0) for 104 units from 5 *rd*^{1}-CAG-*RHO* mice (F) and six units from three control *rd*^{1}-CAG-GFP mice (G) meeting an objective criterion of stimulus-associated change in firing. Color code represents normalized firing rate (−1 and 1 being minimum and maximum firing rate for that unit, respectively). Traces are ordered according to response latency.

(H) Population mean (±SEM) normalized firing rate profiles for *rd*^{1}-CAG-*RHO* units grouped according to response latency (horizontal white lines in F delineate extent of clusters).

(I) Mean ± SEM normalized firing rate (mean firing rate from −2 s to 6 s was normalized to maximum and minimum, and the normalized pre-stimulus firing rate (−2 to 0 s) was then subtracted) for all light-responsive units exposed to 2-s pulses (starting at 0 s) at 4 3 10^{14}, 4 3 10^{13}, and 4 3 10^{12} rod photons/cm^{2}/s.

(J and K) Distribution of response amplitudes (J; mean change in firing rate) and latencies (K; mean time at which mean firing rate first fell outside 2 SDs of baseline firing) for units in (F) responding with increases (excit'n) or decreases (inhib'n) in firing at 4 3 10^{14}, 4 3 10^{13}, and 4 3 10^{12} rod photons/cm^{2}/s.

(L) Perievent rasters for three single units showing firing of three units across multiple repeats of a 2-s light pulse (4 3 10^{14} rod photons/cm^{2}/s) without (above) and with (below; shaded in green) application of GABA receptor antagonists (TPMP 25 mM and picrotoxin 50 mM).

Characterization of Restored Responses In Vivo

To determine whether endogenous levels of *cis*-retinal in the degenerate retina were sufficient to allow ectopic rod opsin to function in vivo and how the signal recorded in the retina appeared in the brain, we turned to recording from the dLGN of anaesthetized mice using multi-electrode probes. For these experiments, we used animals in which one eye had been injected with the AAV2-CAG-*RHO* virus and the other with a control GFP virus (AAV2-CAG-GFP; Figure 2A). This enabled us to compare responses to stimuli presented to treated and control retinas in the same individual. We found that 2-s full-field flashes of 410-nm light (estimated retinal irradiance rv10^{14} rod photons/cm^2/s) produced many more responses when presented to the treated (Figure 2B) than controls (Figure 2C) eyes. In controls, we found 10 units (out of 736 single units in or around the dLGN) that met our objective criterion of light responsiveness. Several of these had very low baseline firing rate (Figure 2C), making them prone to appear as false positives according to our criterion of responsiveness, while the remainder had very sustained and/or delayed increases in firing as previously described for melanopsin-driven responses [23]. By contrast, stimuli presented to the treated eye induced changes in firing for 31 out of 736 units (Figure 2B). These could be either ipsi- or contra-lateral to the stimulated eye. Bleaching was not a problem for in vivo light responses, which showed robust firing across many repeated trials (Figure 2D) and even to light steps against a background (Figure 2E).

dLGN responses downstream from *rd*^{1}-CAG-*RHO* retinas were mostly excitatory in nature. Their response duration (0.56 ± 0.84 s; mean ± SD), amplitude, and latency were variable (Figures 2F and 2G), but a cluster of units responded within 500 ms of lights on. There were examples of cells that maintained elevated firing throughout light exposure, and in some cases beyond, while others showed more transient responses (Figure 2D). Responses could be discerned for stimuli at estimated retinal irradiance of 10^{14} and 10^{13}, but not 10^{12}, photons/cm^2/s (Figure 2D).

Restricting Ectopic Expression of Rod Opsin Using a Cell-Specific Promoter

A potential problem with untargeted expression of rod opsin is that the pigment will appear in cells that ordinarily would have quite different visual feature selectivity. This could make visual information in the brain incoherent. Therefore, we next selectively targeted rod opsin to ON-bipolar cells (Figure 3A) using an enhancer element derived from the grm6 promoter [24, 25] previously shown to drive expression in this cell type [6, 7, 8, 9, 12]. Viral transduction of a grm6-*RHO* construct resulted in rod opsin expression in cells of the INL across the retina (Figures S2A, S2B, and S2F) often clustered in patches of high transduction (Figure 3B; Figures S2C and S2D). Multi-electrode array recordings of the GCL of two grm6-*RHO*-treated retinas revealed stimulus-associated increases in firing in 30 out of 135 units (Figure 3C). Response latencies (Figure 3D; 1.14 ± 0.778 s; mean ± SD), durations (0.49 ± 0.76 s; mean ± SD), and amplitudes (Figure 3E; 2.8 ± 3.42 spikes/s; mean ± SD) varied significantly. Robust excitatory responses were observed at maximum light intensity (rv10^{14} rod photons/cm^2/s) and also when the intensity was reduced to rv10^{12} rod photons/cm^2/s (Figure 3F). Inhibition of GABAergic signaling abolished these responses (Figure 3G), consistent with the view that they arose primarily from a light-dependent disinhibition of ganglion cell firing.

Electrophysiological responses to light could be readily detected in the dLGN of grm6-*RHO*-treated animals. Thus, when presented with 2-s full-field flashes (410 nm; rv10^{14} rod equivalent photons/cm^2/s), numerous units (73 out of 481 units in or around the dLGN) showed a significant change in firing (Figure 3H). Once again, most responses were excitatory, but a number of inhibitory responses (n = 14) were also recorded in this case. Response latencies (Figure 3I; 1.07 ± 0.6; mean ± SD) and amplitudes (Figure 3J; 6.93 ± 9.377; mean ± SD) varied significantly, although many units responded within 500 ms of stimulus onset. Mean (±SD) response duration was 0.41(±0.28) s for increases and 1.21 (±0.75) s for decreases in firing. Responses were apparent at rv10^{14} and 10^{13} rod photons/cm^2/s but were less convincing when the stimulus intensity was dropped to 10^{12} rod photons/cm^2/s (Figure 3K).

Light-Induced Behavioral Responses

Next, we asked whether ectopic rod opsin could support visual discrimination. For this purpose, we set out to establish a behavioral test of vision that was higher throughput and less stressful than maze navigation tasks (which in our experience require very long training times for animals with poor vision [26]) and could be used in conjunction with a variety of visual features. Based upon previous light/dark box tests [7, 14, 27, 28] and other reports of behavioral responses to simple visual stimuli [29], we hypothesized that abrupt alterations in the visual scene might induce changes in spontaneous locomotor activity (either increases or decreases) that could be measured objectively with available image analysis software. Mice were placed in a modified light/dark box and allowed free movement between two arenas via an opening in the separating wall. Ordinary LCD computer monitors set to provide corneal irradiance 0.12 W/m^2 (rv40 lux; retinal irradiance rv10^{11}–10^{12} rod-equivalent photons/cm^2/s at maximum brightness ''white screen'' and a contrast ratio of 1:100) were placed behind transparent walls at either end of the arena. We started by asking whether mice could detect a simple luminance step by switching one of the monitors to ''white'' after the animals had been allowed to explore the box for several minutes with both monitors set to ''black.'' Wild-type mice responded to the change with an immediate increase in locomotor activity (Figure 4A). This response was absent from control *rd*^{1}-CAG-GFP mice, while both CAG-*RHO*- and grm6-*RHO*-treated mice responded to the appearance of the white screen with a statistically significant reduction in activity, indicating that they had detected the luminance increment (Figure4A).

To probe temporal resolution of the restored vision, we investigated whether treated mice could detect the transition from a gray to a flickering screen of equivalent time-averaged irradiance (0.066 W/m^2). *rd*^{1}-grm6-*RHO* mice responded to appearance of either 2-Hz or 4-Hz flicker with decreased activity, while 10 Hz drove a significant increase (Figures 4B and 4C; two-way repeated measures [RM] ANOVA; $p < 0.0001$ for interaction between flicker frequency and gray versus flicker, post hoc Bonferroni correction $p < 0.05$ for gray versus flicker at 4 and 10 Hz; paired t test $p < 0.01$ also for 2 Hz). *rd*^{1}-CAG-*RHO* responded only to the 2-Hz flicker, while *rd*^{1}-CAG-GFP controls showed

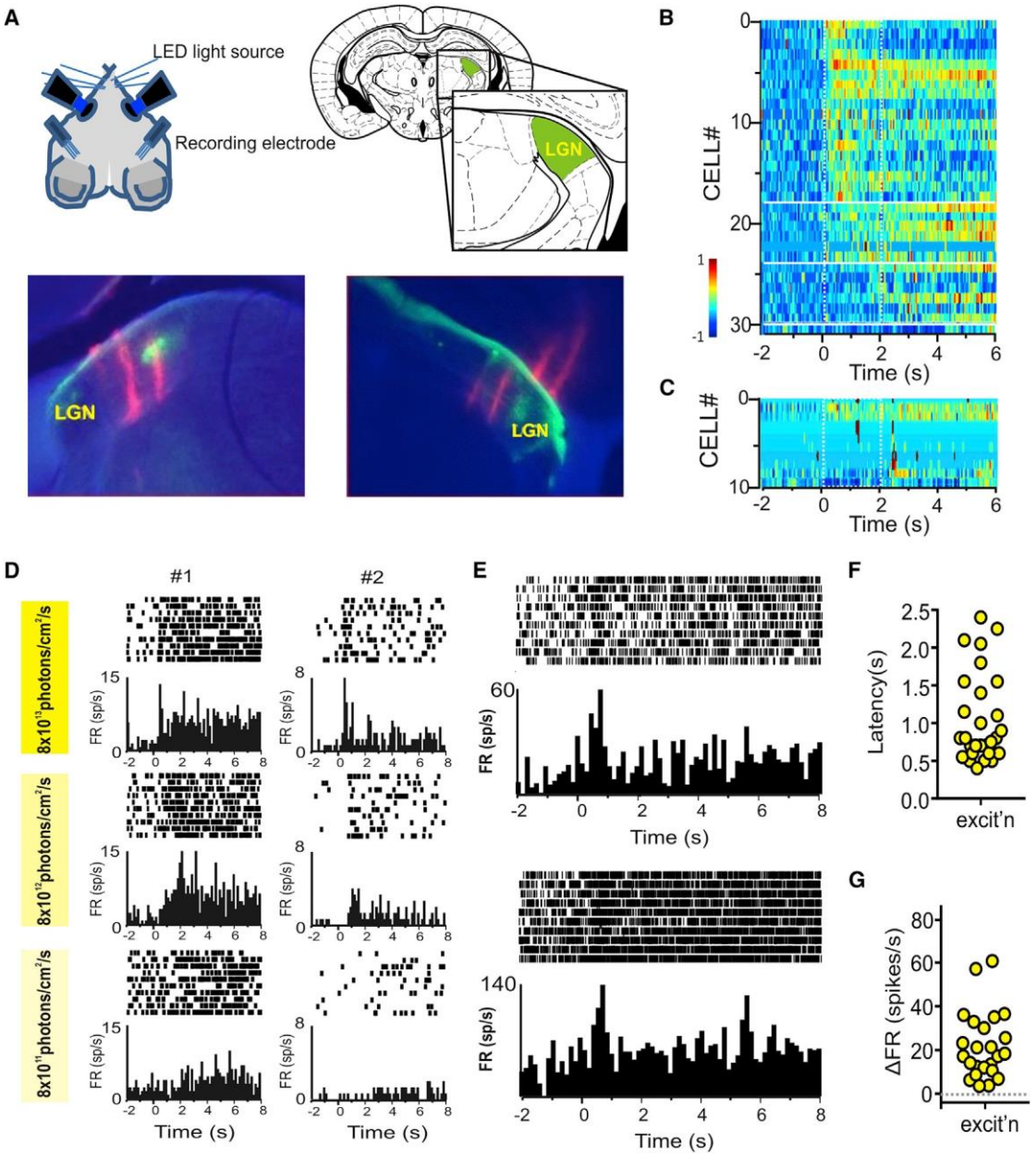

Figure 2. Rod Opsin Expression Driven by the Ubiquitous CAG Promoter Restores Light Responses in Blind *rd*^{1} Mouse Thalamus

(A) Schematic of recording apparatus allowing presentation of separate light stimuli to each eye and insertion of silicone multi-channel recording electrode probes to the dorsal lateral geniculate nuclei (dLGNs) in either hemisphere. Representative histological sections through the left and right dLGN with DiI tracks (in red) showing path of insertion for recording probes.

(B and C) Heatmap representations of mean firing rate across multiple presentations of 2-s stimulus (ON at time 0) to *rd*^{1}-CAG-*RHO* (B) and control *rd*^{1}-CAG-GFP (C) eyes of units showing a significant change in firing associated with stimulus presentation (n = 31 units downstream of 5 treated eyes and n = 10 units downstream of 5 control eyes). Color code represents normalized firing rate (−1 and 1 being minimum and maximum firing rate for that unit, respectively). Traces are ordered according to response latency.

(D) Sensitivity response profile (perievent rasters and associated perievent firing rate histograms) for two representative dLGN single units isolated from (B) at three different retinal irradiances: 8 3 10^{13}, 8 3 10^{12}, and 8 3 10^{11} rod-equivalent photons/cm^2/s.

(E) Light-adapted responses (perievent rasters and associated perievent firing rate histograms) for two representative dLGN units from *rd*^{1}-CAG-*RHO* eyes recorded under light-adapted conditions (retinal irradiance 8 3 10^{13} rod-equivalent photons/cm^2/s and Michelson contrast 96%).

(F and G) Distribution of response latencies (F; time at which mean firing rate first fell outside 2 SDs of baseline for units responding within 2.5 s of lights on) and amplitude (G; mean change in firing rate) for units in (B) responding with increases (excit'n) or decreases (inhib'n) in firing. CAG is a hybrid CMV enhancer/chickenb-actin promoter. *RHO* is human rod opsin coding sequence.

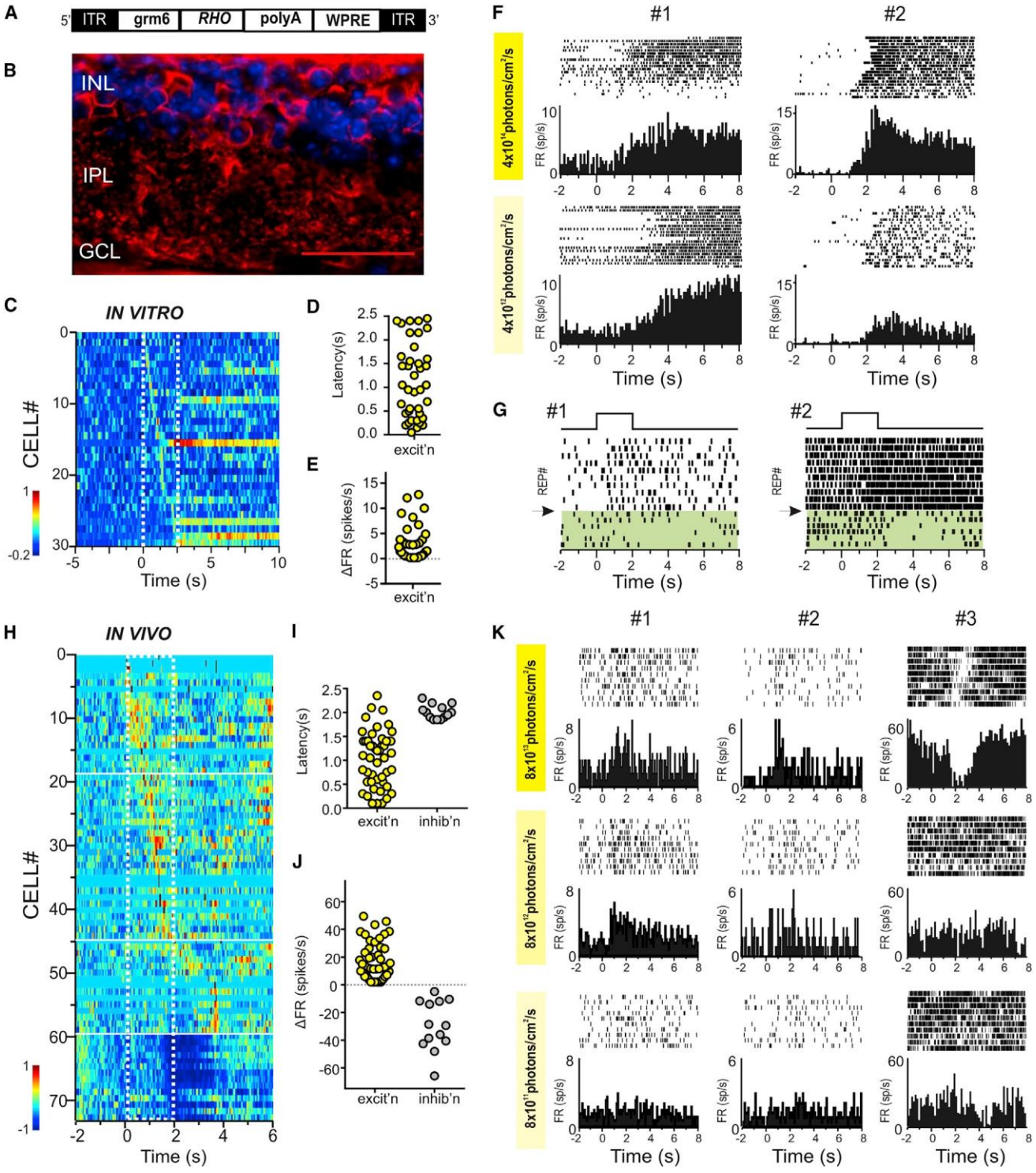

Figure 3. Selective Expression of Rod Opsin Using a Cell-Specific grm6 Promoter Restores Visual Responses in the dLGN of *rd*[1] Mice

(A) Schematic of the DNA expression cassette delivered by AAV2/2 vector to the retina, comprising *RHO* under the ON-bipolar cell-specific (grm6) promoter flanked by ITRs and stabilized by polyA and WPRE.

(B) Exemplar image of a section through an *rd*[1] mouse retina >4 months after intravitreal delivery of viral vector in (A) in conjunction with glycosidic enzymes. Expression of human rod opsin in cells of the INL and processes in the IPL are revealed by staining (red) with an a-hRho antibody and counterstaining of nuclei with DAPI (blue). Calibration bar = 50mm.

(legend continued on next page)

no behavioral response in this paradigm (Figure S4A). Using the 4-Hz flicker, we next explored the contrast sensitivity of the flicker detection by reducing the difference in brightness between white and black elements of the flicker (Figure 4D). We found that *rd*^{1}-grm6-*RHO*-treated mice continued to respond when the contrast ratio was reduced from 1:100 to 1:50, but not 1:7 or lower (Figure 4D).

We used a different cohort of *rd*^{1}-grm6-*RHO* mice to assess spatial acuity for the restored vision. In this case, we asked whether there was a change in locomotor activity associated with the switch from a uniform gray screen to a drifting grating (black:white contrast ratio = 1:7.5; stimuli matched for irradiance). We started by applying this paradigm to wild-type mice to confirm its suitability for our purpose. Appearance of these gratings induced increases in locomotor activity in wild-types at frequencies %0.4 or 0.6 cycles per degree (cpd) (Figure 4E, #1; first trial and Figure 4F average of seven trials; two-way RM ANOVA; $p < 0.01$ for gray versus gratings, post hoc Bonferroni correction $p < 0.05$ at 0.1 and 0.4 cpd; paired t test $p < 0.05$ also for 0.2 and 0.6 cpd). Importantly, this finding is consistent with published estimates of spatial acuity in mice from optokinetic and maze navigation methods [30, 31]. We tested treated mice first with a considerably lower grating frequency (0.04 cpd; equivalent to viewing 15-cm bars at 60-cm distance). We found that the grating induced an increase in activity in *rd*^{1}-grm6-*RHO* mice (Figure 4E, #2 and #3). Across the population of treated mice, this approached statistical significance for the first single trial ($p = 0.05$) and was statistically significant ($p < 0.05$) over five (Figure 4G) or ten repeats ($p < 0.05$, data not shown). *rd*^{1}-grm6-GFP mice showed no response to this stimulus (data not shown). When tested with a finer grating (0.08 cpd) neither *rd*^{1}-grm6-*RHO* (Figure 4G) nor *rd*^{1}-grm6-GFP (data not shown) mice showed a significant change in activity.

Visual Responses to Naturalistic Scenes

The ability of *rd*^{1}-grm6-*RHO* to distinguish spatial patterns at contrast ratios (1:7.5) well within those experienced in natural scenes [32] led us to ask whether ectopic rod opsin might allow discrimination of more naturalistic scenes. We recorded electrophysiological activity in the dLGN across multiple repeats of a 30-s movie comprising mice moving around an open arena [33]. In both *rd*^{1}-grm6-*RHO* and *rd*^{1}-CAG-*RHO* mice, we found units whose firing rate appeared to increase at particular phases on multiple repeats of the movie, suggesting a response to features of the stimulus. However, only one of these from an *rd*^{1}-grm6-*RHO* met an objective criterion of response (Figures 5A–5C). We finally asked whether treated mice could show behavioral responses to a natural movie by presenting a clip of a swooping owl (Figure 5D) to mice in the behavioral test arena. *rd*^{1}-grm6-*RHO* mice responded to this stimulus with a significant increase in activity (Figures 5E and 5F), which was also observed in wild-type mice but was absent in control *rd*^{1}-CAG-GFP mice or *rd*^{1}-CAG-*RHO*-treated animals (Figure 5F).

DISCUSSION

We have found that ectopic expression of human rod opsin is an effective method of restoring vision in blind mice. Using electrophysiological recordings in the retina and visual thalamus, we find that ectopic rod opsin supports reproducible responses to light pulses and steps over a range of intensities typical of our everyday experience. At the single-unit level, restored responses can be excitatory or inhibitory, sustained or transient, mirroring the richness of the visual code seen in wild-type mice. Using a behavioral test, we find that rod opsin-treated mice are able to detect visual stimuli presented using an ordinary LCD visual display unit (VDU) in a dimly lit room. Under these conditions, they can distinguish flicker at a range of frequencies (up to 10 Hz), differences in luminance commonly encountered in visual scenes, coarse spatial patterns, and elements of a natural movie.

The quality of recreated vision reported here for human rod opsin has a number of encouraging characteristics and overall compares favorably with previous approaches. An important feature is its relatively high sensitivity. We find electrophysiological responses at retinal irradiances as low as rv10^{12} photons/cm^2/s. This represents a significant improvement in sensitivity compared to previous studies using microbial opsins (thresholds between 10^{14} and 10^{17} photons/cm^2/s) [5–10], LiGluR/MAG photoswitches (10^{15}–10^{16} photons/cm^2/s) [11, 12], or photoactivated ligands (AAQ at 4 3 10^{15} photons/cm^2/s [13] and DENAQ at 4 3 10^{13} photons/cm^2/s) [14] and is similar to the most recent work with the synthetic Opto-mgluR6 receptor (6 3 10^{12} photons/cm^2/s) [15]. Importantly, this threshold for rod opsin-driven responses falls within the range of irradiances encountered in normal indoor environments.

(C) Heatmap representations of mean firing rate across multiple presentations of 2-s stimulus (ON at time 0) for 30 single retinal units from two *rd*^{1}-grm6-*RHO* mice showing a significant change in firing associated with stimulus presentation. Color code represents normalized firing rate (-1 and 1 being minimum and maximum firing rate for that unit, respectively). Traces are ordered according to response latency.

(D and E) Distribution of response latencies (D; time at which mean firing rate fell outside 2 SDs of baseline for units responding within 2.5 s of lights on) and amplitude (E; mean change in firing rate) for units in (C) responding with increases (excit'n) in firing.

(F) Sensitivity response profile (perievent rasters and associated perievent firing rate histograms) for two representative retinal single units isolated from (C) at two different retinal irradiances: 4 3 10^{14} and 4 3 10^{12} rod-equivalent photons/cm^2/s.

(G) Perievent rasters for two single units showing inhibition of excitatory responses after application of GABA receptor antagonists (TPMP 25 mM and picrotoxin 50 mM; lower part of raster plots shaded in green).

(H) Heatmap representations of mean firing rate across multiple presentations of 2-s stimulus (ON at time 0) for 73 single dLGN units from *rd*^{1}-grm6-*RHO* eyes showing a significant change in firing associated with stimulus presentation. Color code represents normalized firing rate (-1 and 1 being minimum and maximum firing rate for that unit, respectively). Traces are ordered according to response latency.

(I and J) Distribution of response latencies (I; time at which mean firing rate fell outside 2 SDs of baseline for units responding within 2.5 s of lights on) and amplitude (J; mean change in firing rate) for units in (C) responding with increases (excit'n) or decreases (inhib'n) in firing.

(K) Sensitivity response profile (perievent rasters and associated perievent firing rate histograms) for representative dLGN single units isolated from (H) at three different retinal irradiances: 8 3 10^{13}, 8 3 10^{12}, and 8 3 10^{11} rod-equivalent photons/cm^2/s.

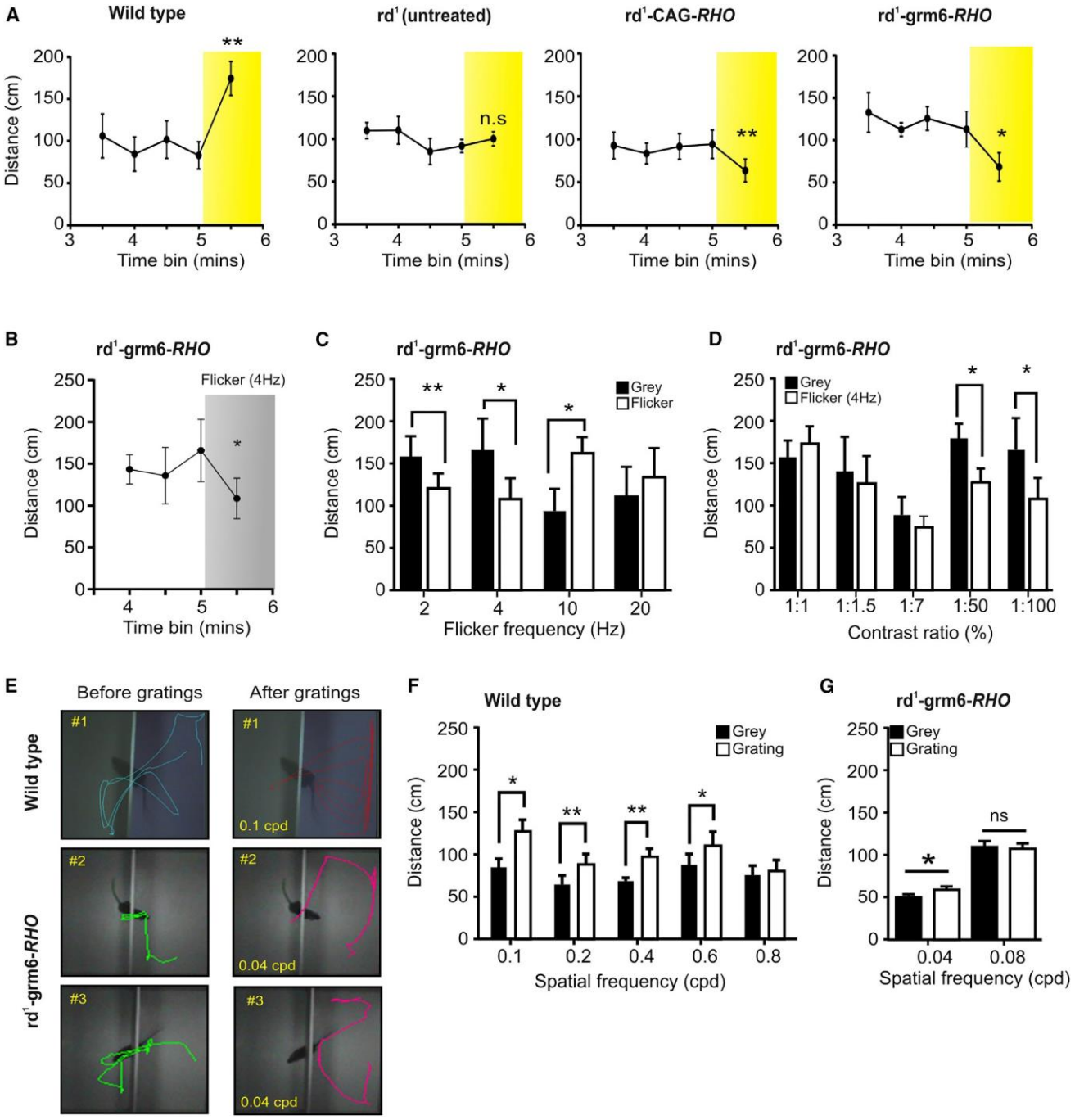

Figure 4. Ectopic Expression of Rod Opsin Restores Visual Behavior in Blind *rd*^{1} Mice

(A) Open box activity plots for freely moving mice with LCD screens switched from "black" to "white" at time 5 min (illuminance 40 lux; estimated retinal irradiance 1 3 10^{12} rod-equivalent photons/cm^2/s).

(B) Open box activity plot for *rd*^{1}-grm6-*RHO* mice exposed to 4-Hz flicker starting at 5 min (illuminance 20 lux; estimated retinal irradiance 8 3 10^{11} rod-equivalent photons/cm^2/s.

(C and D) Histograms of activity for *rd*^{1}-grm6-*RHO* mice showing distance traveled in 30 s before (black bars) and 30 s after (white bars) presentation of "white" screen at different flicker frequencies (C) and at 4-Hz flicker at different contrast ratios (D).

(E) Representative movement trajectories for a wild-type and two different *rd*^{1}-grm6-*RHO* mice in the open field box in the 30 s before (left) and 30 s after (right) presentation of gratings.

(F) Histogram of activity for wild-type mice showing distance traveled in 30 s before (black bars) and 30 s after (white bars) presentation of drifting squarewave gratings (contrast ratio 1:8) at different spatial frequencies.

(G) Histogram of change in activity in response to two different spatial frequencies (0.04 and 0.08 cpd) for *rd*^{1}-grm6-*RHO* mice. Sample sizes for data in (A)–(D) are five wild-type, six *rd*^{1}-CAG-GFP, six *rd*^{1}-CAG-*RHO*, and five *rd*^{1}-grm6-*RHO* mice; in (F) eight wild-type; in (G) nine *rd*^{1}-grm6-*RHO*.

(legend continued on next page)

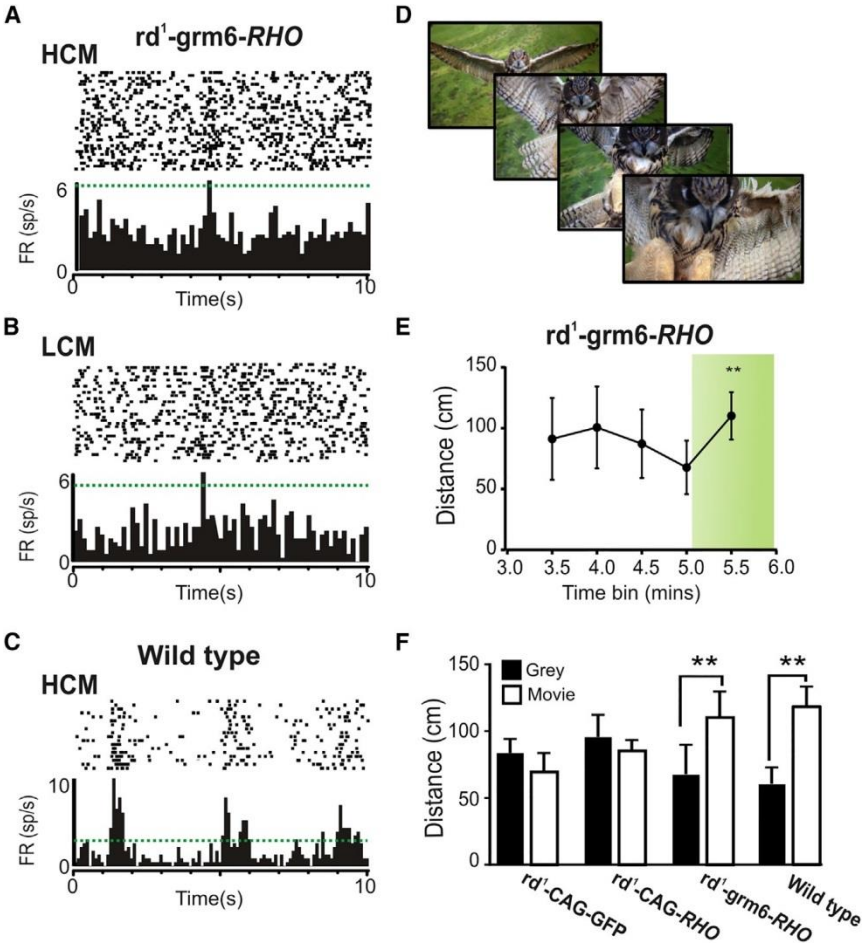

Figure 5. Rod Opsin Restores Visual Behavior in Response to Natural Scenes

(A and B) Perievent rasters and associated perievent firing rate histograms for a dLGN unit to multiple presentations of a 30-s naturalistic movie (mice moving in an open arena in horizontal view; mean estimated retinal irradiance 1 3 10^{13} rod-equivalent photons/cm^2/s) to an *rd*^{1}-grm6-*RHO* eye. (A) and (B) show presentations of the high-contrast movie (HCM; black:white contrast ratio = 1:100) and low-contrast movie (LCM; contrast ratio reduced 1:50), respectively. Horizontal line on histograms shows the 99% confidence interval for firing rate across the movie presentation; note the increase in firing above this line at the same time point for both movie presentations.

(C) Firing pattern of a representative dLGN unit from a wild-type mouse exposed to the HCM is presented for comparison.

(D) Example frames from a naturalistic movie featuring a swooping owl presented to mice in a behavioral arena.

(E) Open box activity plots for *rd*^{1}-grm6-*RHO* mice presented with a naturalistic swooping owl movie starting at 5 min (shaded in green; estimated retinal irradiance 8 3 10^{11} rod-equivalent photons/cm^2/s).

(F) Histogram of activity (mean ± SEM distance traveled by each animal) for *rd*^{1}-CAG-GFP (n = 6), *rd*^{1}-CAG-*RHO* (n = 6), *rd*^{1}-grm6-*RHO* (n = 5), and wild-type (n = 10) mice showing distance traveled in 30 s before (black bars) and after (white bars) presentation of the swooping owl movie. Two-tailed paired t tests comparing activity before and after stimulus appearance (**p < 0.01).

The relatively high sensitivity of the light responses driven by ectopic rod opsin raises the possibility that this intervention could allow visual discrimination under natural viewing conditions. We employed a new behavioral paradigm to determine the extent to which this was realized. Although developed independently, it is similar to a recently published approach shown to assay cortical vision [28]. At its heart is the prediction that an abrupt change in the visual scene may induce an alteration in behavioral state that can be measured as a change in locomotor activity. As commercially available software can measure mouse locomotor activity in open fields, we hoped that this would provide a simple and objective method to determine whether mice could distinguish between pairs of visual stimuli. That proved to be the case, and in wild-type mice, the new test replicates previous estimates of spatial acuity (Figure 4F) [30, 31]. When applied to treated animals, this behavioral test provides evidence for impressive visual discrimination in *rd*^{1}-grm6-*RHO* mice. These animals showed changes in activity not only to simple luminance increments but also to the appearance of more subtle visual cues including relatively fast flicker (up to 10 Hz) and simple spatial gratings.

Importantly, these responses were elicited under moderate illumination (rv20–150 lux; rv10^{13} rod equivalent photons/cm^2/s) and at physiological levels of visual contrast. To our knowledge, this is the first time that a clinically amenable optogenetic intervention has been shown to support spatiotemporal discrimination under such natural viewing conditions. Optokinetic responses to drifting gratings have been recreated using both channelrhodopsin and halorhodopsin, but at much higher irradiances [8, 10]. In a recent study employing opto-mgluR6, such optokinetic responses were recorded at more physiological light levels [15]. However, that work was undertaken in a mouse line in which germline genetic modification was used to express the pigment in all ON-bipolar cells, confounding comparison with the effects of the more clinically relevant viral gene transfer employed here.

The behavioral responses of *rd*^{1}-grm6-*RHO* mice to relatively fast flicker (4 and 10 Hz) indicate that vision in these animals has

In all panels, activity is represented by mean ± SEM of the mean distance traveled by each animal in a 30-s time bin; time in min since introduction to testing arena. Two-tailed paired t tests comparing activity before and after stimulus appearance (*p < 0.05, **p < 0.01). For Figures 4B and 4C, two-way RM ANOVA; p < 0.0001 for interaction between flicker frequency and gray versus flicker, post hoc Bonferroni correction p < 0.05 for gray versus flicker at 4 and 10 Hz. For Figure 4F, two-way RM ANOVA; p < 0.01 for gray versus gratings, post hoc Bonferroni correction p < 0.05 at 0.1 and 0.4 cpd.

reasonable temporal resolution and that they can detect stimuli as short as 50 ms. However, it does not follow that they are able to actually resolve the flicker (i.e., detect the train of flashes) at these frequencies. Interactions with head and eye movements could produce apparent modulations at lower frequencies. Moreover, a temporal modulation in irradiance would also be apparent for a photoreceptor integrating over timescales that are not a perfect multiple of the flicker period (although note that the contrast of any such apparent temporal modulation would be strongly negatively correlated with integration period).

One potential advantage of rod opsin therapy is that it relies upon a light-absorbing chromophore (*cis*-retinal) that is naturally produced in the retina. A natural concern, however, is how the availability of the chromophore might be altered in retinal disease. On the one hand, degeneration of photoreceptors (which normally represent a substantial sink for chromophore) might make *cis*-retinal especially abundant in the surviving inner retina. On the other, secondary degeneration of the retinal pigment epithelium (RPE) can be a feature of advanced retinal degeneration, and some forms of dystrophy originate with visual-cycle defects. The effectiveness of rod opsin therapy in *rd*^{1} mice (which exhibit RPE dystrophy [34]) argues that in many cases, the degenerate retina would contain sufficient chromophore. In other cases, augmentation with exogenous *cis*-retinal could be considered [35, 36].

In summary, the data presented here indicate that the level of vision recovered by ectopic expression of rod opsin compares favorably with that produced by other optogenetic actuators. Given the simplicity of the intervention and the inherent appeal of a therapy that entails introducing a human protein into a tissue in which it is ordinarily expressed, we suggest that human rod opsin warrants consideration as a method for restoring vision in advanced retinal degeneration.

EXPERIMENTAL PROCEDURES

See Supplemental Information for details on experimental procedures.

Adult C57BL/6J (wild-type) and C3H/HeJ (*rd*^{1}) mice were used in this study. All animal experiments and care were conducted in accordance with the UK Animals (Scientific Procedures) Act (1986). Physiological and behavioral experiments were undertaken in mice between 8 and 12 weeks after intravitreal injection of AAV vector administered in isofluorane-anaesthetized mice between 8 and 10 weeks of age. Each eye was injected with 3 ml virus (1 3 10^{13} genomic counts) containing either a rod opsin (AAV2-ITR-CAG-*RHO*-polyA-WPRE-ITR for untargeted expression or AAV2-ITR-grm6-*RHO*-polyA-WPRE-ITR for targeted expression) or GFP (AAV2-ITR-CAG-GFP-polyA-WPRE-ITR for untargeted expression or AAV2-ITR-grm6-GFP-polyA-WPRE-ITR for targeted expression) expression construct, in combination with 0.5 ml of glycosidic enzyme solution containing 0.125 units each of heparinise III and hyaluronan lyase (E.C. 4.2.2.8 and E.C. 4.2.2.1; Sigma-Aldrich). Eyes were retrieved >6 weeks post vector injection, fixed, and cryosectioned before immunohistochemistry and microscopy. For details of gene delivery via AAV vector, histology, immunohistochemistry, and bio-imaging, see Supplemental Experimental Procedures.

Multi-electrode Array Recordings

Recordings were performed on rod opsin-treated *rd*^{1} mice (n = 8) and GFP-injected *rd*^{1} controls (n = 3) using a multi-electrode array system (Multi Channel Systems). Light stimuli (2-s full-field flashes of white light, 20-s interstimulus interval, at three different intensities 4 3 10^{12}, 4 3 10^{13}, and 4 3 10^{14} rod photons/cm^{2}/s) were presented by a customized light engine source (Lumencor or Thorlab LEDs). Spike-sorted, single-unit data were further analyzed using Neuroexplorer (Nex Technologies) and MATLAB R2010a (MathWorks).

In Vivo Electrophysiology

Lateral geniculate nucleus (LGN) recordings were performed on two groups of anaesthetized *rd*^{1} mice using a 32-channel probe (Neuronexus). Group 1 (n = 7) had one eye injected with AAV2-CAG-*RHO* and the other with AAV2- CAG-GFP, and group 2 (n = 5) had one eye injected with AAV2-grm6-*RHO* and the other with AAV2-grm6-GFP. Visual stimuli were provided by LEDs (Thorlab $\mathbf{l}_{max}$: 410 nm) and delivered via fiber optic to purpose-made eye cones tightly positioned onto each eye to minimize any potential light leak. Light flashes were delivered according to a light protocol consisting of two parts. Part 1 included flashes from darkness: 2-s light ON, 20-s light OFF, with 10-s offset between each eye. This paradigm was repeated at least ten times at each neutral density (ND) filter. Retinal irradiance ranged from 8 3 10^{11} photons/cm^{2}/s at ND2 to 8 3 10^{13} photons/cm^{2}/s at ND0. Part 2 of the light protocol involved recording in light-adapted conditions where 5-s steps of light were applied to a steady background illumination at Michelson contrast of 96%. There was a 20-s interstimulus interval and a 10-s offset between two eyes. This paradigm was repeated ten times. Naturalistic movies were presented with a digital mirror device projector (DLP LightCommanderTM, Logic PD), whose intrinsic light engine had been replaced with our own multispectral LED light source containing four independently controlled LEDs ($\mathbf{l}_{max}$ at 405 nm, 455 nm, 525 nm, and 630nm; Phlatlight PT-120 Series (Luminus Devices). For details, see Supplemental Information. We used the same objective criterion to identify light-responsive units in both in vitro and in vivo recordings—that firing rate within 4 s of the start of a 2-s pulse fell >2 SDs outside mean of baseline firing prior to light exposure. Applying this criterion to recordings from control *rd*^{1} eyes provides confidence that it returns few false positives; the rate of false negatives is harder to determine. In addition to the responses shown here, it was our impression that in some cases, a light response appeared to have interacted with some underlying oscillatory mechanism, inducing a modest increase in firing around light stimulation and a more substantial change several seconds later. Response duration was estimated by the time over which firing rate fell outside 2 SDs of baseline. A few cells (n = 7 for CAG in vivo; n = 6 for grm6 in vitro; n = 7 for grm6 in vivo) in which the stimulus appeared to have induced a longer-lasting change in baseline firing patterns were not included in this analysis.

Behavior

Although developed independently, our test is similar to that in a recently published study [28] and shown by them to be a reflection of cortical vision. Using a modification of a light/dark box, mice were allowed free movement between two equal arenas (left and right halves) via an opening in the separating wall. The visual stimuli were displayed from two computer monitors (Acer V173b and either Dell E173FP or ViewSonic matched for power by adjusting screen brightness) facing clear walls of each arena, using a DualHead2Go Digital Edition external multi-display adaptor (Matrox Graphics). A variety of visual stimuli were generated using a custom-written program and displayed on one monitor at a time. For further details on behavioral set up and stimuli used, see Supplemental Information.

SUPPLEMENTAL INFORMATION

Supplemental Information includes Supplemental Experimental Procedures and four figures and can be found with this article online at http://dx.doi.org/10.1016/j.cub.2015.07.029.

AUTHOR CONTRIBUTIONS

J.C.-K., A.E.A., C.E., N.M., K.E.D., P.N.B., and R.J.L. designed the research. J.C.-K. performed intraocular injections, retinal histology, LGN recordings, and behavioral experiments. J.C.-K. and C.E. performed MEA recordings. A.P. performed behavioral experiments involving spatial stimuli with assistance from K.E.D., R.B., and N.M. J.C.-K. performed data processing and analysis with assistance from A.E.A. N.M. assisted with histology. J.C.-K., P.N.B., and R.J.L. wrote the manuscript with input from all authors. P.N.B. and R.J.L. supervised the research.

ACKNOWLEDGMENTS

We thank Franck Martial for assistance with light measurements for behavioral experiments; Jonathan Wynne and Dave Green for assistance with behavioral setup; and Timothy M. Brown for assistance with design and advice on electrophysiology experiments. J.C.-K. was supported by a Medical Research Council Clinical Research Training Fellowship (G1000268/1). This study was supported by grants from the ERC (268970 to R.J.L.), BBSRC (BB/K002252/1 to R.J.L.), and MRC (Confidence in Concept award MC_PC_13070 to R.J.L., P.N.B., and J.C.-K.).

Received: May 15, 2015
Revised: June 19, 2015
Accepted: July 10, 2015
Published: July 30, 2015

REFERENCES

1. Mazzoni, F., Novelli, E., and Strettoi, E. (2008). Retinal ganglion cells survive and maintain normal dendritic morphology in a mouse model of inherited photoreceptor degeneration. J. Neurosci. *28*, 14282–14292.
2. Santos, A., Humayun, M.S., de Juan, E., Jr., Greenburg, R.J., Marsh, M.J., Klock, I.B., and Milam, A.H. (1997). Preservation of the inner retina in retinitis pigmentosa. A morphometric analysis. Arch. Ophthalmol. *115*, 511–515.
3. Busskamp, V., Picaud, S., Sahel, J.A., and Roska, B. (2012). Optogenetic therapy for retinitis pigmentosa. Gene Ther. *19*, 169–175.
4. Lin, B., Koizumi, A., Tanaka, N., Panda, S., and Masland, R.H. (2008). Restoration of visual function in retinal degeneration mice by ectopic expression of melanopsin. Proc. Natl. Acad. Sci. USA *105*, 16009–16014.
5. Bi, A., Cui, J., Ma, Y.P., Olshevskaya, E., Pu, M., Dizhoor, A.M., and Pan, Z.H. (2006). Ectopic expression of a microbial-type rhodopsin restores visual responses in mice with photoreceptor degeneration. Neuron *50*, 23–33.
6. Doroudchi, M.M., Greenberg, K.P., Liu, J., Silka, K.A., Boyden, E.S., Lockridge, J.A., Arman, A.C., Janani, R., Boye, S.E., Boye, S.L., et al. (2011). Virally delivered channelrhodopsin-2 safely and effectively restores visual function in multiple mouse models of blindness. Mol. Ther. *19*, 1220–1229.
7. Cronin, T., Vandenberghe, L.H., Hantz, P., Juttner, J., Reimann, A., Kacsó, A.E., Huckfeldt, R.M., Busskamp, V., Kohler, H., Lagali, P.S., et al. (2014). Efficient transduction and optogenetic stimulation of retinal bipolar cells by a synthetic adeno-associated virus capsid and promoter. EMBO Mol. Med. *6*, 1175–1190.
8. Lagali, P.S., Balya, D., Awatramani, G.B., Münch, T.A., Kim, D.S., Busskamp, V., Cepko, C.L., and Roska, B. (2008). Light-activated channels targeted to ON bipolar cells restore visual function in retinal degeneration. Nat. Neurosci. *11*, 667–675.
9. Macé, E., Caplette, R., Marre, O., Sengupta, A., Chaffiol, A., Barbe, P., Desrosiers, M., Bamberg, E., Sahel, J.A., Picaud, S., et al. (2015). Targeting channelrhodopsin-2 to ON-bipolar cells with vitreally administered AAV Restores ON and OFF visual responses in blind mice. Mol. Ther. *23*, 7–16.
10. Busskamp, V., Duebel, J., Balya, D., Fradot, M., Viney, T.J., Siegert, S., Groner, A.C., Cabuy, E., Forster, V., Seeliger, M., et al. (2010). Genetic reactivation of cone photoreceptors restores visual responses in retinitis pigmentosa. Science *329*, 413–417.
11. Caporale, N., Kolstad, K.D., Lee, T., Tochitsky, I., Dalkara, D., Trauner, D., Kramer, R., Dan, Y., Isacoff, E.Y., and Flannery, J.G. (2011). LiGluR restores visual responses in rodent models of inherited blindness. Mol. Ther. *19*, 1212–1219.
12. Gaub, B.M., Berry, M.H., Holt, A.E., Reiner, A., Kienzler, M.A., Dolgova, N., Nikonov, S., Aguirre, G.D., Beltran, W.A., Flannery, J.G., and Isacoff, E.Y. (2014). Restoration of visual function by expression of a light-gated mammalian ion channel in retinal ganglion cells or ON-bipolar cells. Proc. Natl. Acad. Sci. USA *111*, E5574–E5583.
13. Polosukhina, A., Litt, J., Tochitsky, I., Nemargut, J., Sychev, Y., De Kouchkovsky, I., Huang, T., Borges, K., Trauner, D., Van Gelder, R.N., and Kramer, R.H. (2012). Photochemical restoration of visual responses in blind mice. Neuron *75*, 271–282.
14. Tochitsky, I., Polosukhina, A., Degtyar, V.E., Gallerani, N., Smith, C.M., Friedman, A., Van Gelder, R.N., Trauner, D., Kaufer, D., and Kramer, R.H. (2014). Restoring visual function to blind mice with a photoswitch that exploits electrophysiological remodeling of retinal ganglion cells. Neuron *81*, 800–813.
15. van Wyk, M., Pielecka-Fortuna, J., Löwel, S., and Kleinlogel, S. (2015). Restoring the ON switch in blind retinas: Opto-mGluR6, a next-generation, cell-tailored optogenetic tool. PLoS Biol. *13*, e1002143.
16. Li, X., Gutierrez, D.V., Hanson, M.G., Han, J., Mark, M.D., Chiel, H., Hegemann, P., Landmesser, L.T., and Herlitze, S. (2005). Fast noninvasive activation and inhibition of neural and network activity by vertebrate rhodopsin and green algae channelrhodopsin. Proc. Natl. Acad. Sci. USA *102*, 17816–17821.
17. Gutierrez, D.V., Mark, M.D., Masseck, O., Maejima, T., Kuckelsberg, D., Hyde, R.A., Krause, M., Kruse, W., and Herlitze, S. (2011). Optogenetic control of motor coordination by Gi/o protein-coupled vertebrate rhodopsin in cerebellar Purkinje cells. J. Biol. Chem. *286*, 25848–25858.
18. Cao, P., Sun, W., Kramp, K., Zheng, M., Salom, D., Jastrzebska, B., Jin, H., Palczewski, K., and Feng, Z. (2012). Light-sensitive coupling of rhodopsin and melanopsin to G(i/o) and G(q) signal transduction in Caenorhabditis elegans. FASEB J. *26*, 480–491.
19. Bailes, H.J., and Lucas, R.J. (2013). Human melanopsin forms a pigment maximally sensitive to blue light ($\lambda_{max} \approx$ 479 nm) supporting activation of G(q/11) and G(i/o) signalling cascades. Proc. Biol. Sci. *280*, 20122987.
20. Pugh, E.N., Jr., Nikonov, S., and Lamb, T.D. (1999). Molecular mechanisms of vertebrate photoreceptor light adaptation. Curr. Opin. Neurobiol. *9*, 410–418.
21. Perlman, I., and Normann, R.A. (1998). Light adaptation and sensitivity controlling mechanisms in vertebrate photoreceptors. Prog. Retin. Eye Res. *17*, 523–563.
22. Cehajic-Kapetanovic, J., Le Goff, M.M., Allen, A., Lucas, R.J., and Bishop, P.N. (2011). Glycosidic enzymes enhance retinal transduction following intravitreal delivery of AAV2. Mol. Vis. *17*, 1771–1783.
23. Brown, T.M., Gias, C., Hatori, M., Keding, S.R., Semo, M., Coffey, P.J., Gigg, J., Piggins, H.D., Panda, S., and Lucas, R.J. (2010). Melanopsin contributions to irradiance coding in the thalamo-cortical visual system. PLoS Biol. *8*, e1000558.
24. Masu, M., Iwakabe, H., Tagawa, Y., Miyoshi, T., Yamashita, M., Fukuda, Y., Sasaki, H., Hiroi, K., Nakamura, Y., Shigemoto, R., et al. (1995). Specific deficit of the ON response in visual transmission by targeted disruption of the mGluR6 gene. Cell *80*, 757–765.
25. Kim, D.S., Matsuda, T., and Cepko, C.L. (2008). A core paired-type and POU homeodomain-containing transcription factor program drives retinal bipolar cell gene expression. J. Neurosci. *28*, 7748–7764.
26. Brown, T.M., Tsujimura, S., Allen, A.E., Wynne, J., Bedford, R., Vickery, G., Vugler, A., and Lucas, R.J. (2012). Melanopsin-based brightness discrimination in mice and humans. Curr. Biol. *22*, 1134–1141.
27. Bourin, M., and Hascoët, M. (2003). The mouse light/dark box test. Eur. J. Pharmacol. *463*, 55–65.
28. Cooke, S.F., Komorowski, R.W., Kaplan, E.S., Gavornik, J.P., and Bear, M.F. (2015). Visual recognition memory, manifested as long-term habituation, requires synaptic plasticity in V1. Nat. Neurosci. *18*, 262–271.
29. Yilmaz, M., and Meister, M. (2013). Rapid innate defensive responses of mice to looming visual stimuli. Curr. Biol. *23*, 2011–2015.
30. Gianfranceschi, L., Fiorentini, A., and Maffei, L. (1999). Behavioural visual acuity of wild type and bcl2 transgenic mouse. Vision Res. *39*, 569–574.
31. Prusky, G.T., West, P.W., and Douglas, R.M. (2000). Behavioral assessment of visual acuity in mice and rats. Vision Res. *40*, 2201–2209.

32. Mante, V., Frazor, R.A., Bonin, V., Geisler, W.S., and Carandini, M. (2005). Independence of luminance and contrast in natural scenes and in the early visual system. Nat. Neurosci. *8*, 1690–1697.

33. Allen, A.E., Storchi, R., Martial, F.P., Petersen, R.S., Montemurro, M.A., Brown, T.M., and Lucas, R.J. (2014). Melanopsin-driven light adaptation in mouse vision. Curr. Biol. *24*, 2481–2490.

34. Neuhardt, T., May, C.A., Wilsch, C., Eichhorn, M., and Lu¨tjen-Drecoll, E. (1999). Morphological changes of retinal pigment epithelium and choroid in rd-mice. Exp. Eye Res. *68*, 75–83.

35. Van Hooser, J.P., Aleman, T.S., He, Y.G., Cideciyan, A.V., Kuksa, V., Pittler, S.J., Stone, E.M., Jacobson, S.G., and Palczewski, K. (2000). Rapid restoration of visual pigment and function with oral retinoid in a mouse model of childhood blindness. Proc. Natl. Acad. Sci. USA *97*, 8623–8628.

36. Ablonczy, Z., Crouch, R.K., Goletz, P.W., Redmond, T.M., Knapp, D.R., Ma, J.X., and Rohrer, B. (2002). 11-cis-retinal reduces constitutive opsin phosphorylation and improves quantum catch in retinoid-deficient mouse rod photoreceptors. J. Biol. Chem. *277*, 40491–40498.

CellPress

Current Biology

Supplemental Information

Restoration of Vision with Ectopic Expression of Human Rod Opsin

Jasmina Cehajic-Kapetanovic, Cyril Eleftheriou, Annette E. Allen, Nina Milosavljevic, Abigail Pienaar, Robert Bedford, Katherine E. Davis, Paul N. Bishop, and Robert J. Lucas

Figure S1

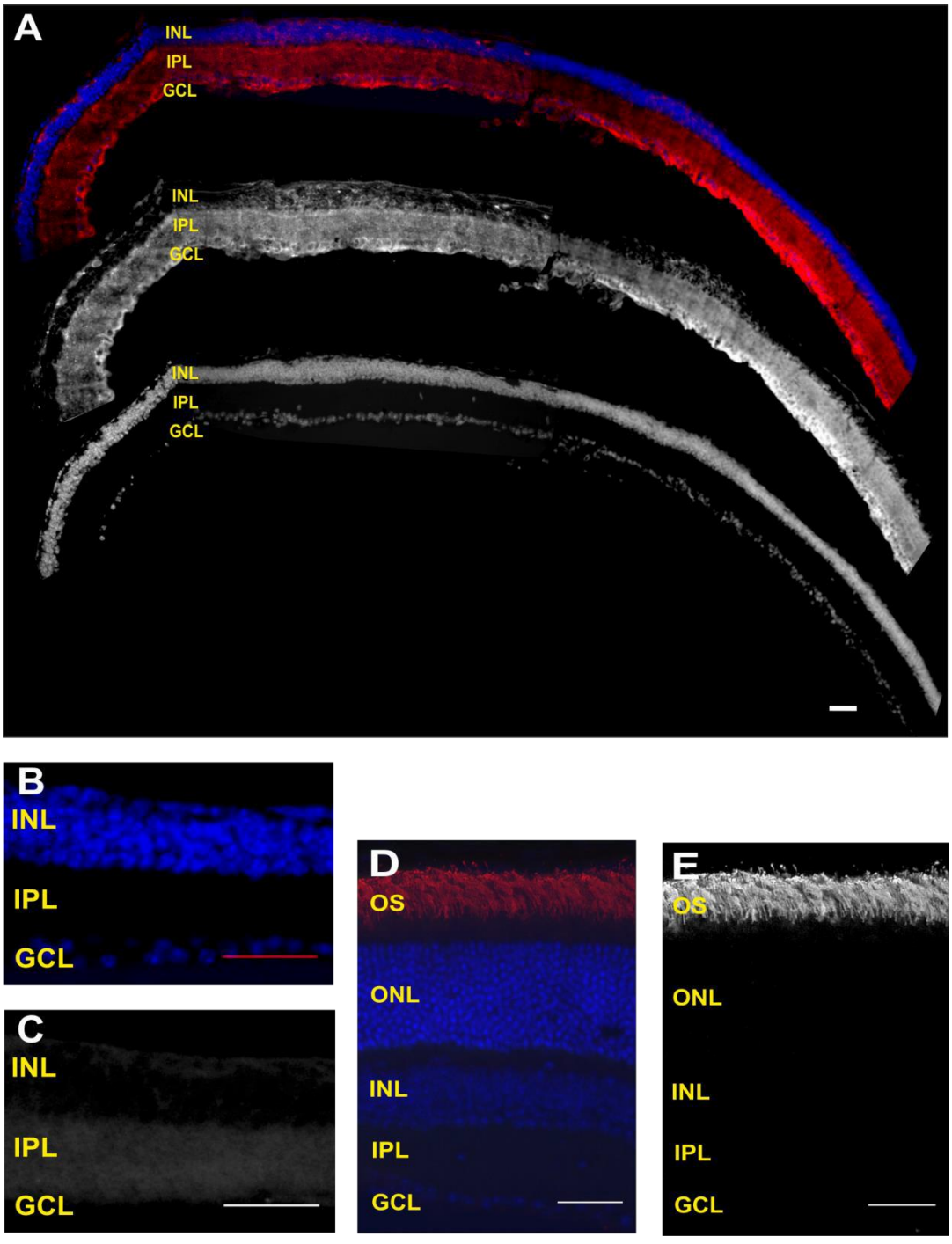
A
INL
IPL
GCL
INL
IPL
GCL
INL
IPL
GCL
B
INL
IPL
GCL
C
INL
IPL
GCL
D
OS
ONL
INL
IPL
GCL
E
OS
ONL
INL
IPL
GCL

Figure S2

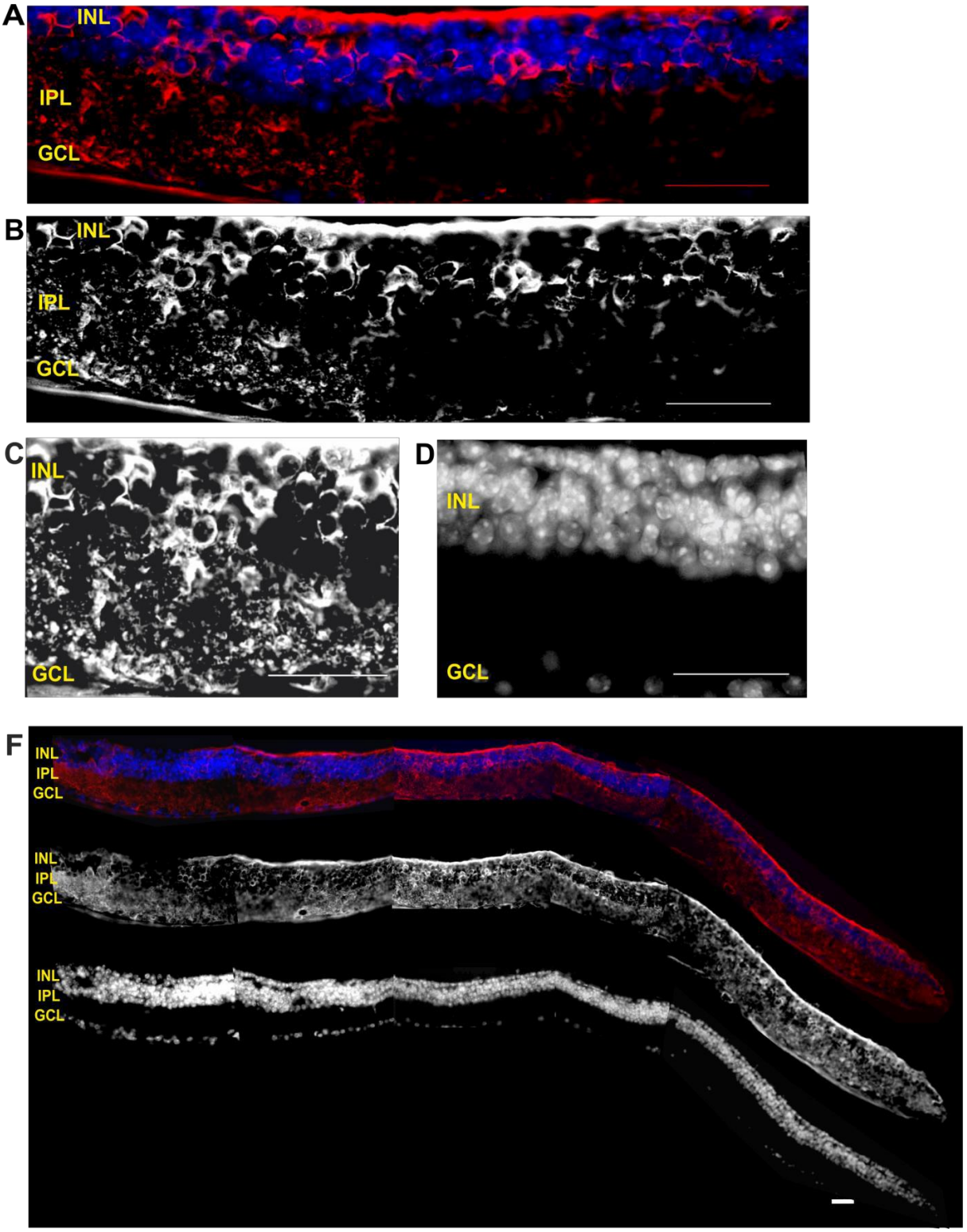
A
INL
IPL
GCL
B
INL
IPL
GCL
C
INL
GCL
D
INL
GCL
F
INL
IPL
GCL
INL
IPL
GCL
INL
IPL
GCL

Figure S3

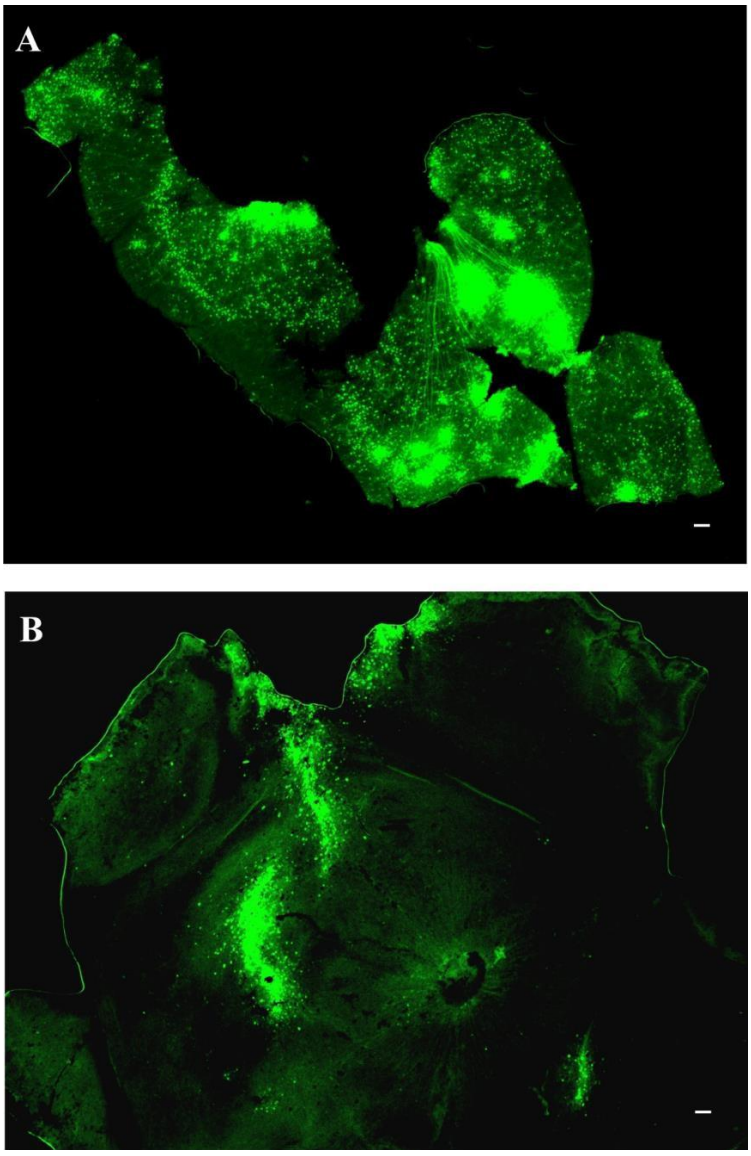

Figure S4

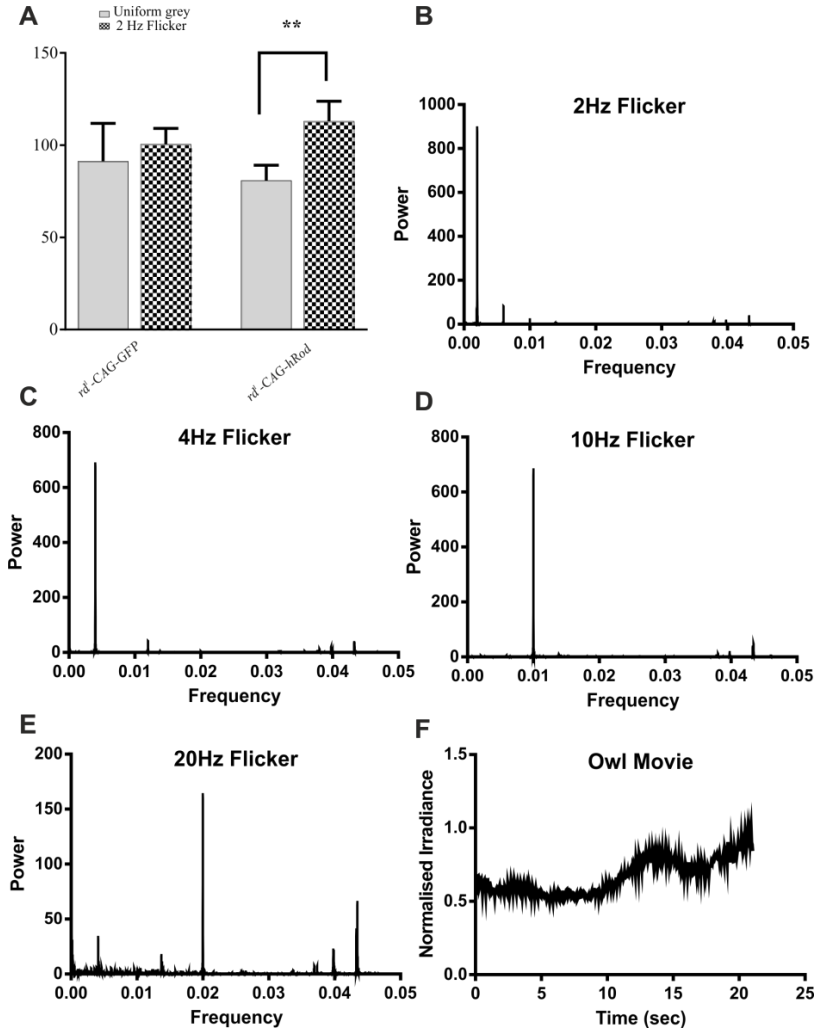
A
Uniform grey
2 Hz Flicker
**
150
100
50
0
rd-CAG-GFP
rd-CAG-hRod
B
2Hz Flicker
Power
1000
800
600
400
200
0
0.00
0.01
0.02
0.03
0.04
0.05
Frequency
C
4Hz Flicker
Power
800
600
400
200
0
0.00
0.01
0.02
0.03
0.04
0.05
Frequency
D
10Hz Flicker
Power
800
600
400
200
0
0.00
0.01
0.02
0.03
0.04
0.05
Frequency
E
20Hz Flicker
Power
200
150
100
50
0
0.00
0.01
0.02
0.03
0.04
0.05
Frequency
F
Owl Movie
Normalised Irradiance
1.5
1.0
0.5
0.0
0
5
10
15
20
25
Time (sec)

Figure S1. Rod opsin expression in *rd*^{1} retinas using a non-selective (CAG) promoter and control *rd*^{1} and *wild-type* stains. Relating to Figure 1.
(A) Exemplar images of a section through an *rd*^{1} mouse retina >4 months after intravitreal delivery of AAV2/2-CAG-*RHO* in conjunction with glycosidic enzymes. Uneven density of rod opsin expression is shown after staining with α-hRho antibody (upper image in red; middle image in white, a monochrome version of antibody staining). Nuclei are stained with DAPI (upper image in blue; lower monochrome image in white). Note that this impression of staining across a retinal section was produced by splicing together several high magnification images of smaller portions of the retina. (B to E) images of sections through PBS injected *rd*^{1} (B and C) and *wild-type* (D and E) mouse retina showing no staining (B and C) and photoreceptor outer segment (OS) staining (D and E) after treatment with α-hRho antibody; nuclei are stained with DAPI (blue); C and E are monochrome versions of α-hRho antibody staining in (B) and (D) respectively; nuclei are stained with DAPI (blue). INL – inner nuclear layer, IPL- inner plexiform layer, GCL – ganglion cell layer, ONL – outer nuclear layer. CAG - a hybrid CMV enhancer/chickenβ-actin promoter. *RHO* - human rod opsin coding sequence. Calibration bar = 50μm.

Figure S2. Rod opsin expression in *rd*^{1} retina using an ON-bipolar specific (grm6) promoter. Relating to Figure 3.
(A) A longer section of the retina presented in Figure 3B >4 months after intravitreal delivery of AAV2/2-grm6-*RHO* in conjunction with glycosidic enzymes showing the extent of rod opsin expression in cells of the inner nuclear layer (INL) and processes in the inner plexiform layer (IPL) after staining (red) with an α-hRho antibody and counterstaining of nuclei with DAPI (blue). (B) A monochrome version of α-hRho antibody staining in (A) clearly depicting rod opsin expression in white. (C) A monochrome version of α-hRho antibody staining in Figure 3B showing a cluster of moderately high rod opsin expression (white). (D) A monochrome version of DAPI staining in Figure 3B. (F) Exemplar images of a section through an *rd*^{1} mouse retina >4 months after intravitreal delivery of AAV2/2-grm6-hRho in conjunction with glycosidic enzymes. Uneven density of rod opsin expression is shown after staining with α-hRho antibody (upper image in red) and (middle image in white, a monochrome version of antibody staining). Nuclei are stained with DAPI (upper image in blue and lower monochrome image in white). Note that this impression of staining across a retinal section was produced by splicing together several high magnification images of smaller portions of the retina. GCL - ganglion cell layer. grm6 - ON bipolar cell specific promoter. *RHO* - human rod opsin coding sequence. Calibration bar = 50μm.

Figure S3. GFP localisation in whole mount *rd*^{1} retinas following intravitreal injection of AAV2 driving transgene expression under a non-selective (CAG) promoter or an ON-bipolar specific (grm6) promoter. Relating to Figure 1 and Figure 3. Retinal wholemounts in both A (using a non-selective (CAG) promoter) and B (using an ON-bipolar specific (grm6) promoter) depict uneven expression of a marker (GFP) driven by these promoters. Transduced cells are shown in green. Calibration bar = 50μm.

Figure S4. Behavioural activity in treated and control *rd*^{1} mice in response to 2Hz flicker and visual stimuli used for behavioural experiments. Relating to Figure 4 and Figure 5. (A) Histogram of activity for *rd*^{1}-CAG-GFP (n = 6) and *rd*^{1}-CAG-*RHO* (n = 6) mice showing

distance travelled in an open field box 30s before (grey bars) and 30s after (chequered bars) presentation of a 2Hz full field flicker. Activity is represented by mean±SEM of the mean distance travelled by each animal in a 30-sec time bin; time in minutes since introduction to testing arena. Two tailed paired t-tests comparing activity before and after stimulus appearance (**$p < 0.01$). CAG - a hybrid CMV enhancer/chickenβ-actin promoter. *RHO* - human rod opsin coding sequence. (B-F) Flicker and naturalistic movie stimuli were generated using standard LCD monitors. To assess the characteristics of these stimuli we measured irradiance with a photodiode (Advanced Photonix SLD-70 BG2A) connected to a 10-bit analog-to-digital converter of a microcontroller board (Arduino UNO). The sampling rate of acquisition was 100 Hz. The power spectrum graphs show frequency in kHz and power in arbitrary unit. B-E show power spectrum analyses for irradiance traces at 2, 4, 10 and 20Hz. Note the contamination of lower frequency components at 20Hz (as we approach the limit of hardware performance) but not other frequencies. F shows the change in irradiance (normalised to max=1) over the course of a single repeat of the swooping owl movie.

Supplemental Experimental Procedures

Gene delivery via AAV

AAV vector was administered via intravitreal injection in isofluorane anaesthetised mice aged 8 to 10 weeks. Prior to injections, pupils were dilated with tropicamide and phenylephrine. A custom made ultra-fine needle (Hamilton RN needle 34 gauge, supplied by ESSLAB) was attached to a 5µl Hamilton glass syringe and was passed at 45 degrees through the pars plana into the vitreous cavity, carefully avoiding the lens and blood vessels. The injection was performed under a direct visualisation of the needle tip through cover-slipped eyes under an operating microscope (Microscopes Inc., USA). The vectors, rAAV serotype 2 (rAAV2/2, or simply AAV2) expressing rod opsin or GFP under the control of a strong ubiquitous pan-neuronal promoter (CAG) or ON-bipolar cell specific (grm6) promoter were obtained from Vector Biolabs, Philadelphia, USA. The CAG promoter is a fusion of CMV early enhancer and chicken β-actin promoter. The grm6 promoter is a fusion of 200-base pair enhancer sequence of the mouse grm6 gene encoding for ON-bipolar cell specific metabotropic glutamate receptor, mGluR6, and an SV40 eukaryotic promoter. The gene of interest in each case was flanked by inverted terminal repeat (ITR) domains and stabilised by polyadenylation signal sequence (polyA) and a woodchuck hepatitis posttranscriptional regulatory element (WPRE).

Each eye was injected with 3µl virus ($1x10^{13}$ genomic counts) containing either a rod opsin (AAV2-ITR-CAG-*RHO*-polyA-WPRE-ITR for untargeted expression or AAV2-ITR-grm6-*RHO*-polyA-WPRE-ITR for targeted expression) or GFP (AAV2-ITR-CAG-GFP-polyA-WPRE-ITR for untargeted expression or AAV2-ITR-grm6-GFP-polyA-WPRE-ITR for targeted expression) expression construct, in combination with 0.5µl of glycosidic enzyme solution containing 0.125 units each of heparinise III and hyaluronan lyase (E.C. 4.2.2.8 & E.C. 4.2.2.1; Sigma-Aldrich, Dorset, UK). The enzyme solutions were made fresh on the day of injection by dissolving the enzymes in sterile phosphate-buffered saline (PBS). The vector and enzymes were mixed in a syringe immediately before an eye injection and were given in a single combined injection.

Histology

Retrieved eyecups (>6 weeks post vector injection) were fixed in 4% paraformaldehyde (PFA) for 24 hours at 4^{o} C. The tissue was then washed in PBS and further fixed in 30% sucrose in PBS overnight at 4^{o} C. Fixed eyes were cryo-protected in optimal-cutting temperature medium (Raymond A Lamb Ltd., Eastbourne, UK) and frozen at -80^{o} C until further processing. Cryo-protected retinal section were sectioned on a cryostat (Leica, Microsystems) horizontally through the eyecup at 8-10µm thickness from ventral to dorsal side, so that each section contained a complete nasal to temporal cross-section of the retina. Ten-twelve sections were collected on each slide containing sections representative of the entire retina. Slides were stored at -80^{o} C.

For immunohistochemistry, slides were removed from the freezer and allowed to air-dry at room temperature for 1 hour. Sections were permeabilised by immersing slides in PBS with 0.2% Triton for 20 minutes at room temperature. Following this sections were background blocked with PBS with 0.2% Triton X-100 containing 10% donkey serum (D9663; Sigma, UK) for 1 hour at room temperature. Primary antibody (Rabbit Anti-Human Rhodopsin, Abcam, Ab112576) was applied at 1:200 dilution in blocking buffer (PBS with 0.2% Triton X-100 and 2.5% donkey serum) for 3 hours at room temperature. After washing in tween 0.05% PBS, four times for 10 minutes, sections were incubated with secondary antibody (Alexa Fluor® 546 Donkey Anti-Rabbit IgG (H+L) Antibody, Life technologies, lot: 1504518) diluted 1:200 in PBS with 0.2% Triton X-100 and 2.5% donkey serum for 2 hours at room temperature. Slides were then washed four times for 10 minutes in 0.05% tween PBS followed by one final wash with dH_20. After removing excess fluid, slides were mounted with fluorescent mounting media containing DAPI (Vectashield, Vector Laboratories Ltd., Peterborough, UK) to stain cell nuclei. For bio-imaging, sections were analysed under an Olympus BX51 upright microscope using x4, x10 and x20 Plan Fln objectives and captured using a Coolsnap ES camera (Photometrics, Tucson, AZ) through MetaVue Software (Molecular Devices Ltd. Wokingham, UK). Images were taken under specific band pass filter sets and colour-combined images were used for further processing using ImageJ.

Multi-electrode array recordings

Enucleated eyes were placed in a petri dish filled with carboxygenated (95% CO2/5%CO2) aCSF (artificial cerebro-spinal fluid, concentration in mM: 118 NaCl, 25 NaHCO3, 1 NaH2PO4, 3 KCl, 1 MgCl2, 2 CaCl2, 10 C6H12O6, 0.5 L-Glutamine). Retinas were then carefully isolated in diffuse red light under a dissecting microscope and mounted, ganglion cell side down, onto a 60- or 256-channel multi-electrode array (Multi Channel Systems, Reutlingen, Germany). Retinal explants were coupled in place with a weighted dialysis membrane, and continuously perfused with carboxygenated aCSF at 2.2 ml per minute using a peristaltic pump (SCI400, Watson Marlow, UK), and maintained at 32˚C using a Universal Serial Bus temperature controller regulating an inline heater for the inflow of aCSF. Light stimuli (white light) were presented by a customised light engine source (Lumencor, USA or Thorlab LEDs). At brightest intensity (ND0) LEDs were $1x10^{15}$ total photons/cm^2/s for Lumencore and $8x10^{14}$ total photons/cm^2/s for Thorlab LEDs. Arduino Due card (Italy) controlled by programmes written in LabVIEW (Version 8.6, National Instruments, TX, USA) was used to control stimulus duration and intensity by altering LED output and adjusting filter wheel containing neutral-density filters (ThorLabs, UK) which reduce the intensity by x10. Stimuli were delivered at 2-second pulses of light (20s inter-stimulus interval) for 20-30 repeats at ND0, ND1 (10x dimmer) and ND2 (100x dimmer). Data were sampled at 25 kHz during the acquisition of both spontaneous and evoked activity and recorded for off-line sorting using Offline Sorter (Plexon). After removing clear

artifacts common to all channels, principal component analyses were used to discriminate single units, identified as distinct clusters of spikes within the principal component space, with a clear refractory period in the interspike interval distribution. Spike-sorted, single-unit data were then further analysed using Neuroexplorer (Nex Technologies) and MATLAB R2010a (The Mathworks Inc.).

In-vivo electrophysiology

Recordings were performed on two groups of *rd*[1] mice: group 1 (n = 7), one eye injected with AAV2-CAG-*RHO* and the other with AAV2-CAG-GFP; and group 2 (n = 5), one eye injected with AAV2-grm6-*RHO* and the other with AAV2-grm6-GFP. Mice were anaesthetised with urethane (intraperitoneal injection 1.55g/kg; 20% w/v; Sigma Aldrich, Poole, UK), ketamine and xylazine (100mg/kg ketamine and 10mg/kg xylazine; intraperitoneally) or isofluorane (initial dose of 2-3% and maintenance dose of 0.6-1.0% administered via a nose cone; GM-4, Narishige, Japan). Animals were mounted in a stereotaxic frame (SR-15M; Narishige International Ltd, London, UK) and core body temperature was maintained at 37 °C via a homeothermic heat mat (Harvard Apparatus, Edenbridge, UK). Pupils were dilated with atropine and mineral oil (Sigma Aldrich) was applied to retain corneal moisture. A small craniotomy and durotomy (~1 mm^2) was performed directly above each lateral geniculate nucleus (LGN) using stereotaxic coordinates according to mouse atlas (Paxinos and Franklin, 2001; hole centre= bregma: −2.46 mm; midline: −2.8). A 32-channel electrode (NeuroNexus Technologies Inc., MI, USA) was introduced to each LGN in the centre of the hole (medial shank: -2.5 mm relative to midline; depth: −2.6 mm relative to brain surface at 18 degrees angle) for simultaneous recording from both LGNs. A second recording was performed where electrodes were re-positioned and advanced 250µm dorsally with respect to bregma (at -2.71mm). Following electrode insertion mice were dark adapted for 30 minutes to allow neuronal activity to stabilize. Data were acquired using a Recorder64 system (Plexon, TX, USA) with signal amplification by a 20x gain AC-coupled head stage (Plexon, TX) followed by preamplifier conditioning providing a total gain of 3500x. Data were high-pass (300Hz) filtered and time-stamped neural waveforms were digitized simultaneously from all channels at a rate of 40 kHz. Multiunit data was then stored for offline sorting and analysis as for the MEA data described above. To confirm the location of recording sites, the recording electrode was dipped in fluorescent dye (Cell Tracker CM-DiI; Invitrogen) prior to insertion into the brain. After in-vivo recordings, the mouse's brain was removed and post-fixed overnight in 4% paraformaldehyde, prior to cryoprotection for 24 hours in 30% sucrose. 100µm coronal sections were then cut using a sledge microtome, mounted onto glass slides and cover slipped using Vectashield (Vector Laboratories, Inc.).

Visual stimuli

Visual stimuli were provided by LEDs (Thorlab λmax: 410 nm) and delivered via fiber optic to purpose-made eye cones tightly positioned onto each eye to minimise any potential light leak. A National Instruments card (USB-6229) controlled by programmes written in LabVIEW (Version 8.6, National Instruments, TX, USA) was used to control stimulus duration and intensity by altering LED output and adjusting filter wheel containing neutral-density (ND) filters (ThorLabs, UK). At brightest intensity (ND0) LEDs gave a corneal irradiance of 47 W/m^2 or $4x10^{15}$ of effective flux for rod opsin; estimated retinal irradiance is $8x10^{13}$ log photons/cm^2/s based upon the method [S1]. Light was measured using a spectroradiometer (Bentham Instruments Ltd., UK or Cambridge Research Systems Ltd., UK), which measured the relative power in mW/cm^2 at

wavelengths between 350-700nm. The effective quantal flux (in photons/cm^2/s) for each opsin was then estimated by weighting spectral irradiance according to pigment spectral efficiency using the formula: effective photon flux = $\int P(\lambda).s(\lambda).l(\lambda)d\lambda$ where $P(\lambda)$ is spectral irradiance in photons/cm^2/s/nm; $s(\lambda)$ is pigment spectral sensitivity approximated by the Govardovskii visual template [S2]; and $l(\lambda)$ is mouse lens transmission as measured by Jacobs and Williams [S3].

Light flashes were delivered according to a light protocol consisting of 2 parts. Part 1 included flashes from darkness: 2s light ON, 20s light OFF with 10s offset between each eye. This paradigm was repeated at least 10x at each ND filter. Retinal irradiance ranged from $8x10^{11}$ photons/cm^2/s at ND2 to $8x10^{13}$ photons/cm^2/s at ND0. Part 2 of the light protocol involved recording in light adapted conditions where 5-second steps of light were applied to a steady background illumination at Michelson contrast of 96%. There was a 20-second inter-stimulus interval and a 10-second offset between two eyes. This paradigm was repeated ten times.
Naturalistic movies were presented with a digital mirror device projector (DLP® LightCommanderTM; Logic PD Inc.), whose intrinsic light engine had been replaced with our own multispectral LED light source containing four independently controlled LEDs (λ_{max} at 405nm, 455nm, 525nm and 630nm; Phlatlight PT-120 Series (Luminus Devices). Light from the LEDs was combined by a series of dichroic mirrors (ThorLabs), and directed onto the mirror device. The movie was presented using Python running PsychoPy Version 1.70.00 software. It featured mice moving around a behavioural arena including movement and looming of different sized objects (subtending visual angles ranging from 0.5° to 36°) at a range of orientations, speeds and contrasts (maximum Michelson contrast at 96%). The movie was presented at irradiance 0.81 W/m^2 with estimated retinal irradiance of $1x10^{13}$ rod equivalent photons/cm^2/s). The movie lacked differences in colour, and changes in irradiance across time were minimal (standard deviation of irradiance = 5.94%). Previous validations in *wild-type* mice have shown undetectable responses for presentations of de-focussed versions, indicating that most activity was elicited by changes in spatial patterns and object motion.

Behaviour
The modified light/dark box (dimensions: length=40cm width=40cm and height=30cm, open top) was made of Perspex and its walls painted white except for the two long sides of each arena, which were kept clear. Two identical infra-red lamps were placed centrally above each arena, to allow visualisation under dark conditions.
The visual stimuli were displayed from two 17-inch flat screen computer monitors (Acer V173b or Dell E173FP and ViewSonic matched for power by adjusting screen brightness) facing clear walls of each arena, using a DualHead2Go Digital Edition external multi-display adapter (Matrox Graphics Inc.). A variety of visual stimuli were generated using a custom written program and displayed on one monitor at a time. Stimuli included switching from 'black' (minimum brightness) to 'white', from steady grey to full screen flicker (Figure S4B to S4E) or square-wave gratings without an associated change in irradiance. The stimuli were presented when the mouse was in the middle of one half of the arena and the spatial frequency of gratings are reported for this viewing distance. Spatial frequency would become lower (by up to 2x) if the mouse moved towards the monitor and higher if it moved away. In addition a natural movie (colour rendition of an owl swooping in slow motion Figure S4F) was presented. Light intensity from 400-700nm was measured using a spectroradiometer (Bentham Instruments Ltd., UK or Cambridge Research Systems Ltd., UK). For full screen modulations, corneal irradiance for a

mouse looking directly at the screen was measured (for ease of comparison with other studies) by using a cosine diffuser light placed in the appropriate location in the arena.
Before the experimental period, mice were handled and habituated to their novel environment over 5 days, at the same time each day, by leaving them in the experimental box with their cagemates for 30 min. Following the habituation period, behaviour experiments were conducted over several weeks at the same time each day. Each group of mice was allowed to undergo only one testing condition per day. On each test day, mice were brought into the testing room in their home cages, allowed to accommodate to the testing room conditions for 30 minutes and then each mouse was tested individually. Mice were placed into the open field box (randomly to east or west half) and allowed to move freely between two arenas. All test trials were recorded under infra-red conditions through a camcorder fitted with an infra-red filter (λ=665nm). The box was thoroughly cleaned with 70% ethanol after each test trial and allowed to air-dry before next mouse was placed into the box.
A recording trial began after 3 minutes of habituation. Each trial run consisted of 5 minutes of control stimulus, following which a test stimulus was presented on a screen facing an arena that contained a mouse at this time point. The recorded trials were stored for off-line analysis using a video tracking software device (EthoVision® XT 10.1 Noldus, Tracksys Ltd., UK). We analysed distance travelled by each mouse in the entire box and outputted results in 30 second bins. The mouse's ability to detect the visual stimuli was assessed as a change in distance travelled in the 30s either side of test stimulus appearance. As we had no strong *a priori* expectation that stimuli would increase vs. decrease activity, we used a two-tailed paired *t* test to detect changes in locomotion. To account for habituation to the novel stimulus, we tested for statistically significant response across the group of treated mice in a single presentation for most tests here. The exception was the drifting grating, in which we explored the robustness of responses over repeated presentations in *wild-type* and *rd*^{1} (treated and control) mice. We found that responses were retained over multiple presentations, but that high repeat numbers did not necessarily maximise the likelihood of detecting small effect sizes, as mouse behaviour appeared to change as they became increasingly accustomed to the task. Thus, e.g. we found that baseline activity progressively increased in both *rd*^{1}-grm6-*RHO* and *rd*^{1}-grm6-GFP animals and the magnitude of increases in activity decreased beyond 10 repeats (data not shown).

Supplemental references

S1. Lyubarsky, A.L., Daniele, L.L., and Pugh, E.N., Jr. (2004). From candelas to photoisomerizations in the mouse eye by rhodopsin bleaching in situ and the light-rearing dependence of the major components of the mouse ERG. Vision Res *44*, 3235-3251.

S2. Govardovskii, V.I., Fyhrquist, N., Reuter, T., Kuzmin, D.G., and Donner, K. (2000). In search of the visual pigment template. Vis Neurosci *17*, 509-528.

S3. Jacobs, G.H., and Williams, G.A. (2007). Contributions of the mouse UV photopigment to the ERG and to vision. Doc Ophthalmol *115*, 137-144.

Chapter 6: Discussion

6.1. Summary of main findings

The ultimate aim of the research has been to restore vision using human opsins. Specifically the first aim has been to optimise and evaluate safety of AAV2 based gene delivery to the retina following intravitreal injection with glycosidic enzymes. The second aim was to investigate whether retinal transduction with the optimised vector delivery system carrying melanopsin or rod opsin can restore visual function in mice with an advanced retinal degeneration. We hypothesised the both melanopsin and rod opsin, native human G-protein coupled receptors can restore optogenetic visual responses in retinal degeneration with enhanced sensitivity compared to current optogenetic tools. Furthermore, we hypothesised that optogenetic targeting of one specific retinal cell type, the ON bipolar cell, would improve the quality of recreated vision compared to non-specific targeting of all surviving cells in the degenerate retina.

We identified a combination of AAV2 vector and extracellular matrix degrading enzymes, heparinase III and hyaluronan lyase, which allowed us to achieve sufficient retinal transduction via intravitreal route necessary for restoration of photoreceptive function. In addition, assays of retinal function have shown that this treatment is safe up to at least 12 months post treatment. Next, we have shown that both melanopsin and rod opsin, when expressed ectopically, outside their native retinal cells, can restore visual function in a mouse model of advanced retinal degeneration with much higher sensitivity than current optogenetic strategies. Furthermore, due to its faster kinetics, rod opsin has been able to recreate a more diverse, higher quality, set of visual responses compared with melanopsin. Indeed, mice with rod opsin expression driven by ON bipolar specific promoter were able to use this recreated visual code to display behavioural responses to spatial stimuli, flicker and natural scenes.

An array of experimental techniques was employed in this thesis but what sets this work apart from many other studies, are two techniques in particular: *in vivo* LGN recordings and the novel behavioural paradigm. By directly assaying the light-evoked activity within the LGN, we have gained a much greater insight into the response

properties of optogenetically driven responses. In addition, we developed a novel behavioural paradigm that successfully assayed the efficacy and quality of restored vision in a simple, stress-free and high-throughput test.

Collectively, these data revealed that virally mediated ectopic expression of human rod opsin can restore vision under natural viewing conditions and at moderate light intensities. This was the first time that anyone has been able to restore visual responses with appropriate timing and sensitivity in any model of retinal degeneration. The inherent advantages in employing a human protein, the simplicity of this intervention, and the quality of vision restored, all suggest that this type of approach has the potential to restore vision in patients with advanced IRDs and that it should be evaluated in clinical trials.

A discussion follows on a few key areas that have emerged from the results as well as on ideas for future directions.

6.2. Why intravitreal gene therapy?

To be successful, gene therapy requires efficient, specific and widely distributed transduction of target cells. In the retina, this is by large determined by the route of vector administration, the AAV capsid serotype and titre used. The two main vector delivery approaches in the eye are subretinal and intravitreal injections (Figure 6.1). In the current climate of growing experience in vitreo-retinal surgery, the subretinal injection is a procedure of choice for retinal gene therapy (Bainbridge et al., 2008; Maguire et al., 2008; Hauswirth et al., 2008; MacLaren et al., 2014). To date, this is the most efficient method of targeting RPE and PR cells, which are affected in retinal degenerations. However, intravitreal approach would be greatly preferred on several accounts.

First, subretinal administration is technically more challenging and associated with greater surgical morbidity then intravitreal injections. The subretinal route deposits the vector solution in a virtual space created between the RPE and the neurosensory retina, called the subretinal space. This detachment of photoreceptors from the RPE or 'bleb' is temporary (usually flattens after few days following vector diffusion) but can be damaging to the retina. Furthermore, before the bleb can be induced, surgeons need to perform a vitrectomy (in humans and large animals) to provide access to the subretinal space and prevent excessive intraocular pressure rise following subretinal injection. In small animals surgical vitrectomy is impossible to perform, so injections are given into intact eyeballs with additional technical difficulties.

In both cases, retinal detachment can cause retinal holes and intraocular haemorrhage with often, irreversible damage. This is especially true in degenerating retina, which is often extremely thin and fragile. Indeed, the latest communications on gene therapy human trials report adverse effects as a direct consequence of detachment of neurosensory retina (including foveal thinning and reduction in visual acuity) in some participants after subfoveal delivery of the AAV vector (Bainbridge et al., 2015; Jacobson et al., 2012). In addition, retinal remodelling associated with degeneration activates Muller glia and their distal processes form a scar that isolates the retina from the subretinal space (Jones and Marc, 2005). Thus, subretinal treatments that occur after Muller seal formation must involve traumatic surgical detachment of the glial seal. Thus, in clinical setting in particular, the ability to target photoreceptors from the vitreous would be extremely beneficial.

The other route for vector delivery, the intravitreal route, deposits the vector into the vitreous cavity. The intravitreal injection is increasingly becoming a routine clinical practice, especially in recent years with the advent of anti-angiogenic macular therapies. This approach is less technically challenging, does not require retinal detachment or vitrectomy and has a much lower risk of surgical complications. This is particularly relevant when both eyes require treatment. Hence, this approach is suitable for repeated, bilateral injections, which might be necessary for long-term

efficacy as well as allowing for combined delivery of other pharmaco-therapeutic agents.

Another advantage of the intravitreal route over subretinal injections is that it allows for greater volumes of vector solution to be used per injection with potentially more homogenous vector distribution. Unlike with subretinal approach, vector transduction from the vitreous is not limited to the outer retinal cells in a localized area under the 'bleb' and could potentially lead to pan-retinal transduction of inner and outer retina, broadening its therapeutic potential. In fact, evidence that non–cell-autonomous mechanisms can contribute to retinal cell death (Kedzierski et al., 1998) indicates that widespread transduction of viable retina may enhance protection against degeneration.

However, one of the greatest challenges in current AAV-mediated gene therapy research is to achieve an efficient transduction of inner or indeed outer retinal cells using intravitreal injections, and has been a subject of a number of recent pre-clinical studies (reviewed in Boye et al., 2013). Several AAV variants have emerged from these studies with enhanced transduction properties, some of which are able to target the photoreceptors in the outer retina (Hellstorm et al., 2009; Petrs-Silva et al., 2009; Klimczak et al., 2009; Dalkara et al., 2013). However, the processes by which these vectors are being developed, rational mutagenesis and directed evolution, are costly and time consuming. In addition, the new variants are species specific, i.e. a variant that has been developed via *in vivo* directed evolution in a mouse, worked well in this model, but demonstrated very limited transduction properties in the primate retina (Dalkara et al., 2009).

A further limitation of an intravitreal injection is that it is more likely to induce a self-limiting immune response than a subretinal injection (Maclachlan et al., 2011). In addition, the likely increased amount of AAV required in the human eye following intravitreal delivery may result in even greater immune responses than those arising from subretinal approach. A recent report on one of the current clinical trials shows evidence of immune responses with high AAV loads (Bainbridge et al., 2015).

Our approach to overcome this barrier was to use extracellular matrix degrading enzymes, the glycosidic enzymes, in conjunction with naturally occurring AAV2 vector as described in Chapter 3. Indeed, we have shown that a combination of heparinase III and hyaluronan lyase produced the greatest enhancement of gene delivery to the neurosensory retina in both healthy wild-type eyes and eyes with an advanced retinal degeneration. It is likely, that the enzymatic lysis of these extracellular barriers increases the size of matrix pores and/or affects cell-surface interactions to promote the AAV to move into and across the retina with more ease. Short and long-term safety studies indicated that retinal function was unaffected by these enzymes, confirming the value of this simple, species-independent approach in experimental models of retinal degenerations and potentially allowing the development of intravitreal injection of gene therapy vectors for clinical applications. Perhaps yet further improvements in retinal transduction could be made by combining engineered vectors with these glycosidic enzymes. However, further rigorous safety studies are needed to develop this enzyme-based intravitreal therapy for clinical use.

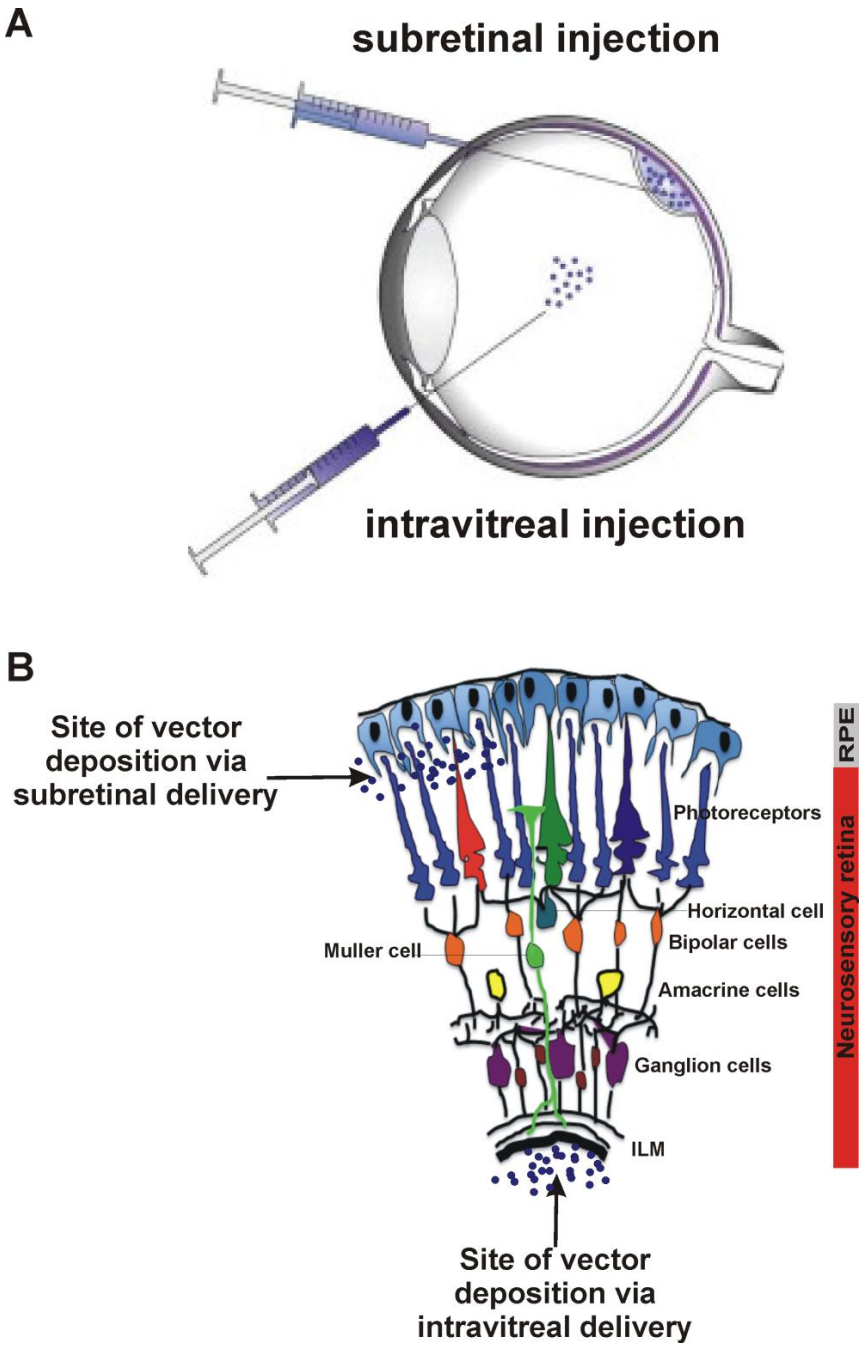

Figure 6.1. Routes of vector delivery to the retina. (A) Subretinal administration creates a temporary separation bleb between the neurosensory retina and the RPE, providing gene delivery to cells in this localized area, the photoreceptor and RPE cells. Intravitreal administration of naturally occurring vectors targets inner retinal cells but could potentially result in diffuse retinal transduction across the retinal layers. (B) Schematic of the retina in cross section showing the major cell layers and the sites of delivery for viral vectors. ILM – internal limiting membrane, RPE – retinal pigment epithelium (A, adapted from Dalkara et al., 2014).

6.3. Which cell to target?

The retina has significant computational ability and can simultaneously extract several different visual features from the natural movie projected to its photoreceptors (Gollisch and Meister, 2010). A key element of retinal computation is the divergence of signals, at the bipolar cell level, into two parallel pathways: ON and OFF, activated by increments or decrements in light respectively. In addition, horizontal cells interact with photoreceptors leading to lateral inhibition and excitatory bipolar and ganglion cells interact with inhibitory amacrine cells leading to selective responses to e.g. direction of motion, blue versus yellow signals etc. by different types of ganglion cells. It transpires therefore that the higher upstream the cellular target, the greater the chance of preserving normal retinal computation.

In order to preserve retinal processing, optogenetic sensors must be targeted to the appropriate cells types. There are two distinct approaches to creating artificial photoreceptors and reanimating blind retinas (Figure 6.2). First, the non-specific targeting where expressing 'optogenes' to one particular cell type is not important (Figure 6.2A). This 'shot-gun' approach can be achieved using a ubiquitous promoter to drive gene expression in all surviving neurons of the degenerate retina. Indeed two pioneering optogenetic studies restored visual sensitivity to *rd1* retinas employing this approach (Bi et al., 2006) and visually guided behaviour was reported in rats (Tomita et al., 2010). In addition, non-targeted reagents are currently used in optopharmacology. It is reasoned that the natural, sophisticated processing of the retina can be sidelined and that the cortical plasticity is a powerful process allowing the brain to extract relevant features from no matter what visual information it is presented with from the retina. Thus treated subjects can relearn interpreting the interpretation of visual scenes using the new and simplified language that the reanimated retina provides.

The second approach involves cell-specific targeting of surviving retinal cells (Figure 6.2 B and C). In retinas with a specific cone sparing degeneration, despite the loss of cone outer segments, the inner segments remained electrically viable and amenable

to optogenetic reactivation. Indeed, AAV-delivery of halorhodopsin driven by a cone-specific promoter bestowed light sensitivity to the surviving cones and drove ON and OFF pathways. The light responses were transmitted to the visual cortex and the animals demonstrated optomotor behaviour (Busskamp et al., 2010).

In cases where no photoreceptors remain, the highest order surviving cell is the bipolar cell (Figure 6.2B), which is suitable for optogenetic manipulation. Indeed several studies have targeted optogenes to bipolar cells using the ON-bipolar cell-specific grm6 cell-specific promoter, either through electroporation (Lagali et al, 2008) or via AAV-systems (Doroudchi et al., 2011; Mace et al., 2015; Cronin et al., 2014). The responses observed by Lagali et al. and Doroudchi et al. were of ON type only whereas those in studies by Mace et al. and Cronin et al. were of both ON and OFF polarity. The signals were sent to the visual cortex where they induced light behavioural changes in mice. The level of transgene expression in bipolar cells seems to have been the limiting factor in both approaches. The electroporation approach (which is not compatible with clinical applications) resulted in transient, low level gene expression and although synthetically engineered vectors produced higher expression levels (Mace et al., 2015; Cronin et al., 2014; Gaub et al., 2014) and led to more diverse signals at the retinal and cortical levels no major advances in restoration of more complex spatio-temporal vision were reported. Indeed, from a translational perspective, it is clear that achieving high levels of expression in inner retinal neurons has been elusive (Yin et al., 2011) and even the 'enhanced' engineered AAVs can only transduce deeper cells in the foveal region (Dalkara et al., 2013) when delivered via the vitreous.

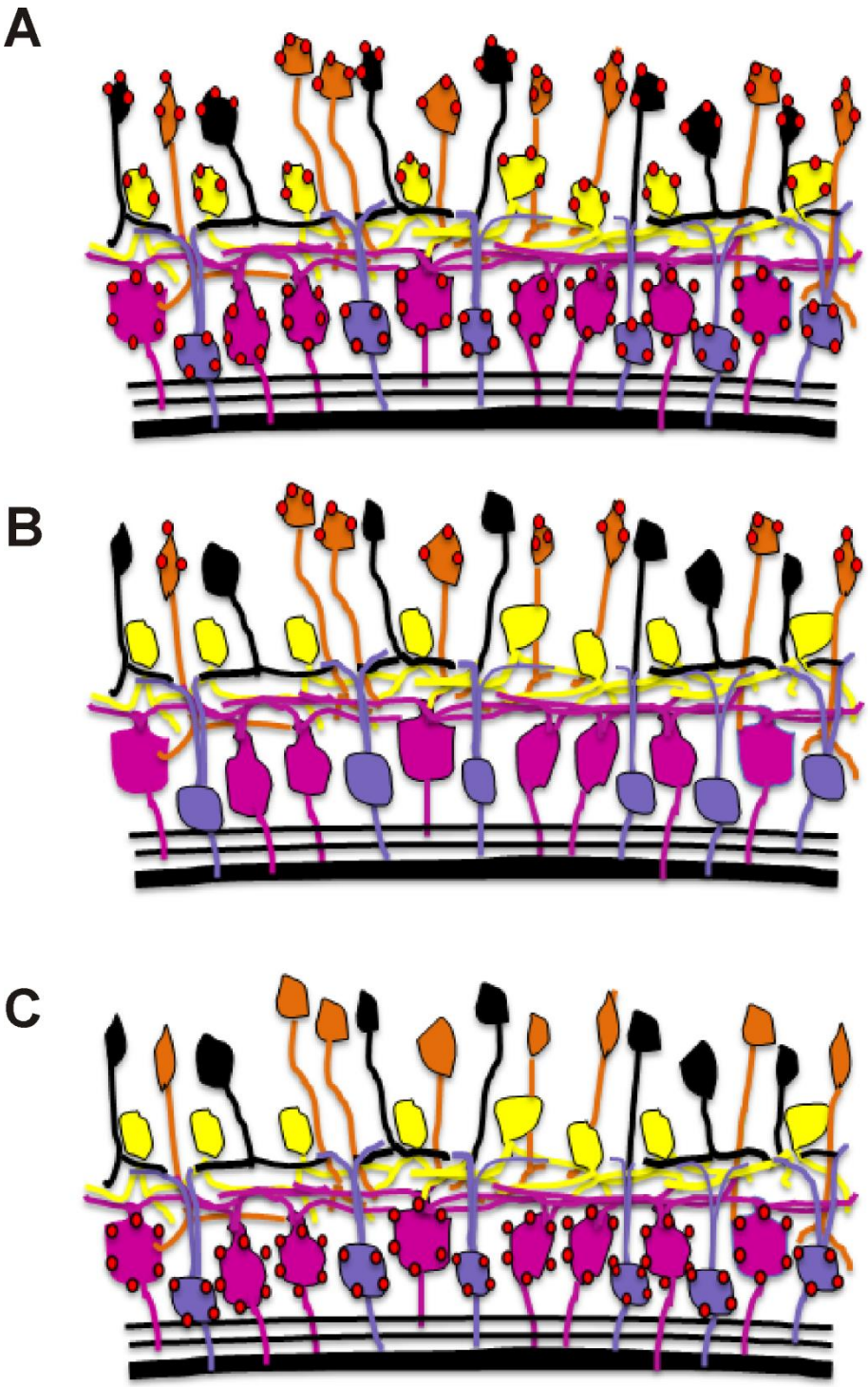

Figure 6.2. Untargeted versus targeted optogenetic approach. (A) Untargeted approach delivers optogenetic sensors to all surviving cells in the degenerating retina. (B-C) Targeted approach delivers optogenetic sensors to one specific cell type e.g. ON-bipolar cells (B) or RGCs (C). Targeting ON-bipolar cells can potentially drive all RGCs with correct polarities and waveforms, re-creating the '20-circuit mosaics' each extracting a different feature from the visual scene. Targeting RGCs directly potentially generates homogeneous waveform in all classes, which my compromise useful vision. ON-bipolar cells- orange; OFF bipolar cells – black; amacrine cells- yellow; RGCs – purple and violet; AAV-red circles.

Lastly, specific targeting of RGCs (Figure 6.2C) is more easily achievable with high levels of optogene expression from the AAV-delivery into the vitreous (Greenberg et al., 2011; Gaub et al., 2014). In addition, the RGCs are most resistant to degenerative changes and remain stable in very advanced stages of retinal degeneration (Mazzoni et al., 2008). However, being the innermost layer of cells in the retina, the sophisticated image processing mediated by retinal interneurons would be bypassed. Indeed, key elements of visual processing are not restored (ON/OFF pathways or centre-surround organisation) if RGCs are targeted specifically (Gaub et al., 2014) or via an untargeted approach (Bi et al., 2006; Greenberg et al. 2011).

In this thesis we explored both untargeted and targeted therapy. We used glycosidic enzyme enhanced intravitreal delivery of AAV2 vector with cell ubiquitous CAG promoter for non-specific cell targeting and an ON-bipolar cell-specific promoter, grm6, to successfully target rod opsin to ON-bipolar cells (Chapter 5). Interestingly, neuronal responses driven by grm6 promoter were more numerous with a greater proportion of OFF responses compared with those driven by the ubiquitous promoter. However, there were no major differences in the diversity or amplitude of the response or observed latency between the two promoters. None-the-less, behaviourally, mice treated with rod opsin driven by the grm6 promoter were able to respond to a much greater range of visual stimuli including relatively fast flickers (10 Hz, contrast, spatial stimuli and natural scenes. In contrast, mice that expressed rod opsin driven by the ubiquitous pan neuronal promoter could only detect changes in luminance and low flicker frequency (2Hz). This data lends support to the hypothesis that with untargeted expression of rod opsin, the pigment appears in cells that ordinarily would have quite different visual feature selectivity making visual information in the brain incoherent. One such confounding effect would be to simultaneously activate both excitatory ON and inhibitory OFF channels in the retina. By contrast, specific targeting of higher order surviving cells, the ON-bipolar cells, produces more coherent visual information in the brain that mice are able to 'use' to guide their behaviour.

6.4. Human opsins as optogenetic sensors: melanopsin versus rod opsin

A viable optogenetic therapy with translational potential depends on the ability of the optogenetic sensor to adequately stimulate their target cells. In order to achieve this, the sensor must be at sufficiently high concentration, photosensitivity and fast kinetics to induce phototransduction. The amount of photopigment produced by newly created inner retinal 'photoreceptors' is always going to be small compared with true rods and cones. Therefore, the efficacy of photon capture is going to be very low. For this the sensor system must ideally incorporate amplification and adaptation, or the vision will only be restored at very high light levels. In this thesis we used two human opsins for the purpose of imparting light-sensitive function to the surviving cells of the retina in a mouse model of advanced retinal degeneration. Both opsins are designed to separate the light sensing molecules from the ion channel effectors through an amplifying signalling cascade thereby allowing vision under natural light levels.

This concept is distinct from the current optogenetic approaches to vision restoration in which the light sensing molecule (such as ChR2, halorhodopsin, LiGluR and azobenzene) is also the ion channel effector. The single molecule approaches have an inherent sensitivity restriction due to the limited surface area of retinal neurons and the lack of an amplifying cascade. They therefore remain so insensitive that they require extreme non-physiological levels of light and hardware-dependent intensification. In addition ChR based systems require UV light stimulation which is clearly problematic. Our data shows that by separating the light sensor from the ion channel effector and activating an existing G-protein cascade to interconnect the two, we increase the light sensitivity by at least two-three orders of magnitude and introduce two log units of adaptation into the system (Figure 6.3). This concept is fundamentally more similar to the phototransduction cascade in photoreceptors than the 'single component' microbial opsins.

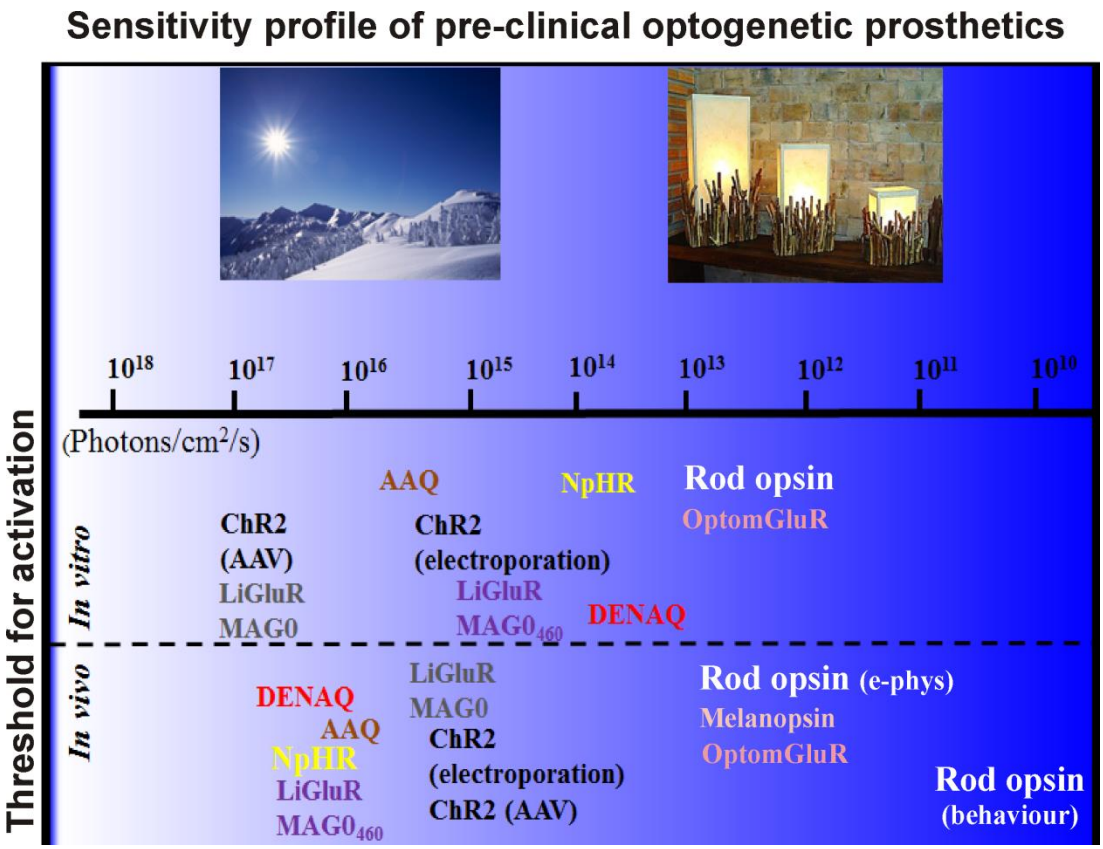

Figure 6.3. Sensitivity profile of pre-clinical optogenetic prosthetics. Values include recent work on OptomGluR (chimeric melanopsin/mGluR metabotropic glutamate receptor) and our current work on melanopsin and rod opsin.

A priori, rod opsin would seem to be poor candidate for an ideal optogenetic sensor. Its phototransduction is intrinsically tied to G-protein transducin which is not expressed at high levels outside the photoreceptors. In addition, the mechanisms evolved to rapidly terminate the light response in rod photoreceptors (rhodopsin kinase and arrestin) are not known to be present outside photoreceptors significantly slowing down the recovery from the light activated to the dark adapted state. Moreover, this visual recovery cycle requires continual chromophore replenishment from the RPE and it thought to be dependent upon the intimate contact between photoreceptors and the RPE. Inner retinal cells, even in the presence of retinal dystrophies where rods and cones have been lost, would not be physically associated with the RPE in the same way. Remarkably, we have shown that rod opsin does not bleach *in vivo* and is able to work under light adapted conditions. This proved our

hypothesis that there was enough *cis*-retinal produced by the retina for rod opsin to use. In fact in the absence of rods and cones in the degenerated retina (a natural sink for the chromophore) *cis*-retinal should be present in excess. This should further balance the RPE degeneration (often a feature of retinal dystrophies) which would reduce chromophore levels.

One potential advantage of using melanopsin or melanopsin-based systems is that the bleaching would be of low importance altogether. Melanopsin is similar to the invertebrate rhodopsin in chromophore association (and use of G_q protein signalling) and its reversal whilst bound to the opsin – 'pigment bistability'. This property makes melanopsin highly resistant to bleaching at high light intensities and allows successive light activation without response dissipation. Indeed, we have shown that when it is ectopically expressed in the surviving inner retinal cells it can drive robust light-dependent responses in the brain at physiological light levels. Importantly, it can also detect changes in luminance from background illumination. However, the latency of response (order of seconds) observed, although a significant improvement from those recorded from control *rd1* mice, may preclude melanopsin from signalling useful environmental cues. Neuronal light evoked responses driven by ectopic expression of rod opsin were similar in sensitivity to melanopsin but they were more diverse, had both ON and OFF properties, they were generally larger in amplitude and had much shorter latencies. Indeed such responses, when driven by ON-bipolar cells, were compatible with visually guided behaviour in treated mice in response to a range of artificial and natural stimuli.

A similar concept has recently been described for a chimeric melanopsin/mGluR metabotropic glutamate receptor (OptomGluR) (Van Wyk et al., 2015) with comparable sensitivity to our work with native human melanopsin and rod opsin. However, the study was undertaken in a transgenic *rd1* mouse line modified to express the pigment in all ON-bipolar cells (i.e. OptomGluR6 expressed under the full-length GRM6 promoter in *rd1*_Opto-mGluR6 knock-in founder line), preventing direct comparison with the effects of the more clinically relevant viral gene transfer

employed in this thesis. In addition, the presence of non-degenerate retina that has not undergone any remodelling further confounds comparisons of response kinetics and behavioural data with our experiments. Indeed, using a different test for visual acuity (optokinetic reflex testing) mGluR6-rescued mice achieved 0.15 cycles/degree compared to 0.04 cycles/degree achieved by rod opsin-treated mice in this work. Although developed independently, another group has shown similar sensitivity for rod opsin (Gaub et al., 2015) and detection of moving compared to static stimuli in their treated mice.

Elucidating biochemical pathways was beyond the scope of this work but one such hypothesis is that rod opsin, when expressed in ON-bipolar cells, activates a native ion channel via an amplifying signalling cascade that is triggered by an endogenous G-protein. The cascade is normally activated by glutamate release from photoreceptor cells, which activates mGluR6 in ON bipolar cells, in turn activating the ion channel TRPM1 (Figure 6.4). However, given that rod opsin normally acts through $G\alpha_{i/o}$ class G proteins one would expect its primary response to light to be hyperpolarising (the brain's equivalent of inhibiting or switching the cells OFF). Nevertheless, stimulus-induced ON excitatory responses were much more numerous than OFF inhibitory responses. Indeed, this could produce excitatory responses from RGCs if it were to reduce the activity of inhibitory amacrine-cell synapses. This proved to be the case, as application of GABA antagonists abolished most excitatory responses, which must have primarily originated with light-evoked disinhibition of RGC firing (Figure 6.5).

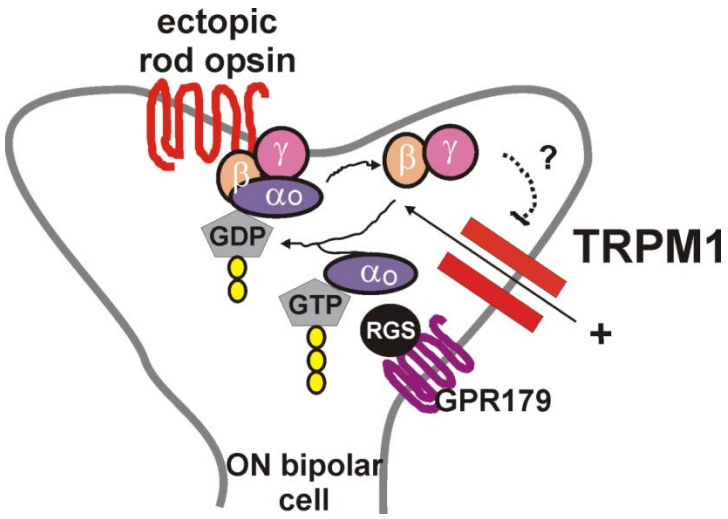

Figure 6.4. Schematic of proposed biochemical pathway of ectopic rod opsin in ON-bipolar cell. G-protein coupled receptor, rod opsin, in ON-bipolar cells can activate a native channel, TPRM1, via an amplifying secondary signalling cascade that is normally triggered by an endogenous G-protein, mGluR6 (see Figure 1.8). The cascade is normally activated by reducing glutamate levels from photoreceptors, which in turn activates mGluR6 in rod ON-bipolar cells which in turn activates TRPM1.

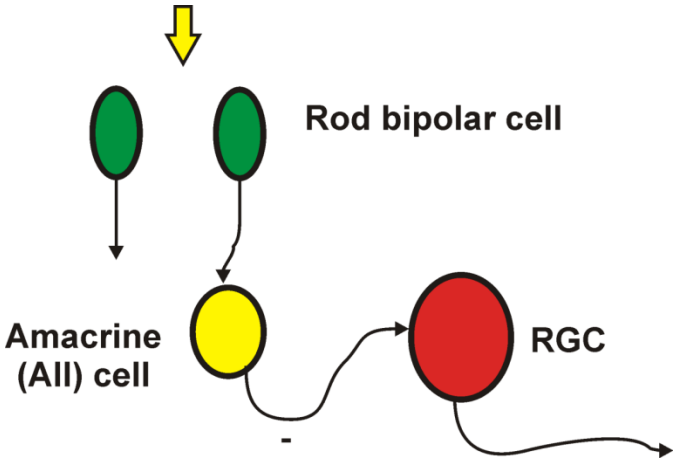

Figure 6.5. Schematic of proposed pathway of ectopic rod opsin driven ON responses. Inhibitory rod opsin responses mediated through $G\alpha_{i/o}$ class proteins could reduce the activity of inhibitory amacrine-cell (AII) synapses disinhibition the RGC firing which would lead to overall ON excitatory responses in RGCs.

6.5. Limitations of *rd1* model and possible rodent alternatives

The *rd1* founder mutation is present in more than one hundred currently used laboratory mouse lines allowing researches to choose the necessary genetic background. However, secondary mutations in any one of those lines are well-known to modify the phenotypic onset and progression of photoreceptor degeneration making direct comparisons between '*rd1*-based' studies somewhat challenging (van Wyk et al., 2015). In particular, the efficacy of potential therapies depends on the rate of progression of retinal degeneration and therefore, measured success may differ between *rd1* substrains. This indeed may at least in part explain the large heterogeneity in optogenetically-driven neuronal response properties we observed in this work.

It has recently been highlighted that many C3H mouse lines, especially those derived from parental C3H/HeJ colony, might carry a secondary mutation in *GPR179* gene, called the no-b wave or *nob5* mutation (Nishiguchi et al., 2015). This leads to aberrant ON-bipolar cell activity due to dysfunctional TrpM1 output channels (Peachey et al., 2012). We cannot exclude the possibility that our mice carried this mutation, thus questioning the proposed biochemical pathway for ectopic rod opsin in ON bipolar cells. This opens a possibility that if rod opsin acted through this most direct pathway, involving the TRPM1 channels, would the speed of responses be further improved. To test this, a mouse model carrying the *rd1* mutation crossed on a C57 wild-type, rather than C3H background would provide a suitable alternative.

Testing our strategy in different models of retinal degeneration might provide further clues on the characteristics of restored responses. In this respect, choosing a model with less aggressive degeneration, such as the *rd10* model (which also carries a mutation in *Pde6b* gene; Gargini et al., 2007) might inform on the visual responses following rod opsin-based optogenetic treatment in the presence of some surviving photoreceptors. Furthermore, the aggressive degeneration in *rd1* mice means that during their lifespan they may have never dedicated much cortical processing power

to visual inputs. As such, they may not be an ideal model for evaluating whether the plasticity of the brain can adapt to make sense of restored visual inputs, and so the *rd*^{10} mouse with slower degeneration and better ability to 'use' the visual information they are presented with during behavioural testing, may again be preferred.

Another widely studied model of retinal degeneration that should to consider is the Royal College of Surgeons (RCS) rat model with photoreceptor degeneration as a result of the failure of the RPE to phagocytose shed rods and cones (D'Cruz et al., 2000). Rats have an inherent evolutionary advantage over mice for visual studies; with greater visual acuity (Prusky et al., 2000) and ability to attend to and solve more complex visual tasks. In addition their larger eye size makes the intraocular gene delivery much easier.

6.6. Limitations of animal models of retinal degeneration

Currently, there is no ideal animal model that allows straightforward evaluation of the translational potential of optogenetic therapies for retinal degenerations. Each model is limiting in its ability to simulate the human retina, so only limited conclusions can be drawn with respect to efficacy and safety.

As discussed, murine models of retinal degeneration are widely used as a first model. There are many naturally occurring strains with genetic mutations that lead to retinal degeneration at various speed and indeed many commonly used transgenic models. The costs of breeding and housing rodents are relatively low compared with larger animal models. However, several important differences exist in murine models when compared to human eyes. Rodent eyes are much smaller compared to human eyes, resulting in a relatively larger area of transduction by either subretinally or intravitreally delivered vectors and therefore potential for overestimating the efficacy of the treatment. Equally, a small rodent eye with proportionally much larger crystalline lens compared to humans, is potentially prone to more intraoperative

complications such as lenticular damage, vitreous haemorrhage and retinal detachment, ultimately limiting the efficacy of the treatment.

In addition, the small eye size in rodents, limits the volume of vector particles that can be delivered. Furthermore, the permeability of the ILM is different in mice than in humans or primates. The ILM is much thinner in mice and lacks the variations in thickness in different parts of the retina that is present in larger animals (Dalkara et al., 2009) and is thus likely to be more permissive to the virus. Significantly, in nocturnal species such as the mouse, photoreception is rod-dominated with relatively few cones and a lack of a fovea, making the development of cone-based therapies or those for central retinal degenerations or more complex disease processes such as AMD very challenging. In addition, the lack of high-acuity vision in rodents makes behavioural studies and estimates of visual acuity and therefore of a full therapeutic potential of an optogenetic actuator very difficult.

Alternatively, naturally occurring canine models of retinal degeneration such as Briard dog (Kijas et al., 2002) have been used in visual restoration studies (Acland et al., 2001; Beltran et al., 2012). Dogs' eyes that are more comparable in size with humans, and their ILMs are more similar (Balaratnasingam et al., 2009). However, they do not have a true fovea, but instead possess a bouquet of cones that can be affected in IRDs (Beltran et.al, 2014). In addition, the process of retinal degeneration in dogs is much slower than in rodents typically taking a year or longer for the retina to degenerate making optogenetic studies for advanced degenerations less practical, costly and difficult to evaluate (Kijas et al., 2002; Ropstad et al., 2008).

A recently developed transgenic mini-pig model of IRD (autosomal dominant mutation in rhodopsin; Ross at al., 2012; Scott et al., 2014) has advantages in that the eyes are of comparable size to human eyes. The progression of the retinal degeneration is quicker than that of the Briard dog, although some robust cones do survive in this model. However, although pigs have a 'pseudomacula', they lack a true fovea.

Indeed, the closest animal model of human fovea that has been used in the evaluation of gene therapies for IHDs is the macaque monkey. Their eyes, including the ILM, are structurally similar to humans (Yin et al., 2011). In addition, monkeys can be trained to perform complex visual tasks mimicking human behaviour. However, there are no naturally occurring models of IRDs in this animal. It is possible to induce photoreceptor death by laser photocoagulation but this would not be a true model of IRD.

6.7. Future directions

This work lends itself to a few naturally progressing future studies. First, it would be important to further improve the AAV targeting system. Since the gene expression patterns of retinal cell types are different, it would be desirable in the future to target more cell types specifically, e.g. OFF-bipolar cells, amacrine cells or any one type of ~20 different RGCs. Indeed, it may be possible to target more than one cell type and use optogenetic tools with different spectral sensitivities to play back their own neural code. Unfortunately to date there are no known vectors or promoters that would specifically target OFF-bipolar cells, amacrine cells or indeed any single type of RGCs. Therefore development of these optimised expression systems, preferably in primates, would greatly improve the translational potential of gene delivery for optogenetic treatments. However, there needs to be a careful balance between increasing the level of expression of an optogenetic protein in any one given cell, to produce a larger response of the cell to light, and the possibility of inducing immune responses, cell toxicity and off-target expression.

Our data shows convincing evidence that rod opsin works remarkably well when ectopically expressed in inner retinal cells, superseding *a priori* expectations that it might not. It transpires that indeed inner retinal neurons possess the necessary intracellular machinery and that there is enough endogenous *cis*-retinal for ectopic rod opsin to work. Furthermore, rod opsin's natural 'OFF' signalling to neurons would

mean that neurons expressing rod opsin would be switched 'OFF' by light. In theory, if neurons were completely silent in the dark this would not generate a physiological signal. In fact the resting membrane potential of neurons is always set to give some background activity that can be inhibited, and indeed hyperactivity is observed in 'deafferented' neuronal states in retinal degeneration. Changing this neuronal polarity to inhibitory signals (from excitatory that normally occur in the intact retina) we reasoned would not be a huge problem; at worst subjects would see a 'negative' image of the world but that most likely there would be sufficient plasticity in the brain to recreate normal percepts. However, restoring function in a rod-dominant mouse retina might be quite different to that of a cone-dominant human retina, especially in terms of chromacy perceived.

Following on from this it seems pertinent to identify the biochemical mechanisms and pathways of ectopic rod opsin, confirming or indeed disputing our proposed mechanisms described above (see Figures 6.4 and 6.5). In addition, valuable information on the dynamic range of rod opsin responses would be obtained if the system was stressed at higher light intensities or presented with high frequency flickers to determine its rate of recovery from bleached states. Furthermore, dampening the pathological neuronal hyperactivity with gap-junction blockers, such as meclofenamic acid, might improve the optogenetically evoked light responses as recently shown for transgenic *rd1* mouse line expressing ChR2 in RGCs (Barrett et al., 2015).

This thesis describes important advances in the development of therapeutic optogenetics therapeutics to treat IRDs by showing that human opsins confer enhancement in light sensitivity over current strategies by orders of magnitude. However there is a trade-off in that native opsins have longer response latencies (especially melanopsin) that could ultimately compromise temporal resolution of restored vision. A recent study using cone opsins has shown that they may be inherently faster (Masseck et al., 2014) and could therefore lead to improved response kinetics. In addition, cone opsins may be less dependent on the RPE for

recycling of the chromophore, as unlike native rod opsin, they are able to use an alternative source of *11-cis*-retinal from Muller cells (Tang et al., 2013). This way they might be better able to avoid bleach and support vision at higher light intensities than rod opsin. Moreover, introducing cone opsins with different spectral sensitivities might be able to recreate colour vision, if two or more opsins are introduced at the same time. Alternatively, engineering bleach-resistant chimeric proteins based on human opsins, with improved temporal properties, is an attractive line of future work.

As discussed above there is no ideal animal model that mimics human retina or recapitulate human disease phenotype. Post-mortem human retinal explants are compelling alternative to evaluate the translational potential of optogenetic sensors with a caveat of them being *ex vivo* and having limited post-mortem viability. However, methods have been established to culture human retina for up to two weeks, although photoreceptor outer segments are lost (Johnson and Martin, 2008). These cultured retinas could be used to evaluate the gene expression profile and vector tropism (Fradot et al., 2011) in a limited timeframe relative to onset of expression. However they would not model host immunity or the delivery methods, since the retina is bathed in the virus. Indeed, the only way to truly evaluate the quality of vision achievable through gene therapies and optogenetics may be through human trials.

6.8. Progressing optogenetics to the clinic

Optogenetics provides a tremendous potential for treating visual loss secondary to IRDs. The treatment is applicable to any late stage retinal degeneration with significant loss of photoreceptors. The approach is mutation independent and gene independent and is applicable to any patient with surviving inner retinal neurons.

This is a major advantage over current mutation dependent approach involving gene replacement therapy. The rare nature of IRDs and the genotypic and phenotypic heterogeneity means that only a relatively small number of patients might benefit from treatments targeting specific gene mutations. In addition, patients affected by autosomal dominant disease and gain-of-function mutations are not amenable to simple augmentation therapy and might require alternative strategies which are still in pre-clinical stage. Moreover, gene replacement therapy is currently limited by the cargo capacity of AAV based vectors restricting its use to the delivery of relatively small genes. In addition, as currently used, subretinal delivery of vectors limits the dose and size of the transduced area, the procedure requires a high level of clinical skill and there are potential risks of complications and damage to foveal cones.

In addition to optogenetics, two major interventions for late stage degenerations include electronic retinal implants and cell transplantation. Electronic retinal prosthetic devices have restored functional vision in some patients but are fundamentally limited by low resolution due to the limitation of the size of implantable chips (Argus II device has 60 electrodes and occupies 10x20 degrees of visual angle). Retinal-cell transplantation has great potential to restore vision in diverse forms of retinal degeneration and extend beyond IRDs to include millions of individuals who are affected by more common diseases including AMD, diabetic retinopathy and glaucoma. However, significant challenges including the source of donor cells and integration capacity of transplanted cells limit this therapy. In addition there are significant risks associated with retinal cell transplantation, including loss of remaining vision due to potential surgical damage, inflammatory responses, immune rejection, and/or induction of proliferative vitreoretinopathy.

Optogenetics therefore has potential to bypass the limitations of above therapies, and through a single, routine intravitreal injection, provide a lasting therapy to patients with IRDs. However, likelihood is that no one single optogenetic treatment would fit all patients with IRDs, but different optogenetic approaches and cellular targets would be required for different subgroups of patients with different forms and stages

of retinal degeneration. In addition, the therapeutic window of opportunity is likely to be limited in advanced stage disease before retinal remodelling and disorganisation takes place that could limit useful vision. Yet, if there was an attempt to use current data to provide a basis for translation of optogenetics to clinical trials, how would we direct a therapeutic plan?

The choice of light-sensing molecule would be human rod opsin, considering the advantages it offers in terms of simplicity of intervention, sensitivity, low immunogenicity and the quality of restored vision over other actuators. The current cellular target of choice would be the ON-bipolar cell, given the quality of vision that is recreated when rod opsin is specifically expressed in this cell type. The caveat however, is that transducing the large number of bipolar cells has yet to be achieved and that late stage degeneration may cause enough remodelling to distort retinal processing. Indeed a downregulation of expression of mGluR6 receptor in ON-bipolar cells has been observed, as well as reprogramming of their signalling from the classical mGluR6-based ON polarity to an iGluR-based OFF polarity in an *rd*^{1} model of retinal degeneration (Marc et al., 2007).

RGC targeting remains an attractive alternative for advanced degenerations where there has been extensive loss of bipolar cells or extensive remodelling of the retinal circuitry. Importantly, GCL integrity has been demonstrated in post-mortem human donor retinas with advanced retinal degenerations (Santos et al., 1997; Humayun et al., 1999). In addition, a small subset of patients with rod-cone dystrophies may have residual foveal cones (which have lost outer segments) that can persist in advanced stages of degeneration and may be amenable to targeting using an optogenetic approach. Combining optogenetic approaches with a neuroprotective therapy (Busskamp and Roska, 2011, Leveillard and Sahel, 2010) to protect cell function and increase the cell lifespan could provide further benefits. With an advent of novel imaging techniques, such as adaptive optics, the morphology of retinal neurons can be studied during the course of the disease in order to choose suitable patients for clinical trials. Important questions that need to be addressed in future studies are

those of longevity of the proposed therapies and whether any of them would prevent or slow down retinal degeneration process and remodelling and ultimate cell death.

6.8.1. Forward vision: the next five years

Ideal optogenetic therapy needs to be safe, effective, low cost and beneficial for a large number of patients with many different retinal dystrophies. There are currently several optogenetic therapies that are very close to human trials. All of the preclinical data so far shows that optogenetic therapy for IRDs is safe with clear evidence of efficacy and ability to induce light-driven activity in the degenerate retina. Developing optogenetic therapy that is mutation independent, and could potentially be applicable to any patient with advanced stage degeneration, would significantly lower the cost-per-dose relative to current mutation dependent gene therapy approaches.

Although it is our hope and belief that optogenetics will prove beneficial for the treatment of multiple retinal dystrophies, a critical step in the development of this intervention is the design of well thought-out clinical trials. First, there is a need to identify clear target patient groups and standardise outcome measures and their ways of testing in order to successfully interpret clinical trials. The development of a shared database to enhance recruitment of eligible patients for inclusion in specific trials would be beneficial. Primary outcome measures should (in addition to conventional visual acuity measures) focus on improvement of both independence and social connectedness.

In addition, there needs to be a better classification system of patients with different stages of retinal disease, so that window of opportunity for optogenetic treatment is not missed. It will thus be important to define this window of opportunity when optogenetic intervention will be most successful. This window is likely to be small as optogenetic therapy in the first instance is likely to include patients with advanced stage disease after all functional photoreceptors have been lost, but before remodelling has negatively impacted remaining retinal circuitry.

The success of these strategies for vision rescue will likely depend on better understanding of the mechanisms of retinal remodelling (and its prevention) and incorporation of this knowledge into design of optimal therapeutics. In addition, development of new imaging modalities to visualise surviving retinal cells and identify target patients as well as to measure the efficacy of these treatments and to monitor disease progression is needed. Importantly, patients who are recruited into clinical trials need to be given a clear explanation of expected outcomes. This leads us to a key question: what will success look like?

The level of vision achieved by an optogenetic therapy will be determined by the surviving neuronal targets (photoreceptors, bipolar cells, RGCs) and the level of preservation of neuronal wiring in the remaining retinal circuitry, especially in the foveal region. Many people with IRDs have a rod-cone dystrophy, where despite outer cone segment degeneration, light insensitive cone cell bodies survive for many years. Targeting cones, and therefore utilising most of the retinal processing, has the potential to recreate vision with the greatest similarity to normal vision. However, in more advanced stages of degeneration, all cones will be lost and those patients will likely benefit from targeting bipolar cells, whilst the most severely affected would require RGC targeting.

By targeting inner cone segments or bipolar cells optogenetics has potential to recreate meaningful vision in patients who have become severely sight impaired due to retinal degeneration. Current success for late stage degenerations is evaluated against Argus II implants which directly stimulate RGC and where successful treatment has recovered navigational vision as well as crude object and face recognition for some patients. Optogenetics has a potential to improve on this outcome as light-sensitive protein expression will not be limited to a few cells in a small area of the retina to the 60 evenly spaced electrodes in the Argus II chip (covering a few mms of retina only), but could transduce millions of surviving inner retinal cells creating in effect millions of artificial photoreceptors. These cells would have uneven spacing as found in the normal retina (assuming no remodelling has taken place at the time of the therapy) with highly organised mosaic arrangement of cells at every level. Visual information would therefore be sent in a relatively straight

line from the photoreceptor to the bipolar cell to the RGC mapping elements of the visual scene in straightforward fashion to locations on the retina. Targeting retinal periphery would therefore preserve the map, dramatically improve the degree of recovered field of vision and therefore the quality of spatial navigation as well as more detailed vision such as object recognition (more central transduction). However, this would not provide the same acuity as the fovea, which is the area that is the most useful to patients.

In the fovea cones are still arranged in the spatial map that correlates with the spatial properties of the image. Therefore, for patients with remnant cone cell bodies in the fovea there would be the greatest potential to recreate high-acuity vision. In patients with no surviving cones optogenetic therapy will rely on targeting bipolar cells and RGCs. However, RGCs and bipolar cells are pushed aside in a ring around the fovea and are not found directly under the photoreceptors in a mosaic as elsewhere in the retina. Thus, if bipolar or RGCs express optogenetic proteins in the fovea, images projecting onto the fovea are likely to lead to distorted neuronal representation of the retina. One way to remedy this problem would be to purposely pre-distort images by a goggle type device to compensate for the ring-arrangement of the light sensitive targeted cells. The device would also have to be capable of eye tracking to follow changes in fixation.

In summary, optogenetics has potential to restore vision beyond that achieved by current retinal prosthesis – best visual acuity achieved was 20/1262 with an Argus II device. Beyond visual acuity, some patients demonstrated object localisation, discrimination and large letter identification. Others gained ability to perform simple orientation and mobility tasks in daily activities, whilst some realised only rudimentary functional gains, like simple light perception or localisation of bright versus dark areas, which although of limited use is appreciated by patients with no vision. In addition, there were some patients who had no benefit at all. It is therefore vital to carefully manage patients' expectations and not to oversell the intervention and build false hopes. Lastly, one of the most important aspects of successful therapy is rehabilitation of prosthetic vision as patients will have to learn new visual language. Nearly all patient studies to date have shown that training and motivation

maximise the benefit of the treatment. Therefore, the role of rehabilitation and the potential for retinal and cortical plasticity post treatment should not be underestimated.

On a final note, Russel Van Gelder and Kuldeep Kaur give an excellent synopsis on the rod opsin work in a recent Current Biology Dispatch: Can rhodopsin cure blindness? (Van Gelder and Kaur, 2015).

References

Abedin, M., and King, N. (2010). Diverse evolutionary paths to cell adhesion. Trends Cell Biol *20*, 734-742.

Acland, G.M., Aguirre, G.D., Ray, J., Zhang, Q., Aleman, T.S., Cideciyan, A.V., Pearce-Kelling, S.E., Anand, V., Zeng, Y., Maguire, A.M.*, et al.* (2001). Gene therapy restores vision in a canine model of childhood blindness. Nat Genet *28*, 92-95.

Acland, G.M., Aguirre, G.D., Bennett, J., Aleman, T.S., Cideciyan, A.V., Bennicelli, J., Dejneka, N.S., Pearce-Kelling, S.E., Maguire, A.M., Palczewski, K.*, et al.* (2005). Long-term restoration of rod and cone vision by single dose rAAV-mediated gene transfer to the retina in a canine model of childhood blindness. Mol Ther *12*, 1072-1082.

Adackapara, C.A., Sunness, J.S., Dibernardo, C.W., Melia, B.M., and Dagnelie, G. (2008). Prevalence of cystoid macular edema and stability in oct retinal thickness in eyes with retinitis pigmentosa during a 48-week lutein trial. Retina *28*, 103-110.

Allen, A.E., Storchi, R., Martial, F.P., Petersen, R.S., Montemurro, M.A., Brown, T.M., and Lucas, R.J. (2014). Melanopsin-driven light adaptation in mouse vision. Curr Biol *24*, 2481-2490.

Ali, R.R., Reichel, M.B., De Alwis, M., Kanuga, N., Kinnon, C., Levinsky, R.J., Hunt, D.M., Bhattacharya, S.S., and Thrasher, A.J. (1998). Adeno-associated virus gene transfer to mouse retina. Hum Gene Ther *9*, 81-86.

Ali, R.R., Reichel, M.B., Thrasher, A.J., Levinsky, R.J., Kinnon, C., Kanuga, N., Hunt, D.M., and Bhattacharya, S.S. (1996). Gene transfer into the mouse retina mediated by an adeno-associated viral vector. Hum Mol Genet *5*, 591-594.

Allocca, M., Mussolino, C., Garcia-Hoyos, M., Sanges, D., Iodice, C., Petrillo, M., Vandenberghe, L.H., Wilson, J.M., Marigo, V., Surace, E.M.*, et al.* (2007). Novel adeno-associated virus serotypes efficiently transduce murine photoreceptors. J Virol *81*, 11372-11380.

Allocca, M., Manfredi, A., Iodice, C., Di Vicino, U., and Auricchio, A. (2011). AAV-mediated gene replacement, either alone or in combination with physical and pharmacological agents, results in partial and transient protection from photoreceptor degeneration associated with betaPDE deficiency. Invest Ophthalmol Vis Sci *52*, 5713-5719.

Akache, B., Grimm, D., Pandey, K., Yant, S.R., Xu, H., and Kay, M.A. (2006). The 37/67-kilodalton laminin receptor is a receptor for adeno-associated virus serotypes 8, 2, 3, and 9. J Virol *80*, 9831-9836.

Annear, M.J., Bartoe, J.T., Barker, S.E., Smith, A.J., Curran, P.G., Bainbridge, J.W., Ali, R.R., and Petersen-Jones, S.M. (2011). Gene therapy in the second eye of RPE65-deficient dogs improves retinal function. Gene Ther *18*, 53-61.

Auricchio, A., Kobinger, G., Anand, V., Hildinger, M., O'Connor, E., Maguire, A.M., Wilson, J.M., and Bennett, J. (2001). Exchange of surface proteins impacts on viral vector cellular specificity and transduction characteristics: the retina as a model. Hum Mol Genet *10*, 3075-3081.

Auricchio A, Trapani I, Allikmets R. (2015). Gene Therapy of ABCA4-Associated Diseases.Cold Spring Harb Perspect Med. *8*;5(5):a017301.

Ayuso, C., and Millan, J.M. (2010). Retinitis pigmentosa and allied conditions today: a paradigm of translational research. Genome Med *2*, 3.

Bailes, H.J., and Lucas, R.J. (2013). Human melanopsin forms a pigment maximally sensitive to blue light (lambdamax approximately 479 nm) supporting activation of G(q/11) and G(i/o) signalling cascades. Proc Biol Sci *280*, 20122987.

Balaggan KS Ali RR. (2012). Ocular gene delivery using lentiviral vectors. Gene Ther.; *19*: 145–153.

Bainbridge, J.W., Smith, A.J., Barker, S.S., Robbie, S., Henderson, R., Balaggan, K., Viswanathan, A., Holder, G.E., Stockman, A., Tyler, N.*, et al.* (2008). Effect of gene therapy on visual function in Leber's congenital amaurosis. N Engl J Med *358*, 2231-2239.

Bainbridge, J.W., Mehat, M.S., Sundaram, V., Robbie, S.J., Barker, S.E., Ripamonti, C., Georgiadis, A., Mowat, F.M., Beattie, S.G., Gardner, P.J.*, et al.* (2015). Long-term effect of gene therapy on Leber's congenital amaurosis. N Engl J Med *372*, 1887-1897.

Balaratnasingam, C., Morgan, W.H., Johnstone, V., Pandav, S.S., Cringle, S.J., and Yu, D.Y. (2009). Histomorphometric measurements in human and dog optic nerve and an estimation of optic nerve pressure gradients in human. Exp Eye Res *89*, 618-628.

Barabas, P., Cutler Peck, C., and Krizaj, D. (2010). Do calcium channel blockers rescue dying photoreceptors in the Pde6b (rd1) mouse? Adv Exp Med Biol *664*, 491-499.

Barrett, J.M., Degenaar, P., and Sernagor, E. (2015). Blockade of pathological retinal ganglion cell hyperactivity improves optogenetically evoked light responses in rd1 mice. Front Cell Neurosci *9*, 330.

Bartel, M.A., Weinstein, J.R., and Schaffer, D.V. (2012). Directed evolution of novel adeno-associated viruses for therapeutic gene delivery. Gene Ther *19*, 694-700.

Bell, C.L., Vandenberghe, L.H., Bell, P., Limberis, M.P., Gao, G.P., Van Vliet, K., Agbandje-McKenna, M., and Wilson, J.M. (2011). The AAV9 receptor and its modification to improve in vivo lung gene transfer in mice. J Clin Invest *121*, 2427-2435.

Bell, C.L., Gurda, B.L., Van Vliet, K., Agbandje-McKenna, M., and Wilson, J.M. (2012). Identification of the galactose binding domain of the adeno-associated virus serotype 9 capsid. J Virol *86*, 7326-7333.

Beltran, W.A., Cideciyan, A.V., Lewin, A.S., Iwabe, S., Khanna, H., Sumaroka, A., Chiodo, V.A., Fajardo, D.S., Roman, A.J., Deng, W.T.*, et al.* (2012). Gene therapy rescues photoreceptor blindness in dogs and paves the way for treating human X-linked retinitis pigmentosa. Proc Natl Acad Sci U S A *109*, 2132-2137.

Bennett, J. (2003). Immune response following intraocular delivery of recombinant viral vectors. Gene Ther *10*, 977-982.

Bennett, J., Maguire, A.M., Cideciyan, A.V., Schnell, M., Glover, E., Anand, V., Aleman, T.S., Chirmule, N., Gupta, A.R., Huang, Y.*, et al.* (1999). Stable transgene expression in rod photoreceptors after recombinant adeno-associated virus-mediated gene transfer to monkey retina. Proc Natl Acad Sci U S A *96*, 9920-9925.

Bennett LD, Wang YZ, Klein M, Pennesi ME, Jayasundera T, Birch DG. (2016) Structure/Psychophysical Relationships in X-Linked Retinoschisis. Invest Ophthalmol Vis Sci. *57*(2):332-7.

Berson, D.M., Dunn, F.A., and Takao, M. (2002). Phototransduction by retinal ganglion cells that set the circadian clock. Science *295*, 1070-1073.

Bessant, D.A., Ali, R.R., and Bhattacharya, S.S. (2001). Molecular genetics and prospects for therapy of the inherited retinal dystrophies. Curr Opin Genet Dev *11*, 307-316.

Bi, A., Cui, J., Ma, Y.P., Olshevskaya, E., Pu, M., Dizhoor, A.M., and Pan, Z.H. (2006). Ectopic expression of a microbial-type rhodopsin restores visual responses in mice with photoreceptor degeneration. Neuron *50*, 23-33.

Biedermann, B., Frohlich, E., Grosche, J., Wagner, H.J., and Reichenbach, A. (1995). Mammalian Muller (glial) cells express functional D2 dopamine receptors. Neuroreport *6*, 609-612.

Binley K Widdowson P Loader J (2013). Transduction of photoreceptors with equine infectious anemia virus lentiviral vectors: safety and biodistribution of StarGen for Stargardt disease. Invest Ophthalmol Vis Sci.; *54*: 4061–4071.

Bither, P.P., and Berns, L.A. (1988). Stargardt's disease: a review of the literature. J Am Optom Assoc *59*, 106-111.

Booij, J.C., Baas, D.C., Beisekeeva, J., Gorgels, T.G., and Bergen, A.A. (2010). The dynamic nature of Bruch's membrane. Prog Retin Eye Res *29*, 1-18.

Boughman, J.A., Vernon, M., and Shaver, K.A. (1983). Usher syndrome: definition and estimate of prevalence from two high-risk populations. J Chronic Dis *36*, 595-603

Bourges, J.L., Gautier, S.E., Delie, F., Bejjani, R.A., Jeanny, J.C., Gurny, R., BenEzra, D., and Behar-Cohen, F.F. (2003). Ocular drug delivery targeting the retina and retinal pigment epithelium using polylactide nanoparticles. Invest Ophthalmol Vis Sci *44*, 3562-3569.

Bourin, M., and Hascoet, M. (2003). The mouse light/dark box test. Eur J Pharmacol *463*, 55-65.

Bowes, C., Li, T., Danciger, M., Baxter, L.C., Applebury, M.L., and Farber, D.B. (1990). Retinal degeneration in the rd mouse is caused by a defect in the beta subunit of rod cGMP-phosphodiesterase. Nature *347*, 677-680.

Bowes, C., Li, T., Frankel, W.N., Danciger, M., Coffin, J.M., Applebury, M.L., and Farber, D.B. (1993). Localization of a retroviral element within the rd gene coding for the beta subunit of cGMP phosphodiesterase. Proc Natl Acad Sci U S A *90*, 2955-2959.

Boye, S.E., Alexander, J.J., Boye, S.L., Witherspoon, C.D., Sandefer, K.J., Conlon, T.J., Erger, K., Sun, J., Ryals, R., Chiodo, V.A., *et al.* (2012). The human rhodopsin kinase promoter in an AAV5 vector confers rod- and cone-specific expression in the primate retina. Hum Gene Ther *23*, 1101-1115.

Boye, S.L., Conlon, T., Erger, K., Ryals, R., Neeley, A., Cossette, T., Pang, J., Dyka, F.M., Hauswirth, W.W., and Boye, S.E. (2011). Long-term preservation of cone photoreceptors and restoration of cone function by gene therapy in the guanylate cyclase-1 knockout (GC1KO) mouse. Invest Ophthalmol Vis Sci *52*, 7098-7108.

Boye, S.E., Boye, S.L., Lewin, A.S., and Hauswirth, W.W. (2013). A comprehensive review of retinal gene therapy. Mol Ther *21*, 509-519.

Breuninger, T., Puller, C., Haverkamp, S., and Euler, T. (2011). Chromatic bipolar cell pathways in the mouse retina. J Neurosci *31*, 6504-6517.

Bridges, C.D. (1959). Visual pigments of some common laboratory mammals. Nature *184(Suppl 22)*, 1727-1728.

Brown, T.M., Gias, C., Hatori, M., Keding, S.R., Semo, M., Coffey, P.J., Gigg, J., Piggins, H.D., Panda, S., and Lucas, R.J. (2010). Melanopsin contributions to irradiance coding in the thalamo-cortical visual system. PLoS Biol *8*, e1000558.

Brown, T.M., Tsujimura, S., Allen, A.E., Wynne, J., Bedford, R., Vickery, G., Vugler, A., and Lucas, R.J. (2012). Melanopsin-based brightness discrimination in mice and humans. Curr Biol *22*, 1134-1141.

Buning, H., Perabo, L., Coutelle, O., Quadt-Humme, S., and Hallek, M. (2008). Recent developments in adeno-associated virus vector technology. J Gene Med *10*, 717-733.

Busskamp, V., and Roska, B. (2011). Optogenetic approaches to restoring visual function in retinitis pigmentosa. Curr Opin Neurobiol *21*, 942-946.

Busskamp, V., Picaud, S., Sahel, J.A., and Roska, B. (2012). Optogenetic therapy for retinitis pigmentosa. Gene Ther *19*, 169-175.

Busskamp, V., Duebel, J., Balya, D., Fradot, M., Viney, T.J., Siegert, S., Groner, A.C., Cabuy, E., Forster, V., Seeliger, M.*, et al.* (2010). Genetic reactivation of cone photoreceptors restores visual responses in retinitis pigmentosa. Science *329*, 413-417.

Byrne, L.C., Dalkara, D., Luna, G., Fisher, S.K., Clerin, E., Sahel, J.A., Leveillard, T., and Flannery, J.G. (2015). Viral-mediated RdCVF and RdCVFL expression protects cone and rod photoreceptors in retinal degeneration. J Clin Invest *125*, 105-116.

Caporale, N., Kolstad, K.D., Lee, T., Tochitsky, I., Dalkara, D., Trauner, D., Kramer, R., Dan, Y., Isacoff, E.Y., and Flannery, J.G. (2011). LiGluR restores visual responses in rodent models of inherited blindness. Mol Ther *19*, 1212-1219.

Carter-Dawson, L.D., LaVail, M.M., and Sidman, R.L. (1978). Differential effect of the rd mutation on rods and cones in the mouse retina. Invest Ophthalmol Vis Sci *17*, 489-498

Carter-Dawson, L.D., and LaVail, M.M. (1979). Rods and cones in the mouse retina. I. Structural analysis using light and electron microscopy. J Comp Neurol *188*, 245-262.

Cehajic-Kapetanovic, J., Le Goff, M.M., Allen, A., Lucas, R.J., and Bishop, P.N. (2011). Glycosidic enzymes enhance retinal transduction following intravitreal delivery of AAV2. Mol Vis *17*, 1771-1783.

Chai, L., and Morris, J.E. (1994). Distribution of heparan sulfate proteoglycans in embryonic chicken neural retina and isolated inner limiting membrane. Curr Eye Res *13*, 669-677.

Chang, B., Hawes, N.L., Hurd, R.E., Davisson, M.T., Nusinowitz, S., and Heckenlively, J.R. (2002). Retinal degeneration mutants in the mouse. Vision Res *42*, 517-525.

Chen, C.K., Burns, M.E., Spencer, M., Niemi, G.A., Chen, J., Hurley, J.B., Baylor, D.A., and Simon, M.I. (1999). Abnormal photoresponses and light-induced apoptosis in rods lacking rhodopsin kinase. Proc Natl Acad Sci U S A *96*, 3718-3722.

Chuang, A.T., Margo, C.E., and Greenberg, P.B. (2014). Retinal implants: a systematic review. Br J Ophthalmol *98*, 852-856.

Cideciyan, A.V., Jacobson, S.G., Beltran, W.A., Sumaroka, A., Swider, M., Iwabe, S., Roman, A.J., Olivares, M.B., Schwartz, S.B., Komaromy, A.M.*, et al.* (2013). Human retinal gene therapy for Leber congenital amaurosis shows advancing retinal degeneration despite enduring visual improvement. Proc Natl Acad Sci U S A *110*, E517-525.

Clark, S.J., Keenan, T.D., Fielder, H.L., Collinson, L.J., Holley, R.J., Merry, C.L., van Kuppevelt, T.H., Day, A.J., and Bishop, P.N. (2011). Mapping the differential distribution of glycosaminoglycans in the adult human retina, choroid, and sclera. Invest Ophthalmol Vis Sci *52*, 6511-6521.

Coombs, J.L., Van Der List, D., and Chalupa, L.M. (2007). Morphological properties of mouse retinal ganglion cells during postnatal development. J Comp Neurol *503*, 803-814.

Coppieters, F., Lefever, S., Leroy, B. P. and De Baere, E. (2010). CEP290, a gene with many faces: mutation overview and presentation of CEP290base. Hum. Mutat. *31*, 1097–1108.

Couchman, J.R., and Pataki, C.A. (2012). An introduction to proteoglycans and their localization. J Histochem Cytochem *60*, 885-897.

Cronin, T., Vandenberghe, L.H., Hantz, P., Juttner, J., Reimann, A., Kacso, A.E., Huckfeldt, R.M., Busskamp, V., Kohler, H., Lagali, P.S.*, et al.* (2014). Efficient transduction and optogenetic stimulation of retinal bipolar cells by a synthetic adeno-associated virus capsid and promoter. EMBO Mol Med *6*, 1175-1190.

Dacey, D., Packer, O.S., Diller, L., Brainard, D., Peterson, B., and Lee, B. (2000). Center surround receptive field structure of cone bipolar cells in primate retina. Vision Res *40*, 1801-1811.

Dalkara, D., Kolstad, K.D., Caporale, N., Visel, M., Klimczak, R.R., Schaffer, D.V., and Flannery, J.G. (2009). Inner limiting membrane barriers to AAV-mediated retinal transduction from the vitreous. Mol Ther *17*, 2096-2102.

Dalkara, D., Byrne, L.C., Klimczak, R.R., Visel, M., Yin, L., Merigan, W.H., Flannery, J.G., and Schaffer, D.V. (2013). In vivo-directed evolution of a new adeno-associated virus for therapeutic outer retinal gene delivery from the vitreous. Sci Transl Med *5*, 189ra176.

Dalkara, D., and Sahel, J.A. (2014). Gene therapy for inherited retinal degenerations. C R Biol *337*, 185-192.

Davis, K.E., Eleftheriou, C.G., Allen, A.E., Procyk, C.A., and Lucas, R.J. (2015). Melanopsin-derived visual responses under light adapted conditions in the mouse dLGN. PLoS One *10*, e0123424.

D'Cruz, P.M., Yasumura, D., Weir, J., Matthes, M.T., Abderrahim, H., LaVail, M.M., and Vollrath, D. (2000). Mutation of the receptor tyrosine kinase gene Mertk in the retinal dystrophic RCS rat. Hum Mol Genet *9*, 645-651.

Deisseroth, K., Feng, G., Majewska, A.K., Miesenbock, G., Ting, A., and Schnitzer, M.J. (2006). Next-generation optical technologies for illuminating genetically targeted brain circuits. J Neurosci *26*, 10380-10386.

Deisseroth, K. (2011). Optogenetics. Nat Methods *8*, 26-29.

Dejneka, N.S., Surace, E.M., Aleman, T.S., Cideciyan, A.V., Lyubarsky, A., Savchenko, A., Redmond, T.M., Tang, W., Wei, Z., Rex, T.S*., et al.* (2004). In utero gene therapy rescues vision in a murine model of congenital blindness. Mol Ther *9*, 182-188.

den Hollander, A.I., Roepman R., Koenekoop, R.K., Cremers, F.P. (2008). Leber congenital amaurosis: genes, proteins and disease mechanisms. Prog Retin Eye Res *27*,391-419.

Di Pasquale, G., Davidson, B.L., Stein, C.S., Martins, I., Scudiero, D., Monks, A., and Chiorini, J.A. (2003). Identification of PDGFR as a receptor for AAV-5 transduction. Nat Med *9*, 1306-1312.

Diamond, J.S., and Copenhagen, D.R. (1995). The relationship between light-evoked synaptic excitation and spiking behaviour of salamander retinal ganglion cells. J Physiol *487 (Pt 3)*, 711-725.

Do, M.T., Kang, S.H., Xue, T., Zhong, H., Liao, H.W., Bergles, D.E., and Yau, K.W. (2009). Photon capture and signalling by melanopsin retinal ganglion cells. Nature *457*, 281-287.

Doroudchi, M.M., Greenberg, K.P., Liu, J., Silka, K.A., Boyden, E.S., Lockridge, J.A., Arman, A.C., Janani, R., Boye, S.E., Boye, S.L*., et al.* (2011). Virally delivered channelrhodopsin-2 safely and effectively restores visual function in multiple mouse models of blindness. Mol Ther *19*, 1220-1229.

Dowling, J.E., and Werblin, F.S. (1969). Organization of retina of the mudpuppy, Necturus maculosus. I. Synaptic structure. J Neurophysiol *32*, 315-338.

Dryja, T.P., McGee, T.L., Hahn, L.B., Cowley, G.S., Olsson, J.E., Reichel, E., Sandberg, M.A., and Berson, E.L. (1990). Mutations within the rhodopsin gene in patients with autosomal dominant retinitis pigmentosa. N Engl J Med *323*, 1302-1307.
Emanuel, A.J., and Do, M.T. (2015). Melanopsin tristability for sustained and broadband phototransduction. Neuron *85*, 1043-1055.

Falk, M.J., Zhang, Q., Nakamaru-Ogiso, E., Kannabiran, C., Fonseca-Kelly, Z., Chakarova, C., Audo, I., Mackay, D.S., Zeitz, C., Borman, A.D.*, et al.* (2012). NMNAT1 mutations cause Leber congenital amaurosis. Nat Genet *44*, 1040-1045.

Famiglietti, E.V., Jr., Kaneko, A., and Tachibana, M. (1977). Neuronal architecture of on and off pathways to ganglion cells in carp retina. Science *198*, 1267-1269.

Farber, D.B., Flannery, J.G., Bowes-Rickman, C. (1994). The rd mouse story: seventy years of research on an animal model of inherited retinal degeneration. Prog Ret Eye Res *13*, 31–64.

Farber, D.B., and Lolley, R.N. (1974). Cyclic guanosine monophosphate: elevation in degenerating photoreceptor cells of the C3H mouse retina. Science *186*, 449-451.

Farber, D.B., and Lolley, R.N. (1976). Enzymic basis for cyclic GMP accumulation in degenerative photoreceptor cells of mouse retina. J Cyclic Nucleotide Res *2*, 139-148.

Forsythe, E., and Beales, P.L. (2013). Bardet-Biedl syndrome. Eur J Hum Genet *21*, 8-13.

Fradot, M., Busskamp, V., Forster, V., Cronin, T., Leveillard, T., Bennett, J., Sahel, J.A., Roska, B., and Picaud, S. (2011). Gene therapy in ophthalmology: validation on cultured retinal cells and explants from postmortem human eyes. Hum Gene Ther *22*, 587-593.

Fritsche, L. G., Fariss, R. N., Stambolian, D., Abecasis, G. R., Curcio, C. A. and Swaroop, A. (2014). Age-related macular degeneration: genetics and biology coming together. Annu. Rev. Genomics Hum. Genet. *15*, 151–171.

Gabriel, N., Hareendran, S., Sen, D., Gadkari, R.A., Sudha, G., Selot, R., Hussain, M., Dhaksnamoorthy, R., Samuel, R., Srinivasan, N.*, et al.* (2013). Bioengineering of AAV2 capsid at specific serine, threonine, or lysine residues improves its transduction efficiency in vitro and in vivo. Hum Gene Ther Methods *24*, 80-93.

Gao, G., Vandenberghe, L.H., Alvira, M.R., Lu, Y., Calcedo, R., Zhou, X., and Wilson, J.M. (2004). Clades of Adeno-associated viruses are widely disseminated in human tissues. J Virol *78*, 6381-6388.

Garcia-Fernandez, J.M., Jimenez, A.J., and Foster, R.G. (1995). The persistence of cone photoreceptors within the dorsal retina of aged retinally degenerate mice (rd/rd): implications for circadian organization. Neurosci Lett *187*, 33-36.

Gargini, C., Terzibasi, E., Mazzoni, F., and Strettoi, E. (2007). Retinal organization in the retinal degeneration 10 (rd10) mutant mouse: a morphological and ERG study. J Comp Neurol *500*, 222-238.

Gaub, B.M., Berry, M.H., Holt, A.E., Reiner, A., Kienzler, M.A., Dolgova, N., Nikonov, S., Aguirre, G.D., Beltran, W.A., Flannery, J.G.*, et al.* (2014). Restoration of visual function by expression of a light-gated mammalian ion channel in retinal ganglion cells or ON-bipolar cells. Proc Natl Acad Sci U S A *111*, E5574-5583.

Gaub, B.M., Berry, M.H., Holt, A.E., Isacoff, E.Y., and Flannery, J.G. (2015). Optogenetic Vision Restoration Using Rhodopsin for Enhanced Sensitivity. Mol Ther.

George, N.D., Yates, J.R., and Moore, A.T. (1995). X linked retinoschisis. Br J Ophthalmol *79*, 697-702.

Gibson, R., Fletcher, E.L., Vingrys, A.J., Zhu, Y., Vessey, K.A., and Kalloniatis, M. (2013). Functional and neurochemical development in the normal and degenerating mouse retina. J Comp Neurol *521*, 1251-1267.

Goldberg, N.R., Greenberg, J.P., Laud, K., Tsang, S., and Freund, K.B. (2013). Outer retinal tubulation in degenerative retinal disorders. Retina *33*, 1871-1876.

Gollisch, T., and Meister, M. (2010). Eye smarter than scientists believed: neural computations in circuits of the retina. Neuron *65*, 150-164.

Goncalves, M.A. (2005). Adeno-associated virus: from defective virus to effective vector. Virol J *2*, 43.

Gooley, J.J., Ho Mien, I., St Hilaire, M.A., Yeo, S.C., Chua, E.C., van Reen, E., Hanley, C.J., Hull, J.T., Czeisler, C.A., and Lockley, S.W. (2012). Melanopsin and rod-cone photoreceptors play different roles in mediating pupillary light responses during exposure to continuous light in humans. J Neurosci *32*, 14242-14253.

Govardovskii, V.I., Fyhrquist, N., Reuter, T., Kuzmin, D.G., and Donner, K. (2000). In search of the visual pigment template. Vis Neurosci *17*, 509-528.

Greenberg, K.P., Pham, A., and Werblin, F.S. (2011). Differential targeting of optical neuromodulators to ganglion cell soma and dendrites allows dynamic control of center-surround antagonism. Neuron *69*, 713-720.

Gruter, O., Kostic, C., Crippa, S.V., Perez, M.T., Zografos, L., Schorderet, D.F., Munier, F.L., and Arsenijevic, Y. (2005). Lentiviral vector-mediated gene transfer in adult mouse photoreceptors is impaired by the presence of a physical barrier. Gene Ther *12*, 942-947.

Halder, S., Van Vliet, K., Smith, J.K., Duong, T.T., McKenna, R., Wilson, J.M., and Agbandje-McKenna, M. (2015). Structure of neurotropic adeno-associated virus AAVrh.8. J Struct Biol.

Hamblion, E.L., Moore, A.T., Rahi, J.S., and British Childhood Onset Hereditary Retinal Disorders, N. (2012). Incidence and patterns of detection and management of childhood-onset hereditary retinal disorders in the UK. Br J Ophthalmol *96*, 360-365.

Handa, J.T. (2012). How does the macula protect itself from oxidative stress? Mol Aspects Med *33*, 418-435.

Hart, A.W., McKie, L., Morgan, J.E., Gautier, P., West, K., Jackson, I.J., and Cross, S.H. (2005). Genotype-phenotype correlation of mouse pde6b mutations. Invest Ophthalmol Vis Sci *46*, 3443-3450.

Hartong, D.T., Berson, E.L., and Dryja, T.P. (2006). Retinitis pigmentosa. Lancet *368*, 1795-1809.

Hattar, S., Liao, H.W., Takao, M., Berson, D.M., and Yau, K.W. (2002). Melanopsin-containing retinal ganglion cells: architecture, projections, and intrinsic photosensitivity. Science *295*, 1065-1070.

Hargrave, P.A., and McDowell, J.H. (1992). Rhodopsin and phototransduction: a model system for G protein-linked receptors. FASEB J *6*, 2323-2331.

Hauswirth, W.W., Aleman, T.S., Kaushal, S., Cideciyan, A.V., Schwartz, S.B., Wang, L., Conlon, T.J., Boye, S.L., Flotte, T.R., Byrne, B.J.*, et al.* (2008). Treatment of leber congenital amaurosis due to RPE65 mutations by ocular subretinal injection of adeno-associated virus gene vector: short-term results of a phase I trial. Hum Gene Ther *19*, 979-990.

Haverkamp, S., Grunert, U., and Wassle, H. (2001). Localization of kainate receptors at the cone pedicles of the primate retina. J Comp Neurol *436*, 471-486.

Hecht, S., Shlaer, S., and Pirenne, M.H. (1942). Energy, Quanta, and Vision. J Gen Physiol *25*, 819-840.

Heegaard, S., Jensen, O.A., and Prause, J.U. (1986). Structure and composition of the inner limiting membrane of the retina. SEM on frozen resin-cracked and enzyme-digested retinas of Macaca mulatta. Graefes Arch Clin Exp Ophthalmol *224*, 355-360.

Heinegard, D. (2009). Proteoglycans and more--from molecules to biology. Int J Exp Pathol *90*, 575-586.

Hellstrom, M., Ruitenberg, M.J., Pollett, M.A., Ehlert, E.M., Twisk, J., Verhaagen, J., and Harvey, A.R. (2009). Cellular tropism and transduction properties of seven adeno-associated viral vector serotypes in adult retina after intravitreal injection. Gene Ther *16*, 521-532.

Henriksen, B.S., Marc, R.E., and Bernstein, P.S. (2014). Optogenetics for retinal disorders. J Ophthalmic Vis Res *9*, 374-382.

Hermonat, P.L., and Muzyczka, N. (1984). Use of adeno-associated virus as a mammalian DNA cloning vector: transduction of neomycin resistance into mammalian tissue culture cells. Proc Natl Acad Sci U S A *81*, 6466-6470.

Histed, M.H., Ni, A.M., and Maunsell, J.H. (2013). Insights into cortical mechanisms of behavior from microstimulation experiments. Prog Neurobiol *103*, 115-130.

Holt, C.E., and Dickson, B.J. (2005). Sugar codes for axons? Neuron *46*, 169-172.

Herzer, S. Beckett, P., Wegman, T., *et al*. (2003) Isoelectric titration curves of viral particles as an evaluation tool for ion exchange chromatography. Amersham Biosciences. Life Sci News 13.

Hood, D.C., Wladis, E.J., Shady, S., Holopigian, K., Li, J., and Seiple, W. (1998). Multifocal rod electroretinograms. Invest Ophthalmol Vis Sci *39*, 1152-1162.

Humayun, M.S., Dorn, J.D., da Cruz, L., Dagnelie, G., Sahel, J.A., Stanga, P.E., Cideciyan, A.V., Duncan, J.L., Eliott, D., Filley, E.*, et al.* (2012). Interim results from the international trial of Second Sight's visual prosthesis. Ophthalmology *119*, 779-788

Ichijo, H. (2004). Proteoglycans as cues for axonal guidance in formation of retinotectal or retinocollicular projections. Mol Neurobiol *30*, 23-33.

Iozzo, R.V., and Schaefer, L. (2015). Proteoglycan form and function: A comprehensive nomenclature of proteoglycans. Matrix Biol *42*, 11-55.

Jacobs, G.H., and Williams, G.A. (2007). Contributions of the mouse UV photopigment to the ERG and to vision. Doc Ophthalmol *115*, 137-144.

Jackson, T.L., Antcliff, R.J., Hillenkamp, J., and Marshall, J. (2003). Human retinal molecular weight exclusion limit and estimate of species variation. Invest Ophthalmol Vis Sci *44*, 2141-2146.

Jacobson, S.G., Acland, G.M., Aguirre, G.D., Aleman, T.S., Schwartz, S.B., Cideciyan, A.V., Zeiss, C.J., Komaromy, A.M., Kaushal, S., Roman, A.J.*, et al.* (2006). Safety of recombinant adeno-associated virus type 2-RPE65 vector delivered by ocular subretinal injection. Mol Ther *13*, 1074-1084.

Jacobson, S.G., Cideciyan, A.V., Ratnakaram, R., Heon, E., Schwartz, S.B., Roman, A.J., Peden, M.C., Aleman, T.S., Boye, S.L., Sumaroka, A.*, et al.* (2012). Gene therapy for leber congenital amaurosis caused by RPE65 mutations: safety and efficacy in 15 children and adults followed up to 3 years. Arch Ophthalmol *130*, 9-24.

Johnson, T.V., and Martin, K.R. (2008). Development and characterization of an adult retinal explant organotypic tissue culture system as an in vitro intraocular stem cell transplantation model. Invest Ophthalmol Vis Sci *49*, 3503-3512.

Jones, B.W., and Marc, R.E. (2005). Retinal remodeling during retinal degeneration. Exp Eye Res *81*, 123-137.

Kaludov, N., Brown, K.E., Walters, R.W., Zabner, J., and Chiorini, J.A. (2001). Adeno-associated virus serotype 4 (AAV4) and AAV5 both require sialic acid binding for hemagglutination and efficient transduction but differ in sialic acid linkage specificity. J Virol *75*, 6884-6893.

Kamei, M., Misono, K., and Lewis, H. (1999). A study of the ability of tissue plasminogen activator to diffuse into the subretinal space after intravitreal injection in rabbits. Am J Ophthalmol *128*, 739-746.

Kamenarova, K., Corton, M., Garcia-Sandoval, B., Fernandez-San Jose, P., Panchev, V., Avila-Fernandez, A., Lopez-Molina, M.I., Chakarova, C., Ayuso, C., and Bhattacharya, S.S. (2013). Novel GUCA1A mutations suggesting possible mechanisms of pathogenesis in cone, cone-rod, and macular dystrophy patients. Biomed Res Int *2013*, 517570.

Kashiwakura, Y., Tamayose, K., Iwabuchi, K., Hirai, Y., Shimada, T., Matsumoto, K., Nakamura, T., Watanabe, M., Oshimi, K., and Daida, H. (2005). Hepatocyte growth factor receptor is a coreceptor for adeno-associated virus type 2 infection. J Virol *79*, 609-614.

Kay, C.N., Ryals, R.C., Aslanidi, G.V., Min, S.H., Ruan, Q., Sun, J., Dyka, F.M., Kasuga, D., Ayala, A.E., Van Vliet, K.*, et al.* (2013). Targeting photoreceptors via intravitreal delivery using novel, capsid-mutated AAV vectors. PLoS One *8*, e62097.

Kedzierski, W., Bok, D., and Travis, G.H. (1998). Non-cell-autonomous photoreceptor degeneration in rds mutant mice mosaic for expression of a rescue transgene. J Neurosci *18*, 4076-4082.

Keenan, T.D., Clark, S.J., Unwin, R.D., Ridge, L.A., Day, A.J., and Bishop, P.N. (2012). Mapping the differential distribution of proteoglycan core proteins in the adult human retina, choroid, and sclera. Invest Ophthalmol Vis Sci *53*, 7528-7538.

Kern, A., Schmidt, K., Leder, C., Muller, O.J., Wobus, C.E., Bettinger, K., Von der Lieth, C.W., King, J.A., and Kleinschmidt, J.A. (2003). Identification of a heparin-binding motif on adeno-associated virus type 2 capsids. J Virol *77*, 11072-11081.

Kettenmann, H., and Verkhratsky, A. (2011). [Neuroglia--living nerve glue]. Fortschr Neurol Psychiatr *79*, 588-597.

Kijas, J.W., Cideciyan, A.V., Aleman, T.S., Pianta, M.J., Pearce-Kelling, S.E., Miller, B.J., Jacobson, S.G., Aguirre, G.D., and Acland, G.M. (2002). Naturally occurring rhodopsin mutation in the dog causes retinal dysfunction and degeneration mimicking human dominant retinitis pigmentosa. Proc Natl Acad Sci U S A *99*, 6328-6333.

Kim, H., Robinson, S.B., and Csaky, K.G. (2009). Investigating the movement of intravitreal human serum albumin nanoparticles in the vitreous and retina. Pharm Res *26*, 329-337.

Klimczak, R.R., Koerber, J.T., Dalkara, D., Flannery, J.G., and Schaffer, D.V. (2009). A novel adeno-associated viral variant for efficient and selective intravitreal transduction of rat Muller cells. PLoS One *4*, e7467.

Koenekoop, R.K. (2004). An overview of Leber congenital amaurosis: a model to understand human retinal development. Surv Ophthalmol *49*, 379-398.

Kohl, S., Coppieters, F., Meire, F., Schaich, S., Roosing, S., Brennenstuhl, C., Bolz, S., van Genderen, M.M., Riemslag, F.C., European Retinal Disease, C.*, et al.* (2012). A nonsense mutation in PDE6H causes autosomal-recessive incomplete achromatopsia. Am J Hum Genet *91*, 527-532.

Kohl, S., and Hamel, C. (2013). Clinical utility gene card for: Achromatopsia - update 2013. Eur J Hum Genet *21*.

Kolstad, K.D., Dalkara, D., Guerin, K., Visel, M., Hoffmann, N., Schaffer, D.V., and Flannery, J.G. (2010). Changes in adeno-associated virus-mediated gene delivery in retinal degeneration. Hum Gene Ther *21*, 571-578.

Komaromy, A.M., Alexander, J.J., Rowlan, J.S., Garcia, M.M., Chiodo, V.A., Kaya, A., Tanaka, J.C., Acland, G.M., Hauswirth, W.W., and Aguirre, G.D. (2010). Gene therapy rescues cone function in congenital achromatopsia. Hum Mol Genet *19*, 2581-2593.

Komaromy, A.M., Alexander, J.J., Rowlan, J.S., Garcia, M.M., Chiodo, V.A., Kaya, A., Tanaka, J.C., Acland, G.M., Hauswirth, W.W., and Aguirre, G.D. (2010). Gene therapy rescues cone function in congenital achromatopsia. Hum Mol Genet *19*, 2581-2593.

Kramer, R.H., Mourot, A., and Adesnik, H. (2013). Optogenetic pharmacology for control of native neuronal signaling proteins. Nat Neurosci *16*, 816-823.

Lagali, P.S., Balya, D., Awatramani, G.B., Munch, T.A., Kim, D.S., Busskamp, V., Cepko, C.L., and Roska, B. (2008). Light-activated channels targeted to ON bipolar cells restore visual function in retinal degeneration. Nat Neurosci *11*, 667-675.

Lazarus, H.S., and Hageman, G.S. (1992). Xyloside-induced disruption of interphotoreceptor matrix proteoglycans results in retinal detachment. Invest Ophthalmol Vis Sci *33*, 364-376.

Le Meur, G., Stieger, K., Smith, A.J., Weber, M., Deschamps, J.Y., Nivard, D., Mendes-Madeira, A., Provost, N., Pereon, Y., Cherel, Y.*, et al.* (2007). Restoration of vision in RPE65-deficient Briard dogs using an AAV serotype 4 vector that specifically targets the retinal pigmented epithelium. Gene Ther *14*, 292-303.

Lebherz, C., Maguire, A., Tang, W., Bennett, J., and Wilson, J.M. (2008). Novel AAV serotypes for improved ocular gene transfer. J Gene Med *10*, 375-382.

Leveillard, T., and Sahel, J.A. (2010). Rod-derived cone viability factor for treating blinding diseases: from clinic to redox signaling. Sci Transl Med *2*, 26ps16.

Li, C., Diprimio, N., Bowles, D.E., Hirsch, M.L., Monahan, P.E., Asokan, A., Rabinowitz, J., Agbandje-McKenna, M., and Samulski, R.J. (2012). Single amino acid modification of adeno-associated virus capsid changes transduction and humoral immune profiles. J Virol *86*, 7752-7759.

Lin, B., Martin, P.R., and Grunert, U. (2002). Expression and distribution of ionotropic glutamate receptor subunits on parasol ganglion cells in the primate retina. Vis Neurosci *19*, 453-465.

Lin, B., Koizumi, A., Tanaka, N., Panda, S., and Masland, R.H. (2008). Restoration of visual function in retinal degeneration mice by ectopic expression of melanopsin. Proc Natl Acad Sci U S A *105*, 16009-16014.

Lois, N., Holder, G.E., Bunce, C., Fitzke, F.W., and Bird, A.C. (2001). Phenotypic subtypes of Stargardt macular dystrophy-fundus flavimaculatus. Arch Ophthalmol *119*, 359-369.

Lopes VS, Williams DS. (2015). Gene Therapy for the Retinal Degeneration of Usher Syndrome Caused by Mutations in MYO7A. Cold Spring Harb Perspect Med. *20*;5(6).

Lotery, A.J., Yang, G.S., Mullins, R.F., Russell, S.R., Schmidt, M., Stone, E.M., Lindbloom, J.D., Chiorini, J.A., Kotin, R.M., and Davidson, B.L. (2003). Adeno-associated virus type 5: transduction efficiency and cell-type specificity in the primate retina. Hum Gene Ther *14*, 1663-1671.

Lucas, R.J., Douglas, R.H., and Foster, R.G. (2001a). Characterization of an ocular photopigment capable of driving pupillary constriction in mice. Nat Neurosci *4*, 621-626.

Lucas, R.J., Freedman, M.S., Lupi, D., Munoz, M., David-Gray, Z.K., and Foster, R.G. (2001). Identifying the photoreceptive inputs to the mammalian circadian system using transgenic and retinally degenerate mice. Behav Brain Res *125*, 97-102.

Lucas, R.J., Hattar, S., Takao, M., Berson, D.M., Foster, R.G., and Yau, K.W. (2003). Diminished pupillary light reflex at high irradiances in melanopsin-knockout mice. Science *299*, 245-247.

Lyubarsky, A.L., Daniele, L.L., and Pugh, E.N., Jr. (2004). From candelas to photoisomerizations in the mouse eye by rhodopsin bleaching in situ and the light-rearing dependence of the major components of the mouse ERG. Vision Res *44*, 3235-3251..

Mace, E., Caplette, R., Marre, O., Sengupta, A., Chaffiol, A., Barbe, P., Desrosiers, M., Bamberg, E., Sahel, J.A., Picaud, S.*, et al.* (2015). Targeting channelrhodopsin-2 to ON-bipolar cells with vitreally administered AAV Restores ON and OFF visual responses in blind mice. Mol Ther *23*, 7-16

MacLaren, R.E., Groppe, M., Barnard, A.R., Cottriall, C.L., Tolmachova, T., Seymour, L., Clark, K.R., During, M.J., Cremers, F.P., Black, G.C.*, et al.* (2014). Retinal gene therapy in patients with choroideremia: initial findings from a phase 1/2 clinical trial. Lancet *383*, 1129-1137.

MacLaren, R.E., Pearson, R.A., MacNeil, A., Douglas, R.H., Salt, T.E., Akimoto, M., Swaroop, A., Sowden, J.C., and Ali, R.R. (2006). Retinal repair by transplantation of photoreceptor precursors. Nature *444*, 203-207.

MacNeil, M.A., and Masland, R.H. (1998). Extreme diversity among amacrine cells: implications for function. Neuron *20*, 971-982.

Maguire, A.M., High, K.A., Auricchio, A., Wright, J.F., Pierce, E.A., Testa, F., Mingozzi, F., Bennicelli, J.L., Ying, G.S., Rossi, S.*, et al.* (2009). Age-dependent effects of RPE65 gene therapy for Leber's congenital amaurosis: a phase 1 dose-escalation trial. Lancet *374*, 1597-1605.

Maguire, A.M., Simonelli, F., Pierce, E.A., Pugh, E.N., Jr., Mingozzi, F., Bennicelli, J., Banfi, S., Marshall, K.A., Testa, F., Surace, E.M.*, et al.* (2008). Safety and efficacy of gene transfer for Leber's congenital amaurosis. N Engl J Med *358*, 2240-2248.

Manookin, M.B., Beaudoin, D.L., Ernst, Z.R., Flagel, L.J., and Demb, J.B. (2008). Disinhibition combines with excitation to extend the operating range of the OFF visual pathway in daylight. J Neurosci *28*, 4136-4150.

Maclachlan, T.K., Lukason, M., Collins, M., Munger, R., Isenberger, E., Rogers, C., Malatos, S., Dufresne, E., Morris, J., Calcedo, R.*, et al.* (2011). Preclinical safety evaluation of AAV2-sFLT01- a gene therapy for age-related macular degeneration. Mol Ther *19*, 326-334.

Mandel, Y., Goetz, G., Lavinsky, D., Huie, P., Mathieson, K., Wang, L., Kamins, T., Galambos, L., Manivanh, R., Harris, J.*, et al.* (2013). Cortical responses elicited by photovoltaic subretinal prostheses exhibit similarities to visually evoked potentials. Nat Commun *4*, 1980.

Marc, R.E., Jones, B.W., Anderson, J.R., Kinard, K., Marshak, D.W., Wilson, J.H., Wensel, T., and Lucas, R.J. (2007). Neural reprogramming in retinal degeneration. Invest Ophthalmol Vis Sci *48*, 3364-3371.

Martin, K.R., Klein, R.L., and Quigley, H.A. (2002). Gene delivery to the eye using adeno-associated viral vectors. Methods *28*, 267-275.

Martin, K.R., and Quigley, H.A. (2004). Gene therapy for optic nerve disease. Eye (Lond) *18*, 1049-1055.

Masseck, O.A., Spoida, K., Dalkara, D., Maejima, T., Rubelowski, J.M., Wallhorn, L., Deneris, E.S., and Herlitze, S. (2014). Vertebrate cone opsins enable sustained and highly sensitive rapid control of Gi/o signaling in anxiety circuitry. Neuron *81*, 1263-1273.

Mazzoni, F., Novelli, E., and Strettoi, E. (2008). Retinal ganglion cells survive and maintain normal dendritic morphology in a mouse model of inherited photoreceptor degeneration. J Neurosci *28*, 14282-14292.

McLaughlin, M.E., Ehrhart, T.L., Berson, E.L., and Dryja, T.P. (1995). Mutation spectrum of the gene encoding the beta subunit of rod phosphodiesterase among patients with autosomal recessive retinitis pigmentosa. Proc Natl Acad Sci U S A *92*, 3249-3253.

McLaughlin, M.E., Sandberg, M.A., Berson, E.L., and Dryja, T.P. (1993). Recessive mutations in the gene encoding the beta-subunit of rod phosphodiesterase in patients with retinitis pigmentosa. Nat Genet *4*, 130-134.

Melyan, Z., Tarttelin, E.E., Bellingham, J., Lucas, R.J., and Hankins, M.W. (2005). Addition of human melanopsin renders mammalian cells photoresponsive. Nature *433*, 741-745.

Merbs, S.L., and Nathans, J. (1992). Absorption spectra of human cone pigments. Nature *356*, 433-435.

Michaelides, M., Aligianis, I.A., Ainsworth, J.R., Good, P., Mollon, J.D., Maher, E.R., Moore, A.T., and Hunt, D.M. (2004). Progressive cone dystrophy associated with mutation in CNGB3. Invest Ophthalmol Vis Sci *45*, 1975-1982.

Michaelides, M., Hunt, D.M., and Moore, A.T. (2004). The cone dysfunction syndromes. Br J Ophthalmol *88*, 291-297.

Mordenti, J., Cuthbertson, R.A., Ferrara, N., Thomsen, K., Berleau, L., Licko, V., Allen, P.C., Valverde, C.R., Meng, Y.G., Fei, D.T.*, et al.* (1999). Comparisons of the intraocular tissue distribution, pharmacokinetics, and safety of 125I-labeled full-length and Fab antibodies in rhesus monkeys following intravitreal administration. Toxicol Pathol *27*, 536-544.

Morgans, C.W., Zhang, J., Jeffrey, B.G., Nelson, S.M., Burke, N.S., Duvoisin, R.M., and Brown, R.L. (2009). TRPM1 is required for the depolarizing light response in retinal ON-bipolar cells. Proc Natl Acad Sci U S A *106*, 19174-19178.

Min, S.H., Molday, L.L., Seeliger, M.W., Dinculescu, A., Timmers, A.M., Janssen, A., Tonagel, F., Tanimoto, N., Weber, B.H., Molday, R.S.*, et al.* (2005). Prolonged recovery of retinal structure/function after gene therapy in an Rs1h-deficient mouse model of x-linked juvenile retinoschisis. Mol Ther *12*, 644-651.

Mussolino, C., della Corte, M., Rossi, S., Viola, F., Di Vicino, U., Marrocco, E., Neglia, S., Doria, M., Testa, F., Giovannoni, R.*, et al.* (2011). AAV-mediated photoreceptor transduction of the pig cone-enriched retina. Gene Ther *18*, 637-645.

Murano, E., Perin, D., Khan, R., and Bergamin, M. (2011). Hyaluronan: from biomimetic to industrial business strategy. Nat Prod Commun *6*, 555-572.

Muzyczka N. Parvoviridae: The viruses and their replication. Fundamental virology. Philadelphia: Lippincott Williams & Wilkins 2001;2327-59.

Nishiguchi, K.M., Carvalho, L.S., Rizzi, M., Powell, K., Holthaus, S.M., Azam, S.A., Duran, Y., Ribeiro, J., Luhmann, U.F., Bainbridge, J.W.*, et al.* (2015). Gene therapy restores vision in rd1 mice after removal of a confounding mutation in Gpr179. Nat Commun *6*, 6006.

Novarino, G., Akizu, N., and Gleeson, J.G. (2011). Modeling human disease in humans: the ciliopathies. Cell *147*, 70-79.

Orth, D.H., Fine, B.S., Fagman, W., and Quirk, T.C. (1977). Clarification of foveomacular nomenclature and grid for quantitation of macular disorders. Trans Sect Ophthalmol Am Acad Ophthalmol Otolaryngol *83*, OP506-514.

Palchewski, K (2006). G protein coupled receptor rhodopsin. Annu. Rev. Biochem. *75*, 743-767.

Panda, S., Nayak, S.K., Campo, B., Walker, J.R., Hogenesch, J.B., and Jegla, T. (2005). Illumination of the melanopsin signaling pathway. Science *307*, 600-604.

Panda, S., Sato, T.K., Castrucci, A.M., Rollag, M.D., DeGrip, W.J., Hogenesch, J.B., Provencio, I., and Kay, S.A. (2002). Melanopsin (Opn4) requirement for normal light-induced circadian phase shifting. Science *298*, 2213-2216.

Panda, S., Provencio, I., Tu, D.C., Pires, S.S., Rollag, M.D., Castrucci, A.M., Pletcher, M.T., Sato, T.K., Wiltshire, T., Andahazy, M.*, et al.* (2003). Melanopsin is required for non-image-forming photic responses in blind mice. Science *301*, 525-527.

Pang, J.J., Chang, B., Kumar, A., Nusinowitz, S., Noorwez, S.M., Li, J., Rani, A., Foster, T.C., Chiodo, V.A., Doyle, T.*, et al.* (2006). Gene therapy restores vision-dependent behavior as well as retinal structure and function in a mouse model of RPE65 Leber congenital amaurosis. Mol Ther *13*, 565-572.

Pang, J.J., Dai, X., Boye, S.E., Barone, I., Boye, S.L., Mao, S., Everhart, D., Dinculescu, A., Liu, L., Umino, Y.*, et al.* (2011). Long-term retinal function and structure rescue using capsid mutant AAV8 vector in the rd10 mouse, a model of recessive retinitis pigmentosa. Mol Ther *19*, 234-242.

Pang, J.J., Deng, W.T., Dai, X., Lei, B., Everhart, D., Umino, Y., Li, J., Zhang, K., Mao, S., Boye, S.L.*, et al.* (2012). AAV-mediated cone rescue in a naturally occurring mouse model of CNGA3-achromatopsia. PLoS One *7*, e35250.

Park, T.K., Wu, Z., Kjellstrom, S., Zeng, Y., Bush, R.A., Sieving, P.A., and Colosi, P. (2009). Intravitreal delivery of AAV8 retinoschisin results in cell type-specific gene expression and retinal rescue in the Rs1-KO mouse. Gene Ther *16*, 916-926.

Park, J.C., Moura, A.L., Raza, A.S., Rhee, D.W., Kardon, R.H., and Hood, D.C. (2011). Toward a clinical protocol for assessing rod, cone, and melanopsin contributions to the human pupil response. Invest Ophthalmol Vis Sci *52*, 6624-6635.

Paxinos G, Franklin KBJ (2001) The Mouse Brain in Stereotaxic Coordinates (Second Edition): Academic Press.

Peachey, N.S., Goto, Y., al-Ubaidi, M.R., and Naash, M.I. (1993). Properties of the mouse cone-mediated electroretinogram during light adaptation. Neurosci Lett *162*, 9-11.

Peachey, N.S., Pearring, J.N., Bojang, P., Jr., Hirschtritt, M.E., Sturgill-Short, G., Ray, T.A., Furukawa, T., Koike, C., Goldberg, A.F., Shen, Y.*, et al.* (2012). Depolarizing bipolar cell dysfunction due to a Trpm1 point mutation. J Neurophysiol *108*, 2442-2451.

Pearson, R.A., Barber, A.C., Rizzi, M., Hippert, C., Xue, T., West, E.L., Duran, Y., Smith, A.J., Chuang, J.Z., Azam, S.A.*, et al.* (2012). Restoration of vision after transplantation of photoreceptors. Nature *485*, 99-103.

Petit, C. (2001). Usher syndrome: from genetics to pathogenesis. Annu Rev Genomics Hum Genet *2*, 271-297.

Petrs-Silva, H., Dinculescu, A., Li, Q., Min, S.H., Chiodo, V., Pang, J.J., Zhong, L., Zolotukhin, S., Srivastava, A., Lewin, A.S.*, et al.* (2009). High-efficiency transduction of the mouse retina by tyrosine-mutant AAV serotype vectors. Mol Ther *17*, 463-471.

Petrs-Silva, H., Dinculescu, A., Li, Q., Deng, W.T., Pang, J.J., Min, S.H., Chiodo, V., Neeley, A.W., Govindasamy, L., Bennett, A.*, et al.* (2011). Novel properties of tyrosine-mutant AAV2 vectors in the mouse retina. Mol Ther *19*, 293-301.

Petersen-Jones, S.M., Bartoe, J.T., Fischer, A.J., Scott, M., Boye, S.L., Chiodo, V., and Hauswirth, W.W. (2009). AAV retinal transduction in a large animal model species: comparison of a self-complementary AAV2/5 with a single-stranded AAV2/5 vector. Mol Vis *15*, 1835-1842.

Pittler, S.J., and Baehr, W. (1991). Identification of a nonsense mutation in the rod photoreceptor cGMP phosphodiesterase beta-subunit gene of the rd mouse. Proc Natl Acad Sci U S A *88*, 8322-8326.

Polosukhina, A., Litt, J., Tochitsky, I., Nemargut, J., Sychev, Y., De Kouchkovsky, I., Huang, T., Borges, K., Trauner, D., Van Gelder, R.N.*, et al.* (2012). Photochemical restoration of visual responses in blind mice. Neuron *75*, 271-282.

Provencio, I., Jiang, G., De Grip, W.J., Hayes, W.P., and Rollag, M.D. (1998). Melanopsin: An opsin in melanophores, brain, and eye. Proc Natl Acad Sci U S A *95*, 340-345.

Provencio, I., Rodriguez, I.R., Jiang, G., Hayes, W.P., Moreira, E.F., and Rollag, M.D. (2000). A novel human opsin in the inner retina. J Neurosci *20*, 600-605.

Prusky, G.T., West, P.W., and Douglas, R.M. (2000). Behavioral assessment of visual acuity in mice and rats. Vision Res *40*, 2201-2209

Prusky, G.T., and Douglas, R.M. (2004). Characterization of mouse cortical spatial vision. Vision Res *44*, 3411-3418.

Pugh, E.N., Jr., Nikonov, S., and Lamb, T.D. (1999). Molecular mechanisms of vertebrate photoreceptor light adaptation. Curr Opin Neurobiol *9*, 410-418.

Qi, X., Hauswirth, W.W., and Guy, J. (2007). Dual gene therapy with extracellular superoxide dismutase and catalase attenuates experimental optic neuritis. Mol Vis *13*, 1-11.

Qing, K., Mah, C., Hansen, J., Zhou, S., Dwarki, V., and Srivastava, A. (1999). Human fibroblast growth factor receptor 1 is a co-receptor for infection by adeno-associated virus 2. Nat Med *5*, 71-77.

Qing, K., Khuntirat, B., Mah, C., Kube, D.M., Wang, X.S., Ponnazhagan, S., Zhou, S., Dwarki, V.J., Yoder, M.C., and Srivastava, A. (1998). Adeno-associated virus type 2-mediated gene transfer: correlation of tyrosine phosphorylation of the cellular single-stranded D sequence-binding protein with transgene expression in human cells in vitro and murine tissues in vivo. J Virol *72*, 1593-1599.

Rabinowitz, J.E., Rolling, F., Li, C., Conrath, H., Xiao, W., Xiao, X., and Samulski, R.J. (2002). Cross-packaging of a single adeno-associated virus (AAV) type 2 vector genome into multiple AAV serotypes enables transduction with broad specificity. J Virol *76*, 791-801.

Reich SJ Auricchio A Hildinger M (2003). Efficient trans-splicing in the retina expands the utility of adeno-associated virus as a vector for gene therapy. Hum Gene Ther.; *14*: 37–44.

Reichenbach, A., Fromter, C., Engelmann, R., Wolburg, H., Kasper, M., and Schnitzer, J. (1995). Muller glial cells of the tree shrew retina. J Comp Neurol *360*, 257-270.

Rizzo, S., Belting, C., Cinelli, L., Allegrini, L., Genovesi-Ebert, F., Barca, F., and di Bartolo, E. (2014). The Argus II Retinal Prosthesis: 12-month outcomes from a single-study center. Am J Ophthalmol *157*, 1282-1290.

Robson, A.G., El-Amir, A., Bailey, C., Egan, C.A., Fitzke, F.W., Webster, A.R., Bird, A.C., and Holder, G.E. (2003). Pattern ERG correlates of abnormal fundus autofluorescence in patients with retinitis pigmentosa and normal visual acuity. Invest Ophthalmol Vis Sci *44*, 3544-3550.

Roepman, R., Bauer, D., Rosenberg, T., van Duijnhoven, G., van de Vosse, E., Platzer, M., Rosenthal, A., Ropers, H.H., Cremers, F.P., and Berger, W. (1996). Identification of a gene disrupted by a microdeletion in a patient with X-linked retinitis pigmentosa (XLRP). Hum Mol Genet *5*, 827-833.

Ronquillo, C.C., Bernstein, P.S., and Baehr, W. (2012). Senior-Loken syndrome: a syndromic form of retinal dystrophy associated with nephronophthisis. Vision Res *75*, 88-97.

Romani, M., Micalizzi, A., and Valente, E.M. (2013). Joubert syndrome: congenital cerebellar ataxia with the molar tooth. Lancet Neurol *12*, 894-905.

Ropstad, E.O., Narfstrom, K., Lingaas, F., Wiik, C., Bruun, A., and Bjerkas, E. (2008). Functional and structural changes in the retina of wire-haired dachshunds with early-onset cone-rod dystrophy. Invest Ophthalmol Vis Sci *49*, 1106-1115.

Rosenfeld, P.J., Cowley, G.S., McGee, T.L., Sandberg, M.A., Berson, E.L., and Dryja, T.P. (1992). A null mutation in the rhodopsin gene causes rod photoreceptor dysfunction and autosomal recessive retinitis pigmentosa. Nat Genet *1*, 209-213.

Roska, B., Molnar, A., and Werblin, F.S. (2006). Parallel processing in retinal ganglion cells: how integration of space-time patterns of excitation and inhibition form the spiking output. J Neurophysiol *95*, 3810-3822.

Ross, J.W., Fernandez de Castro, J.P., Zhao, J., Samuel, M., Walters, E., Rios, C., Bray-Ward, P., Jones, B.W., Marc, R.E., Wang, W.*, et al.* (2012). Generation of an inbred miniature pig model of retinitis pigmentosa. Invest Ophthalmol Vis Sci *53*, 501-507.

Russell, S.R., Shepherd, J.D., and Hageman, G.S. (1991). Distribution of glycoconjugates in the human retinal internal limiting membrane. Invest Ophthalmol Vis Sci *32*, 1986-1995.

Sahel, J., Bonnel, S., Mrejen, S., and Paques, M. (2010). Retinitis pigmentosa and other dystrophies. Dev Ophthalmol *47*, 160-167.

Sahel, J.A., Marazova, K., and Audo, I. (2015). Clinical characteristics and current therapies for inherited retinal degenerations. Cold Spring Harb Perspect Med *5*, a017111.

Sakmar, T.P. (2002). Structure of rhodopsin and the superfamily of seven-helical receptors: the same and not the same. Curr Opin Cell Biol *14*, 189-195.

Sakurai, E., Ozeki, H., Kunou, N., and Ogura, Y. (2001). Effect of particle size of polymeric nanospheres on intravitreal kinetics. Ophthalmic Res *33*, 31-36.

Sancho-Pelluz, J., Arango-Gonzalez, B., Kustermann, S., Romero, F.J., van Veen, T., Zrenner, E., Ekstrom, P., and Paquet-Durand, F. (2008). Photoreceptor cell death mechanisms in inherited retinal degeneration. Mol Neurobiol *38*, 253-269.

Sanders, N.N., Peeters, L., Lentacker, I., Demeester, J., and De Smedt, S.C. (2007). Wanted and unwanted properties of surface PEGylated nucleic acid nanoparticles in ocular gene transfer. J Control Release *122*, 226-235.

Santos, A., Humayun, M.S., de Juan, E., Jr., Greenburg, R.J., Marsh, M.J., Klock, I.B., and Milam, A.H. (1997). Preservation of the inner retina in retinitis pigmentosa. A morphometric analysis. Arch Ophthalmol *115*, 511-515.

Schmidt, M., Voutetakis, A., Afione, S., Zheng, C., Mandikian, D., and Chiorini, J.A. (2008). Adeno-associated virus type 12 (AAV12): a novel AAV serotype with sialic acid- and heparan sulfate proteoglycan-independent transduction activity. J Virol *82*, 1399-1406.

Schmidt, T.M., Do, M.T., Dacey, D., Lucas, R., Hattar, S., and Matynia, A. (2011). Melanopsin-positive intrinsically photosensitive retinal ganglion cells: from form to function. J Neurosci *31*, 16094-16101.

Schwartz SD, Regillo CD, Lam BL, Eliott D, Rosenfeld PJ, Gregori NZ, Hubschman JP, Davis JL, Heilwell G, Spirn M, Maguire J, Gay R, Bateman J, Ostrick RM, Morris D, Vincent M, Anglade E, Del Priore LV, Lanza R. (2015). Human embryonic stem cell-derived retinal pigment epithelium in patients with age-related macular degeneration and Stargardt's macular dystrophy: follow-up of two open-label phase 1/2 studies. Lancet. *7;385*(9967):509-16.

Scott, P.A., Fernandez de Castro, J.P., Kaplan, H.J., and McCall, M.A. (2014). A Pro23His mutation alters prenatal rod photoreceptor morphology in a transgenic swine model of retinitis pigmentosa. Invest Ophthalmol Vis Sci *55*, 2452-2459.

Shen, S., Bryant, K.D., Brown, S.M., Randell, S.H., and Asokan, A. (2011). Terminal N-linked galactose is the primary receptor for adeno-associated virus 9. J Biol Chem *286*, 13532-13540.

Simonelli, F., Maguire, A.M., Testa, F., Pierce, E.A., Mingozzi, F., Bennicelli, J.L., Rossi, S., Marshall, K., Banfi, S., Surace, E.M.*, et al.* (2010). Gene therapy for Leber's congenital amaurosis is safe and effective through 1.5 years after vector administration. Mol Ther *18*, 643-650.

Singhal, S., Lawrence, J.M., Bhatia, B., Ellis, J.S., Kwan, A.S., Macneil, A., Luthert, P.J., Fawcett, J.W., Perez, M.T., Khaw, P.T.*, et al.* (2008). Chondroitin sulfate proteoglycans and microglia prevent migration and integration of grafted Muller stem cells into degenerating retina. Stem Cells *26*, 1074-1082.

Skaat, A., Sher, I., Kolker, A., Elyasiv, S., Rosenfeld, E., Mhajna, M., Melamed, S., Belkin, M., and Rotenstreich, Y. (2013). Pupillometer-based objective chromatic perimetry in normal eyes and patients with retinal photoreceptor dystrophies. Invest Ophthalmol Vis Sci *54*, 2761-2770

Smith, A.J., Bainbridge, J.W., and Ali, R.R. (2012). Gene supplementation therapy for recessive forms of inherited retinal dystrophies. Gene Ther *19*, 154-161.

Smith, A.J., Schlichtenbrede, F.C., Tschernutter, M., Bainbridge, J.W., Thrasher, A.J., and Ali, R.R. (2003). AAV-Mediated gene transfer slows photoreceptor loss in the RCS rat model of retinitis pigmentosa. Mol Ther *8*, 188-195.

Sohocki, M.M., Daiger, S.P., Bowne, S.J., Rodriquez, J.A., Northrup, H., Heckenlively, J.R., Birch, D.G., Mintz-Hittner, H., Ruiz, R.S., Lewis, R.A.*, et al.* (2001). Prevalence of mutations causing retinitis pigmentosa and other inherited retinopathies. Hum Mutat *17*, 42-51.

Stasheff, S.F., Shankar, M., and Andrews, M.P. (2011). Developmental time course distinguishes changes in spontaneous and light-evoked retinal ganglion cell activity in rd1 and rd10 mice. J Neurophysiol *105*, 3002-3009.

Stasheff, S.F. (2008). Emergence of sustained spontaneous hyperactivity and temporary preservation of OFF responses in ganglion cells of the retinal degeneration (rd1) mouse. J Neurophysiol *99*, 1408-1421.

Stieger, K., Colle, M.A., Dubreil, L., Mendes-Madeira, A., Weber, M., Le Meur, G., Deschamps, J.Y., Provost, N., Nivard, D., Cherel, Y.*, et al.* (2008). Subretinal delivery of recombinant AAV serotype 8 vector in dogs results in gene transfer to neurons in the brain. Mol Ther *16*, 916-923.

Stingl K, Bartz-Schmidt KU, Besch D, Chee CK, Cottriall CL, Gekeler F, Groppe M, Jackson TL, MacLaren RE, Koitschev A, Kusnyerik A, Neffendorf J, Nemeth J, Naeem MA, Peters T, Ramsden JD, Sachs H, Simpson A, Singh MS, Wilhelm B, Wong D, Zrenner E. (2015) Subretinal Visual Implant Alpha IMS--Clinical trial interim report. Vision Res. *111*(Pt B):149-60.

Strettoi, E., and Pignatelli, V. (2000). Modifications of retinal neurons in a mouse model of retinitis pigmentosa. Proc Natl Acad Sci U S A *97*, 11020-11025.

Summerford, C., and Samulski, R.J. (1998). Membrane-associated heparan sulfate proteoglycan is a receptor for adeno-associated virus type 2 virions. J Virol *72*, 1438-1445.

Summerford, C., Bartlett, J.S., and Samulski, R.J. (1999). AlphaVbeta5 integrin: a co-receptor for adeno-associated virus type 2 infection. Nat Med *5*, 78-82.

Surace, E.M., Auricchio, A., Reich, S.J., Rex, T., Glover, E., Pineles, S., Tang, W., O'Connor, E., Lyubarsky, A., Savchenko, A.*, et al.* (2003). Delivery of adeno-associated virus vectors to the fetal retina: impact of viral capsid proteins on retinal neuronal progenitor transduction. J Virol *77*, 7957-7963.

Surace, E.M., and Auricchio, A. (2008). Versatility of AAV vectors for retinal gene transfer. Vision Res *48*, 353-359.

Tang, P.H., Kono, M., Koutalos, Y., Ablonczy, Z., and Crouch, R.K. (2013). New insights into retinoid metabolism and cycling within the retina. Prog Retin Eye Res *32*, 48-63.

Terakita, A. (2005). The opsins. Genome Biol *6*, 213.

Testa, F., Maguire, A.M., Rossi, S., Pierce, E.A., Melillo, P., Marshall, K., Banfi, S., Surace, E.M., Sun, J., Acerra, C.*, et al.* (2013). Three-year follow-up after unilateral subretinal delivery of adeno-associated virus in patients with Leber congenital Amaurosis type 2. Ophthalmology *120*, 1283-1291.

Thyagarajan, S., van Wyk, M., Lehmann, K., Lowel, S., Feng, G., and Wassle, H. (2010). Visual function in mice with photoreceptor degeneration and transgenic expression of channelrhodopsin 2 in ganglion cells. J Neurosci *30*, 8745-8758.

Tochitsky, I., Polosukhina, A., Degtyar, V.E., Gallerani, N., Smith, C.M., Friedman, A., Van Gelder, R.N., Trauner, D., Kaufer, D., and Kramer, R.H. (2014). Restoring visual function to blind mice with a photoswitch that exploits electrophysiological remodeling of retinal ganglion cells. Neuron *81*, 800-813.

Tomita, H., Sugano, E., Isago, H., Hiroi, T., Wang, Z., Ohta, E., and Tamai, M. (2010). Channelrhodopsin-2 gene transduced into retinal ganglion cells restores functional vision in genetically blind rats. Exp Eye Res *90*, 429-436.

Tsujikawa, M., Wada, Y., Sukegawa, M., Sawa, M., Gomi, F., Nishida, K., and Tano, Y. (2008). Age at onset curves of retinitis pigmentosa. Arch Ophthalmol *126*, 337-340.

Twyford, P., Cai, C., and Fried, S. (2014). Differential responses to high-frequency electrical stimulation in ON and OFF retinal ganglion cells. J Neural Eng *11*, 025001.

Valeri S., Lazar C. H., Chang B., Banin S. E., Swaroop A., (2015). Biology and therapy of inherited retinal degenerative disease: insights from mouse models; Disease Models and Mechanisms *8*: 109-129.

Vandenberghe, L.H., Bell, P., Maguire, A.M., Cearley, C.N., Xiao, R., Calcedo, R., Wang, L., Castle, M.J., Maguire, A.C., Grant, R.*, et al.* (2011). Dosage thresholds for AAV2 and AAV8 photoreceptor gene therapy in monkey. Sci Transl Med *3*, 88ra54.

Van Gelder, R.N., and Kaur, K. (2015). Vision Science: Can Rhodopsin Cure Blindness? Curr Biol *25*, R713-715.

van Wyk, M., Pielecka-Fortuna, J., Lowel, S., and Kleinlogel, S. (2015). Restoring the ON Switch in Blind Retinas: Opto-mGluR6, a Next-Generation, Cell-Tailored Optogenetic Tool. PLoS Biol *13*, e1002143

van Wyk, M., Schneider, S., and Kleinlogel, S. (2015). Variable phenotypic expressivity in inbred retinal degeneration mouse lines: A comparative study of C3H/HeOu and FVB/N rd1 mice. Mol Vis *21*, 811-827.

Wang, J.S., and Kefalov, V.J. (2009). An alternative pathway mediates the mouse and human cone visual cycle. Curr Biol *19*, 1665-1669.

Wang, J.S., and Kefalov, V.J. (2011). The cone-specific visual cycle. Prog Retin Eye Res *30*, 115-128.

Waters, A.M., and Beales, P.L. (2011). Ciliopathies: an expanding disease spectrum. Pediatr Nephrol *26*, 1039-1056.

Walters, R.W., Yi, S.M., Keshavjee, S., Brown, K.E., Welsh, M.J., Chiorini, J.A., and Zabner, J. (2001). Binding of adeno-associated virus type 5 to 2,3-linked sialic acid is required for gene transfer. J Biol Chem *276*, 20610-20616.

Weber, M., Rabinowitz, J., Provost, N., Conrath, H., Folliot, S., Briot, D., Cherel, Y., Chenuaud, P., Samulski, J., Moullier, P.*, et al.* (2003). Recombinant adeno-associated virus serotype 4 mediates unique and exclusive long-term transduction of retinal pigmented epithelium in rat, dog, and nonhuman primate after subretinal delivery. Mol Ther *7*, 774-781.

Wu, Z., Miller, E., Agbandje-McKenna, M., and Samulski, R.J. (2006). Alpha2,3 and alpha2,6 N-linked sialic acids facilitate efficient binding and transduction by adeno-associated virus types 1 and 6. J Virol *80*, 9093-9103.

Wu, Z., Asokan, A., and Samulski, R.J. (2006). Adeno-associated virus serotypes: vector toolkit for human gene therapy. Mol Ther *14*, 316-327.

Xu, J., Dodd, R.L., Makino, C.L., Simon, M.I., Baylor, D.A., and Chen, J. (1997). Prolonged photoresponses in transgenic mouse rods lacking arrestin. Nature *389*, 505-509.

Yang, G.S., Schmidt, M., Yan, Z., Lindbloom, J.D., Harding, T.C., Donahue, B.A., Engelhardt, J.F., Kotin, R., and Davidson, B.L. (2002). Virus-mediated transduction of murine retina with adeno-associated virus: effects of viral capsid and genome size. J Virol *76*, 7651-7660.

Yau, K.W. (1994). Phototransduction mechanism in retinal rods and cones. The Friedenwald Lecture. Invest Ophthalmol Vis Sci *35*, 9-32.

Yin, L., Greenberg, K., Hunter, J.J., Dalkara, D., Kolstad, K.D., Masella, B.D., Wolfe, R., Visel, M., Stone, D., Libby, R.T.*, et al.* (2011). Intravitreal injection of AAV2 transduces macaque inner retina. Invest Ophthalmol Vis Sci *52*, 2775-2783.

Yizhar, O., Fenno, L.E., Davidson, T.J., Mogri, M., and Deisseroth, K. (2011). Optogenetics in neural systems. Neuron *71*, 9-34.

Zallocchi M Binley K Lad Y (2014). EIAV-based retinal gene therapy in the shaker1 mouse model for usher syndrome type 1B: development of UshStat. PLoS One.; *9*: e94272.

Zeitz, C., Jacobson, S.G., Hamel, C.P., Bujakowska, K., Neuille, M., Orhan, E., Zanlonghi, X., Lancelot, M.E., Michiels, C., Schwartz, S.B.*, et al.* (2013). Whole-exome sequencing identifies LRIT3 mutations as a cause of autosomal-recessive complete congenital stationary night blindness. Am J Hum Genet *92*, 67-75.

Zhang, Y., Ivanova, E., Bi, A., and Pan, Z.H. (2009). Ectopic expression of multiple microbial rhodopsins restores ON and OFF light responses in retinas with photoreceptor degeneration. J Neurosci *29*, 9186-9196.

Zhang, F., Aravanis, A.M., Adamantidis, A., de Lecea, L., and Deisseroth, K. (2007). Circuit-breakers: optical technologies for probing neural signals and systems. Nat Rev Neurosci *8*, 577-581.

Zhong, L., Li, B., Mah, C.S., Govindasamy, L., Agbandje-McKenna, M., Cooper, M., Herzog, R.W., Zolotukhin, I., Warrington, K.H., Jr., Weigel-Van Aken, K.A.*, et al.* (2008). Next generation of adeno-associated virus 2 vectors: point mutations in tyrosines lead to high-efficiency transduction at lower doses. Proc Natl Acad Sci U S A *105*, 7827-7832.

Zhong, L., Li, B., Jayandharan, G., Mah, C.S., Govindasamy, L., Agbandje-McKenna, M., Herzog, R.W., Weigel-Van Aken, K.A., Hobbs, J.A., Zolotukhin, S.*, et al.* (2008). Tyrosine-phosphorylation of AAV2 vectors and its consequences on viral intracellular trafficking and transgene expression. Virology *381*, 194-202.

Zhou, Y., Pernet, V., Hauswirth, W.W., and Di Polo, A. (2005). Activation of the extracellular signal-regulated kinase 1/2 pathway by AAV gene transfer protects retinal ganglion cells in glaucoma. Mol Ther *12*, 402-412.

Zinn, E., and Vandenberghe, L.H. (2014). Adeno-associated virus: fit to serve. Curr Opin Virol *8*, 90-97.

Zrenner, E., Bartz-Schmidt, K.U., Benav, H., Besch, D., Bruckmann, A., Gabel, V.P., Gekeler, F., Greppmaier, U., Harscher, A., Kibbel, S.*, et al.* (2011). Subretinal electronic chips allow blind patients to read letters and combine them to words. Proc Biol Sci *278*, 1489-1497.

Zrenner, E. (2013). Fighting blindness with microelectronics. Sci Transl Med *5*, 210